POLITECNICO DI MILANO

DEPARTMENT OF ENERGY

EXECUTIVE DOCTORAL PROGRAMME IN ELECTRIC ENGINEERING

MODELING OF DISTRIBUTED GENERATORS INTERFACED WITH POWER ELECTRONICS TO MEDIUM VOLTAGE NETWORKS: ANALYSIS OF POWER QUALITY, FAULT RIDE THROUGH AND PROTECTIONS COORDINATION

PhD Dissertation of:
Chiara Gandolfi

Tutor:
Morris Brenna

Supervisor:
Dario Lucarella

Co- supervisor:
Riccardo Chiumeo

The Chair of the Doctoral Program:
Alberto Berizzi

Year 2014 – Cycle XXV

to my daughter Elena

Index

INTRODUCTION 5

1 DISTRIBUTED GENERATION AND POWER QUALITY 7
1.1 Overview on the main disturbances present in electrical networks 7
1.2 Analysis of the impact of harmonic inverter connected to the distribution network 10
1.2.1 Two-level three phase Inverter 11
1.2.2 Three-level three phase Inverter 17
1.2.3 Three phase Inverter interleaved 22
1.2.4 Comparison of the different inverter configurations 26
1.3 Interaction between inverter and network in the presence of variable generation: the flicker 33
1.3.1 Flicker impact of the wind generators interfaced on the network with power electronics devices 33
1.3.2 Flicker evaluation 34
1.3.3 Flickermeter Model 34
1.3.4 Flicker dependence on the power oscillations amplitude 37
1.3.5 Flicker dependence on the frequency of the oscillations of power 38
1.3.6 Flicker dependence on the short circuit power of the connection point 39
1.3.7 Flicker dependence on the impedance line ratio X/R 40
1.3.8 Flicker dependence on the value of inverter DC-link capacitance 41
1.4 Final Considerations 42

2 DISTRIBUTED GENERATOR CONNECTED TO DISTRIBUTION NETWORK THROUGH INVERTER 43
2.1 Electromagnetic transient simulations: network model 44
2.2 The model of the photovoltaic installation: power and control 46
2.2.1 Photovoltaic equivalent model 46
2.2.2 DC/DC Boost Converter 48
2.2.3 Voltage Source Inverter (VSI) 50
2.2.4 Converters control Strategies and switching 54
2.2.5 Simulation in the absence of networks disturbances 58
2.3 The model of power and control in a wind generator with permanent magnets and power electronics to interface to the network 59
2.3.1 Wind Turbine 60
2.3.2 Permanent Magnet Synchronous Generator 61
2.3.3 Converters and transformers for connection to the network of a wind generator 71
2.3.4 Control and modulation strategies of the converters 72
2.3.5 Simulation in the absence of networks disturbances 75
2.4 Final Considerations 76
2.5 Structure simulated model in ATPDraw 77

3 INTERACTION BETWEEN INVERTER AND ACTIVE NETWORKS: THE FAULT RIDE THROUGH 79
3.1 FRT strategies 81
3.2 External devices to overcome the voltage dips 81
3.3 Inverter current limitation 84
3.4 Control logics implementation 85
3.4.1 The voltage dip detection system 85
3.4.2 FRT control logics 88
3.4.3 Simulation results for the implementation of control logics for PV generators 88
3.4.4 Simulation results for the implementation of control logics for wind generators 97
3.5 Final Considerations 101

4 ANALYSIS OF THE IMPACT ON THE NETWORK OF MORE DISTRIBUTED GENERATORS: DIGSILENT SIMULATIONS 103
4.1 Equivalence ATPDraw - DIgSILENT 103
4.2 MV and LV network model 104
4.2.1 Simulation results of LV and MV network voltage support from PV generation 106
4.3 Network extension (HV) 109
4.3.1 HV network protection model 111
4.4 Wind generators model 113
4.5 Simulation results of LV and MV network voltage support from wind generator 115
4.6 FRT logic 118
4.7 Simulation results of HV network voltage support from wind generator 120
4.8 Final Considerations 124

5 THE INVERTER BEHAVIUOR IN PRESENCE OF UNBALANCED NETWORKS AND VOLTAGE DIPS 125
5.1 Inverter behavior with classical control over axis d-q in case of unbalanced network 125
5.2 Dq-axes control with negative sequence compensation 129
5.3 Second Order Generalized Integral (SOGI) control 131
5.4 Simulation results in presence of unbalanced network 133
5.4.1 Unbalanced Network during steady state 134
5.4.2 Phase to phase inductive fault 136
5.4.3 Three phase inductive fault 138
5.4.4 Three phase resistive fault and FRT strategies 139
5.4.5 Phase to phase resistive fault with current limitations 141
5.5 Final Considerations 142

6 LABORATORY TESTS OF INNOVATIVE INVERTER CAPABILITIES 143
6.1 Test bed description 143
6.1.1 Linear programmable network simulator 145
6.1.2 DC source with PV characteristic curves emulation 146
6.1.3 RLC variables loads 146
6.1.4 The inverter under test 146
6.1.5 Data acquisition system 147
6.2 Innovative capabilities required to the inverter 147

6.2.1 Overcoming network disturbances 148
6.2.2 Supply controlled reactive power 148
6.2.3 Active power regulation 150
6.3 Test Procedure 151
6.4 Experimental activities results 152
6.4.1 6 kW single phase inverter 153
6.4.2 10 kW three phase inverter 154
6.5 Final Considerations 157

7 ANALYSIS OF THE INTERACTION BEETWEEN INVERTERS WITH FRT STRATEGIES AND NETWORK PROTECTIONS 159
7.1 Distribution networks description 159
7.2 The Italian protection philosophy 160
7.3 Actions on MV distribution networks to improve quality of service 161
7.4 Protection issues for active networks exercise 163
7.5 Italian Standards: brief description 165
7.5.1 Interface Protection for generators connected to MV and HV networks 166
7.5.2 Interface Protection for generators connected to LV networks 167
7.6 Simulation Models 168
7.6.1 The instrument transformers 168
7.6.2 Protection relays: models and settings 181
7.7 Operation protections simulations 192
7.7.1 Three phase direct ground fault 192
7.7.2 Three phase resistive fault 193
7.7.3 Three phase resistive fault with high impedance 194
7.7.4 Single phase to ground fault 195
7.7.5 Unwanted island 196
7.7.6 Reclosing on island network 204
7.8 A protection coordination scheme 207
7.8.1 Network protections coordination: the logic selectivity 208
7.8.2 Coordination logic verification 210
7.8.3 Faulty line segment selection and reverse feeding 216
7.9 Communication delays effects 220
7.10 Final Considerations 224

CONCLUSIONS 225

BIBLIOGRAPHY 227

INTRODUCTION

The increasing widespread of the distributed generators connected to the Medium Voltage (MV) and Low Voltage (LV) distribution networks has come to point out a series of new phenomena and new issues related to interactions between the networks themselves and new types of generators, in the first place those interfaced through electronic power converters. The areas involved are very different and cover, for example, aspects of Power Quality, network operating and automation, regulation and standardization of the service and the market.
From the point of view of Power Quality, the activity performed, in the context of an Executive PhD in the research center RSE Ricerca sul Sistema Energetico S.p.A.[1], in collaboration with the Department of Energy of Politecnico di Milano, has studied in deep the base knowledge of the interaction between inverter and electrical network. In particular, it has been oriented toward the analysis of the harmonic impact on the distribution network and the effects of the variability of the primary source, feature typical of renewable energy sources. In addition, in the frame of the recent national and international Standards, it has been evaluated the distributed generators behavior in case of voltage dips and the possibility for the electronic power devices to support the network. This new perspective makes it necessary also to consider the new strategies for DG control, alternatives to those currently implemented, for the overcoming of voltage dips (Fault Ride Through - FRT).
A significant presence of Distributed Generation (DG) also leads to review the coordination strategies for network protection, that will have to maintain generators connected during network voltage dips avoiding, at the same time, the unwanted islands occurrence and the interference with the automatic reclosing procedures.

On the base of these premises, the activity has been developed along the following main directions:

- analysis of the harmonic impact of the inverters connected to the distribution network and the effect of the variability of the power available from primary source on Power Quality;
- analysis of the new features requested by the most recent Standards to distributed generators in case of a network disturb;
- study of the behavior of electronic converters interface to DG (photovoltaic and wind) in case of voltage dips and evaluation of possible control strategies for overcoming them (FRT);
- definition and verification of a possible coordination protection scheme in active networks.

The analysis have been carried out through simulations with software for numerical calculation (Matlab) and programs for transient simulation of electrical networks (ATPDraw, DIgSILENT).

The discussion begins (Chapter 1) with the study of the interaction phenomena between inverter and electrical network analyzing in particular harmonic pollution and the effect on the Power Quality due to the variability of the power available from the primary source of distributed generators.

Subsequently, peculiarities and issues related to the presence of electronic converters interface for distributed generators connected to the Medium Voltage distribution network have been analyzed. In particular, in Chapter 2 the photovoltaic and wind generator models, based on Permanent Magnets Synchronous Generator, are introduced and discussed.

New strategies to overcome voltage dips to avoid sudden loss of generation as a result of disturbances of network have been studied. These new strategies allow to maintain the generators connected to the network during voltage dips, contrary to the nowadays practice, that, in case of a fault, requires the generators disconnection to avoid unwanted islands in the distribution network. The study highlights what are the design characteristics of the inverter and what are the control logics necessary to enable

[1] This work has been financed by the Research Fund for the Italian Electrical System under the Contract Agreement between RSE S.p.A. and the Ministry of Economic Development - General Directorate for Nuclear Energy, Renewable Energy and Energy Efficiency in compliance with the Decree of March 8, 2006.

them to overcome a fault in the network in accordance with the requirements of certain European states Standards (Chapter 3 and 4). Different advanced inverter control solutions for the optimal management of static generators in presence of unbalanced networks have also been investigated (Chapter 5).

At the end of the study of the behavior of the DG interface inverter, an experimental activity, supported by theoretical analysis, indispensable for the forecast and the interpretation of the test results, has been carried out. The scope of these activities has been to identify how to implement the new features required to the inverter from recent national Standard and the issues to be taken into account, in particular relating to the voltage dips overcome and the exchange of active and reactive power with the network. The results are presented in Chapter 6. The tests have been carried out on two commercial inverters: one with basic functionality and one with some advanced features, even if designed before the present Standard.

Finally, the discussion concludes with the proposal and analysis, presented in Chapter 7, of a possible protection scheme for Medium Voltage distribution networks based on logic selectivity, suitable for both passive and active networks, able to operate the faulty line segment selection and to ensure effective management of the distributed generators connected to the network.

1 DISTRIBUTED GENERATION AND POWER QUALITY

The generation interfaced to the network through electronic power converters is rising new challenges both in terms of the Power Quality and of the network exercise itself. These issues arise mainly from the interactions between the network and distributed generators that characterize active users.
In the following paragraphs, a brief description of the different types of disturbances that can occur in the electrical distribution networks has been presented. Especially considering the disturbances that can affect the proper functioning of the consumer devices, with the need, sometimes, to adopt measures to mitigate the disturbance effect.
Then, in particular two types of disturbances has been taken into consideration that are generally due to the interaction between the network and the distributed generators:

- the generation of harmonics in the network by different types of inverter, also considering analytical formulation useful for the study of possible techniques to minimize these contributions;
- the flicker generated by active power variation of the primary source.

Concerning the phenomenon of flicker, the analysis has been carried out starting from models of wind Permanent Magnet Synchronous Generator (PMSG) connected to the network in a back-to-back configuration.

1.1 Overview on the main disturbances present in electrical networks

In general, disturbances caused both by networks faults and by the operation of devices connected to the networks themselves, are composed mainly of voltage variations in terms of:

- frequency;
- waveform;
- amplitude;
- symmetry of three phase voltages.

Among the different types of disturbances, it is possible to define “conducted disturbances” those electromagnetic phenomena that, from a source, propagate in electrical networks through the lines conductors. In some cases an electromagnetic disturbance moves through the transformer windings and then between networks at different voltage levels.

Network frequency variations
The variations in the frequency are deviations from the rated network frequency and depend from events with their origin essentially in the generation and transmission systems. For interconnected networks, transient frequency variations are due to:

- large generators disconnection;
- faults in very high and high voltage network (respectively HHV and HV);
- opening of “important” interconnection lines;
- large loads disconnection.

For the Medium Voltage (MV) and Low Voltage (LV) distribution network, the Standard CEI EN 50160 [1] defines the voltage characteristics in term of maximum frequency variations[2]. Then the Standards for the connection criteria CEI 0-21 [2] and CEI 0-16 [3] define the interval for the frequency variation to set the Interface Protection (IP).

[2] In presence of distributed generation new requirement to the interface protection are requested, in terms of frequency variation (Chapter 7).

Voltage and current harmonics

The harmonics are the spectral components of a periodic signal non-sinusoidal whose frequencies are integer multiples of the fundamental frequency; the inter-harmonics are sinusoidal components with frequencies that are not integer multiples of the fundamental frequency.

The current harmonics are normally generated by "non-linear" loads and/or consumer devices (identifiable as disturbing sources) and may be constant or vary over time depending on the operating conditions of the individual disturbing sources. The current harmonics "injected" into the network from the various sources, flowing through the network impedances, give rise to harmonic voltage drops and consequently to a deformation of the waveform of the supply voltage.

With reference to the voltage, the harmonics can be evaluated individually, through their amplitude (typically as a Root-Mean-Square, RMS, value expressed in Volts or p.u. of fundamental), or globally, through the total harmonic distortion factor calculated by the following expression:

$$THD\_V = \frac{\sqrt{\sum_{n=2}^{N} V_n^2}}{V_1} \tag{1.1}$$

Similar characterization can be applied to the currents, both in terms of RMS value I_n (expressed in Amperes or p.u. of a reference current) both through the total harmonic distortion factor:

$$THD\_I = \frac{\sqrt{\sum_{n=2}^{N} I_n^2}}{I_1} \tag{1.2}$$

The main sources of harmonic currents in the networks are:

- AC/DC and AC/AC converters;
- loads with non-linear characteristics, such as equipment with magnetic saturation, discharge lamps, arc furnaces, arc welders, transformers, etc.

Flicker

The flicker consists of a visual sensation caused by the intensity fluctuations of the lamps lighting; such fluctuations are originated by a series of rapid variations (identical or different) of the voltage that have modulation frequencies different from 50 Hz, ranging from 0.5 to 40 Hz.

The level of feeling instantaneous flicker is a quadratic function of the amplitude of the light variation and therefore of the fluctuation of voltage. Beyond a certain threshold the flicker becomes annoying and the discomfort grows very rapidly with the amplitude of the fluctuations.

At international level the problem of measuring the flicker in an objective way is considered, the solution is to use an instrument that, connected to a network with voltage fluctuations, indicates the level of visual sensation that the human subject would alert if a reference lamp (230 V, 60 W) has been powered by the network considered. This tool, said *flickermeter*, has been developed by the International Union for Electroheat (UIE) and has been adopted by IEC 61000-4-15 [4]. The measure provided by flickermeter is the *feeling of instant flicker*, obtained with an appropriate simulation of the response to the voltage fluctuation of the chain lamp-eye-brain.

The flickermeter output provides two indices of the severity of the flicker (in p.u. of the threshold of flicker irritability), processing online the instantaneous flicker feeling (in p.u. of threshold flicker perceptibility)[3]. These indices are:

[3] The thresholds of perceptibility and irritability of the flicker are defined as follows:

- *Threshold perceptibility* is the flicker level considered perceptible by only 50 % of the persons tested;
- *Threshold of irritability is* the flicker level considered irritable from a substantial part of the persons tested.

- *Indicator of the severity of flicker in the short term P_{st}* (referring to a time of 10 minutes).
- *Indicator of the severity of flicker in the long term P_{lt} (* referring to a time of 2 hours)

The severity of long term (P_{lt}) is calculated on the basis of a series of 12 consecutive values of P_{st}, corresponding generally to an interval of two hours, with the following expression:

$$P_{lt}=\sqrt[3]{\frac{\sum_{i=1}^{12} Psti^3}{12}} \tag{1.3}$$

The flicker is produced by loads variation and in particular the industrial loads are the most important cause. The flicker may be originated also from the combined effect of a population of loads connected to the same distribution system, even if every single load taken individually doesn't originate flicker. The main HV and MV loads with propensity to cause flicker are the arc furnaces, rolling mills, cycle-converters, welders and motor drives. In regards the LV loads some domestic loads (such as PC, monitors, VT), motor drives and small welders can be considered.

Voltage Unbalance

The voltage unbalance can be individuated considering a diversity of RMS values of the phase voltages and/or normal phase shift of 120 degrees between phases.
Generally the degree of unbalance is defined through the ratio between the component of reverse sequence V_i and the direct sequence V_d:

$$V_u = \frac{V_i}{V_d} \tag{1.4}$$

The voltage unbalance in a transmission or distribution network can also be expressed in the following way:

$$V_u = \sqrt{\frac{1-\sqrt{3-6\cdot\beta}}{1+\sqrt{3-6\cdot\beta}}}$$
$$\beta = \frac{V_{LL12}^4 + V_{LL23}^4 + V_{LL31}^4}{\left(V_{LL12}^2 + V_{LL23}^2 + V_{LL31}^2\right)^2} \tag{1.5}$$

or:

$$V_n = V_{neg} = \frac{1}{3}\cdot\left(\overline{V_{L1}} + \alpha^2\overline{V_{L2}} + \alpha\overline{V_{L3}}\right) \tag{1.6}$$

where:

- V_{LL12} Line voltage between phases 1 and 2, scalar value;
- V_{LL23} Line voltage between phases 1 and 2, scalar value;
- V_{LL31} Line voltage between phases 1 and 2, scalar value;
- V_{L1} Phase voltage between phase 1 and neutral, value complex;
- V_{L2} Phase voltage between phase 2 and neutral, value complex;
- V_{L3} Phase voltage between phase 3 and neutral, value complex;
- $\alpha = \frac{1}{2} + j\frac{\sqrt{3}}{2}$.

The main sources of unbalance are single-phase not balanced loads in LV networks and single-phase loads fed phase to phase in MV and LV networks.
Non-negligible source of voltage unbalance on the transmission HHV and HV grid is constituted by the high speed load rail supplied in AC single phase.

Voltage dips
According to the CEI EN 50160 [1], the voltage dip is defined as a sudden variation of the voltage above a certain threshold, in a node of the electric system; this reduction is followed by a return of voltage to the nominal value after a short time interval.
A voltage dip is a "two-dimensional" electromagnetic disturbance, it's determined by the magnitude of the reduction (or alternatively the residual voltage) and by its duration.
The main cause of voltage dips in a public network is represented by the faults and, in some cases, by transient overload due to starting a large motors or insertion of large loads in relation to the network short circuit power.

Voltage Interruptions
An interruption, according to the CEI EN 50160, occurs when the voltage at the terminals of supply is less than 1% and may be scheduled (in cases of network maintenance) or accidental.
These last are usually originated by transient or permanent faults, mainly linked to external events or actions of third parties and may be classified as *short* (with duration less than 3 minutes and caused by a fault transient) or *long* (with duration longer than 3 minutes and caused by permanent failures).
While the effects of a scheduled outage may be "smoothed" by the users, since they are informed in advance they may arrange appropriate measures, in case of accidental interruptions in the presence of unpredictable and uncertain events is particularly difficult to avoid negative effects.

Overvoltages
Overvoltage between a phase conductor and ground, or between phase conductors starts when the pick value exceeds the value corresponding to the highest voltage admissible for the equipment. For the networks with voltage greater than 1 kV the following classification is considered:

- *temporary overvoltages:* these normally arise from network automation, by failures or by sudden reductions of load. A temporary swell at main frequency generally takes place during a ground fault in the system of public distribution or installations users and disappears when the fault is removed.
- *transient overvoltages:* these are usually caused by lightning (direct or indirect), network automation or fuses interventions.

1.2 Analysis of the impact of harmonic inverter connected to the distribution network

The analysis of the harmonic impact on the network of all the devices connected through electronic power converters will be conducted analyzing analytically the harmonic impact. Three phase converters characterized both by two or three-level will be considered. At the end of the study a possible technique for minimizing the harmonic contributions injected into the network will be presented. The obtained results can be extended to any type of generation or device interfaced to the network with power electronic converters.
It's important to consider the different harmonic impact that the different architectures involve, impact that, in general, depends on the type of technology used (three phase inverter at two-level or multi-level), the modulation strategy (Pulse Width Modulation - PWM modulation, fixed-band, etc.), the switching frequency and any presence in the network of harmonic disturbances.
For this purpose, the activity has taken into consideration architecture with both single inverter (three phase inverter with two or three-level) and with modular configuration, both with PWM modulation, focusing the analysis on harmonic voltages and currents associated with these two architectures.

1.2.1 Two-level three phase Inverter

The basic structure of a three phase two-level inverter is shown in Figure 1-1. In Figure 1-2 the switched line to midpoint and line to line voltages produce by a two-level inverter, obtained by Matlab simulations with Pulse Width Modulation (PWM), are presented.

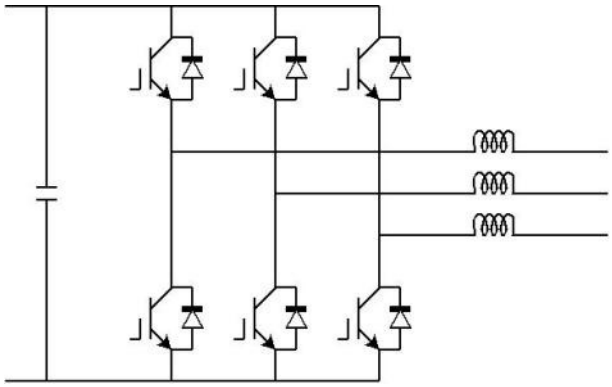

Figure 1-1: Three phase two-level Inverter (Voltage Source Inverter)

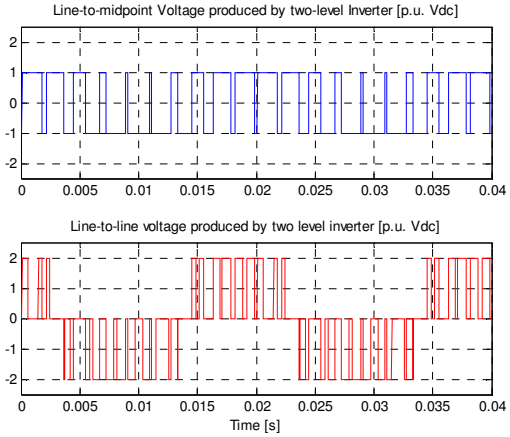

Figure 1-2: Phase voltages and generated line to line by a three phase two-level inverter

In principle, a primary objective of all modulation schemes is to calculate the converter switch-on and switch-off times, which create the desired target output voltage or current. For this purpose, some alternatives are possible [5]:

- *naturally sampled PWM*: switching at the intersection of a target reference waveform and a high frequency carrier;
- *regular sampled PWM*: switching at the intersection of a regularly sampled reference waveform and a high frequency carrier;
- *direct PWM*: switching so that the integrated area of target reference waveform over the carrier interval is the same as the integrated area of the converter switched output.

Many variations of these alternatives have been published; in this study the double-edge naturally sampled modulation strategy has been adopted. The most common form uses a high frequency triangular carrier to compare with a sinusoidal fundamental waveform.
In the assumption to use the PWM strategy with triangular carrier, for a three phase two-level inverter, a balanced set of three phase line to line voltages is obtained if the phase-leg reference are shifted in time by 1/3 of the period (Figure 1-3).

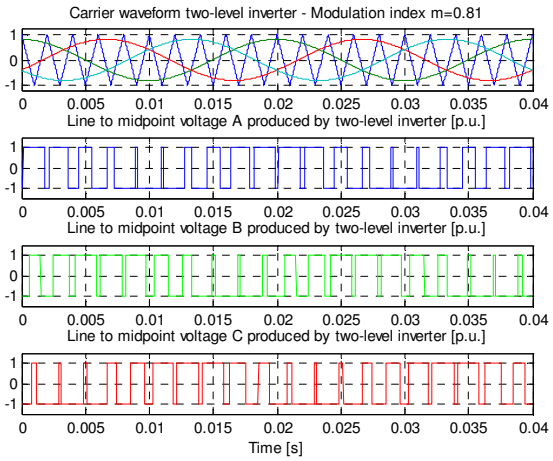

Figure 1-3: Switched line to midpoint and line to line voltages produced by a PWM two-level inverter

The choice of the switching frequency (equal to the frequency of the carrier) is usually conditioned by the characteristics of the valves of the converter, the switching losses and the electromagnetic disturbances caused by variations in voltage *dv/dt.*

Fourier analysis for three phase two-level inverter

The analytical formulation of the general wave of phase voltage generated by a two-level inverter can be written with the following Fourier series transformed:

$$V(t) = \sum_{n=1}^{\infty} \left\{ C_{on} \cos\left[n\left(\omega_0 t + \phi_0\right)\right]\right\} + \sum_{m=1}^{\infty} \sum_{n=-\infty}^{\infty} \left\{ C_{mn} \cos\left[m\left(\omega_c t + \phi_c\right) + n\left(\omega_0 t + \phi_0\right)\right]\right\} \tag{1.7}$$

where ω_0 is the network angular frequency, ω_c is the carrier angular frequency, ϕ_0 and ϕ_c are the offsets of the carrier and modulating waveforms. The summations represent, respectively, the harmonics multiple of the switching frequency and its sidebands harmonics.
To obtain this expression in case of PWM modulation with triangular carrier, it is necessary to proceed as follows [5]

$$V(t) = m_a V_{dc} \sin\left(\omega_0 t + \phi_0\right) \tag{1.8}$$

where m_a is the modulation index, V_{dc} is the direct voltage and ω_0 is the fundamental angular frequency. The transformed in Fourier series can be written in the complex form:

$$V(t) = \sum_{n=-\infty}^{+\infty} C_n e^{jn(\omega_0 t + \phi_0)} \tag{1.9}$$

and the coefficients C_n are :

$$C_n = \frac{1}{T}\int_0^T V(t) e^{-jn\omega_0 t} dt = \frac{1}{2\pi}\int_{-\pi}^{\pi} V(t) e^{-jn\vartheta} d\vartheta \tag{1.10}$$

where $T = \dfrac{2\pi}{\omega_0}$ is the fundamental period and $\vartheta = \omega_0 t$.

Assuming that the width of the pulse is not constant, the phase ϑ can vary between $\pm k'\pi + \phi_c$ and then the (1.10) becomes:

$$C_n = \frac{1}{2\pi}\int_{-k'\pi+\phi_c}^{k'\pi+\phi_c} V(t) e^{-jn\vartheta} d\vartheta = \frac{1}{2\pi}\left[-\frac{1}{jn} e^{-jn\vartheta} \right]_{-k'\pi+\phi_c}^{k'\pi+\phi_c} = \frac{j}{2\pi n} e^{jn\phi_c}\left[e^{jnk'\pi} - e^{-jnk'\pi} \right] \tag{1.11}$$

since $k' = k + m_a V_{dc} \sin\left(\omega_0 t + \phi_0\right)$ and $k = V_{dc}$, the (1.11) becomes:

$$C_n = \frac{j}{2\pi n} e^{jn\phi_c}\left[e^{jnk\pi} e^{jnm_a V_{dc}\pi \sin(\omega_0 t + \phi_0)} - e^{-jnk\pi} e^{-jnm_a V_{dc}\pi \sin(\omega_0 t + \phi_0)} \right] \tag{1.12}$$

and, considering the link with the Bessel function:

$$e^{jx\sin\vartheta} = \sum_{p=-\infty}^{+\infty} J_p(x) e^{jp\vartheta} \tag{1.13}$$

and substituting the (1.13) in (1.12), it's possible to obtain:

$$C_n = \frac{j}{2\pi n} e^{jn\phi_c} \left[e^{jnk\pi} \sum_{p=-\infty}^{+\infty} J_p\left(nm_a V_{dc}\pi\right) e^{jp(\omega_0 t+\phi_0)} - e^{-jnk\pi} \sum_{p=-\infty}^{+\infty} J_{-p}\left(nm_a V_{dc}\pi\right) e^{jp(\omega_0 t+\phi_0)} \right]$$

$$C_n = \frac{j}{2\pi n} e^{jn\phi_c} \left[e^{jnk\pi} \sum_{p=-\infty}^{+\infty} J_p\left(nm_a V_{dc}\pi\right) e^{jp(\omega_0 t+\phi_0)} - e^{-jnk\pi} \sum_{p=-\infty}^{+\infty} (-1)^p J_p\left(nm_a V_{dc}\pi\right) e^{jp(\omega_0 t+\phi_0)} \right] \tag{1.14}$$

$$C_n = \frac{j}{2\pi n} e^{jn\phi_c} \left[\sum_{p=-\infty}^{+\infty} J_p\left(nm_a V_{dc}\pi\right) e^{jp(\omega_0 t+\phi_0)} \left(e^{jnk\pi} - (-1)^p e^{-jnk\pi} \right) \right]$$

In addition, collecting $e^{-jp\frac{\pi}{2}}$, the final expression of the (1.14) can be simplified:

$$C_n = \frac{V_{dc} j}{2\pi n} e^{jn\phi_c} \left[\sum_{p=-\infty}^{+\infty} J_p\left(n\frac{\pi}{2}m_a\right) e^{jp(\omega_0 t+\phi_0)} e^{-jp\frac{\pi}{2}} \left(e^{jnk\pi} e^{jp\frac{\pi}{2}} - e^{-jnk\pi} e^{-jp\frac{\pi}{2}} \right) \right]$$

$$C_n = \frac{V_{dc} j}{2\pi n} e^{jn\phi_c} \left[\sum_{p=-\infty}^{+\infty} J_p\left(n\frac{\pi}{2}m_a\right) e^{jp(\omega_0 t+\phi_0)} e^{-jp\frac{\pi}{2}} \left(e^{jnk\pi} e^{jp\frac{\pi}{2}} - e^{-jnk\pi} e^{-jp\frac{\pi}{2}} \right) \right] \tag{1.15}$$

$$C_n = V_{dc} \sum_{p=-\infty}^{+\infty} J_p\left(n\frac{\pi}{2}m_a\right) \Big/ (2n\pi) e^{jp(\omega_0 t+\phi_0)} e^{-jp\frac{\pi}{2}} e^{jn\phi_c} \left[-\frac{1}{2} j \left(e^{j\left(nk\pi+p\frac{\pi}{2}\right)} - e^{-j\left(nk\pi+p\frac{\pi}{2}\right)} \right) \right]$$

and considering this condition:

$$\left[-\frac{1}{2} j \left(e^{j\left(nk\pi+p\frac{\pi}{2}\right)} - e^{-j\left(nk\pi+p\frac{\pi}{2}\right)} \right) \right] = \sin\left(nk\pi + p\frac{\pi}{2} \right) \tag{1.16}$$

the (1.15) becomes:

$$C_n = V_{dc} \sum_{p=-\infty}^{+\infty} J_p\left(n\frac{\pi}{2}m_a\right) \Big/ (2n\pi) e^{jp(\omega_0 t+\phi_0)} e^{j\left(n\phi_c - p\frac{\pi}{2}\right)} \left[-\sin\left(nk\pi + p\frac{\pi}{2} \right) \right] \tag{1.17}$$

Substituting the coefficients C_n (1.17) in the voltage equation (1.9), the following Fourier series transformed is obtained in case of sinusoidal modulating:

$$V(t) = \sum_{n=-\infty}^{+\infty} C_n e^{jn(\omega_c t+\phi_c)} = 2V_{dc} \sum_{n=+1}^{+\infty} \sum_{p=-\infty}^{+\infty} \frac{J_p\left(n\frac{\pi}{2}m_a\right)}{2n\pi} e^{jp(\omega_0 t+\phi_0)} e^{-jp\frac{\pi}{2}} \left[-\sin\left(nk\pi + p\frac{\pi}{2} \right) \right] e^{jn(\omega_c t+\phi_c)} =$$

$$= 2V_{dc} \sum_{n=+1}^{+\infty} \sum_{p=-\infty}^{+\infty} \left[-\sin\left(nk\pi + p\frac{\pi}{2} \right) \right] \frac{J_p\left(n\frac{\pi}{2}m_a\right)}{2n\pi} e^{j(n\phi_c + p\phi_0 - p\frac{\pi}{2})} e^{j\left(n\omega_c + p\omega_0\right)t} \tag{1.18}$$

$$= 2V_{dc} \sum_{n=+1}^{+\infty} \sum_{p=-\infty}^{+\infty} \left[-\sin\left(nk\pi + p\frac{\pi}{2} \right) \right] \frac{J_p\left(n\frac{\pi}{2}m_a\right)}{2n\pi} e^{-jp\frac{\pi}{2}} e^{jp(\omega_0 t+\phi_0)} e^{jn(\omega_c t+\phi_c)} =$$

If the waveform instead is expressed in cosine, the equation becomes:

$$k' = k + m_a V_{dc} \cos(\omega_0 t + \phi_0) = V_{dc} + m_a V_{dc} \sin\left(\frac{\pi}{2} - \omega_0 t + \phi_0\right) \tag{1.19}$$

and the Fourier series transformed for a single phase is the following:

$$V(t) = 2V_{dc} \sum_{n=+1}^{+\infty} \sum_{p=-\infty}^{+\infty} \left[\sin\left(n\frac{\pi}{2} + p\frac{\pi}{2} \right) \right] \frac{J_p\left(n\frac{\pi}{2} m_a \right)}{2n\pi} e^{j(n\phi_c + p\phi_0)} e^{j(n\omega_c + p\omega_0)t} \tag{1.20}$$

Starting from (1.21), it's possible to underline the main aspects of the analytical solution of the inverter output voltage with PWM modulation as a function of the indices n and p.

$$\begin{aligned} V(t) &= V_{dc} + m_a V_{dc} \cos(\omega_0 t + \phi_0) + \frac{4V_{dc}}{\pi} \sum_{n=+1}^{+\infty} \sin\left(n\frac{\pi}{2} \right) \frac{J_0\left(n\frac{\pi}{2} m_a \right)}{n} \cos\left[n(\omega_c t + \phi_c) \right] + \\ &+ \frac{4V_{dc}}{\pi} \sum_{n=+1}^{+\infty} \sum_{p=-\infty}^{+\infty} \left[\sin\left(n\frac{\pi}{2} + p\frac{\pi}{2} \right) \right] \frac{J_p\left(n\frac{\pi}{2} m_a \right)}{n} \cos\left[n(\omega_c t + \phi_c) + p(\omega_0 t + \phi_0) \right] \end{aligned} \tag{1.21}$$

In case of three phase two-level inverter in presence of balanced three phase voltages displaced by 120°:

$$\begin{aligned} v_a(t) &= V_0 \cos\omega_0 t = m_a V_{dc} \cos\omega_0 t \\ v_b(t) &= V_0 \cos(\omega_0 t - 2\pi/3) = m_a V_{dc} \cos(\omega_0 t - 2\pi/3) \\ v_c(t) &= V_0 \cos(\omega_0 t + 2\pi/3) = m_a V_{dc} \cos(\omega_0 t + 2\pi/3) \end{aligned} \tag{1.22}$$

where V_0 is the peak output voltage, m_a is the modulation index and ω_0 is the fundamental angular frequency, the Fourier series transformed of the phase voltage and line to line voltages become [6]:

$$\begin{aligned} V_{ank}(t) &= V_{dc} + m_a V_{dc} \cos(\omega_0 t - k\frac{2\pi}{3}) + \\ &+ \frac{4V_{dc}}{\pi} \sum_{n=+1}^{+\infty} \sum_{p=-\infty}^{+\infty} \left[\sin\left(n\frac{\pi}{2} + p\frac{\pi}{2} \right) \right] \frac{J_p\left(n\frac{\pi}{2} m_a \right)}{n} \cos\left[n(\omega_c t + \phi_c) + p\left(\omega_0 t - k\frac{2\pi}{3} \right) \right] \end{aligned} \tag{1.23}$$

$$\begin{aligned} V_{abnk}(t) &= V_{dc} + m_a V_{dc} \cos(\omega_0 t + \frac{\pi}{6}) + \\ &+ \frac{4V_{dc}}{\pi} \sum_{n=+1}^{+\infty} \sum_{p=-\infty}^{+\infty} \left[\sin\left(n\frac{\pi}{2} + p\frac{\pi}{2} \right) \right] \frac{J_p\left(n\frac{\pi}{2} m_a \right)}{n} \left(2\sin\left(-p\frac{\pi}{3} \right) \sin\left[n(\omega_c t + \phi_c) + p\left(\omega_0 t - \frac{\pi}{3} \right) \right] \right) \end{aligned} \tag{1.24}$$

In the specific case of a three phase two-level inverter, the voltages (line to midpoint and line to line) harmonics generated by the inverter are depending on the switching frequency and in this case it's possible to use the analytical expression below:

$$V(t) = V_{dc} + m_a V_{dc}\cos(\omega_0 t + \phi_0) + \frac{4V_{dc}}{\pi}\sum_{n=+1}^{+\infty}\sin\left(n\frac{\pi}{2}\right)\frac{J_0\left(n\frac{\pi}{2}m_a\right)}{n}\cos\left[n(\omega_c t + \phi_c)\right] +$$
$$+\frac{4V_{dc}}{\pi}\sum_{n=+1}^{+\infty}\sum_{\substack{p=-\infty \\ p\neq 0}}^{+\infty}\left[\sin\left(n\frac{\pi}{2}+p\frac{\pi}{2}\right)\right]\frac{J_p\left(n\frac{\pi}{2}m_a\right)}{n}\cos\left[n(\omega_c t+\phi_c)+p(\omega_0 t+\phi_0)\right] \quad (1.25)$$

where:

- ω_0 is the angular frequency at the fundamental frequency, ω_c is the angular frequency at the carrier frequency, ϕ_0 [4] and ϕ_c represent the offsets, with respect to an absolute reference, of the modulating and carrier waveforms;
- m_a represents the modulation index;
- the first term (V_{dc}) represents an offset of the waveform generated that in this case, because its symmetry, is not present;
- the second term ($m_a V_{dc}\cos(\omega_0 t + \phi_0)$) corresponds to the fundamental component (f_0) of the voltage generated;
- the first sum represents the harmonics multiple of the switching frequency (f_c), as defined by index n [$\cos(n\omega_c t + n\phi_c)$];
- the double summation identifies the sideband harmonics around each multiple of the switching frequency (n f_c), when $n, p \neq 0$;

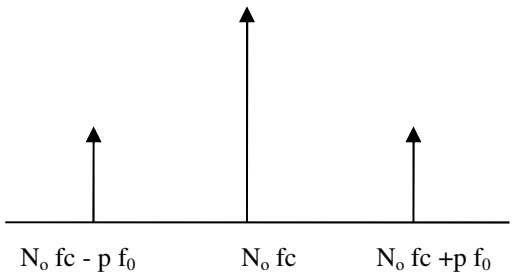

- the functions J_0 and J_p are the Bessel functions of the first type.

The harmonic spectrum of the phase voltage generated has the first "harmonic bell-shaped distribution", after the fundamental component at 50 Hz, at the carrier switching frequency (500 Hz); the subsequent ones are around the multiples of the switching frequency.

In the line to line voltage, considering the equation (1.24), there is a lack in the harmonic spectrum of the following components:

- carrier harmonics, since they are the same for all phase legs;
- third sideband harmonics around each carrier multiple, where n is a multiple of 3;
- sideband harmonics with even combination of $n \pm p$ (since the voltage is an even function and it doesn't produce even harmonics), thanks to the expression $\left[\sin(n+p)\frac{\pi}{2}\right]$ in (2), for odd value of n, harmonics only exist for even value of p and vice versa.

[4] The angle ϕ_c is, for the three phase voltage generated, equal to 0, -2/3π, 2/3.π

According to the last point, if *n=1* in the line to line voltage spectrum all the odd sideband harmonics are eliminated in the first carrier harmonics group, this means that the significant sideband harmonics, with *p* even, in this carrier group will occur at frequency $\omega_c t \pm 2\omega_0 t$, $\omega_c t \pm 4\omega_0 t$ and so on. For the second carrier group (*n=2*), the significant sideband harmonics, with *p* odd, will occur at $2\omega_c t \pm \omega_0 t$, $2\omega_c t \pm 5\omega_0 t$, $2\omega_c t \pm 7\omega_0 t$ and so on.

Figure 1-4 shows the phase voltage and the line to line voltage harmonic components for a three phase two-level inverter operating under naturally sampled PWM, considering f_0=50Hz and f_{sw}=500Hz.

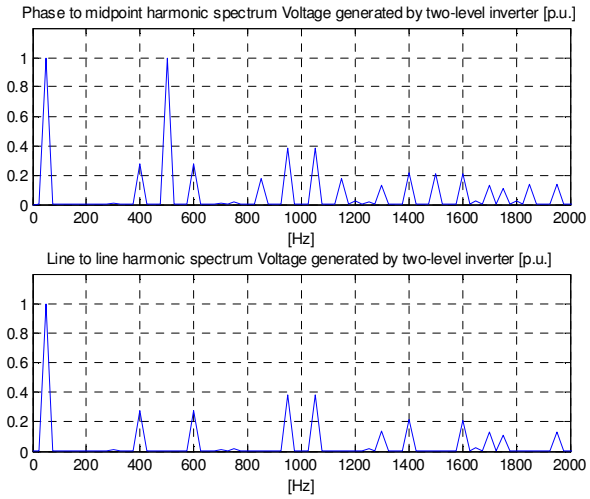

Figure 1-4: Phase and line to line voltages harmonic spectrum for a three phase two-level inverter with PWM modulation

Considering the currents, on the assumption that the inverter is connected to an infinite power network through its switching reactance, the current series Fourier transformed is:

$$I(t) = I\cos(\omega_0 t + \phi_0) + \frac{4I}{\pi}\sum_{n=+1}^{+\infty}\sin\left(n\frac{\pi}{2}\right)\frac{J_0\left(n\frac{\pi}{2}m_a\right)}{n}\cos\left[n\left(\omega_c t + \phi_c\right)\right]$$
$$+\frac{4I}{\pi}\sum_{n=+1}^{+\infty}\sum_{p=-\infty}^{+\infty}\left[\sin\left(n\frac{\pi}{2}+p\frac{\pi}{2}\right)\right]\frac{J_p\left(n\frac{\pi}{2}m_a\right)}{n}\cos\left[n\left(\omega_c t+\phi_c\right)+p\left(\omega_0 t+\phi_0\right)\right] \quad (1.26)$$

From (1.26) it's possible to calculate the harmonic spectrum (in p.u. of the fundamental current), shown in Figure 1-5, that is characterized by the same harmonics present in the phase voltage (Figure 1-4).

Starting from the "base case" of two-level inverter, possible solutions for a reduction of the harmonic impact on the network are analyzed. In particular, in the following the analysis for multilevel inverter structure, for example three-level, and interleaved inverter are presented.

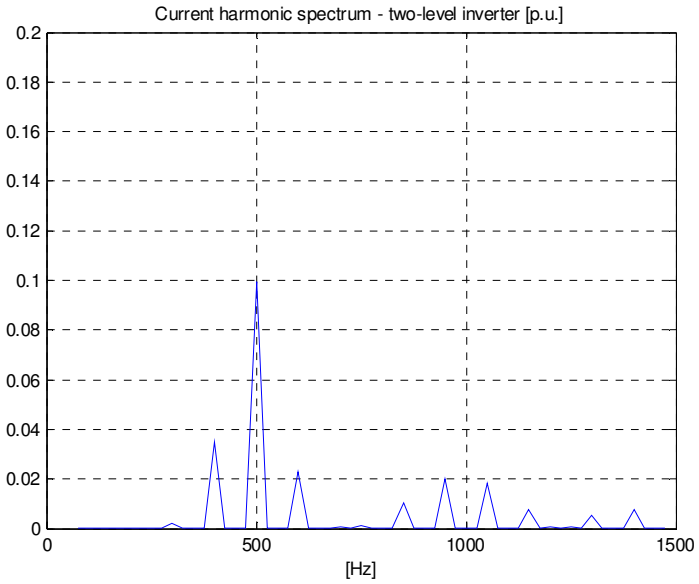

Figure 1-5: Current harmonic spectrum generated by a two-level three phase inverter with PWM modulation (p.u. of fundamental component)

1.2.2 Three-level three phase Inverter

Multilevel Voltage Source Inverter (VSI) are a class of inverters where a DC source with several tabs between the positive and negative terminal is present [6] ÷ [13]. In Figure 1-6 a three-level Neutral Point Clamped (NPC) inverter configuration is shown and in Figure 1-7 the switched line to midpoint and line to line voltages produce by three-level NPC inverter, obtained by Matlab simulations, are presented. The structural feature of a three-level inverter is to have, for each step, a leg constituted by four valves in series and two clamp diodes connected to the central point of the DC capacitors (Figure 1-6).

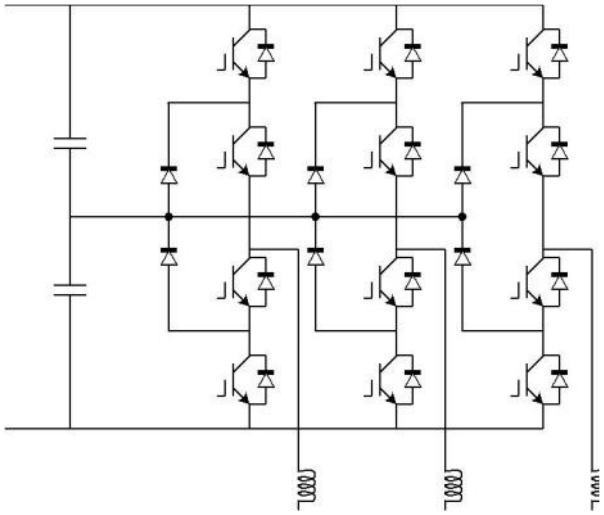

Figure 1-6: Three phase three-level Inverter

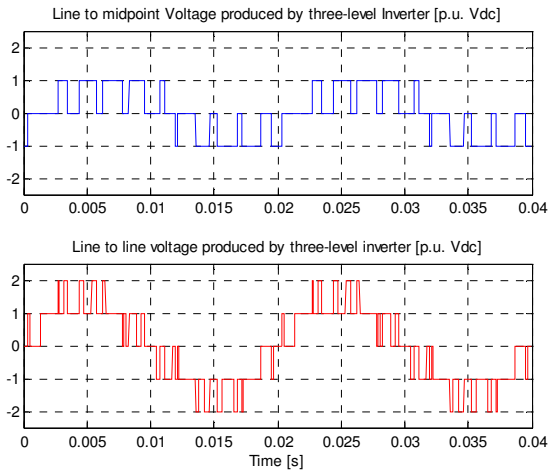

Figure 1-7: Phase voltages and generated line to line by a three phase three-level inverter

The modulation strategies for three phase multilevel inverters are similar to those employed for conventional three phase two-level inverters. In a multilevel inverter the values assumed by the output voltage are defined by the number of the levels of the converter.

An advantage of this structure is that, with the same DC voltage and in condition of "open" (OFF), the voltage applied to each valve is equal to half of that which would occur in case of two-level configuration, with associated benefits for the components design.
The valves are controlled in such a way that only two of the four of each "inverter leg" are ON simultaneously. This means that in case of three-level inverter, the available levels, considering the ON condition of the valves, are (Figure 1-6):

- $+V_{dc}$ - valves S11 and S12;
- the zero level - valves S12 and S13, connecting the phase A to the center point of the capacitors;
- $-V_{dc}$ - valves S13 and S14.

In addition to the capability to withstand higher voltages, the inverter NPC has a less ripple in the output current and reduced amplitude of the output voltage steps, compared to a two-level with the same switching frequency.
At the end comparing a three phase two-level inverter and three-level with the same DC voltage and PWM modulation, it's possible to say that in case of a three-level:

- there is a reduced voltage across the terminals of the individual valve, with a consequent advantage in design and in the choice of the valves;
- phase voltages and line to line are characterized by a greater number of levels and consequently less harmonic content expected, thus favoring the inverter filter output design;
- considering the valves, a single valve in a network period switches the half of the times than in the case of a two-level inverter. In fact, considering the upper valves S11 and S21 in Figure 1-6, it's clear that, in a period, the valve S11 to get the $+V_{dc}$ level switches only 5 times as well as the other, while in case of a two-level the valve switches 10 times (Figure 1-8). This reduction in the number of commutations leads to a reduction in switching losses.

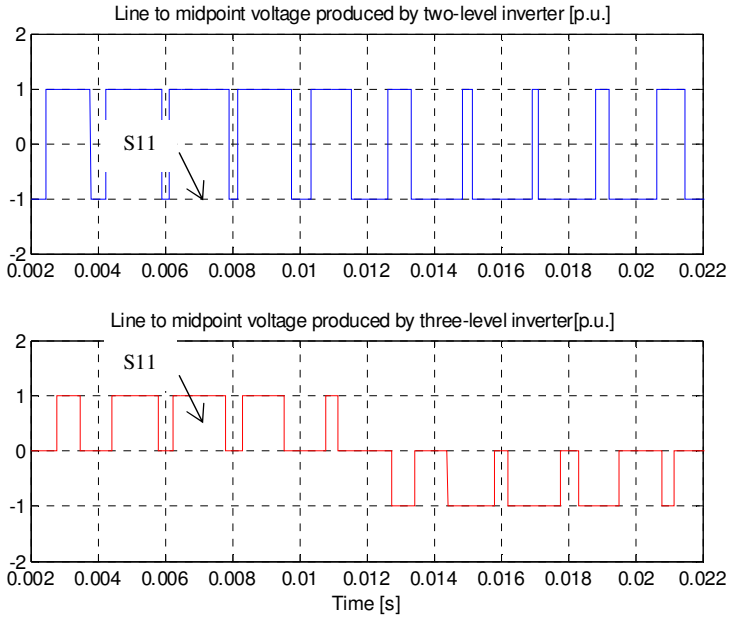

Figure 1-8: Phase voltages from the output of a two-level inverter and three-levels NPC during a fundamental period

Three-level inverter modulation strategies

The double-edge modulation, used for the three phase two-level inverter, can also be implemented, for the three-level, increasing the number of triangular carriers to *L-1*, where *L* is the number of voltage levels of the converter. Three sinusoidal references are then compared with these carriers to determinate the switched voltage. In particular for a three-level inverter:

- *L-1*=2 carriers are arranged;
- the converter is switched to $+V_{dc}$ when the reference is greater than both the carriers;
- the converter is switched to zero when the reference is greater than the lower carrier but less than the upper;
- the converter is switched to $-V_{dc}$ when the reference is less than both the carriers.

In the literature are presented different types of PWM modulation considering different relative phase shift between the carriers [5]:

- Alternative Phase Opposition Disposition (APOD), where the carriers are shifted by 180°;
- Phase Disposition (PD), where all the carriers are in phase.

In Figure 1-9 and Figure 1-10 the carrier and modulation waveforms are shown together with the phase voltages generated by a three phase three-level inverter with different modulation strategy. For example, Figure 1-13 illustrates the carriers and the output voltage of a five-level inverter in case of APOD and PD modulation.

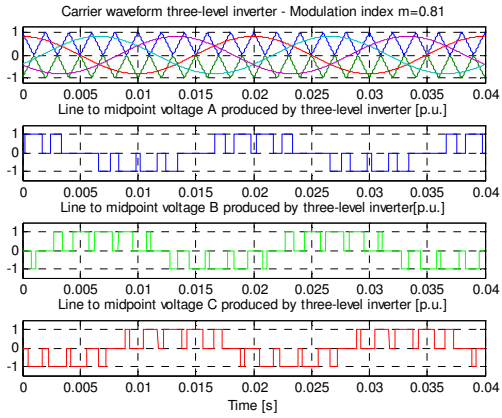

Figure 1-9: Carriers waveform and phase voltages produced by a three-level NPC inverter with naturally sampled APOD modulation

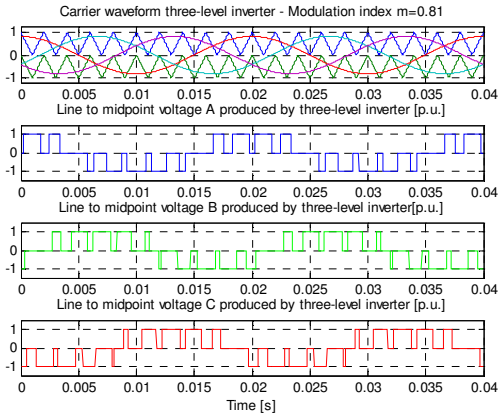

Figure 1-10: Carriers waveform and phase voltages produced by a three-level NPC inverter with naturally sampled PD modulation

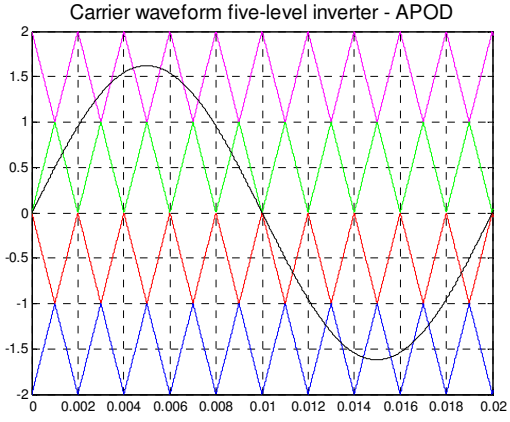

a)

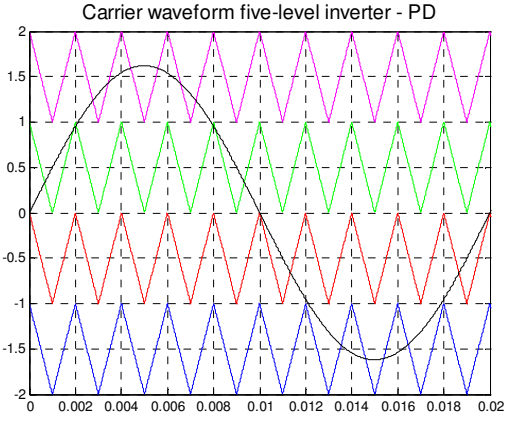

b)

Figure 1-11. Carriers waveform for a five-level NPC inverter configuration with naturally sampled modulation: a) APOD, b) PD

Fourier analysis for three-level three phase inverter

To obtain the analytical expression for the output voltage of a three phase three-level inverter, it is necessary to start from the general expression, which is valid for any converter output waveform:

$$F(t)=\frac{A_0}{2}+\sum_{p=1}^{+\infty}A_{0p}\cos\left(p\left[\omega_0 t+\phi_0\right]\right)+B_{0p}\sin\left(p\left[\omega_0 t+\phi_0\right]\right)+\sum_{n=1}^{+\infty}A_{0n}\cos\left(n\left[\omega_c t+\phi_c\right]\right)+B_{0n}\sin\left(n\left[\omega_c t+\phi_c\right]\right)+$$
$$+\sum_{n=1}^{\infty}\sum_{p=-\infty}^{+\infty}A_{np}\cos\left(n\left[\omega_c t+\phi_c\right]+p\left[\omega_0 t+\phi_0\right]\right)+B_{np}\sin\left(n\left[\omega_c t+\phi_c\right]+p\left[\omega_0 t+\phi_0\right]\right)= \quad (1.27)$$
$$p\neq 0$$
$$=\sum_{n=1}^{+\infty}\sum_{p=-\infty}^{+\infty}C_{np}e^{j[n(\omega_c t+\phi_c)+p(\omega_0 t+\phi_0)]}$$

where the coefficients of the Fourier transformed expressed in the complex notation are:

$$C_{np}=A_{np}+jB_{np}=\frac{1}{2\pi^2}\int_{-\pi}^{\pi}\int_{-\pi}^{\pi}f(x,y)e^{j(nx+py)}dxdy \quad (1.28)$$

with $x=\omega_c t$ and $y=\omega_0 t$.

Considering the solution of the integrals expressed in (1.28), for a three phase three-level inverter with PWM modulation under sinusoidal oscillation PD, the following coefficients C_{np} are obtained [5]:

- for the basic component (n=0 and p= 1):

$$m_a V_{dc} \quad (1.29)$$

- for the multiple harmonics of f_c (n≠0 and p= 0), present only if n is odd [$(1-\cos n\pi)\neq 0$]:

$$\frac{4V_{dc}}{\pi^2}(1-\cos n\pi)\sum_{k=1}^{\infty}\frac{J_{2k-1}(n\pi m_a)}{[2k-1]} \quad (1.30)$$

- for the harmonics in the neighborhood of the multiples of switching frequencies:

$$\frac{V_{dc}}{n\pi}\left\{1-\cos\left(\left[n+p\right]\pi\right)\right\}x\left[J_p\left(n\pi m_a\right)\sin\left(p\frac{\pi}{2}\right)+\frac{4}{\pi}\sum_{k=1}^{\infty}J_{2k-1}\left(n\pi m_a\right)\frac{[2k-1]\cos\left(p\frac{\pi}{2}\right)}{[2k-1+p][2k-1-p]}\right|_{|p|\neq 2k-1}\Bigg] \quad (1.31)$$

This expression is different from zero only for even values of p ($\cos p\frac{\pi}{2}\neq 0$), while the term $J_p\left(n\pi m_a\right)\sin\left(p\frac{\pi}{2}\right)$ is non-null only for odd values of p. As a result:

- ✓ the even harmonics (p even) are present only around the odd multiples (n odd) of the switching frequency.
- ✓ the odd harmonics (p odd) exist only in the neighborhood of even multiple of the switching frequency (n even).

By replacing the coefficients (1.29), (1.30), (1.31) in (1.27), it's possible to obtain the analytical expression of the phase voltage generated by a three phase three-level inverter:

$$v_a(t) = m_a V_{dc}\cos(\omega_0 t + \phi_0) + \frac{8V_{dc}}{\pi^2}\sum_{n=1}^{\infty}\frac{1}{2n-1}\sum_{k=1}^{\infty}\frac{J_{2k-1}([2n-1]\pi m_a)}{[2k-1]}\cos([2n-1]\omega_c t) +$$
$$+\frac{2V_{dc}}{\pi}\sum_{n=1}^{\infty}\frac{1}{2n}\sum_{p=-\infty}^{+\infty}J_{2p+1}(2n\pi m_a)\cos(p\pi)\cos(2n\omega_c t + [2p+1]\omega_0 t) + \quad (1.32)$$
$$+\frac{8V_{dc}}{\pi^2}\sum_{n=1}^{\infty}\frac{1}{2n-1}\sum_{\substack{p=-\infty\\ p\neq 0}}^{+\infty}\sum_{k=1}^{\infty}\frac{J_{2k-1}\left[(2n-1)\pi m_a\right][2k-1]\cos p\pi}{[2k-1+2p][2k-1-2p]}\cos\left[(2n-1)\omega_c t + 2p\omega_0 t\right]$$

In Figure 1-12 and Figure 1-13 the harmonic spectrum the inverter voltages when f_0 = 50Hz and f_c= 500Hz for both modulation strategies Phase Disposition (PD) and Alternative Phase Opposition Disposition (APOD) are shown. In particular, it is possible to verify that:

- in both cases, the amplitude of the harmonics is less than in the case of two-level inverter (Figure 1-4);
- the amplitudes of the harmonics of the phase voltage are lower than in case of modulation PD;
- the presence in the phase voltage, in case of PD modulation, of the 2nd and 4th harmonics (Figure 1-14) (these components are not present in case of a two-level inverter), while with APOD modulation the first relevant harmonic is the 5th (Figure 1-15).

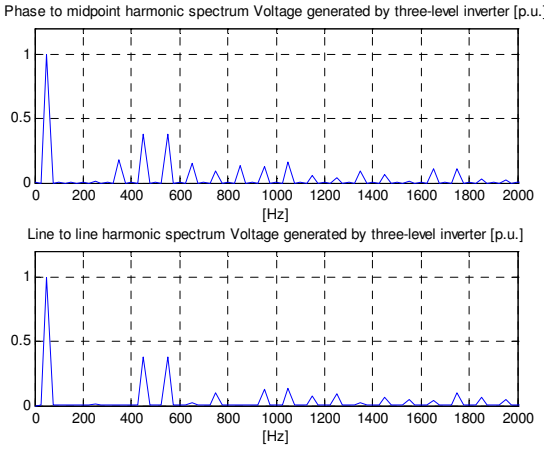

Figure 1-12: Phase and line to line voltages harmonic spectrum with APOD modulation

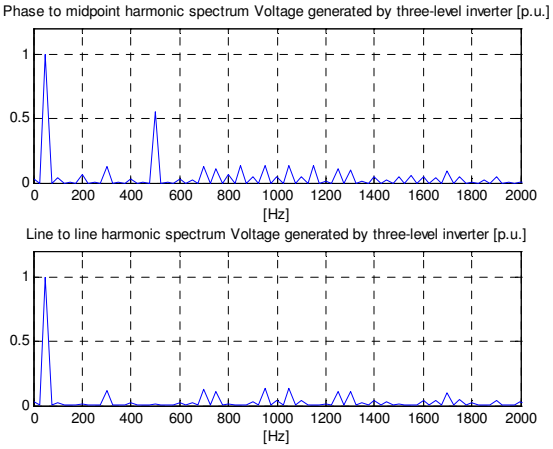

Figure 1-13: Phase and line to line voltages harmonic spectrum with PD modulation

Considering the Figure 1-13 and Figure 1-15, it's possible to verify, in line with the analytical considerations, that in the line to line voltage harmonic spectrum of a three phase three-level inverter with PD modulation:

- for *n* odd (for example n=1, i.e. , at the switching frequency) are present only even harmonics (*p*= ± 2; ± 4);
- for *n* even (for example n=2, i.e. at the double of the switching frequency) the only harmonics in the neighborhood of the multiple of the switching frequency are the odd ones (p = ± 1; ± 3;..).

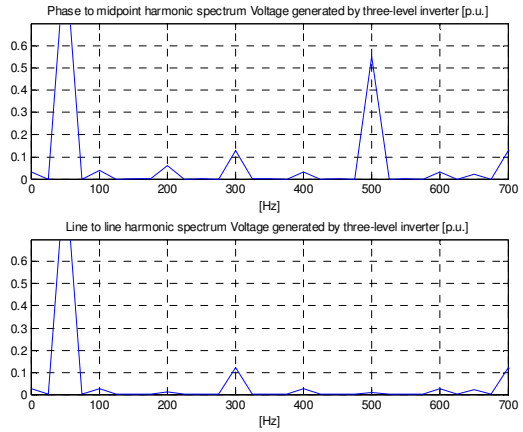

Figure 1-14: Zoom of the harmonic spectrum of voltage at low frequency of a three phase three-level inverter with modulation PD

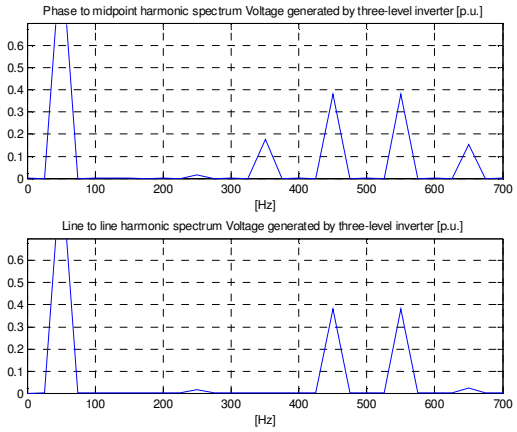

Figure 1-15: Zoom of the harmonic spectrum of voltage at low frequency of a three phase three-level inverter with modulation APOD

The different PWM modulation strategies (APOD and PD) may have different impacts in terms of harmonic contribution to the network even from the point of view of the currents, as highlighted by the spectra of the currents in Figure 1-16 and Figure 1-17 (in p.u. of fundamental component). In particular, it may be underlined that:

- the current harmonics are the same of the phase voltages (the components multiple of f_c in case APOD are not presented);
- in case of PD modulation there are harmonics at low frequency (below the switching frequency) as a consequence of the fact that, being the carriers in phase with each other, the harmonic contributions add up.

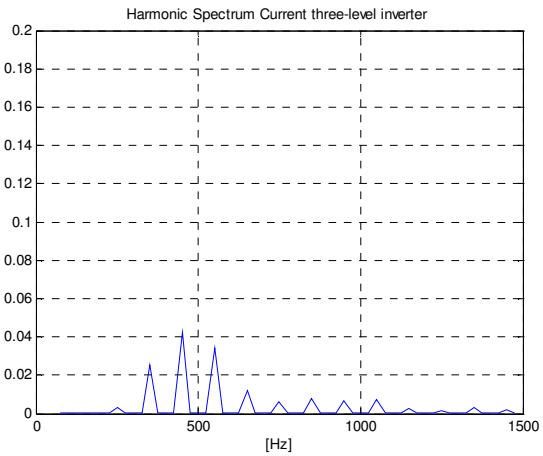

Figure 1-16: Harmonic spectrum of the current generated by a three-level inverter with APOD modulation

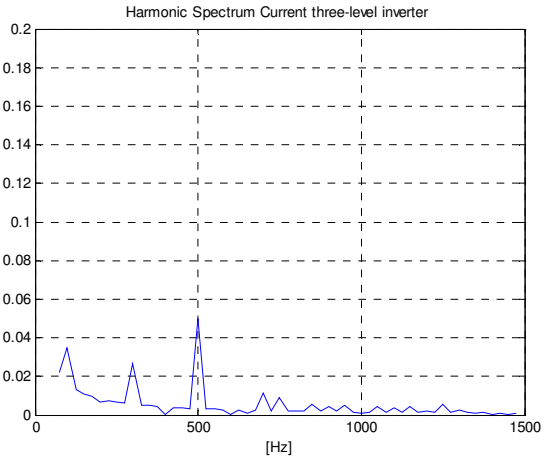

Figure 1-17: Harmonic spectrum of the current generated by a three-level inverter with PD modulation

1.2.3 Three phase interleaved Inverters

In the presence of multiple inverters connected to the Point of Common Coupling (PCC), it becomes relevant to characterize the sum of the harmonic components. The effect of the presence of N inverter connected to the PCC can be represented, in terms of harmonic currents injected into network, from "ratio of harmonics summation" [14][15]:

$$\xi_h^N = \frac{I_h^N}{I_h^1} \frac{P_{n\_INV\_AC}^1}{\sum_{i=1}^{N} P_{n\_INV\_AC}^i} \qquad (1.33)$$

$$0 \le \xi_h^N \le 1$$

where $P_{n\_INV\_AC}^1$ and I_h^1 are referred to the rated power and harmonic currents of a single inverter, while N is the number of inverters connected to the PCC.
For inverters of the same type and of equal power, the expression (1.33) can be simplified by:

$$\xi_h^N = \frac{I_h^N}{NI_h^1} \qquad (1.34)$$

For inverter, whose harmonic currents are in phase, the value of ξ_h^N is equal to the unit (arithmetical sum of harmonic components of various inverters) while the ratio tends to zero (zero-impact on the network) in case of "perfect cancellation" mutual of the harmonics. This condition occurs when the harmonic currents have the same amplitude and the shift angle between the inverter carrier waveforms is:[5]

$$\phi_c = \frac{2\pi}{N} \qquad (1.35)$$

This condition of phase shift can be obtained by generating, in case of PWM modulation under sinusoidal oscillation, carriers shifted among them of the angle ϕ_c [16]. In particular, this modulation strategy is particularly indicated for solutions of photovoltaic installations made with modular architecture where more three phase inverter connected in parallel to the same network node are available [17]÷[19].
Since they interleaved inverters are in parallel connection, the one phase leg line output voltage Fourier series is the same for both inverters (Figure 1-21).

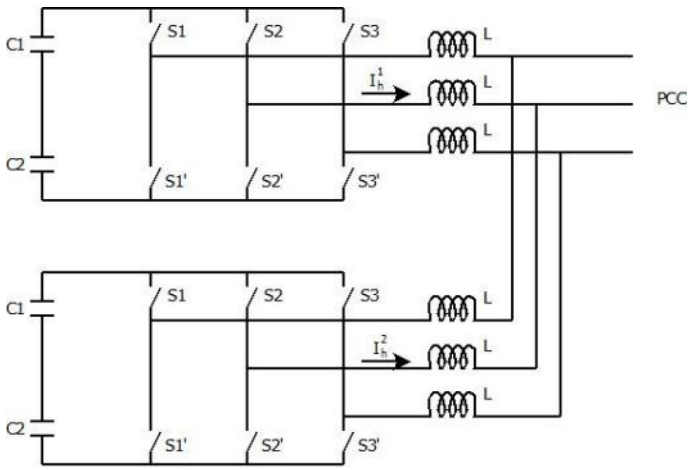

Figure 1-18: Three Phase two-level Voltage Source Inverter in interleaving configuration when N=2

[5] For example, in the case of four inverter (N= 4), the condition of ξ_h^N = 0 would occur for phase shifts of π/2 between the currents supplied by the inverter (0, π/2, π/ 2+π/ 2=π, π+π/ 2 =3/2π).

Here below, to understand the interleaving benefit, two three phase inverters, in two-level configuration, connected in parallel at the PCC have been considered with the carrier waveforms at the same switching frequency (500 Hz) but shifted of 180° and designed so that the total power generated by the two interleaved converters is the same as the single inverter and modulated with PWM modulation providing a 180° phase shift between the carriers (N = 2). The studies are carried out under the assumption of converters connected to a network of infinite power through their switching reactance.

Fourier analysis for three phase two-level interleaved inverter

The modular solution requires that the inverters are connected in parallel to each other and with the network, therefore the analytical expression of the phase voltages generated is the same for both converters and is equal to the equation (1.23) used in § 1.2.1 for the assessment of the harmonic impact on the network of a single two-level inverter.

About the current, in the assumption to have the inverters connected though their output impedance to an infinite power network and to shift the carrier waveform of the second device of 180°, the total current absorbed by the network is the sum of each device, from the equation (1.26), is the following:

$$\begin{aligned} I(t) &= I_1(t) + I_2(t) = (I_1 + I_2)\cos(\omega_0 t + \phi_0) + \\ &+ \frac{4(I_1 + I_2)}{\pi} \sum_{n=+1}^{+\infty} \sin\left(n\frac{\pi}{2}\right) \frac{J_0\left(n\frac{\pi}{2} m_a\right)}{n} \left\{\cos\left[n(\omega_c t + \phi_c)\right] + \cos\left[n(\omega_c t + \phi_c + \pi)\right]\right\} + \\ &+ \frac{4(I_1 + I_2)}{\pi} \sum_{n=+1}^{+\infty} \sum_{\substack{p=-\infty \\ p\neq 0}}^{+\infty} \left[\sin\left(n\frac{\pi}{2} + p\frac{\pi}{2}\right)\right] \frac{J_p\left(n\frac{\pi}{2} m_a\right)}{n} \left\{\cos\left[n(\omega_c t + \phi_c) + p(\omega_0 t + \phi_0)\right] + \cos\left[n(\omega_c t + \phi_c + \pi) + p(\omega_0 t + \phi_0)\right]\right\} \end{aligned} \tag{1.36}$$

where:

- the first term represents the fundamental frequency component;
- the first sum represents the multiple harmonics of the switching frequency. This summation, considering $\cos\alpha + \cos\beta = 2\cos\frac{\alpha+\beta}{2}\cos\frac{\alpha-\beta}{2}$, can be rewritten as follows:

$$+ \frac{4(I_1 + I_2)}{\pi} \sum_{n=+1}^{+\infty} \sin\left(n\frac{\pi}{2}\right) \frac{J_0\left(n\frac{\pi}{2} m_a\right)}{n} \left\{2\cos\frac{(n\omega_c t + n\phi_c + n\omega_c t + n\phi_c + n\pi)}{2} \cos\frac{(n\omega_c t + n\phi_c - n\omega_c t - n\phi_c - n\pi)}{2}\right\} =$$

$$= + \frac{4(I_1 + I_2)}{\pi} \sum_{n=+1}^{+\infty} \sin\left(n\frac{\pi}{2}\right) \frac{J_0\left(n\frac{\pi}{2} m_a\right)}{n} \left\{2\cos\frac{\left[2n(\omega_c t + \phi_c) + n\pi\right]}{2} \cos\left(-n\frac{\pi}{2}\right)\right\}$$

  Which shows the lack of multiple harmonics of the switching frequency in the spectrum of the total current injected (first summation always null), since:
  - ✓ for *n* odd, the term $\cos(-n\pi/2)$ is null;
  - ✓ for *n* even, the term $\sin(-n\pi/2)$ is null.

- The double summation identifies the components around the multiple harmonics of the switching frequency ($n \cdot f_c$) when $n, p \neq 0$. By rewriting the expression it's possible to obtain:

$$+\frac{4(I_1+I_2)}{\pi}\sum_{n=+1}^{+\infty}\sum_{\substack{p=-\infty\\ p\neq 0}}^{+\infty}\left[\sin\left(n\frac{\pi}{2}+p\frac{\pi}{2}\right)\right]\frac{J_p\left(n\frac{\pi}{2}m_a\right)}{n}\left\{\begin{aligned}&\cos\left[\frac{(2p\omega_0+2n\omega_c)t+2p\phi_0+2n\phi_c+n\pi}{2}\right]\left\{\cos\left(-n\frac{\pi}{2}\right)+\sin\left(-n\frac{\pi}{2}\right)\right\}+\\&+\cos\left[\frac{(2p\omega_0-2n\omega_c)t+2p\phi_0-2n\phi_c-n\pi}{2}\right]\left\{\cos\left(-n\frac{\pi}{2}\right)-\sin\left(-n\frac{\pi}{2}\right)\right\}\end{aligned}\right\}$$

where:

- ✓ if *n* and *p* are both odd (or both even) the term $\sin(n+p)\pi/2$ is zero, causing the absence of harmonics in the neighborhood of the multiples of the switching frequency;
- ✓ if *n* is odd and *p* is even and vice versa (i.e. , n ± p is odd), the term $\sin(n+p)\pi/2$ is non-null and therefore in the spectrum the harmonics around multiples of the switching frequency are present (for example, with n=1 and p=2 there will be $f_c \pm 2f_0$).

In Figure 1-19 the spectrum of the current of the individual inverter and the total injected into network (considering f_c=500Hz) are shown, it's possible to highlight:

- the absence of the harmonic bell-shaped distribution at the switching frequency (n= 1);
- the presence of the odd harmonics, in the neighborhood of even multiple of the f_c;
- the presence of the even harmonics, in the neighborhood of the odd multiples of the f_c.

In conclusion, the analytical expression of the output current of two inverters interleaved is the following:

$$I(t)=I_1(t)+I_2(t)=(I_1+I_2)\cos(\omega_0 t+\phi_0)+$$
$$+\frac{4(I_1+I_2)}{\pi}\sum_{n=+1}^{+\infty}\sum_{\substack{p=-\infty\\ p\neq 0}}^{+\infty}\left[\sin\left(n\frac{\pi}{2}+p\frac{\pi}{2}\right)\right]\frac{J_p\left(n\frac{\pi}{2}m_a\right)}{n}\left\{\begin{aligned}&\cos\left[(p\omega_0 t+p\phi_0)+\frac{2n\omega_c t+2n\phi_c+n\pi}{2}\right]\left\{\cos\left(-n\frac{\pi}{2}\right)+\sin\left(-n\frac{\pi}{2}\right)\right\}+\\&-\cos\left[(p\omega_0 t+p\phi_0)-\frac{2n\omega_c t+2n\phi_c+n\pi}{2}\right]\left\{\cos\left(-n\frac{\pi}{2}\right)-\sin\left(-n\frac{\pi}{2}\right)\right\}\end{aligned}\right\} \qquad (1.37)$$

where n = 1, 2, 3, 4, …and p = ±1, ±3, ± 5…

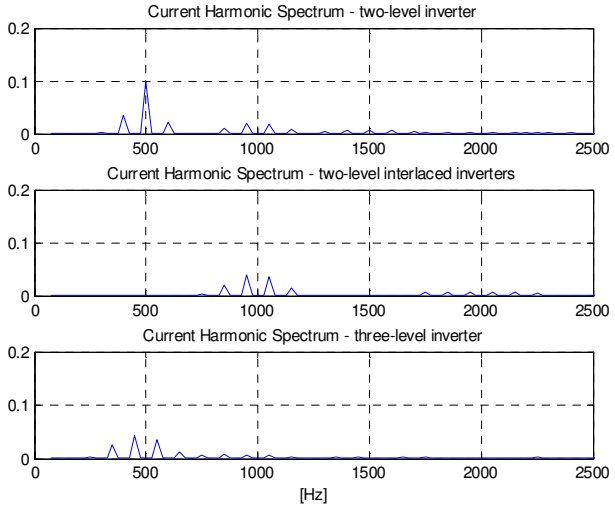

Figure 1-19: Current harmonic Spectrum for each single inverter and interleaving configuration

In Figure 1-20 the current harmonic phases for the two-level interleaved inverter for n=1 (a) and n=2 (b) are shown: since they have the same amplitude, the spectrum of the current injected into the network doesn't have the contribution of these harmonics, while for the second bell (n= 2) the harmonic contributions are added, as shown in the spectrum of Figure 1-19.

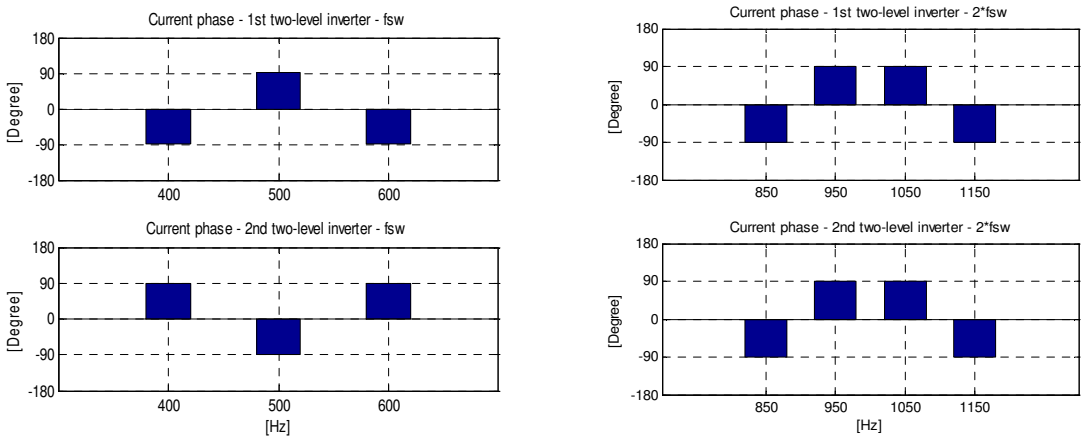

a) b)

Figure 1-20: Current harmonic phases for the two-level interleaved inverter for n=1 (a) and n=2 (b)

1.2.4 Comparison of the different inverter configurations

The assessments are carried out under the assumption of converters connected to a network of infinite power through their switching reactance. In particular, considering different values of the modulation index, the voltage and current behaviors in terms of harmonic spectrum and in terms of Total Harmonic Distortion (THD) are compared. Analysis of "sensitivity" have also been conducted to vary at first the circuit parameters (for example by varying the output reactance of the two inverters interleaved) and the characteristics of modulated and carriers waveforms (for example in the case of error in synchronization during the generation of the two carriers out of phase by 180°).
In regards to the generated voltage, the analysis show that the three-level inverter presents a harmonic contribution lower than the two-level, since the voltage assumes a shape closer to the sinusoidal waveform. Considering the currents injected into the network, the interleaved solution presents an harmonic impact less than in case of a single inverter, both two or three-level one. The detailed comparisons relating to configurations analyzed are shown in the next.

Comparative impact of harmonic voltage

To operate a comparison in terms of harmonic impact of different inverter configurations the THD_V (Total Harmonic Distortion) index is calculated, as stated in §1.1:

$$THD\_V = \frac{\sqrt{\sum_{n=2}^{N} V_n^2}}{V_1}$$

where V_n is the RMS voltage value at the harmonic n, n is the maximum harmonic order considered and V_1 is the RMS value of the voltage at fundamental frequency.

Since the solution interleaved doesn't provide benefit in terms of harmonic voltage impact[6] with respect to the other configurations in examination (two and three-level), it has operated only the comparison in terms of voltage harmonic distortion generated for a single two-level and three-level three phase inverter, both with PWM modulation.
As already mentioned in §1.2.3, also the THD_V comparison confirms the output voltage of a three-level inverter has less harmonic contents than a two-level (Figure 1-22, 1-23).
Only for the three-level inverter, the behavior with the modulations APOD and PD has been analyzed, making sure that for the phase voltage there aren't any differences in THD while the line to line THD_V is lower in case of PD modulation (Figure 1-24), as seen in the § 1.2.3.

[6] This is due to the fact that the two inverters are connected in parallel to the network.

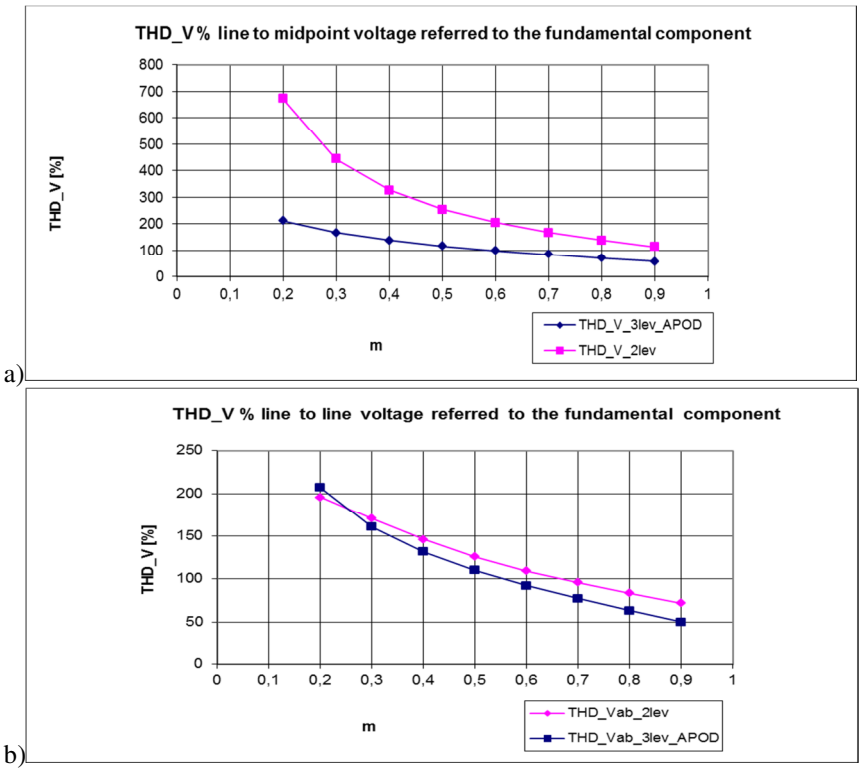

Figure 1-21: THD_V line to midpoint (a) and line to line (b) comparison for a two-level and three-level inverter with APOD modulation

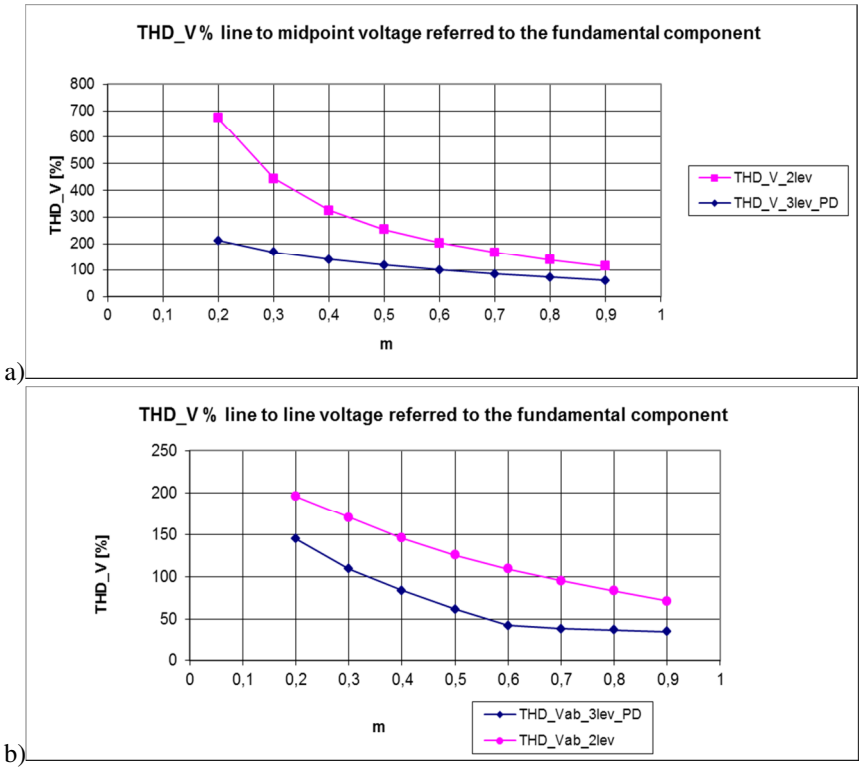

Figure 1-22: THD_V line to midpoint (a) and line to line (b)comparison for a two-level and three-level inverter with PD modulation

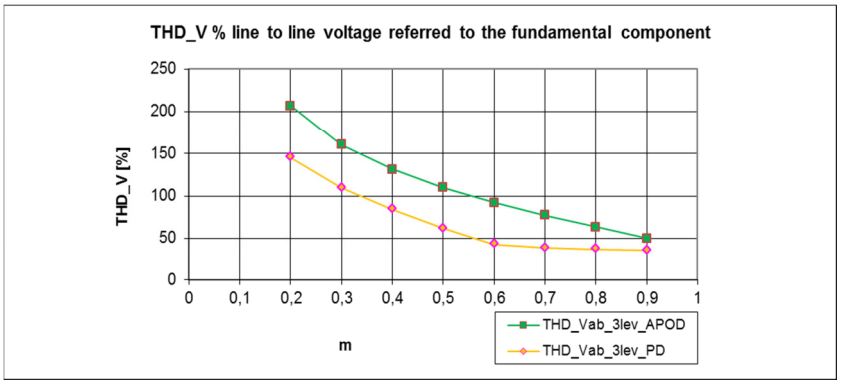

Figure 1-23: THD_V line to line comparison for a three-level levels inverter with modulation APOD and PD

Comparative impact of harmonic current

To make the comparison between the different types of inverter (two, three-level and interleaved converters) it is assumed to have inverters connected to a network of infinite power through the switching reactance. In the interleaved configuration the inverter are designed to have the total power generated by the two converters interleaved the same as the single two or three-level inverter.

Three phase two-level Inverter and interleaved inverter

In Figure 1-24 it's possible to verify that in the spectrum of the overall current generated in the network by the two interleaved inverter there aren't the harmonics multiple of the switching frequency and the related "sidebands", this means a reduced harmonic impact on network with respect to the single inverter.

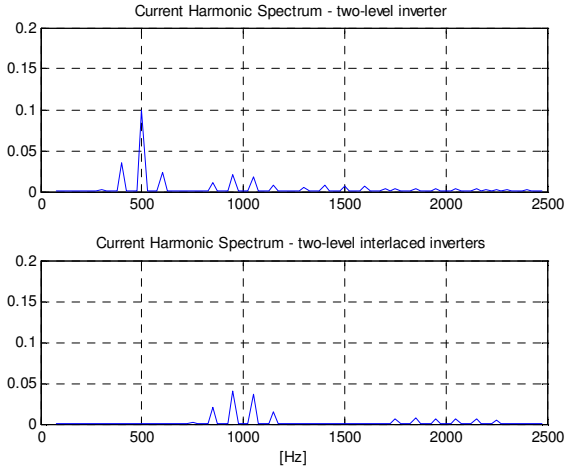

Figure 1-24: Comparison between current harmonic spectrum for two-level and for interleaving inverter configuration

In addition, with reference to the THD_I index, already expressed in (1.2):

$$THD\_I = \frac{\sqrt{\sum_{n=2}^{N} I_n^2}}{I_1}$$

Figure 1-25 represents its trend, considering different modulation index values, and the best performance of the interleaved configuration is confirmed.

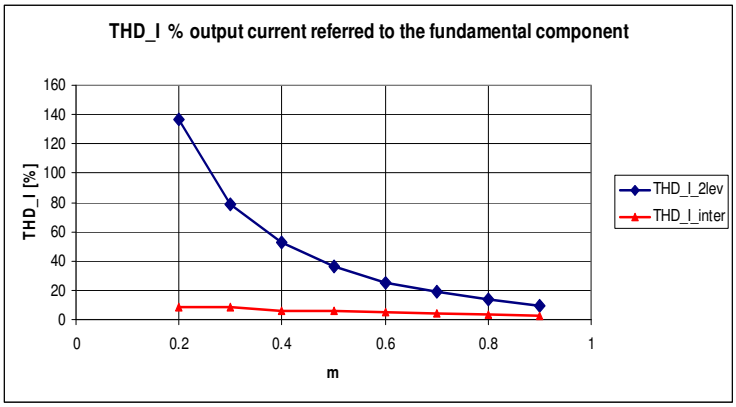

Figure 1-25: THD_I comparison between two-level and interleaved inverter

Comparison between three phase two-level, three-level inverter and interleaved inverters
Operating a comparison between all the three configurations considered, analyzing the current harmonic spectrum[7] there is a lack, for the interleaved inverter, of the bell-shaped distribution centered on the switching frequency and harmonic multiples of the switching frequency. In addition for the three-level configuration with APOD modulation (Figure 1-26) there is an harmonic contribution similar to that of two interleaved inverters even if starting from the bell centered on the switching frequency.

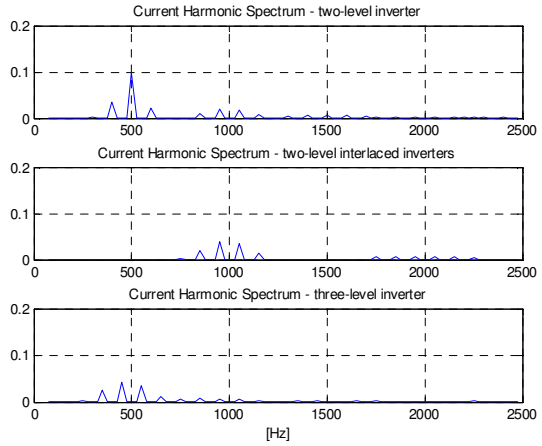

Figure 1-26: Current harmonic spectrum comparison for two-level inverter, three-level inverter with APOD modulation and interleaved inverter

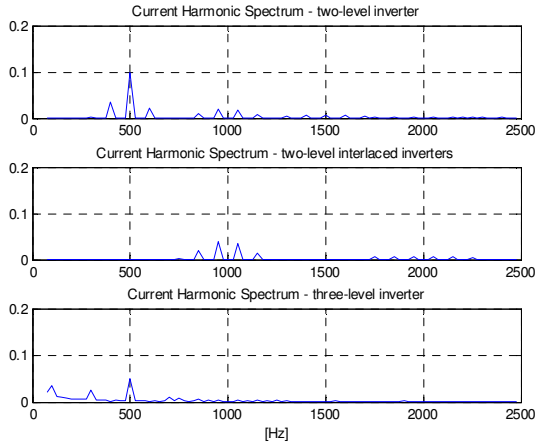

Figure 1-27: Current harmonic spectrum comparison for two-level inverter, three-level inverter with PD modulation and interleaved inverter

Finally, by working the comparison with the THD_I it's verified that the current generated by a three-level inverter (both with modulation APOD and PD) presents an index of total harmonic distortion bigger than the interleaved configuration. In Figure 1-28 the trend of the THD_I for different values of the modulation index is represented, this confirms the lower harmonic impact of the interleaved configuration which is favored in modular multi inverter architectures.

[7] In the case of interleaved inverters this is the overall current injected into the network.

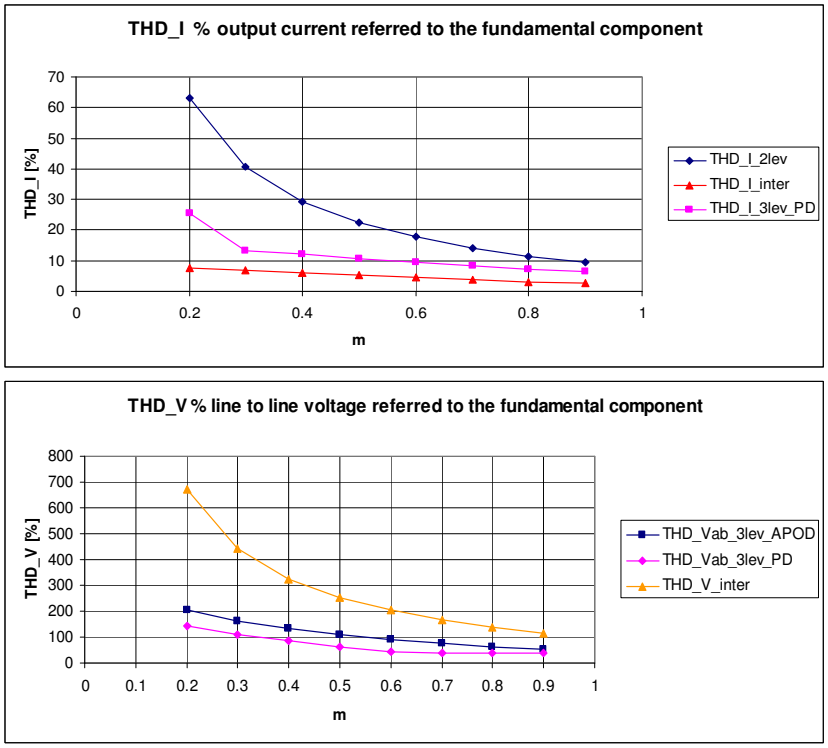

Figure 1-28: THD_I comparison between two-level inverter, three-level inverter with PD and APOD modulation and interleaved inverter

Even if the two-level interleaved inverters are designed with the same power and parameters, it can be useful to analyse what happens, in the current harmonic spectrum, in the hypothesis of "unbalance" between the two interleaved converters, examining the cases with:

- a switching reactance varies in a range of ± 20 %, with respect to the nominal value;
- the angles ϕ_0 and ϕ_c from the equation (1.37), which respectively represent the phase shift of the modulating signal (with respect to the absolute reference) and of the carriers of two inverters interleaved, are variable[8].

Switching reactance variation

In Figure 1-29 the THD_I referred to the fundamental current are shown when the reactance of an inverter varies between ± 20% of the designed value. For the same modulation index, in the range of variation positive or negative, there is an increase in the harmonic distortion injected into the network, even if the variation of the THD_I compared to the ideal case "balanced" is less than 2% (Figure 1-30). From the comparison with the Figure 1-25 it's possible to confirm better performance of the interleaved inverter solution, even in the presence of unbalance between the switching reactance.

[8] These conditions may occur, for example, in the case of synchronization errors in the generation of the waves.

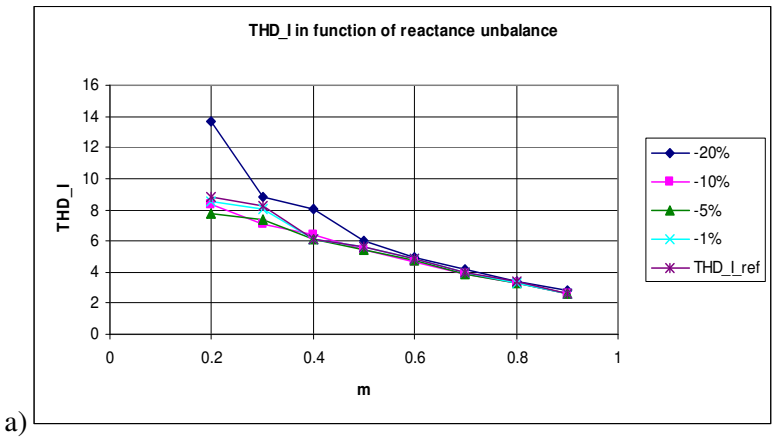

a)

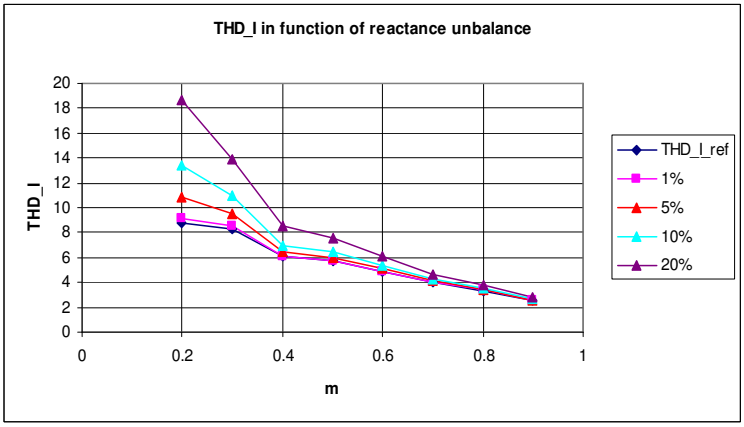

b)

Figure 1-29: THD_I deviation from the nominal case, when the reactance of the second interleaved inverter is less (a) or bigger (b)than the first one

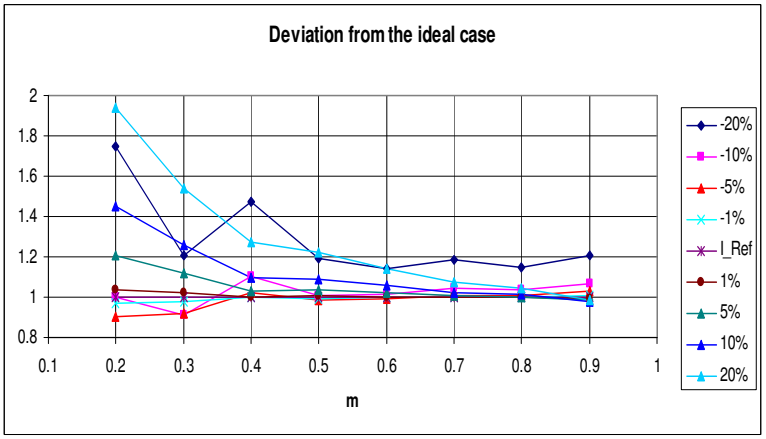

Figure 1-30: THD_I deviation from the ideal case

ϕ_0 and ϕ_c angles variation

At the end, the voltage and current Total Harmonic Distortion are also influenced by the phase shifts ϕ_0 and ϕ_c. The angle ϕ_0 is the shift of the reference current from the zero cross and ϕ_c is an added shift between the carriers waveform of the interleaved inverters evaluated in case of a synchronization error during the generation of these signals.

For instance, the THD_I variation, for all the possible values assumed by these shifts, is less than 10% for a range of modulation index between 0.6 and 0.8 (Figure 1-31 and 1-32) [9].
Regarding the spectrum of the total current injected into the network, it has been reported an influence of the angle ϕ_C: assuming, for example, $\phi_C = 30°$ and a modulation index m=0.7, the harmonic spectrum presents the "first bell", corresponding to the switching frequency, that is not present in the ideal case, due to the not perfect compensation in phase opposition of the harmonics of the two inverters. In Figure 1-31b the spectrum of the current in the event of $\phi_0 = 90°$ is shown: only the sidebands harmonic components appear in correspondence of the switching frequency, since the cancellation of the f_c is ensured by 180° phase shift between the carriers of two inverters.

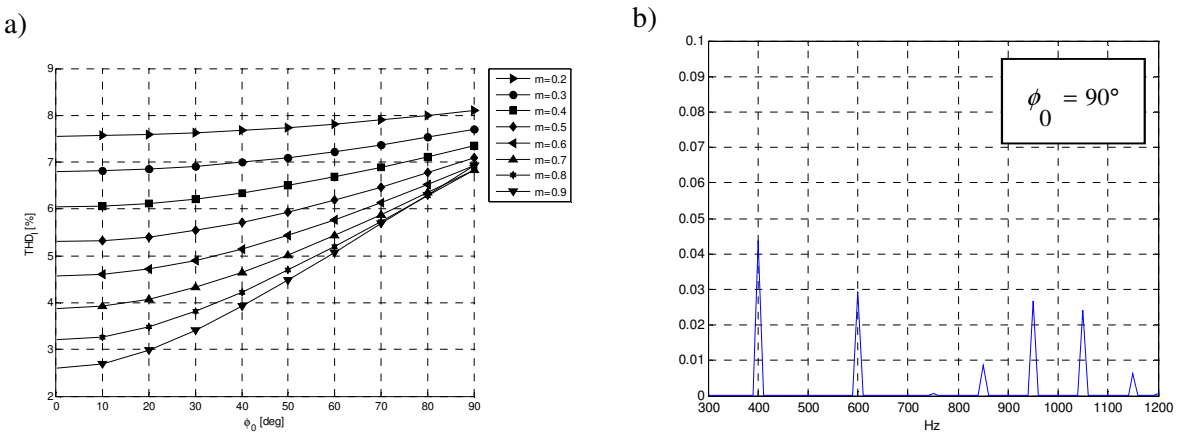

Figure 1-31: THD_I (a) and current harmonic spectrum (b) in case of a ϕ_0 shift of one interleaved inverter

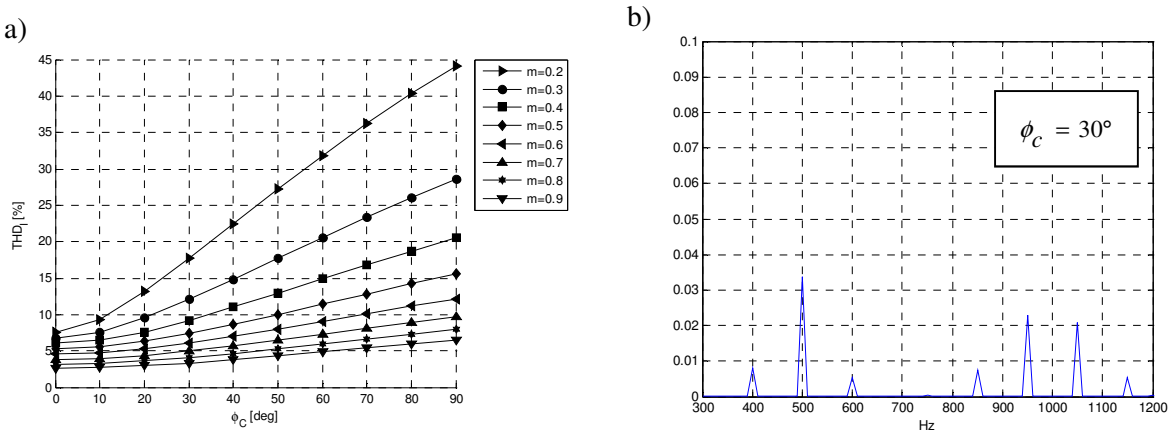

Figure 1-32: THD_I (a) and current harmonic spectrum (b) in case of a ϕ_c shift between the carries waveform of the interleaved inverter

As presented in the previous results, considering the configuration of two three phase two-level interleaved inverters, the positive effects to reduce the current harmonic distortion injected into the network are confirmed in any case.

[9] These considerations are valid in the hypothesis that the angle ϕ_0 is different, from the ideal case, only for one of two inverters interlaced modulating waveform (if the phase shift is identical for both converters, variations in THD_I aren't present).

1.3 Interaction between inverter and network in the presence of variable generation: the flicker

In general, the phenomenon of the flicker is the result of voltage fluctuation typically caused by the effect on the network of time variable powers associated with a particular loads (§1.1) or generation with primary source variable (e.g. photovoltaic or wind). The phenomenon intensity is connected to the network characteristics of the connection point of the generator: weak networks, characterized by a reduced short circuit power, can make this phenomenon more evident, especially in the presence of loads or generators of significant power.
Both photovoltaic generators and wind farms are characterized by variations in the power exchanged with the network due to the variability respectively of the sun and wind. In general, with the same network characteristics, the phenomenon may be more critical for wind power plants since those have, typically, higher power installed and the generators can be directly connected to the network (for example old designed plants with asynchronous generator and DFIG - Double Fed Induction Generator plants). Typically for wind power plants the flicker can manifest itself in two different operation conditions: continuous and "switching".
In the first case, the flicker is caused by the power fluctuations due to: the wind variability, the tower effect[10] and the mechanical characteristics of the turbine. While in case of "switching" operation, the disturbance is manifested as a result of start and stop of wind turbines. In particular the voltage variations caused by wind generator starting can be divided into two fundamental contributions:

- a first contribution due to the reactive power absorption to magnetize the generator, in case of a voltage drop in the network;
- a second contribution related to the input into the network of power, with a consequent increase in the voltage.

In presence of systems that allow the turbine speed control and/or equipment connected to the network through electronic power converters, it's possible to implement control strategies of the mechanical[11] and electronic parts that allow a minimization of the variations in power delivered. In the next session the case of wind generation with Permanent Magnets Synchronous Generator (PMSG) interfaced to the network with power electronics in a back-to-back configuration to verify its effectiveness in terms of disturbance containment and the possible effect on the system behavior in particular on DC section has been analyzed[12][20] ÷ [34].

1.3.1 Flicker impact of the wind generators interfaced to the network with power electronic devices

Initially, the correlation between the level of flicker (§ 1.1) and the following parameters, varying the generator power factor, has been analyzed by digital simulations:

- the characteristics of the generation from primary source (§ 1.3.4 and 1.3.5); in particular, considering the power oscillations amplitude, two possible converters control methods have been analyzed to minimize these oscillations;
- the network short circuit power at the generator connection point and the impedance line parameter X/R (§ 1.3.6 and 1.3.7);
- the electronic power circuits characteristics (§ 1.3.8).

[10] The so-called *tower shadow* is the result of the cyclical passage of each of the blades in front of the tower to support the turbine: the consequent alteration of the wind speed that affects the blade determines power derating and also voltage reduction at a frequency related to the blades number and to the frequency of "crossing" in front of the tower (resulting from the turbine rotation speed).
[11] Control of the angle of blades attack.
[12] The considerations presented for the wind generator and in particular those relating to the effect of the power electronics device can also be transferred to the case of photovoltaic generator interfaced with static converters. The presence of electronic converters in wind power plants, of course, leads to problems in terms of harmonic injected into the network, as seen before.

It should be noted that this study has been carried out using a model of wind PMSG, but the method of survey used and part of the obtained results can be extended to every type of distributed generation characterized by variability in power fed into the grid.
For this study, models of *full converter* wind generators, implemented during the course of the doctoral dissertation and explained in detail in the Chapter 2, have been used. These models allow to implement a power variability available from primary source and they are connected to a simplified Medium Voltage distribution network model. In addition, a flickermeter digital model has been developed for the "off-line" analysis of the data obtained by the digital simulation for the assessment of the severity of the flicker in different conditions of delivery. Then, two different control strategies for the electronic power converters have been considered.

In the study, it is assumed that the variations of power available from primary source are caused by variations "saw tooth" of the wind speed around a constant mean value.

1.3.2 Flicker evaluation

The simulations conducted in environment ATPDraw have been used to assess the correlation between the flicker level, considering different values of the generator power factor cos(φ), and the following parameters:

- amplitude of the power oscillations [24];
- frequency of the power oscillations;
- Short Circuit Power of the network (P_{cc}) at the connection point of the wind generator [24];
- line X/R characteristics [24];
- DC-link capacitance.

1.3.3 Flickermeter Model

For the evaluation of the flicker level produced by wind generator, a digital model of measuring instrument said flickermeter has been developed as reported in IEC 61000-4-15 [32].
The measuring instrument is composed of five stages of signal conditioning of mains voltage, as shown in Figure 1-33. These stages have the aim to reproduce the variations in the brightness of an incandescent lamp due to the fluctuations of the mains voltage, as well as typically perceived by the human eye. A quantitative assessment of the flicker level is carried out by statistical processing of the data obtained by the measuring instrument.

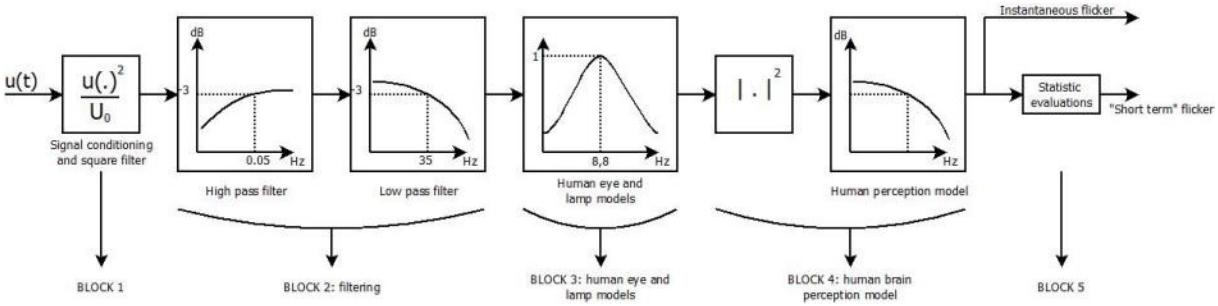

Figure 1-33: Model of flickermeter according to IEC 61000-4-15

The following is a detailed description of the individual blocks which constitute the instrument.

BLOCK 1
In block 1 the voltage signal is squared and then normalized dividing it by its nominal value.

BLOCK 2

In this block a filtering is operated to eliminate the frequency components that are not of interest for the calculation of the flicker. The block is composed of two filters: a first order high-pass filter with cut-off frequency[13] of 0.05 Hz connected in cascade with a Butterworth low pass sixth-order filter with cut-off frequency of 35 Hz. Bode plots of amplitude and phase of the two filters are shown in Figure 1-34.

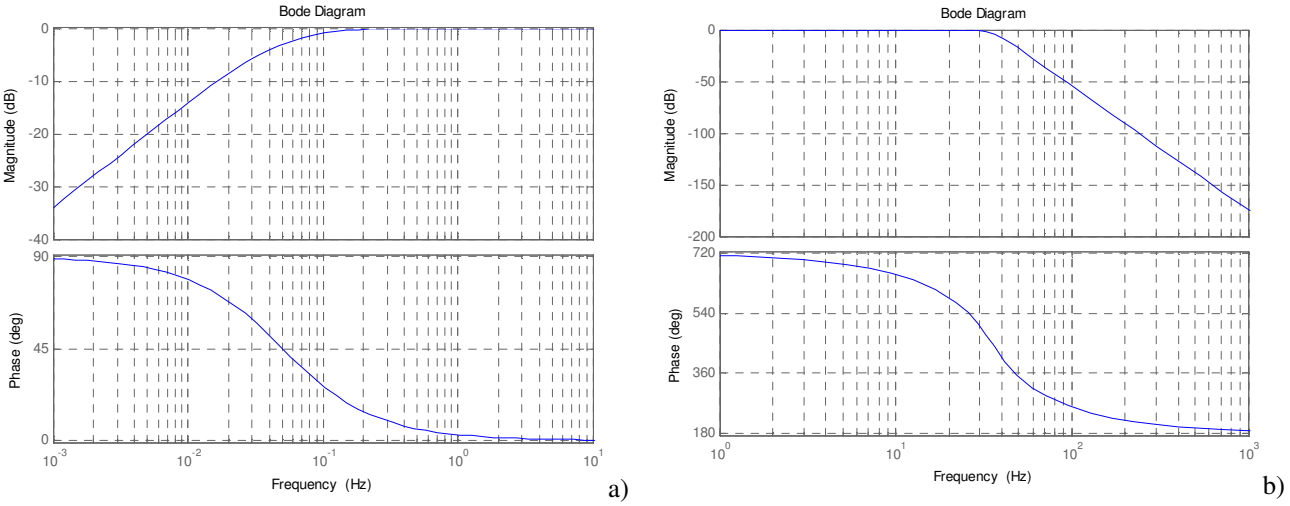

Figure 1-34: Bode diagrams of amplitude and phase of high-pass (a) and low-pass (b) filters that implement the block 2 of the model flickermeter

BLOCK 3

Block 3 consists of a filter weighed that represents the response to voltage variations of an incandescent lamp, powered with a given voltage with fixed frequency and the human eye sensitivity to the frequency of the variations in the lamp brightness. The filter transfer function[14] is the following:

$$H_3(s) = \frac{k\omega_1 s}{s^2 + 2\lambda s + \omega_1^2} * \frac{1 + \frac{s}{\omega_2}}{\left(1 + \frac{s}{\omega_3}\right)\left(1 + \frac{s}{\omega_4}\right)} \tag{1.38}$$

where, for a 60W lamp supplied with a voltage of 230 V_{rms} at 50 Hz[15], it has:

K	λ [rad/s]	ω_1[rad/s]	ω_2[rad/s]	ω_3[rad/s]	ω_4[rad/s]
1.74802	2π4.05981	2π9.15494	2π2.27979	2π1.22535	2π21.9

The Bode diagram of amplitude and phase of the resulting transfer function is shown in Figure 1-35.

[13] The cut-off frequency of a high-pass filter (or low-pass) with a transfer function H(s) is the value of frequency f_c for which occurs that $\left|H(j2\pi f_c)\right|_{dB} = 20\log_{10}\left|H(j2\pi f_c)\right| = -3dB$.

[14] Where "∗" represents the product of convolution defined as: $(f * g)(x) := \int_{-\infty}^{+\infty} f(y)g(x-y)dy$.

[15] For lamps supplied with voltage 120 V_{rms} at frequency 60 Hz, the shape of the filter is the same, but the numerical value of the coefficients are different.

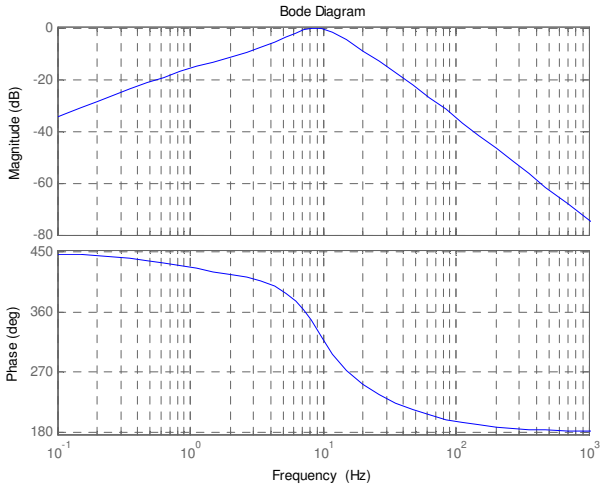

Figure 1-35: Bode diagrams of amplitude and phase of the transfer function of the filter weighed in block 3 of the flickermeter

BLOCK 4

This block represents the model of the effect of the delay of perception introduced by the human brain, this is obtained by the squarer of the output signal of block 3 and a first order low-pass filter with time constant of 300 ms. The output signal of this block is the level of instantaneous voltage flicker that is used for statistical evaluations carried out from the next block.

BLOCK 5

The block 5 is used to calculate an index of the severity of the flicker in the short term, i.e. evaluated over 10 minutes, commonly referred as P_{st} (value *short term*) and defined as:

$$P_{st} = \sqrt{0{,}0314P_{0,1} + 0{,}0525P_{1S} + 0{,}0657P_{3S} + 0{,}28P_{10S} + 0{,}08P_{50S}} \tag{1.39}$$

where:

- P_x denotes the x-th percentile of instantaneous flicker (for example the term $P_{0.1}$);
- the other terms, indicated by the subscript $_S$, constitute a weighted average of the percentiles in agreement with the following expressions:

$$P_{1S} = (P_{0,7} + P_1 + P_{1,3})/3$$
$$P_{3S} = (P_{2,2} + P_3 + P_4)/3$$
$$P_{10S} = (P_6 + P_8 + P_{10} + P_{13} + P_{17})/5$$
$$P_{50S} = (P_{30} + P_{50} + P_{80})/3$$

According to IEC 61000-4-15 [32] it's also possible to calculate an index of severity flicker over 120 minutes, averaging suitably indexes P_{st} calculated in 12 intervals of 10 minutes.

The model of flickermeter described above has been implemented in Matlab environment. The tool allows to acquire in a input voltage signal, coming from a circuit simulation or from an acquisition of real data, and gives as output the instantaneous values of flicker and the index P_{st}. Therefore, for the evaluations carried out in this Chapter, it has been first done the circuit simulations of the different cases in examination and subsequently an offline analysis of the voltages provided by digital simulator has been carries out.
Due to simulation time constrains, only the short term flicker coefficient P_{st} has been evaluated and it's calculated for 1 s. Even though the short term flicker coefficient here calculated is not in accordance to the Standard, it is useful to assess the influence of some grid and generator parameters on flicker severity.

1.3.4 Flicker dependence on the power oscillations amplitude

As anticipated, the type of control adopted for power converters back-to-back to interface the wind generator to the network allows to inject all the active power made available from primary source. Using this approach, therefore, the oscillations of wind turbine power, linked to the variability of the wind speed and repetitive effects such as the *tower shadow,* can cause power fluctuations fed into the grid by the inverter and consequently network voltage variations.

In the analysis, periodical power variations available from primary source have been assumed, for example due to gusts of wind fairly regular, with a given frequency (10 Hz). The short circuit power (P_{cc}) of the MV distribution network at the wind generator connection point is 400 MVA, i.e. 160 times the rated power of the generation plant and the line to which the generator is connected has a total impedance of 1.015 Ω (1.015 p.u.) with a ratio X/R equal to 7 [24]. In this simulation and in all the other cases, the device is designed to inject all the available power from the primary source, up to its design limit (2.5 MVA).

The values of the parameter P_{st}, evaluated over 1 s, as a function of the amplitude of the variations of power, obtained by the model of flickermeter developed in Matlab from the values of simulated voltage, are reported in Figure 1-36. From the calculated values it's possible to establish that the index trend has, with good approximation, a parabolic dependence on the amplitude of the oscillations of power.

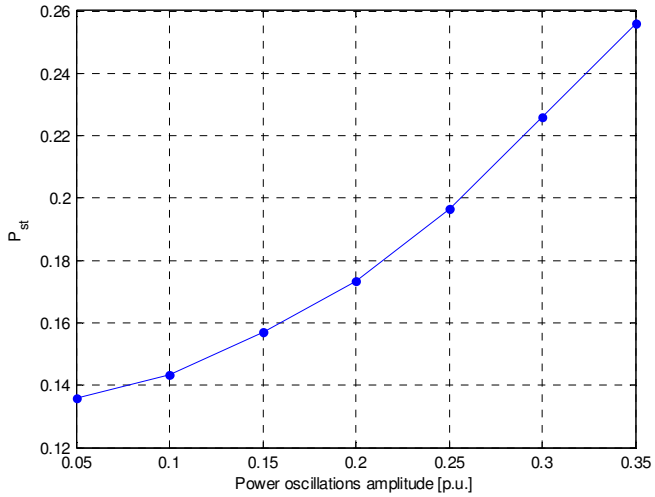

Figure 1-36: Flicker severity dependence on the amplitude of the oscillations of power (1 p.u. = 2.5 MVA)

In order to reduce the severity of the flicker generated by the wind power plant it's possible to adopt controls that make the reference magnitudes for the rectifier control and/or the inverter less sensitive from power oscillations of the primary source. To assess the validity of these controls to reduce the flicker it has been assumed to modify the AC/DC converter control to calculate the current references of axis d-q from the error between the actual power extracted from the primary source and a reference value. It should be noted that this type of control is less efficient than the field oriented control, in terms of Maximum Power Point Tracking (MPPT). In fact, adopting the control in power, the value of the reference of active power must be modified with a logic of the type "perturb and observe (P&O)", or with other logics of MPPT that vary in discrete steps the reference value independent on the maximum power can be extracted as a function of the speed of the wind. The Figure 1-37:a returns the comparison, in the same conditions of the primary source, between the index P_{st} obtained with the two control types and the Figure 1-37:b shows the percentage variation of the index assessed with the method of power control with respect to the method of field oriented control, with the same amplitude of the power oscillations.

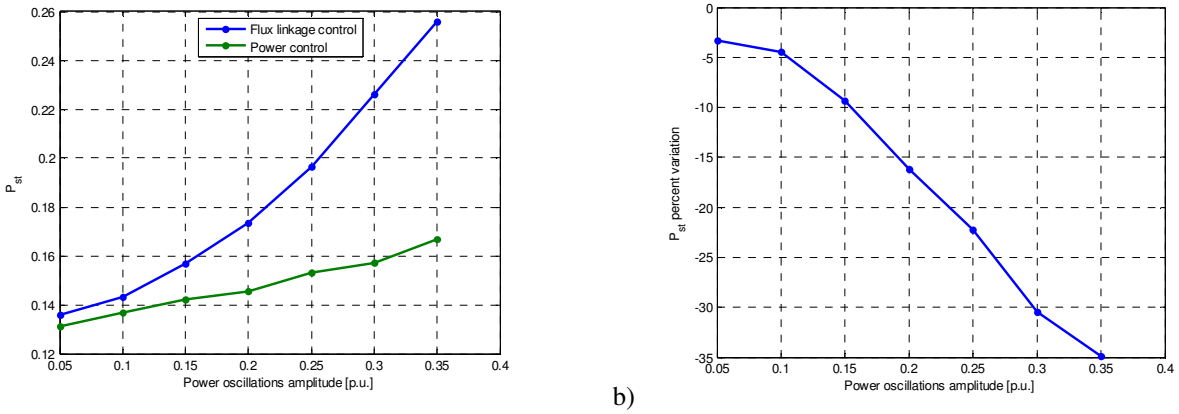

a) b)

Figure 1-37: Flicker severity dependence on power variation of the primary source with different AC/DC converter control methods: (a) comparison of the calculated values, b) percentage variation obtained with the method of power control with respect to the method of field oriented control (1 p.u. = 2.5 MVA)

1.3.5 Flicker dependence on the frequency of the power oscillations

In the same conditions of network used for the analysis above, it has been simulated the impact, in terms of flicker, of a wind generator considering the frequency of the variations in power of the primary source. The AC/DC power converter control, presented in Chapter 2, is designed in order to always inject the maximum power available from primary source. This type of control proved to be more problematic from the point of view of the severity of the flicker generated in network (Figure 1-37:). In this case it's assumed: an amplitude of the variations of constant power equal to 400 kW (0.16 p.u.) and the frequency varies between 0 Hz and 20 Hz in discrete steps. The values of P_{st} calculated by the model of flickermeter are shown in Figure 1-38.

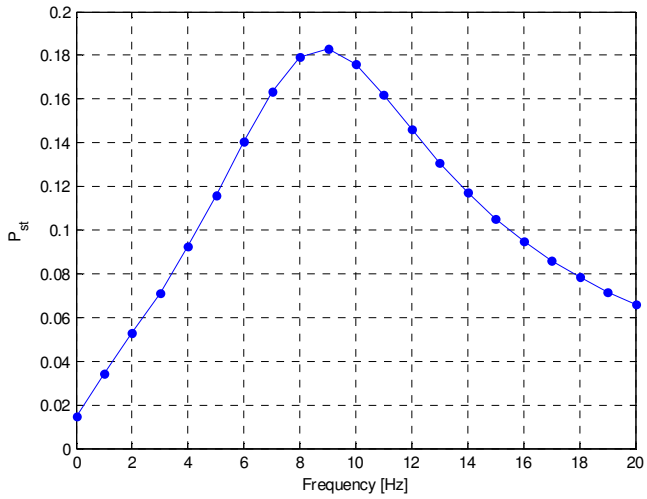

Figure 1-38: Flicker severity dependence on the frequency of the power variations

Figure 1-39 shows the trend of P_{st} index as a function of both amplitude and frequency of the power oscillations, during the network conditions indicated above.

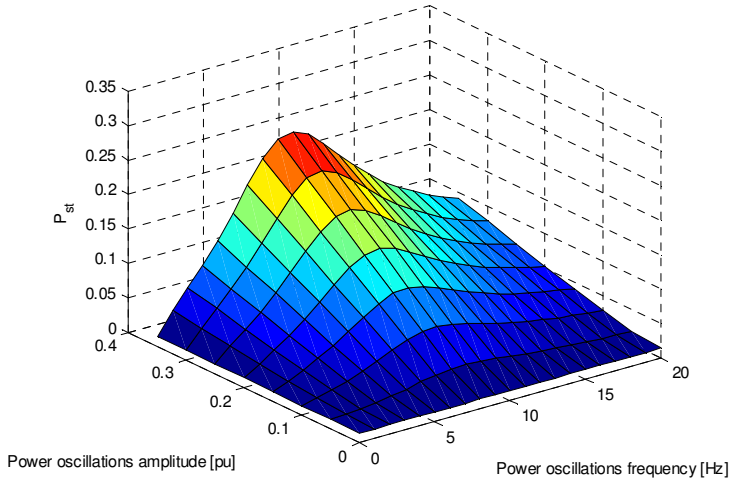

Figure 1-39: Flicker severity dependence on frequency and amplitude of the variations of power of the primary source (1 p.u. = 2.5 MVA)

1.3.6 Flicker dependence on the short circuit power at the connection point

To assess the link between the intensity of P_{st} and the network short circuit power (P_{cc}) at the point of connection of the generator, it is assumed to vary the value of the network impedance, maintaining constant the X/R ratio of the impedance (equal to 7). The calculation of the values of resistance and inductance of line, fixed the P_{cc}, has been done starting from these equations:

$$\begin{aligned} &P_{CC} = \frac{V_{LL}^2}{Z} \\ &Z = \sqrt{R^2 + X^2} \\ &\frac{X}{R} = k \end{aligned} \qquad R = \frac{1}{\sqrt{k+1}} \frac{V_{LL}^2}{P_{CC}} \quad , \quad L = \frac{k}{\sqrt{k+1}} \frac{V_{LL}^2}{2\pi f \cdot P_{CC}} \tag{1.40}$$

where V_{LL} is the line to line voltage network and k is a constant.

The analysis has been carried out setting the amplitude and the frequency of the variations in power, respectively equal to 400 kW (0.16 p.u.) and 10 Hz. The results obtained (Figure 1-40) have been compared with those calculated, always with the variation of the P_{cc} of the network, with a wind generator that injects constant power on the network, with a value equal to 2.5 MVA. In addition three different generators power factors have been analyzed, respectively equal to 1, 0.9 inductive (i.e. reactive power absorbed by the inverter) and 0.9 capacitive (i.e. reactive power delivered by the inverter).

As expected [24], the value of the index of the severity of the flicker *short term* has a dependency of reverse type ($1/P_{cc}$) on network short circuit power. From the analysis it's shown that also the reactive power contributes to the flicker generation, since the inverter operation mode with fixed power factor necessarily implies that a variations of active power match variations that are proportional to reactive power with a consequent increase of the mains voltage variations and therefore of the flicker severity.

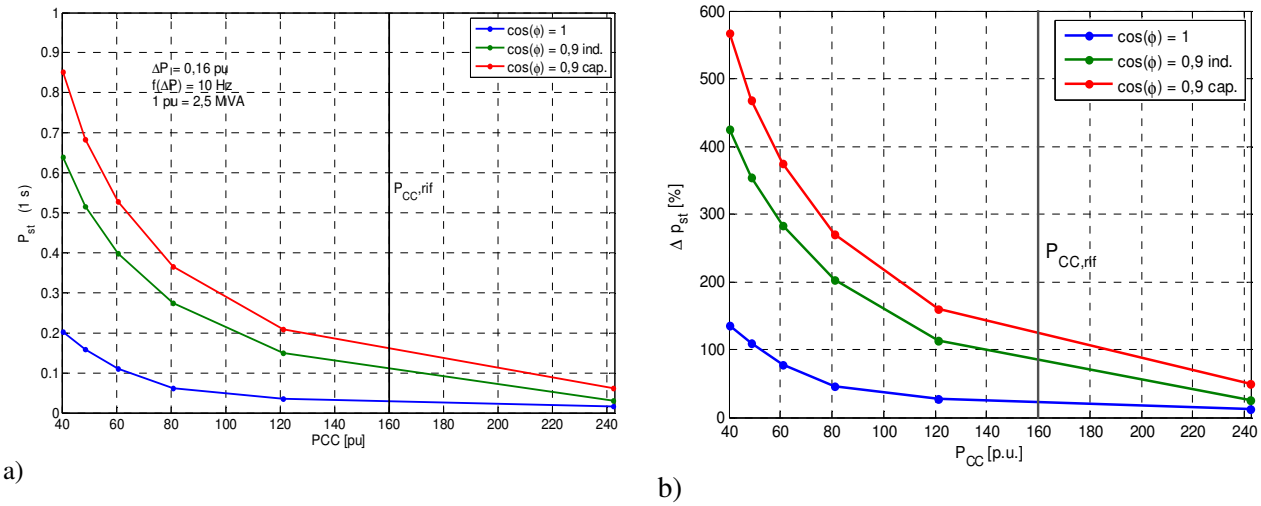

a) b)

Figure 1-40: Flicker severity dependence on the network P_{cc} at the wind generator connection point (a) values calculated by the model of flickermeter under different power factors, (b) percentage variations with respect to the case benchmark with constant power injection (1 p.u. = 2.5 MVA)

1.3.7 Flicker dependence on the impedance line ratio X/R

For this type of analysis the same primary source output variation of the previous case have been used. It is analyzed the P_{st} index dependence on the ratio X/R of the impedance of the network line where the generator is connected. The dependence has been evaluated for different values of short circuit power from the network. Considering a lower P_{cc} (100 MVA corresponding to 40 p.u.), the case of delivery only active power and the case with reactive power injection have been analyzed. The results of the simulations are reported in Figure 1-41: in absolute terms (case a) and in terms of percentage variation with respect to the case of the absence of power variations introduced into the network (case b), if used as a benchmark.

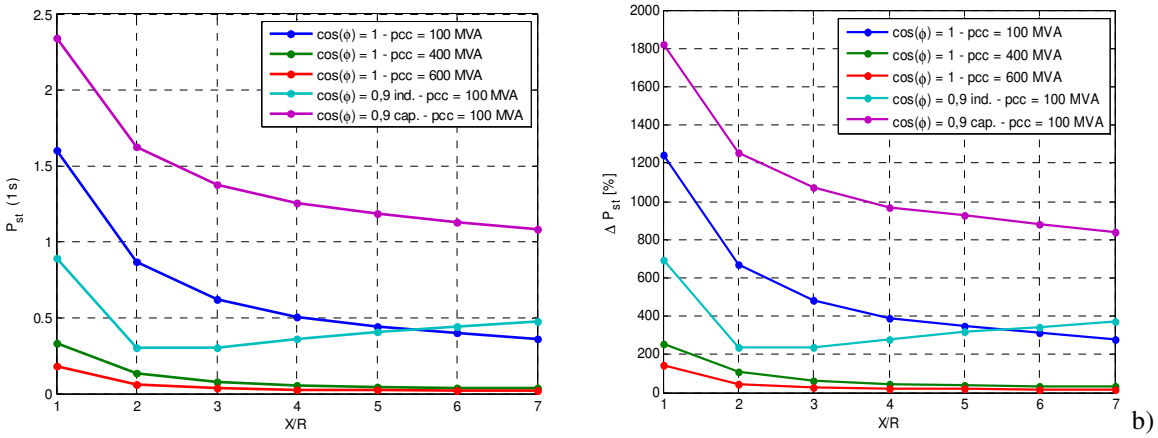

a) b)

Figure 1-41: Flicker severity dependence on X/R line characteristics (a) absolute values obtained under different injection and network conditions, b) percentage variations in respect to the benchmark case

The analysis shows that, for the same short circuit power, the resistive component of the line impedance has the main role in the determination of the severity of the flicker.

1.3.8 Flicker dependence on the value of inverter DC-link capacitance

The capacitor placed in the back-to-back converter DC section, said DC-link, has the purpose of stabilizing the value of the inverter DC voltage, thus limiting the ripple according to the following equation:

$$\Delta V_{dc\max} = \frac{\sqrt{2} I_{CA} + I_{DC}}{2 f_{sw} C_{DC}} \tag{1.41}$$

where I_{CA} is the RMS value of the current delivered by the inverter in the network at rated power, I_{DC} direct current, f_{sw} the inverter switching frequency and C_{DC} the total capacitance of DC-link.

In this case, the capacitor has been designed to obtain a maximum current ripple of 3% with a rated voltage of 1100 V; this design has effects on the DC voltage variations in case of unbalances between the power delivered by primary source and the one injected into the network by the inverter.

From the flicker point of view, an inverter DC voltage stable allows an injection of active power without oscillations obtaining less flicker level. However, it is necessary to consider the interactions with the dynamics of the controls of the two electronic power converters and, therefore, it is not possible to determinate beforehand a simple relation between flicker severity and DC-link capacitance design. This relationship has therefore been investigated by digital simulation, calculating the index P_{st}, using the flickermeter Matlab model, from mains voltages obtained by the ATPDraw simulations. The conditions for the P_{st} calculation are the same of the previous paragraphs and in particular:

- network P_{cc} at the connection point: 100 MVA (40 p.u.);
- line ratio X/R: 7;
- amplitude of the variations of power of the primary source: 400 kW (0.16 p.u.);
- frequency of variations of power of the primary source: 10 Hz.

Figure 1-42 shows the results of simulation from which it emerges that the P_{st} index is less affected by the value of capacitance of the DC-link, considering variations of ± 40%[16] than the value of design chose to limit the ripple of the DC voltage (100 mF equal to 1 p.u.).

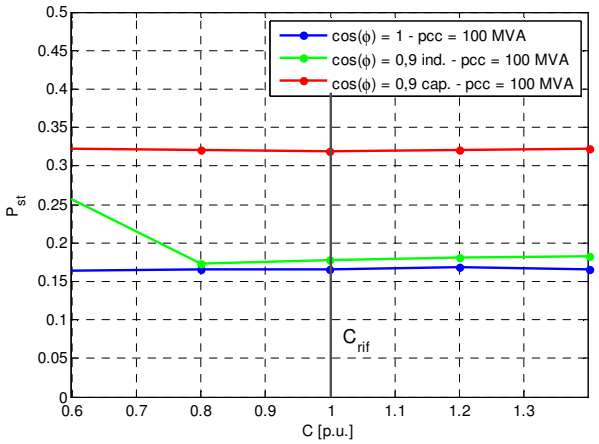

Figure 1-42: Flicker severity dependence on DC-link capacitance

[16] Lower values of capacitance were not taken into consideration because it is known to cause instability of the control implemented.

1.4 Final Considerations

The evolution of the distribution grids toward active type networks with Distributed Generation (DG) leads to analyze which is the impact of DG in terms of Power Quality. In particular, considering DG connected through power electronic converters, the effects related to harmonics and flicker have been deeply examined.

This analysis suggests that the harmonic impact varies with the system architectures and is closely linked to:

- type of technology used (three phase inverter two-level or multi-level);
- modulation strategy (Pulse Width Modulation - PWM modulation, fixed-band, etc.);
- switching frequency;
- any harmonic disturbance present in the network.

The activities take into consideration architectures with single inverter (three phase inverter: two or three-level) and with a modular construction (three phase interleaved inverters), both with PWM modulation, by focusing on the harmonic analysis of the voltages and currents injected into network associated with these two architectures. In particular it has been found that:

- in terms of harmonic voltage contribution the three-levels inverter produces a harmonic pollution lower than the two-levels configuration.
- in terms of harmonic current contribution injected into the network, the configuration with two interleaved inverters is better because it moves the first harmonics bell-shaped distribution toward high frequencies ($n \cdot f_c$) with small amplitudes.

Then, considering the flicker phenomenon, the *short term* flicker severity index has been calculated in case of a wind Permanent Magnets Synchronous Generator interfaced to the network with back-to-back converter configuration. The results have shown that:

- the P_{st} is greater if, considering the variability of the primary source wind, the wind generator converter has the field oriented control, used to extract the maximum power available and injected into the network;
- there is an inverse relationship between network short circuit power at the inverter connection point and the severity of the flicker; in particular, the possible delivery or absorption of reactive power has in general a worsening effect on the severity of the flicker due to the voltage drops on inductive components of the network impedance;
- the P_{st} is more linked to the resistive component of the line impedance in the same short-circuit power network conditions;
- the P_{st} is less affected by the value of DC-link capacitance, if it is designed to limit, during the steady-state operation, the DC voltage ripple within a few percentage of the nominal value.

Finally, it should be underlined that the investigation methods and part of the results obtained can be extended to every type of distributed generators connected to the network through electronic converters or characterized by variable primary power.

2 DISTRIBUTED GENERATORS CONNECTED TO DISTRIBUTION NETWORKS THROUGH INVERTER

The study of the impact of Distributed Generation (DG) on the voltage quality has been conducted with digital simulation of the behavior of such generators in case of voltage dips and proponing possible control strategies to overcome them. In particular, the simulations conducted in ATPDraw environment (Alternative Transient Program) have made it possible to evaluate the Electromagnetic Transient (generally referred EMT) resulting from the disturbance, highlighting:

- the "natural" response of the DG system, i.e. without any external device or any special control strategies;
- the system response in presence of auxiliary devices (hardware and software) to satisfy the new requirements of Fault Ride Through that will be presented in Chapter 3.

Initially the photovoltaic (PV) generation has been taken into consideration, since in Italy this generation had a greatest increase in terms of installed power. But in the European context, for some years, wind generators of various types and sizes have found wide use as well. For example, in Table 2-1 the installed power from wind power plants are reported for all member countries of the European Union in 2009 and 2010 [35]. Figure 2-1 shows the trend of the installed power from wind power plants in the EU as a whole from 1995 to 2010 [35].

Table 2-1: Installed wind capacitance in member countries of the European Union in 2009 and 2010 (in MW)

Country	2009	2010	Country	2009	2010
Austria	995	1011	Latvia	28	31
Belgium	563	911	Lithuania	91	154
Bulgaria	177	375	Luxembourg	35	42
Cyprus	0	82	Malta	0	0
Czech Republic	192	215	Holland	2215	2237
Denmark	3465	3752	Poland	725	1107
Estonia	142	149	Portugal	3535	3898
Finland	147	197	Romania	14	462
France	4574	5660	Slovakia	3	3
Germany	25777	27214	Slovenia	0.03	0.03
Greece	1087	1208	Spain	19160	20676
Hungary	201	295	Sweden	1560	2163
Ireland	1310	1428	United Kingdom	4245	5204
Italy	4849	5797	**Total EU**	**75090**	**84278**

In the recent years, as regards the *on-shore* plants, which represent the majority of plants currently installed, it is becoming a trend to install average power plants, up to 2 MW, based on Permanent Magnets Synchronous Generators (PMSG) instead of the most classic doubly-fed induction generators [36]. The first, in fact, require the use of full power converters to decouple frequency and voltage level generated by the wind turbine from the network. Only in recent years, the power electronics has reached a maturity that allow to make PMSG competitive compared to the traditional solutions, in terms of costs and payback time. In addition, the possibility to easily vary the control strategies of power electronic converters allows to manage the generators in a much more versatile way than the traditional one and, if necessary, to provide also auxiliary services to the network.

The significant presence of wind farms DG with PMSG connected to the network using electronic power converters, it has brought with it the need, as for the photovoltaic generation, to reconsider the management strategies to adopt in the event of disturbances and voltage dips in the network.

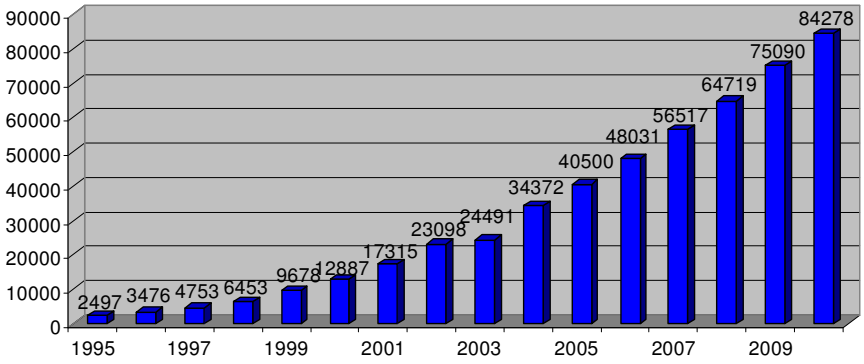

Figure 2-1: Total power from wind plants installed in the EU from 1995 to 2010 [MW]

The study for both types of distributed generators (Photovoltaic and Wind) has been developed by digital simulation (with environments ATPDraw and DIgSILENT PowerFactory) and through theoretical analysis with numerical calculation software and the main results will be presented in the Chapters 3, 4 and 5.

2.1 Electromagnetic transient simulations: network model

For the purposes of the simulations in the environment ATPDraw, a detailed model of a Medium Voltage (MV) distribution network, typical Italian, has been implemented. This network develops from a Primary Substation (PS) with a power transformer HV/MV of 40 MVA; the prevalent High Voltage (HV) network is modeled through a Thevenin equivalent sinusoidal three phase generator with frequency of 50 Hz, voltage 132 kV and an inductance that gives a value of short circuit power equal to 2300 MVA. In the PS a MV bus-bar is present from which five feeders of different lengths start. On each of the lines there are passive loads and at the start of each line a three phase Circuit Breaker (CB) is installed.
The network faults are simulated connecting in different positions a timed circuit breaker with in series an impedances inductive or resistive with different value. In this way, it is possible to simulate faults with voltage dips of different depth and duration, introducing also possibly voltages phase shift.
In particular, the network implemented in the simulations is shown schematically in Figure 2-2.

The different feeders shown are characterized in this way:

- Line 1: cable line, total length 5 km, empty;
- Line 2: cable line, overall length 20 km, total load 6 MVA;
- Line 3: cable line, total length 1 km, total load 6 MVA;
- Line 4: overhead line, overall length 15 km, empty;
- Line 5: overhead line, overall length 30 km, total load 5.4 MVA;
- Line 6: cable line, overall length 10 km, at the end of which will be connected the distributed generator.

Below the characteristics of each component are detailed.

HV Prevalent Network

The network has been represented by an appropriate equivalent at 132 kV (characterized by a three phase fault current of 10 kA and a single phase fault current of 8 kA).

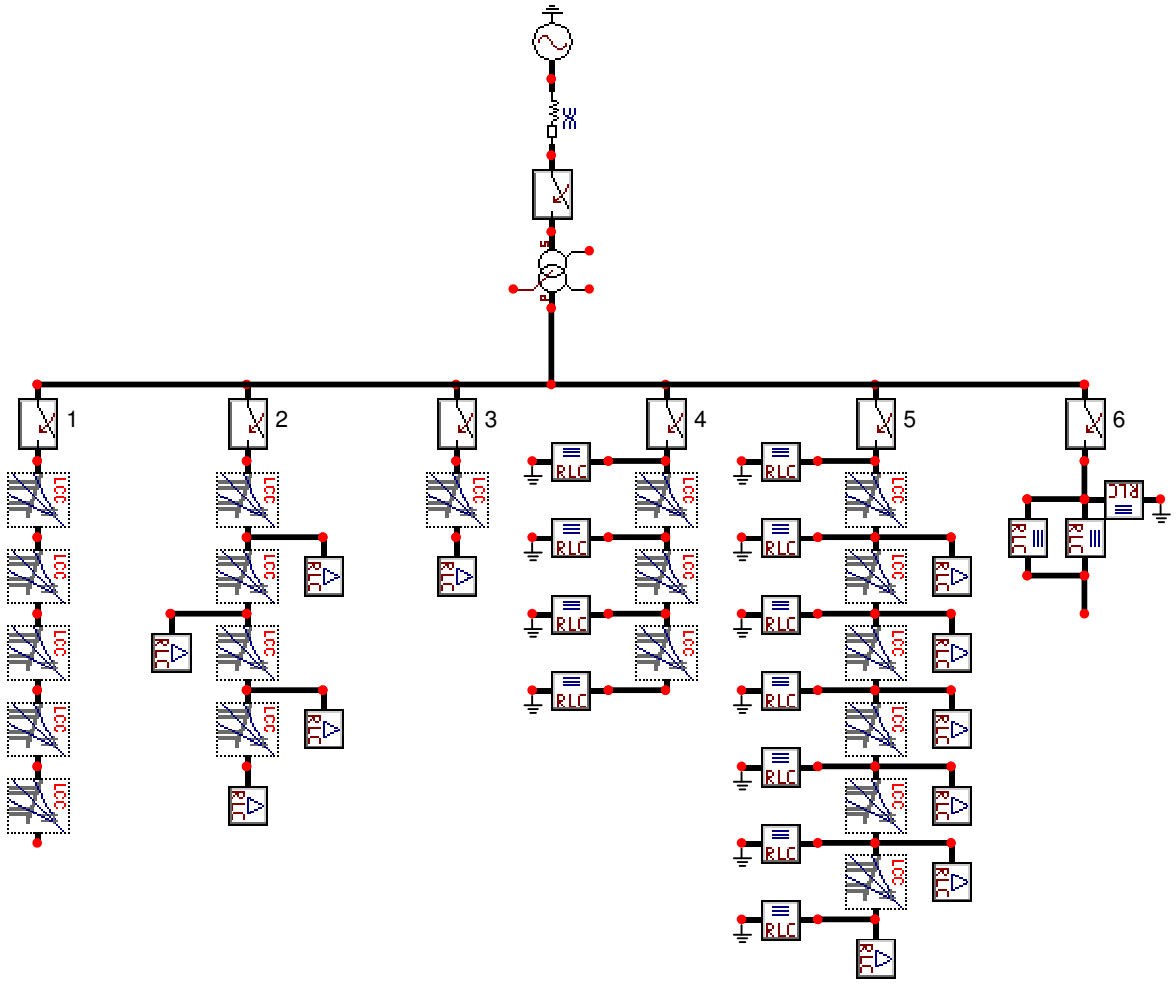

Figure 2-2: Diagram of the main network used for simulations

HV/MV transformer

The main data of the HV/MV transformer used are reported in Table 2-2.

Table 2-2: Main data of the HV/MV transformer

A_n	40 MVA
V_{1n}	132 kV
V_{2n}	20.8 kV
P_{cc}	0.437 %
v_{cc}	15.5 %
I_0	0.5 %
P_0	0.065 %

Overhead lines

The main data relating to the overhead lines considered are reported in Table 2-3. The conductance to ground have been modeled by resistors connected to earth added at the beginning of each segment of the line.

Table 2-3: Main data of the overhead line MV

Conductor Diameter	10.7 mm
$r_{conductor}$	0.289 Ω/Km
Conductances	0.714 μS/Km

Cable Line

The cable lines are MV triple-pole aluminum helix cables, insulated with Cross-linked polyethylene, shielded under thermoplastic sheath. Their main data are reported in Table 2-4. The cable line 6, where the DG will be connected, is modeled by a circuit equivalent to Γ.

Table 2-4: Main Data cable MV

Conductor Diameter	16.5 mm
Insulator Thickness	5.5 mm
Screen Section	16 mm^2
Outside Diameter	36 mm
ε_{XLPE}	3
ε_{PVC}	8
$r_{conductor}$	0.164 Ω/km
r_{shield}	1.15 Ω/km

Distributed Generators

For the photovoltaic (PV) generators a 580 kW power plant directly connected to the MV network is considered (§ 2.2). In regards the wind generation a PMSG in a back-to-back configuration of about 2MVA has been modeled (§ 2.3).

2.2 The model of the photovoltaic installation: power and control

The structure of the simulated system is reported in Figure 2-3 and consists of:

- a PV array;
- a DC/DC BOOST converter to extract the Maximum Power Point Tracking (MPPT) from the PV array and to increase the output voltage to a level suitable for the inverter;
- a two level three phase VSI to connect the DG to the MV network through a MV/LV transformer.

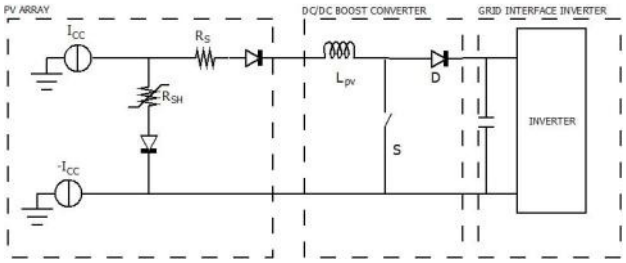

Figure 2-3: Simplified diagram of a typical structure of the system of photovoltaic generation

2.2.1 Photovoltaic equivalent model

A PV array consists of solar cells, each generating a certain voltage and current; by connecting these cells in series and in shunt, the required current and voltage can be generated. The photovoltaic equivalent system has been represented by the following equivalent model shown in Figure 2-4 [37]÷[39].

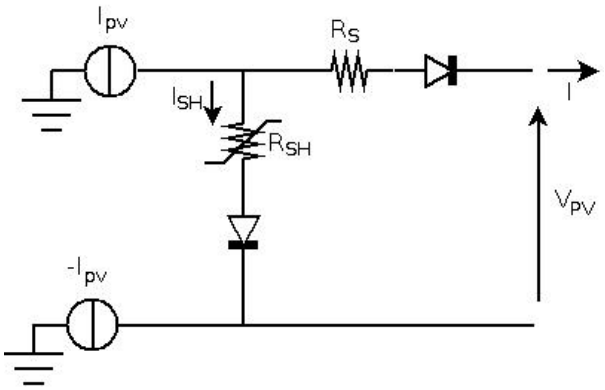

Figure 2-4: Electrical equivalent of a photovoltaic panel

The simplified electric equivalent model of a solar cell is made by a photovoltaic current source I_{pv}, a diode, a shunt resistor (R_{sh}), that takes into account the current to earth under normal operation conditions, and a series resistor (R_s), that represents the internal resistance to the flow of generated current and depends on the thick of the junction P-N, on the present impurities and on the contact resistances. The current-voltage (I-V) characteristic is given by:

$$I = I_{pv} - \frac{V_{pv} + I R_s}{R_{SH}} \tag{2.1}$$

$$I_D = I_0 \left[exp \frac{q\left(V_{pv} + I R_s\right)}{AkT} - 1 \right] \tag{2.2}$$

where:

- I is the current injected by the PV system;
- I_{pv} represent the current generated by the cell that is a constant for a given temperature (T) and Solar irradiation (G);
- I_D the current flowing through the diode that depend from its reverse saturation current I_0;
- A is the identity factor of the diode and depends on the recombination factors inside the diode itself (for crystalline silicon is about 2);
- q is the electron charge (1.60217646E-19 C);
- k is the Boltzmann constant (1.3806503E-23 J/K);
- T is the absolute temperature in K degree.

In the usual cells, the leakage current to earth, flowing through R_{sh}, is negligible with respect to the other two currents. As a consequence, the saturation current of the diode can be experimentally determined by applying the no-load voltage V_{oc} to a not-illuminated cell and measuring the current flowing inside the cell. In this study the output I(V) and P(V) characteristics has been calculated for the following PV system features:

P_{MPPT}	580 kW
V_{MPPT}	610 V
I_{MPPT}	950 A
T	25°C
G	1000 W/m^2

In particular in Figure 2-5 it's possible to evaluate the PV behaviour in case of short circuit or no-load. During these two conditions the electric power produced in the cell is null, whereas starting from the short-circuit condition, when the voltage increases, the produced power rises too: after reaching the maximum power point (P_m), the power suddenly falls near to the no-load voltage value.

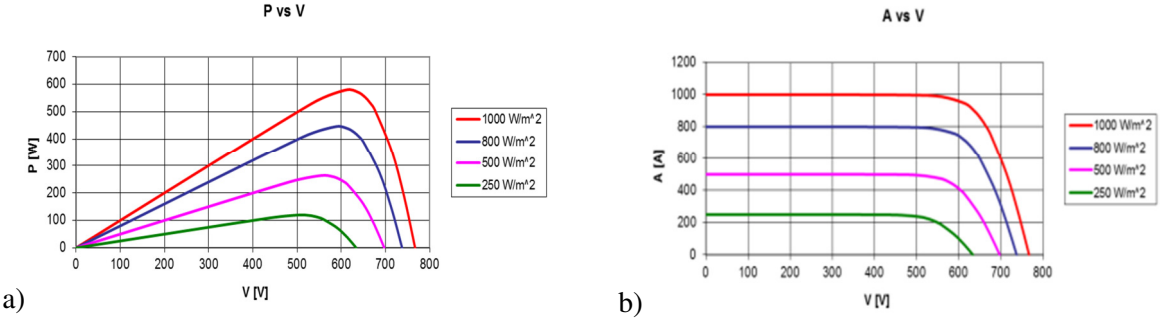

a) b)

Figure 2-5: Characteristics of voltage/power (a) and voltage/current (b) of PV 580 kW generator for constant Temperature (T) and variable Solar Irradiation (G)

Maximum Power Point Tracking

The trends of the power/voltages characteristics in Figure 2-5a have only one maximum at a given voltage, V_{MPP}, which corresponds, from the current/voltage characteristic, a current I_{MPP}. The pair (V_{MPP}, I_{MPP}) therefore represents the working point where the panel produces its maximum power (Maximum Power Point - MPP).

It is therefore necessary to provide a system for the identification of the maximum power point (Maximum Power Point Tracking - MPPT) so that, in order to obtain the maximum efficiency, the panel is "brought to work" around values of voltage/current corresponding to the MPP.

Systems of MPPT can be implemented with different algorithmic solutions [37], although usually it's used a technique called "perturb and observes" (P&O). In this strategy, the point of maximum power is tracked by adjusting, with time deadlines defaults, the output voltage of the photovoltaic panel by following the following steps:

1. to fix a V_{PV} voltage;
2. to measure the power output from the panel P(k);
3. to disturb the value of the voltage with a known variation;
4. to measure again the power delivered by the system P(k+1);
5. If P(k+1) >P(k) to disturb again V_{PV} with a variation of the same sign of the previous one; otherwise to apply a disturbance of opposite sign.

In this way the value of the output voltage of the photovoltaic panel tends to oscillate around the value V_{MPP}. Since this dynamic is generally "slow", compared with the typical dynamics of electronic systems and the phenomena that affect the variations of MPP, the update of the voltage value can also be performed with time intervals of the order of seconds. Under this assumption, the MPPT dynamics can be considered slower than the phenomena subject to analysis (voltage dips) and therefore in the model the MPPT logic has not been implemented. In other words, the voltage/current working point has been fixed beforehand at the value (V_{MPP}, I_{MPP}) and held constant for the entire duration of the transient [39].

2.2.2 DC/DC Boost Converter

The converter placed between the photovoltaic generator and DC bus is a unidirectional chopper. The need for raising or lowering converter voltage derives from the relationship between the DC voltage and PV generator working, considering the variations in relation to different environmental conditions

(sunlight and temperature). For the photovoltaic generator modeled the MPP voltage value is 610 V. In particular, assuming an inverter DC bus voltage of 800 V, the chopper implemented in the study is a DC/DC BOOST converter.
The PV generator interface converter must ensure the operation at the point voltage - current that corresponds to the maximum output power to ensure the provision of all the available power. A schematic diagram of the DC/DC converter is shown in Figure 2-6.

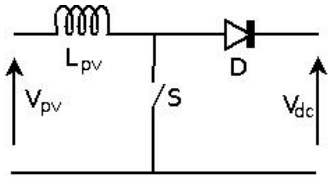

Figure 2-6: Circuit Diagram of the DC/DC converter

For reasons of cost, this converter is usually used in plants for greater power, such as the one taken into account in this study (580 kW). For generators of lower power, connected to the Low Voltage network, on the contrary, the photovoltaic panel can be connected directly to the inverter. If present, the DC/DC converter is used also for the MPPT algorithm implementation; on the other hand, in case of direct interfacing to the inverter, the MPPT is included in the inverter control itself.

With regard to the boost converter design and control modeling, some choices that will ensure a greater simplicity of the system to simulate have been considered, but verifying a match with more complex models.
In particular, the chopper is modulated with a fixed band width current modulation instead of a more common modulation strategy PWM (Pulse Width Modulation). This is because the lack of a proper algorithm for MPPT reduces the boost converter only at the stage of adaptation of the output voltage of the panel to optimal levels for the inverter to interface the generator to the network, making practically indifferent the type of modulation choice for driving. The substantial equivalence between the two modulation strategies, for the purposes of the simulations in this study, will be discussed in § 2.2.4.

Boost converter design
Starting from the chopper equivalent circuit (Figure 2-6) and considering the current trend in the inductance of the chopper shown in Figure 2-7, it's possible to write the functioning equations in the intervals T_{on} and T_{off}, respectively defined as δT and $(1-\delta)T$, where δ represents the duty cycle and T the switching period of the chopper:

$$L_{pv}\frac{\Delta I}{\delta T} = V_{pv} \tag{2.3}$$

$$L_{pv}\frac{\Delta I}{(1-\delta)T} = V_{dc} - V_{pv} \tag{2.4}$$

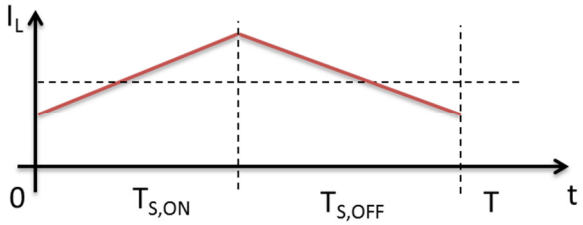

Figure 2-7: Trend of the current in the inductance of the chopper boost

Since the chopper is modulated with a fixed band width current modulation, the variation range of the current, ΔI, can be fixed beforehand. Therefore, obtaining this parameter from (2.3) and replacing it in (2.4) it's possible to obtain the following equations:

$$\begin{aligned} \Delta I &= \frac{V_{pv}}{L_{pv}} \delta T \\ L_{pv} \frac{V_{pv}}{L_{pv}} \delta T &= V_{dc}(1-\delta)T - V_{pv}(1-\delta)T \end{aligned} \tag{2.5}$$

Processing the second expression of the equation (2.5) it is obtained:

$$V_{pv}\delta = -V_{pv} + V_{pv}\delta + V_{dc} - V_{dc}\delta \tag{2.6}$$

$$V_{pv} = +V_{dc}(1-\delta) \tag{2.7}$$

Finally, replacing the expression of the duty cycle in the first equation, the formula for design the inductance of the chopper is determined:

$$\begin{aligned} \delta &= 1 - \frac{V_{pv}}{V_{dc}} \\ L_{pv} &= \frac{V_{pv}}{\Delta I} T \left(1 - \frac{V_{pv}}{V_{dc}}\right) = \frac{V_{pv}}{\Delta I * f_{sw}} \left(1 - \frac{V_{pv}}{V_{dc}}\right) \end{aligned} \tag{2.8}$$

where the parameters V_{PV}, ΔI and the switching frequency f_{sw}= 1/T have been evaluated in the condition of critical operation, that is in case of low irradiation.
The variation in maximum allowable current has been set equal to 10% of the maximum current that can be delivered from the panel (Figure 2-5) and the switching frequency has been chosen to use the same IGBT of the inverter (§ 2.2.3). The main characteristics of the PV system are summarized in the table below:

V_{PV}	617 V
V_{dc}	800 V
ΔI	50 A
f_{sw}	8 kHz
L_{pv}	160 μH

2.2.3 Voltage Source Inverter (VSI)

To connect the PV system to the network a Voltage Source Inverter has been considered, in particular a two-level three phase inverter configuration (Figure 2-8). Depending on the size of the plant, the interfacing with the network can provide, in addition, the presence of a transformer to respond to the Standard requirements for network connection [2][3] (in this case, depending on the device design, the reactance of switching can be "included" in the transformer itself). For the model implemented, it has been necessary to represent the coupling transformer with the network (connected with triangle network side and star to the ground side inverter), the size of which has not provided the opportunity to "include" in its the switching reactance.

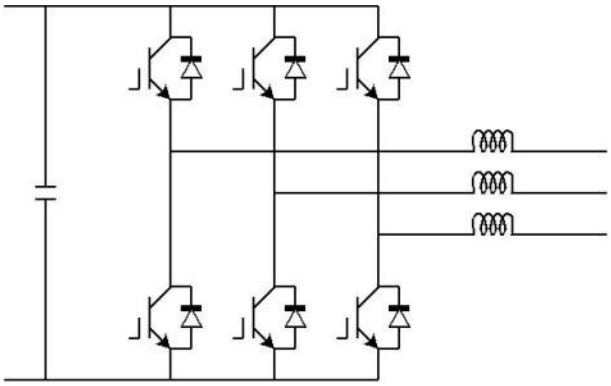

Figure 2-8: Simplified circuit diagram of a two-level three phase inverter

Main inverter parameters

The complete interface system considered to connect the PV array to the network is made of:

- a three phase two-level inverter with forced switching;
- a source of accumulation of energy;
- a three phase transformer coupling with the network MV;
- passive filters RC connected at LV side.

The inverter valves are designed taking into account the maximum continuous voltage can be reached by the inverter and their rated current. In general, the choice of the controlled switches must be made according to the safety operation area in terms of both voltages and currents. Once selected the components, the limitation of instantaneous current of the inverter must be set to a value less than the maximum peak current of the selected valve. In this specific case, the characteristic parameters, adopted in the study, of the valves of the inverter (IGBT) are:

V_{CE} = 1700 V (maximum voltage allowable for the valve that determines the choice of the DC voltage of the inverter)
I_c = 2400 A (maximum RMS current switchable permanently)
I_{CM} = 4800 (Maximum switched current not repetitive - 1 ms)

Given these project constraints it's possible to proceed to the converter design, for which the characteristic of the main components are summarized here below:

- Rated power
  A_n= 630 kVA
  The converter has been overdesigned with respect to the maximum power of the photovoltaic panel to have a transient capability and to ensure a margin of power injection during transient events.

- Three phase transformer coupling with the network (power, voltage and current ratings, transformation ratio, short circuit voltage):
  A_n = 630 kVA
  V_{1n} = 20000 V
  V_{2n} = 278 V
  K_t = 71
  v_{cc} = 6 %
  P_{cc} = 0.35 %
  Connection primary winding: triangle
  Connection secondary windings: star to earth with R_t=0.3 Ω.

- Filter LV side: "RC" filter between the switching inductances and the secondary of the transformer, used to filter the high frequency harmonics introduced into a network from the converter:
  C_{filter}= 662 μF
  R_{filter}= 0.1 Ω;

- Switching output inductance (L_{inv}) is dimensioned imposing an inverter output reactance (which takes into account also of the transformer) equal to 0.16 p.u., referring to the rated power of the device and the nominal LV voltage for the switching inductance is obtained:
  L_{inv}= 0.0396 mH.

- DC-link
  The DC capacitors have many functions involving the system, some during the steady-state operation and others during the transient.
  During steady state, the capacitances have the function of containing the high-frequency ripple voltage on the bus DC due to the switching of the converters valves. These capacitances have to be positioned as close as possible to the converters, to prevent voltage spikes cause by the inductances that can damage the valves.
  However, there are other functions of the smoothing capacitors during the transient operating, that involve the entire system and not just the individual converters. For example, the rapid variations of load and generation must be absorbed by these elements, to give way to the converters regulators to modify their setting to maintain constant voltage on the bus DC. Therefore, these capacitors can be added directly to the DC bus once designed all of the system. It is understood that the higher the installed capacitance, the better is the behavior of the system, but with a greater cost of the system and a larger overall dimensions. In this specific case, the converter has the function of compensator therefore it has been chosen to calculate the capacitance C using the criterion of limit the voltage ripple at the switching frequency in section in DC. The peak-to-peak ripple can be calculated by the following expression evaluated on half of the switching period (T_{sw}):

$$\Delta V_{dc} = \frac{1}{C}\int_{0}^{T_{sw}/2} i_{cond}\,dt = \frac{1}{C}\int_{0}^{T_{sw}/2} \left(I_{cc} - i_{ac}(t)\right)dt \tag{2.9}$$

Starting from this expression, solving the integral and considering that if the switching frequencies is more higher than the network frequency the alternative current may be considered constant at any instant, it's obtained the following equation:

$$\begin{aligned}\Delta V_{dc} &= \frac{1}{C}\int_{t_i}^{t_i+T_{sw}/2} \left(I_{cc} - \sqrt{2} I_{ca}\sin(\omega t_i)\right)dt = \frac{1}{C}\left[I_{cc}t - \sqrt{2} I_{ca}\sin(\omega t_i)t\right]_{t_i}^{t_i+T_{sw}/2} = \\ &= \frac{1}{C}\left[I_{cc}\frac{T_{sw}}{2} - \sqrt{2} I_{ca}\sin(\omega t_i)\frac{T_{sw}}{2}\right] = \frac{1}{2Cf_{sw}}\left[I_{cc} - \sqrt{2} I_{ca}\sin(\omega t_i)\right]\end{aligned} \tag{2.10}$$

To assess the maximum ripple, it is considered the maximum of the function (2.10) that occurs for $\sin(\omega t_i) = -1$ and therefore:

$$\Delta V_{dc\max} = \frac{1}{2Cf_{sw}}\left[I_{cc} + \sqrt{2} I_{ca}\right] \tag{2.11}$$

From which it derives the expression of the capacitance:

$$C = \frac{I_{DC} + \sqrt{2} I_{AC}}{2 f_{sw} \Delta V_{DC\max}} \tag{2.12}$$

where:

- I_{AC}: RMS value of the single phase nominal current;
- I_{DC}: current of the generator connected to the section in DC;
- f_{SW}: converter switching frequency = 1/Tsw;
- ΔV_{DCmax}: maximum voltage ripple acceptable.

Considering the case under study, imposing a switching frequency of 1950Hz and a ripple voltage equal to 1% V_{DC}, the capacitance is approximately equal to 73 mF. In the simulations, in reference to a total capacitance of 100 mF, the results have shown the effectiveness of this capacitance in order to adjust the DC voltage even during transients consequent to voltage dips on the network.

Inverter capability

Below the curves of the inverter theoretical capability are shown, calculated in terms of the maximum power supplied for different values of the mains voltage. The capability indicated in Figure 2-9 as "nominal" has been calculated assuming a current that can be flowed through the inverter equal to the nominal (1310 A), while the other "transient" capability (Figure 2-10) is referred to the maximum current switchable permanently from the valves (2400 A).

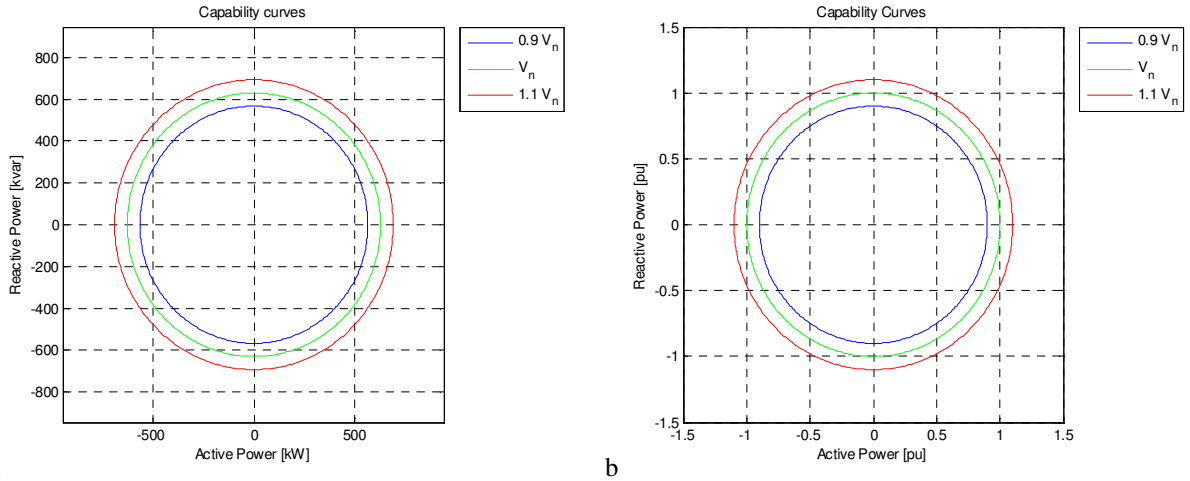

a b

Figure 2-9: Inverter nominal capability: absolute values (a) and p.u. (b)

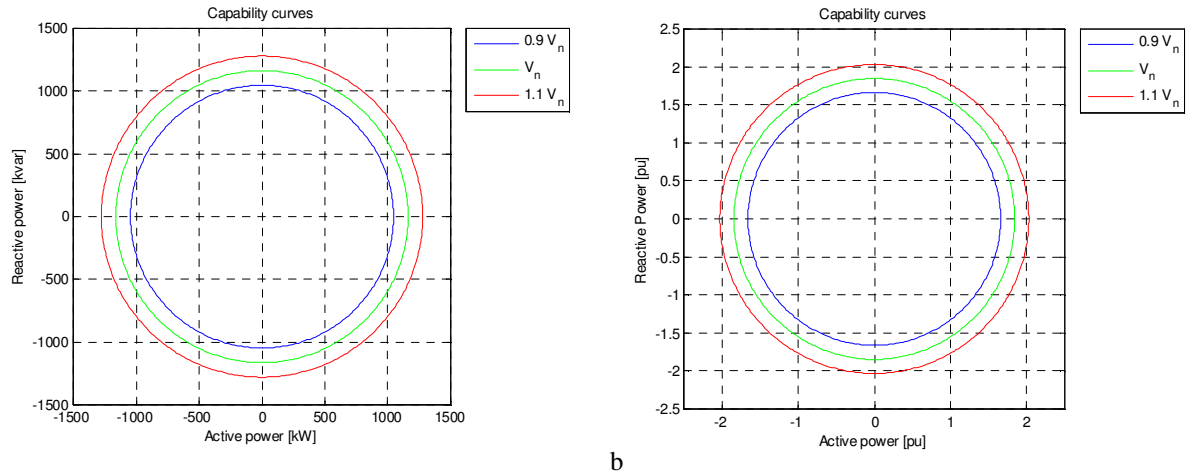

a b

Figure 2-10: Inverter transient capability: absolute values (a) and p.u. (b)

2.2.4 Converters control Strategies and switching

2.2.4.1 Fixed band width modulation for the DC boost converter

For driving the DC boost converter has been initially adopted a current control strategy with a fixed band width. By acting on opening and closing of the switch, the inductor current L_{pv} is maintained within a predetermined band centered around a reference value, since the amplitude is constant, considering the variation of the PV array operation point as a function of the irradiation, the switching frequency of the chopper varies. Conversely, if a PWM modulation is adopted, the switching frequency would be fixed.

In particular, when the inductor current becomes less than the lower limit of the current bandwidth the switch is closed. In this way the inductor current is forced to grow, almost linearly, until, reached the upper limit of the bandwidth, the switch is open, causing the decrease of the current. The value of the reference current can be set using a search algorithm for maximum power (§ 2.2.1). This strategy requires a current reference, equal to I_{MPP} in the cases considered, and to modulate the opening and closing of the converter to keep the inductor current within a range of fixed width around the reference value. In Figure 2-12 the trend of the current is represented, together with the reference signals and the thresholds in the condition of nominal operation of the PV array, according to the CEI EN 60904-3 [39].

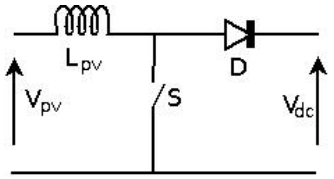

Figure 2-11: Circuit Diagram of the DC/DC converter

The error signal, obtained as the difference between I_{MPPT} and the actual current generated by PV, is compared with the thresholds (±5% I_{MPPT}) and:

- if the PV current is greater than the superior limit, the valve S (Figure 2-11) is open so that the current can flow to the network decreasing and returning to the reference band;
- if the current is less than the lower limit, S valve is closed (brown line upper level), the voltage V_{pv} is applied to the inductor L_{pv} and the current increases energizing the inductor.

The slopes of growth and decrease of the current are influenced by the inductance and the *duty cycle,* according to the equations given above (§ 2.2.2).

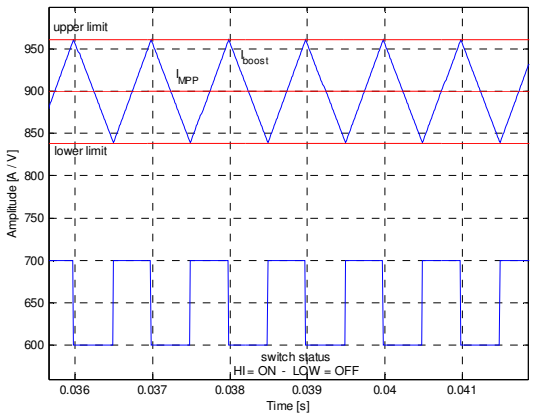

Figure 2-12: Chopper boost modulation: PV current and switching signal

2.2.4.2 PWM modulation for the DC boost converter

This modulation strategy plans to compare the magnitude to check, commonly the output voltage of the converter but it is also possible to current, with a reference value possibly being processed by the difference with appropriate regulators. The error signal thus generated is compared with a signal "saw tooth" (or a triangular waveform) at a fixed frequency. When the error signal is greater than the "saw tooth", the valve S of Figure 2-11 is closed, while otherwise it is kept open. In Figure 2-13 the waveforms of: error, signal "saw tooth", resulting valve control signal and the relative behavior of the inductor current are represented.

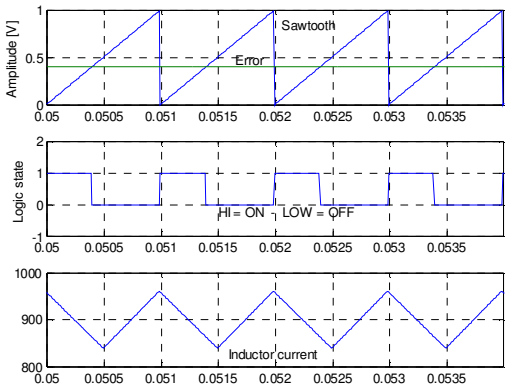

Figure 2-13: Chopper boost PWM modulation signals

2.2.4.3 Equivalence verification between different modulation strategies for the converter

As anticipated at first the substantial equivalence between the use of a fixed band width current modulation and a more common PWM modulation for the boost converter has been verified for the purposes of the simulations carried out. Figure 2-14 shows, for the fixed band width modulation (a, c) and PWM (b, d), the behavior of DC voltage and currents delivered by the inverter at LV side in response to a voltage dip of depth 70% V_n caused by a three phase fault with a resistive impedance which is extinguished in 120 ms[17].

From the simulations results there are not noticed substantial differences between the two modulation strategies. It should be underlined that this equivalence is not verified in the absolute sense since the boost converter responds to disturbances in a different way depending on the type of modulation, however, for the purposes of the study to analyze the behavior of the overall system in presence of voltage dips, it's possible to consider these equivalent modulations[18].

For the greater simplicity and simulations execution speed initially the fixed band width hysteresis modulation has been uses. However, despite the advantage of the simplicity and the precision with which the current follows the reference, the main drawback of this method is the fact that the valves switching frequency is not constant but varies within a band in each half cycle of the mains frequency. This can cause excessive stress to the valves and, especially, makes it more difficult to filter the high-frequency ripple. From these observations, below the simulation results performed with the PWM modulation technique are presented.

[17]The control strategy of the inverter and the solutions used to overcome the voltage dip will be described in the following sections.

[18]During steady state, the system boost converter + panel, or even the only panel, could be represented by an equivalent current generator. In fact, such modeling is very simple and therefore advantageous in terms of simulation speed, but it does not allow to effectively capture the behavior of the real system during transients.

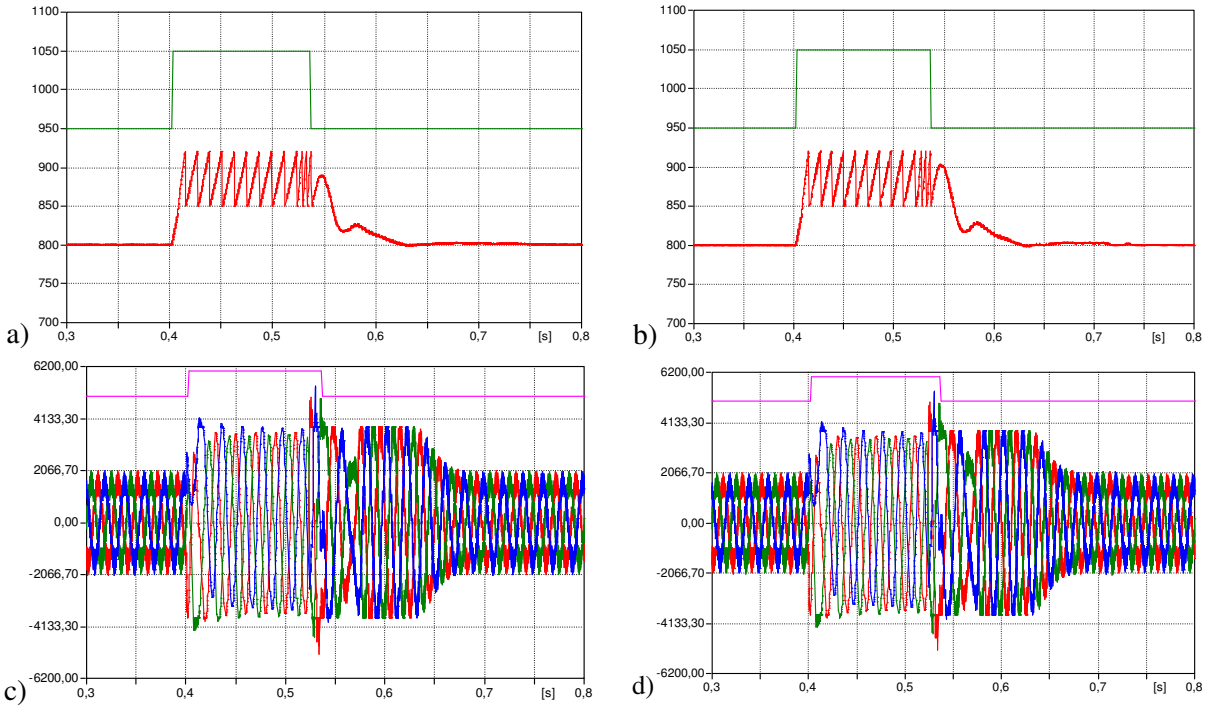

Figure 2-14: Transients of the characteristic values of the inverter in response to a voltage dip: currents supplied by the inverter side LV with fixed hysteresis band modulation (a, c) and PWM modulation (b, d)

2.2.4.4 Interface converter control

The control scheme of the VSI, shown in Figure 2-15, consists of two independent branches for the regulation of active and reactive power delivered by the inverter.

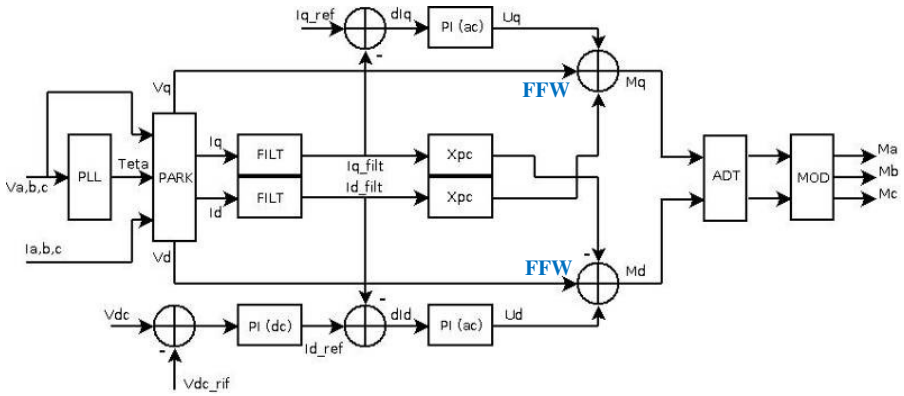

Figure 2-15: Diagram of the inverter control on axis d-q with PWM modulation

The calculation of the two currents of direct and quadrature axes, said i_d and i_q, is carried out starting from the reading of the phase currents by means of a first intermediate processing in the fixed reference αβ:

$$\begin{bmatrix} i_\alpha \\ i_\beta \end{bmatrix} = \sqrt{\frac{2}{3}} \begin{bmatrix} 1 & -1/2 & -1/2 \\ 0 & \sqrt{3}/2 & -\sqrt{3}/2 \end{bmatrix} \begin{bmatrix} i_a \\ i_b \\ i_c \end{bmatrix} \tag{2.13}$$

where i_α and i_β are the currents expressed in the new reference and i_a, i_b, i_c are the phase currents read at network side of the transformer. Then it's used this transformation to pass in the rotating frame d-q:

$$\begin{bmatrix} i_d \\ i_q \end{bmatrix} = \begin{bmatrix} \cos(2\pi ft) & \sin(2\pi f) \\ -\sin(2\pi f) & \cos(2\pi f) \end{bmatrix} \begin{bmatrix} i_\alpha \\ i_\beta \end{bmatrix} \quad (2.14)$$

where f is the network frequency measured by a device for coupling phase (Phase Locked Loop - PLL).

In such a scheme, the inverter DC voltage is compared to a reference value and the obtained error signal is processed by a Proportional Integral (PI) controller to obtain a current reference on the "d" axis.
In particular, the set-point of the reactive power (i.e. proportional to the current on the "q" axis in the frame of the Park transformation) is maintained fixed at the zero value, while the active power set-point (given by the current reference on the "d" axis) aims at maintaining constant the inverter DC voltage, V_{DC}.
The recent national and international Standards, in terms of connection to the networks of DGs (CEI 0-21 [2] and CEI 0-16 [3]), however, requires that under certain conditions the inverter should be able to inject a share of reactive power to provide ancillary services to the network. In order to verify the feasibility of these requests, in the following simulations the calculation of the value of current reference axis q has been modified depending on the cases (Chapter 3). The inverter and the MV/LV network coupling transformer design has been therefore carried out to take into account the additional current which may be required to support the network.
Both current references are compared with the relevant measured component of the inductor current, and the current errors are separately sent to two independent regulators Proportional Integral (PI), whose outputs are summed separately to the voltages expressed on the same rotating axis in order to provide a compensation *feed-forward* (FFW of Figure 2-15). The purpose of this further control loop is to make more rapid the system responses to variations in the mains voltage. In fact, the outputs of the two regulators are thus directly affected by the variations of the voltage, allowing a first response of the control without mediation of integral components. These last have, instead, the purpose of cancelling the errors of current to stationary, i.e. for a long time. The components on the two axis d-q are decoupled in this stage in this way:

$$\begin{aligned} M_d &= V_d - 2\pi f L_{inv} i_q \\ M_q &= V_q + 2\pi f L_{inv} i_d \end{aligned} \quad (2.15)$$

where M_d and M_q are the reference voltages on the axis d and q respectively after the decoupling, V_d and V_q are the same voltages before the decoupling, f is the network frequency, i_d and i_q the currents expressed in rotating reference d-q and L is the total inverter output inductance, sum of the switching inductance and that of the transformer LV/MV.

The signals thus obtained are reported in a synchronous reference to the voltages generated by the inverter, and then reported to the LV side of the transformer. Taking into account a suitable rotation to compensate the windings transformer connection, the controlled voltages can be used for the calculation of the three modulating signals. The switches are driven according to a sinusoidal Pulse Width Modulation (PWM), and the driving signals are generated by comparing the modulation signals with a fixed frequency triangular carrier waveform.

The PI regulators are designed to guarantee a dynamic stability according to the following specifications:

Table 2-5: Regulators features

	Gain bandwidth product	**Phase margin**
PI control on DC Side	4Hz	36°
PI control on AC Side	20Hz	83°

In Figure 2-16 the PI regulators step response are shown.

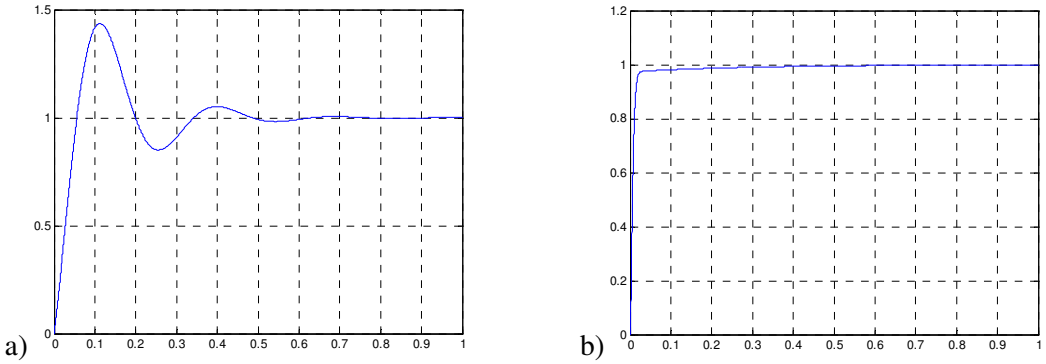

Figure 2-16: Regulator step response: DC side (a) and side AC (b)

2.2.5 Simulation in the absence of networks disturbances

The operation of the PV plant has been simulated in the steady state and transient condition, in order to verify the correctness of the design carried out. Figure 2-17 shows the trends during steady state of some characteristic quantities while Figure 2-18 shows the transient behavior of DC voltages and inverter currents. The transients have been caused by a step variation of the DC voltage reference.

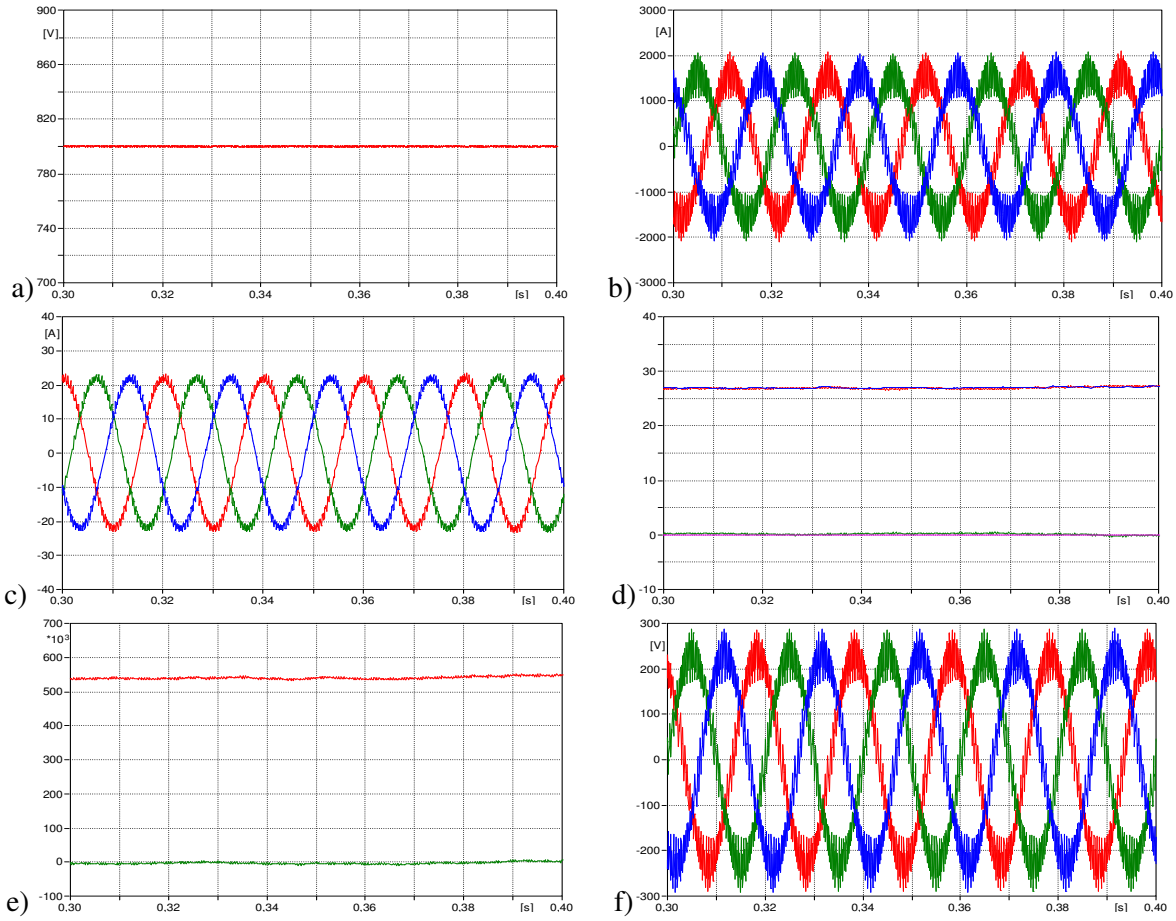

Figure 2-17: Steady state simulation: DC voltage (a), current inverter side (b) and network side (c), current axis d and q with reference values (d), active and reactive powers (e), phase voltages at the secondary of the transformer coupling (f)

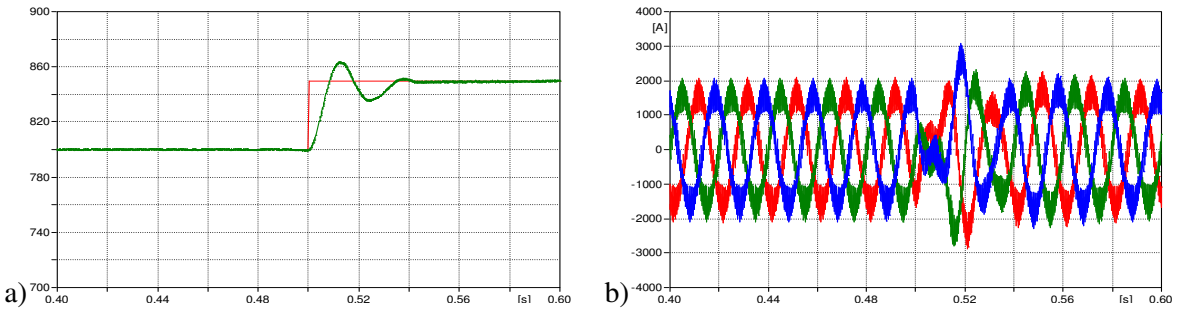

Figure 2-18: Transient behavior: DC voltage and reference value (a), currents through inductances of switching (b)

2.3 The model of power and control in a wind generator with permanent magnets and power electronics to interface to the network

Wind Permanent Magnet Synchronous Generator (PMSG) can be connected to a Medium Voltage (f.i. 20 kV) distribution network through two different configuration of power electronic circuits. In both cases there are:

- a wind turbine;
- a Permanent Magnet Synchronous Generator;
- a three phase grid side Voltage Source Inverter (VSI);
- a LV/MV transformer.

The difference between the two power plant topologies is related to the possibility to connect the generator to the inverter with a diode rectifier or a controlled rectifier.
The diode bridge rectifier generates an unregulated DC voltage from the AC outputs of the PMSG which supplies a boost DC/DC converter (Figure 2-19). This last is controlled with a current mode hysteresis band modulation which sets the current extracted from the generator. The DC/DC converter output voltage is the DC input of the VSI which regulates the voltage across the DC capacitor by controlling the power injected into the distribution network through the LV/MV transformer.

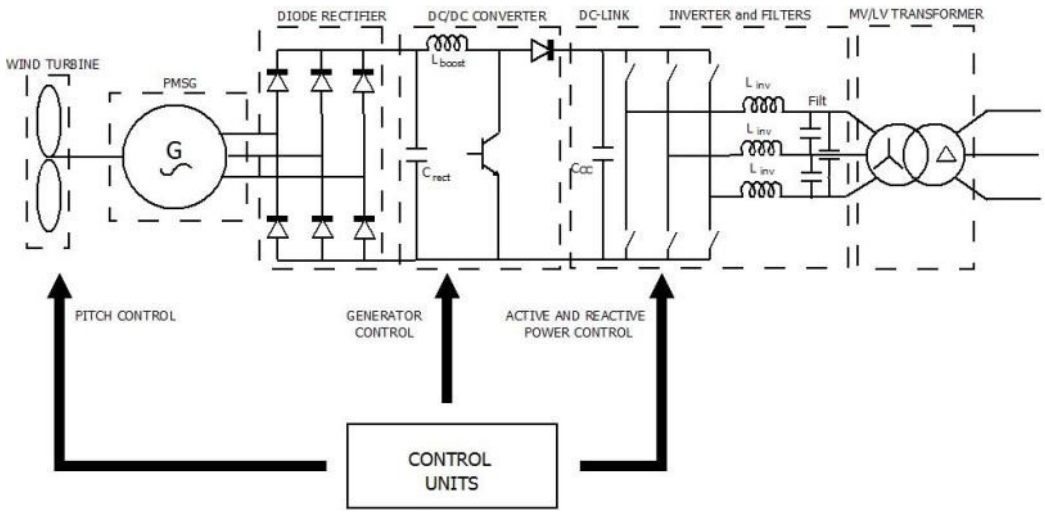

Figure 2-19: Schematic model of a wind synchronous generator with diode-rectifier

In the second plant configuration, the so called *full converter*[19], the use of two controlled power electronic stages (rectifier and inverter) connected through a DC-link (Figure 2-20) allows [40]÷[50]:

- a complete decoupling between grid and generator;
- the control of the active power generated by the PMSG, performed through the rectifier;
- the control of the active and reactive power supplied to the grid, performed through the inverter.

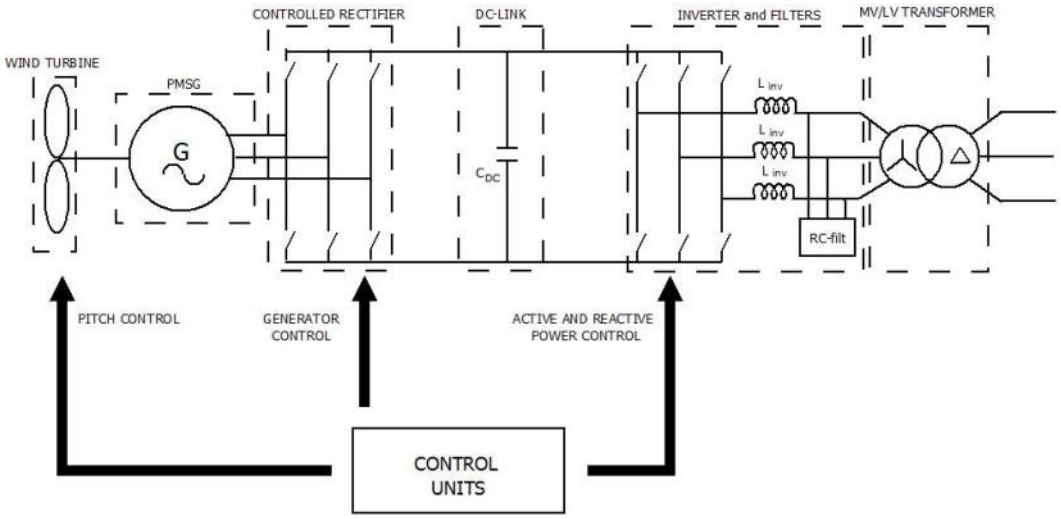

Figure 2-20: Schematic model of a wind synchronous generator *full-converter*

The choice between the two solutions is related to the overall system performance, depending on different voltage and current levels. Another important thing to consider is the cost. The different configurations have instead little impact on the behaviour of the system in case of voltage dips and in presence of Fault Ride Through requirements as it depends mainly on the behaviour of the grid converter (Chapter 3).
In the study both solutions have been analyzed, in detail the analysis results of the converter back-to-back that allows greater flexibility for the control of the converter generator side are given[20].

For the studies presented hereafter, a simplified PMSG model with a Thevenin equivalent has been realized in ATPDraw. The validation of the PMSG model is performed comparing its behaviours with a complete model developed in the environment Matlab/Simulink.
The complete model is composed of wind PMSG developed in Matlab/Simulink, (which takes into account the amount of generation, including the mechanical parts, and the AC/DC converter). The Thevenin equivalent consists of a voltage source connected with the impedances of the stator of the synchronous generator (made in ATPDraw). The verification of the equivalence has the purpose to confirm the possibility to perform the study with the generator representation with the simplified Thevenin model. More details, relating to such equivalence and the conditions postulated for the demonstration are given below.

2.3.1 Wind Turbine

For the simulations purposes the mechanical part of the system has been not modeled, mainly represented by wind turbine and the drive shaft that connects it to the generator rotor. The choice of not represent that section of the system derives from the fact that its dynamics are purely mechanical and therefore time constants are longer than electrical phenomena investigated by the simulations. In particular, these mechanical phenomena include:

[19] This configuration of the connection between the two power converters adopted in these generators is also called back-to-back.
[20] For example, it's possible to adjust the stator currents also setting a null reactive power generator injection.

- fluctuation in the drive shaft rotation speed, due to the elasticity of the shaft torsion itself;
- variations in the inclination angle of the blades with respect to the wind direction (angle of pitch), used as a system for the Maximum Power Point Tracking of the generator (MPPT)[21][45].

Therefore, in these simulations, it is considered that the wind turbine has a constant rotation speed without oscillations, therefore the generator frequency, synchronous to this speed, is also constant.
The power extracted from the wind by the turbine blades is given by:

$$P = \frac{1}{2}\rho\pi r^2 C_p(\lambda,\beta)v_w^3 \tag{2.16}$$

where ρ is the air density, r is the blade radius, v_w is the wind speed and C_p is the power coefficients, depending on the tip speed ratio λ and on the pitch angle β of the blades. λ is equal to the ratio of the blades speed and the wind speed. The dependence of C_p on λ and β is shown in the following figure [47].

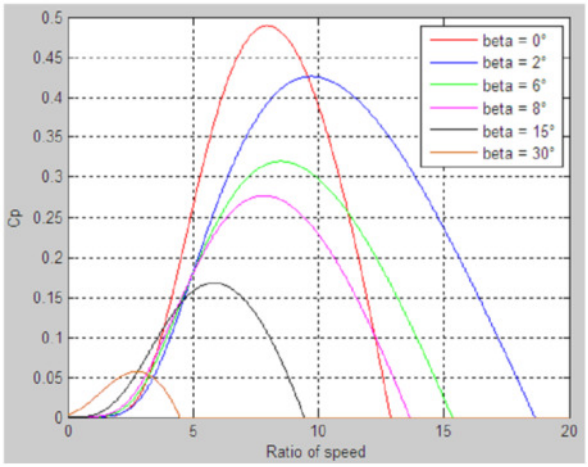

Power curves dependencies from tip speed ratio at different pitch angles

2.3.2 Permanent Magnet Synchronous Generator

Even though Double Fed Induction Generators (DFIG) are still preferred for large installations, Permanent Magnet Synchronous Generator (PMSG) are becoming more and more popular due to higher mechanical reliability and the possibly to avoid the weak point of the gearbox.
The studies of the interactions between the generation system and the grid requires the development of simulation models of PMSG, power electronic converters and their controls.
Below the implementation of a simplified model of a PMSG interconnected to a distribution grid with power electronic circuits has been described. The validation of the PMSG model is performed comparing its behaviors with a complete model developed in the Matlab/Simulink environment.

The simplified model of a wind PMSG system has been developed into the environment Alternative Transient Program Draw (ATPDraw). The 2 MVA PMSG is here represented through an ideal three phase voltage generator with leakage inductances and resistances connected in series to the outputs (Thevenin equivalent) [48]. Such a simplification in the generator representation, that should be

[21] In the case of PMSG, the search for the maximum power point can be made only by acting on the inclination of the blades, while, for the common wound-rotor synchronous generators, the algorithm of MPPT may also act by varying the generator rotor current.

validated, allows reducing the computational complexity to evaluate the solution of (2.18). In this way, it is possible to insert the simplified PMSG model within larger system in order to perform study of Distributed Generators (DG) integration within complex distribution grids. The model validation is discussed in the next section.
Neglecting the dynamic mechanical and electromagnetic, as earlier mentioned, the frequency of the synchronous generator is considered to be constant and equal to:

$$f_{gen} = f_{te} n_{pp} \tag{2.17}$$

where f_{te} is the frequency of rotation of the wind turbine and n_{pp} is the number of pairs poles of the generator.

2.3.2.1 PMSG complete model

The system considered is composed of: a PMSG, a rectifier with IGBT, controlled by a suitable control system, a capacitor connected to the DC output of the rectifier and a resistor connected in parallel with this capacitor, with load function. There is no need to introduce models of inverters and network since the presence of stage of straightening driven decouples the dynamics of the wind turbine and the synchronous generator from that of the other parts of the system (Figure 2-22).

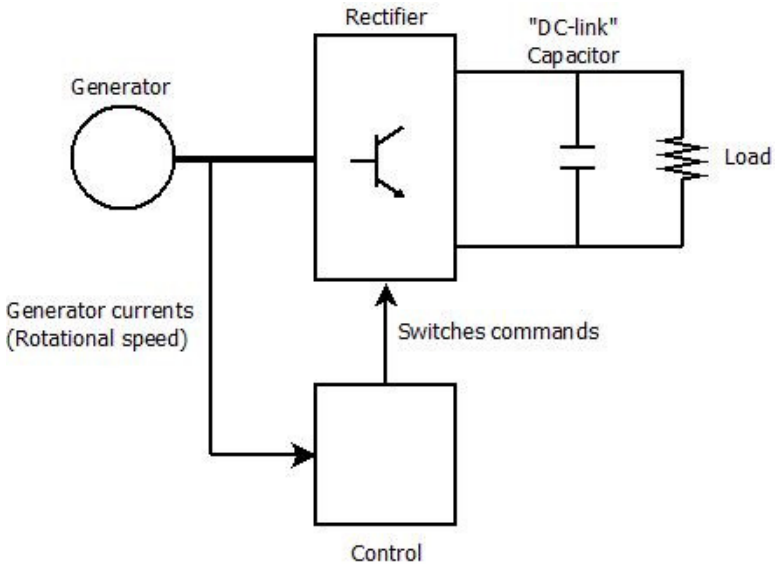

Figure 2-21: Block scheme Simulink model of a PMSG

The resistive load connected in parallel to the output capacitor of the rectifier (Figure 2-21) is designed to dissipate the power rating of the generator with DC voltage equal to 1100 V[22]. Therefore, the value used is:

$$R = \frac{V_{dc}^2}{P_N} = \frac{1100^2}{2 \cdot 10^6} = 0.605 \quad \Omega \tag{2.18}$$

The dynamic equations governing the operations of a PMSG are:

[22] This voltage is used as the reference voltage for the inverter control and therefore represents the nominal voltage for the exercise of the DC bus.

$$\begin{aligned}
\frac{di_d}{dt} &= \frac{\omega_N}{x_d}\left[v_d - r_s i_d + n x_q i_q\right] \\
\frac{di_q}{dt} &= \frac{\omega_N}{x_q}\left[v_q - r_s i_q - \left(x_d i_d + \psi_M\right)n\right] \\
T_e &= \psi_M i_q + \left(x_d - x_q\right) i_d i_q \\
\frac{dn}{dt} &= \left[T_e + T_m - Bn\right]
\end{aligned} \tag{2.19}$$

where the values are expressed in p.u. and have the following meaning:

- i_d, i_q: generator currents over axis d and q;
- v_d, v_q: voltages over axis d and q;
- ω_N: rated electric angular frequency;
- n: turbine rotational speed;
- x_d, x_q: stator reactance over axis d and q;
- r_s: stator resistance;
- ψ_M: rotor permanent magnet flux;
- T_e, T_m: electromagnetic and mechanical torque;
- B: friction coefficient.

All these quantities are expressed in a d-q rotating frame synchronous to the PMSG rotor flux. In a round rotor machine for which x_d=x_q, from the last two equation it emerges that the generator active power is proportional to the quadrature-axis current (i_q) which is the main electrical control parameter. The inputs of the system are the voltages generated by the controlled rectifier, which has been also represented as an averaged model in Simulink. The inputs of the PMSG are the voltages generated by the rectifier, expressed in the rotating d-q frame, and its outputs are the d-axis current, the q-axis currents and the angular speed of the generator[23], which are used as inputs for the rectifier control.

A detailed model of a PMSG has been developed in the environment Matlab/Simulink implementing the equations (2.18) through Simulink blocks, as represented in Figure 2-22, and the main features are reported in Table 2-6.

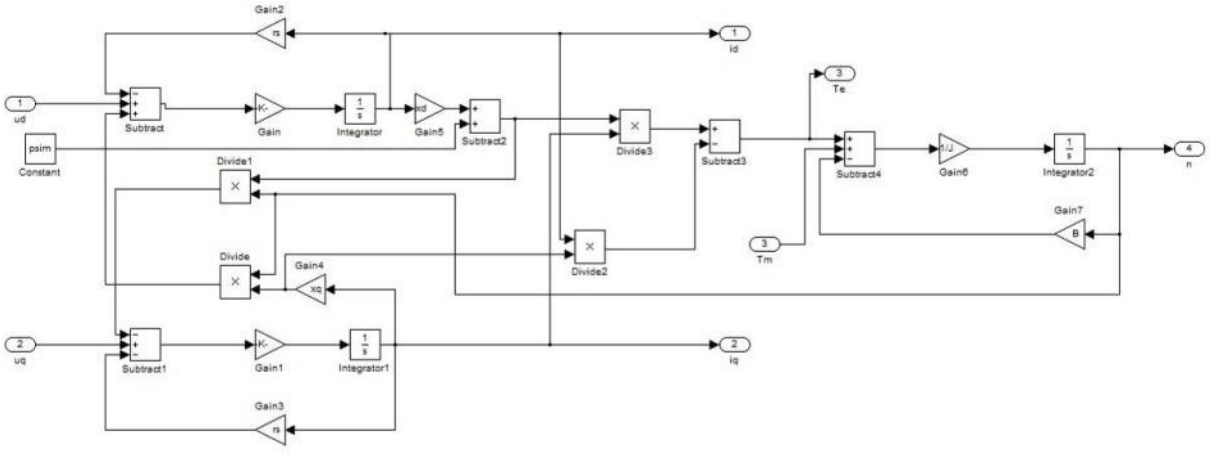

Figure 2-22: Matlab/Simulink detailed implementation of a PMSG

[23] Considering the relation between the angular and the rotational speed $\omega = \frac{2\pi n}{60}$.

Table 2-6: PMSG main design parameters

Magnitude		Value
Rated Power	A_N	2 MVA
AC Voltage	V_{CA}	230 V_{rms}
Rotational Speed	ω_N	$2\pi 30$ rad/s
Stator resistance	r_S	0.02 p.u.
Reactance axis d	X_d	0.5 p.u.
Reactance axis q	X_q	0.5 p.u.
Magnetic rotor flux	ψ_M	0.865 p.u.
Moment of Inertia	J	4 p.u.
Friction mechanical coefficient	B	0.01 p.u.

2.3.2.2 IGBT rectifier: model and control

The controlled rectifier circuit allows the generation of three voltages as outputs of the PMSG with wanted amplitudes and angles acting on the open/close status of the six controlled switches. The currents supplied by the PMSG depends on these voltages and on the leakage inductances of the generator. Starting from the equations (2.18) it is convenient to express voltages over d-q axes, so that the regulator can control the direct and quadrature current exchanged by the generator. Even though different control schemes are applicable, here the so called *field oriented control* (*Field Oriented Control - FOC)* has been implemented. This control aims to maximize the power extracted from the generator and, therefore, includes an MPPT algorithm.

A field oriented control scheme presents two branches: one of the speed of rotation "outside" and one of the stator current "inside" in a reference system over axis d-q where the electromagnetic torque (and therefore, the speed) is controlled by the control of the component over q-axis:

$$T_e = \psi_M i_q \tag{2.20}$$

The reference of the current i_q is obtained from the outer ring of the control. In the case of the "simplified" representation of the generator, the structure of the current loop has been maintained, whereas the active power "extracted" from the generator equivalent must be adjusted by varying the d-axis reference of the stator current. In particular the equivalence between the models has been verified by imposing a reference current over axis d to extract the active power rating of the generator when it rotates at the angular speed rating.

The active power delivered by the generator is transferred entirely to the capacitor DC-link, in the absence of further systems connected to it, the voltage across its terminals would increase. The modulation of the converter is a Pulse Width Modulation (PWM).

The outputs i_d and i_q of the model (Figure 2-22) represent respectively the currents supplied by the generator over the d-q axes, these should then be transformed into phase quantities, i.e. current physical, and sent to the rectifier control. In the model implemented, in order to further simplify the simulations, the control of the converter receives as input the current magnitudes already expressed on rotary axis, even though they are not the physical quantities that would be measured in reality. The phase currents are calculated "offline" to allow a more simple and intuitive view of the transients. The same is done for the control output voltages, which are sent as inputs to the model of synchronous generator described here.

The implemented control acts independently on quantities expressed over the d-axis and the axis q, in accordance with the logic described by the Matlab/Simulink scheme in Figure 2-23.

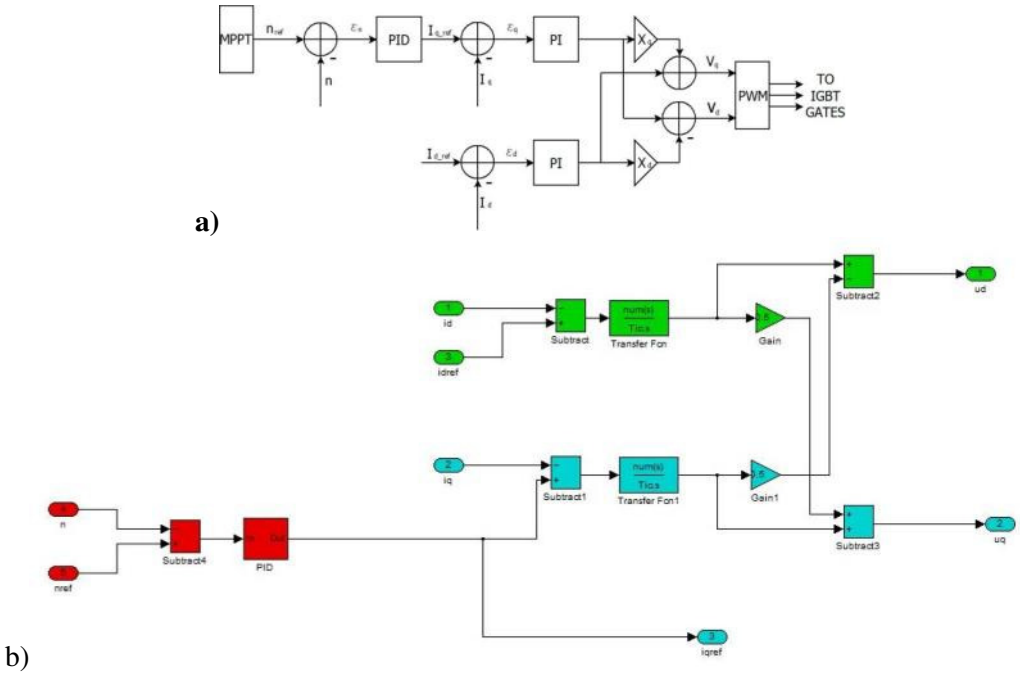

Figure 2-23: Scheme rectifier control (a) and Matlab/Simulink implementation (b): the colors distinguish the three control sections. Red: control of angular speed; blue : current control over axis q; green : current control over axis d

In the adopted control scheme, the rotating speed of the PMSG rotor (n) is compared to a reference value (n_{ref}), calculated by a Maximum Power Point Tracking (MPPT) loop, and the speed error is processed by a Proportional-Integral-Derivative (PID) regulator, in the form:

$$H_{PID\_1}(s) = k_{pw}\left(1 + \frac{k_{iw}}{s} + sk_{dw}\right) \tag{2.21}$$

where k_{pw}, k_{iw} and k_{dw} are numerical coefficients, respectively proportional, integral and differential gain. The output of the PID regulator represents the q-axis current reference for the rectifier, while the d-axis reference is kept to zero in order to minimize losses. Both current references are compared with the relevant current values and errors are processed by two Proportional-Integral (PI) regulators, in the form:

$$H_{PID\_2}(s) = k_{pc}\left(1 + \frac{1}{\tau_{ic}s}\right) \tag{2.22}$$

where k_{pc} is the proportional gain and τ_{ic} the integral time constant. The dimensioning of the magnitudes and the coefficients of the control that is used for the system under test and reported in Table 2-7.

The control scheme aims to maximize the power extracted from the wind adjusting the speed of the wind turbine so that it is equal to a value of optimal reference. The optimal value depends on the speed of the wind and from the angle of blades attack and, usually, varies during the wind generator operation. For the purposes of the following simulations, since transients in wind speed variations or in the angle of blades attack are not introduced, a true search algorithm of the maximum power point is not implemented, but the value of the reference rotational speed is held constant at a calculated optimum value.

Table 2-7: Design the rectifier control IGBT

Magnitude	Value [p.u.]
n_{rif}	1
i_{drif}	0
k_{pw}	1
k_{iw}	0.8
k_{dw}	0.01
K_{pc}	2
τ_{ic}	0.5

2.3.2.3 Results of simulations for the verification of the equivalence of the models

The validation of the simplified model is made by comparing its dynamic behaviour with that of the Matlab detailed model. Even through the following differences should be considered:

- in the Thevenin equivalent model active power is proportional to the d-axis current, while in the detailed model it is proportional to the q-axis current;
- similarly, the reactive power is proportional to the q-axis current for the simplified and to the d-axis current for the detailed model;
- the simplified model rotational speed is fixed, while in the detailed model it can vary around the reference value during transients; so in the simplified model there is no need to check the voltage generator angular speed, which is placed beforehand equal to the rated value; therefore, it is not necessary the section of the control relative to the adjustment of speed (red blocks in Figure 2-23);
- the voltage output of the detailed model can vary, while for the Thevenin equivalent it is fixed at its nominal value.

The simulations of the two systems have been conducted in Matlab/Simulink where a step change of generated active power has been simulated after 20 s: in particular the available power from the wind is reduced of 50% as a result of a decrease in the wind velocity. The decrease in power of the primary source has been simulated in two different ways:

- for the PMSG decreasing appropriately the value of the mechanical moment of the turbine;
- for the ideal voltage generator reducing of 50% the rectifier reference d-axis current.

In a first step, the value of the moment of inertia of the PMSG is chosen in accordance with the machine design equal to a realistic value considering the physical dimensions of a generator of this size of power. However with this value transients characterized by very long constant time are obtained of the order of J/B (in this case corresponding to 400 s), which cannot be replicated during the simulations involving the ideal voltage generator, without the model of the system mechanical parts. For a comparison of the two systems therefore, it has been decided to assign a sufficiently small value at the moment of inertia of the machine, in particular, J = 0.5 p.u.

Dynamic comparisons have been made for a 2 MVA PMSG. Simulation results for both models are reported in Figure 2-25 where in particular:

a) Angular frequency of the generator and its reference value;
b) Current axis d and its reference value;
c) Current of q-axis and its reference;
d) Phase voltages of the generator;
e) Phase currents of the generator;
f) Active generated power;
g) Measured Voltage DC side of the inverter.

As it can be seen, the dynamics of the simplified model is very close to that of the detailed model, a part from the unavoidable differences already pointed out. The detailed model seems to shows less dumped dynamics, probably due to the absence of parasitic in the model of the rectifier and to the missing interactions with the inverter dynamics. For the purposes of this study the two models are equivalent, also considering that both the DC-link capacitor and the inverter decouple the PMSG from the distribution grid. For this reason, all the studies reported hereafter have been performed with the ATPDraw simplified model only.

Synchronous generator **Ideal Generator**

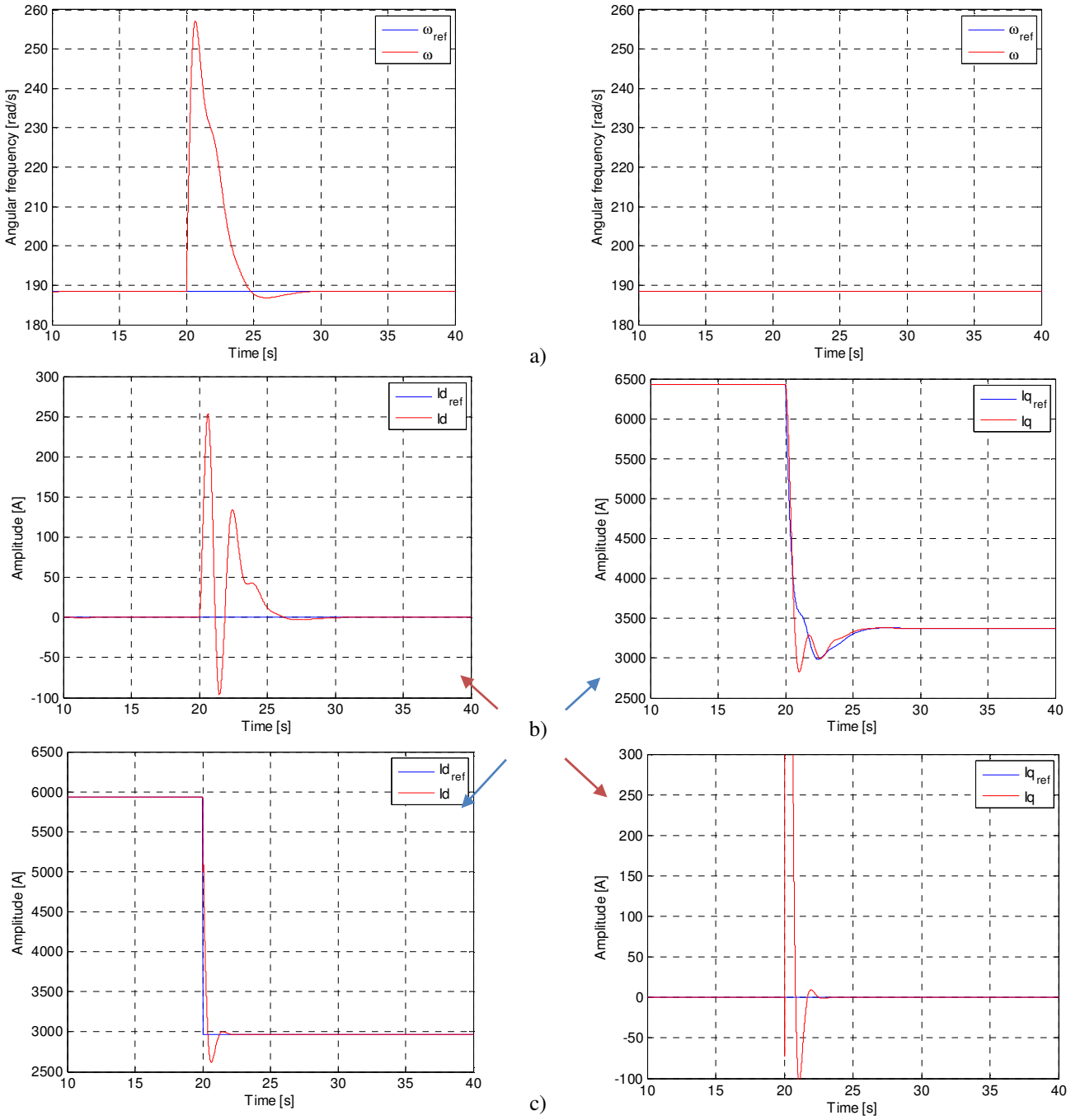

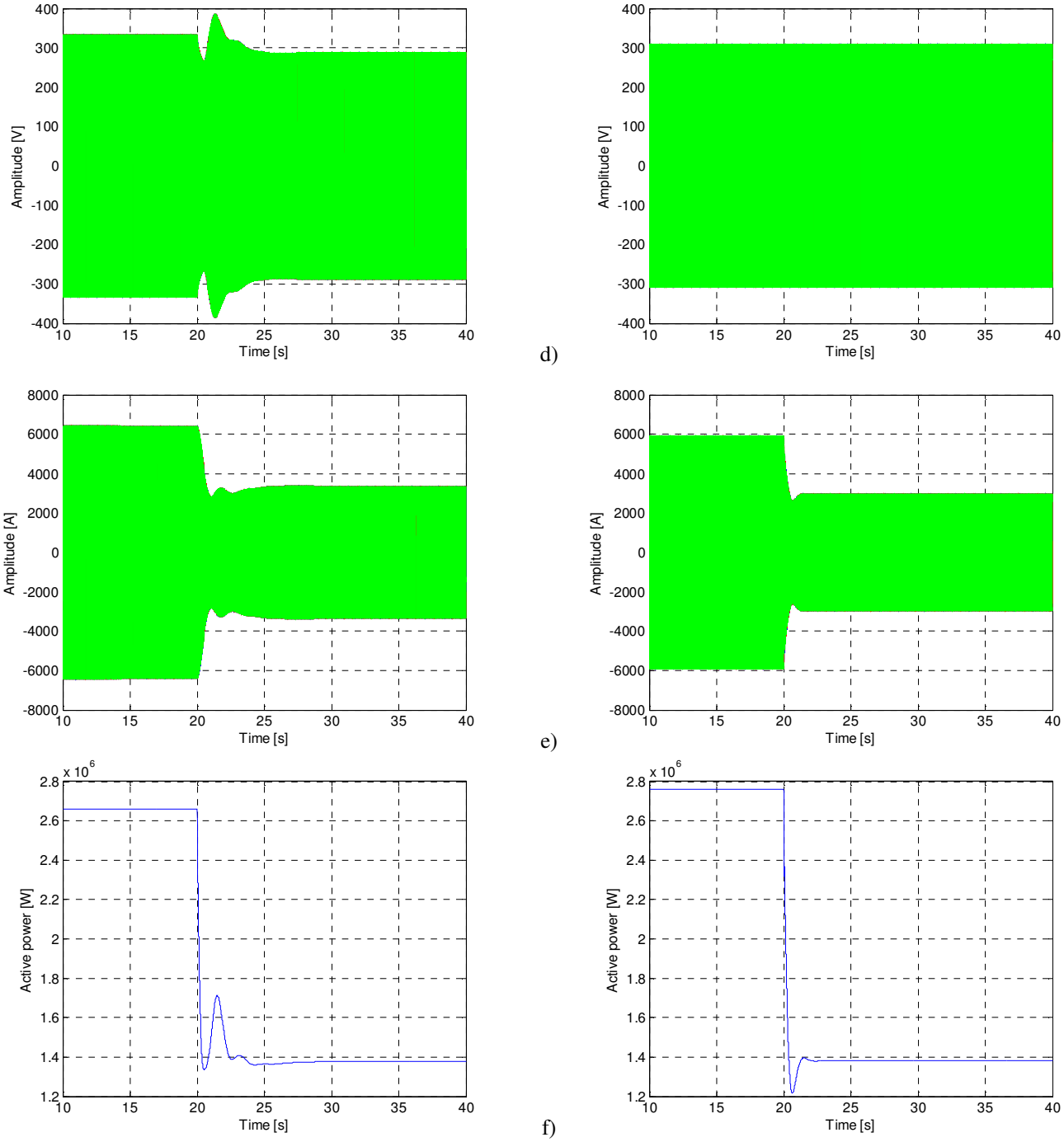

Figure 2-24: Generator dynamic behaviour calculated from the detailed model of a PMSG and from the simplified model in case of a step change of the active power. It should be noted that i_d and i_q exchange their role in the two models

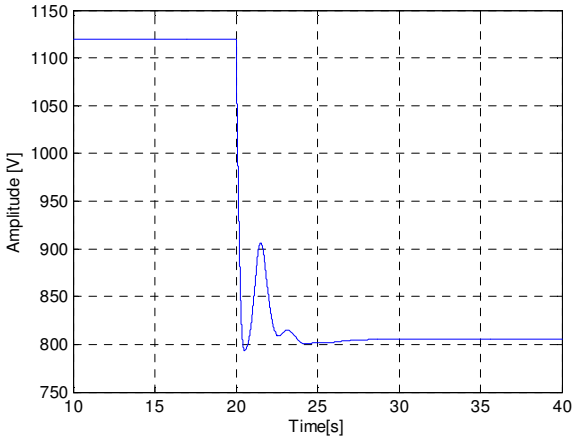

g)

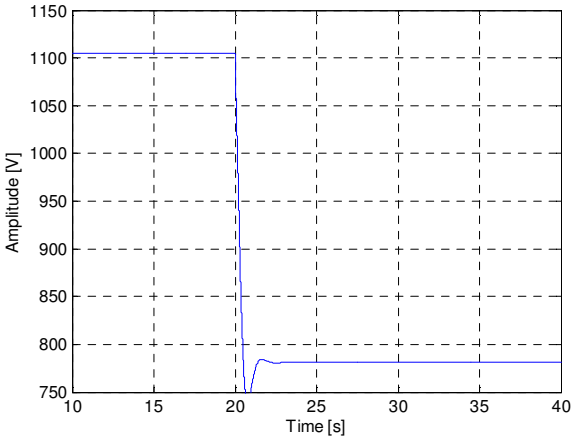

Frequency variations of the synchronous generator

In this section the behavior of the generator is analyzed, and in particular its speed of rotation, as a result of an unbalance between the electrical power consumed from the rectifier and the extracted from the wind by the wind turbine. The results of such analysis will allow to:

- emphasize the possibility of modeling the synchronous generator with a voltage generator;
- evaluate control strategies for the wind power plant to use when during network faults that can introduce variation in the power absorbed by the IGBT rectifier.

The mechanics equation relevant to the generator angular speed variation is:

$$\dot{\omega} = \frac{1}{J}\left(T_e + T_M\right) = \frac{P_e + P_m}{J\omega} \tag{2.23}$$

where:

- ω: angular speed;
- J: moment of inertia of the system (given by the generator, wind turbine and the blades);
- T_e: electromagnetic torque of the generator;
- T_m: mechanical torque of the turbine;
- P_e: electric power drawn by power electronic converters across the terminals of the generator;
- P_m: mechanical power of the turbine.

In the equation (2.23) the mechanical friction coefficient is neglected, however, it would have the effect of further reducing the rotation speed variations. It has been adopted the convention for which the mechanical moment and the mechanical power have a negative sign when the system is working as a generator, while positive one if it worked as a motor. The dynamic response of the system to a step of torque coming from the turbine has been simulated in Matlab environment by varying two parameters and maintaining constant the others, in particular:

- $0{,}5\,pu \le J \le 5\,pu$ (for a power generator 2 MVA it's equivalent to $1\cdot 10^6 kg\cdot m^2 \le J \le 1\cdot 10^7 kg\cdot m^2$);
- $0\,pu \le P_e \le 1\,pu$;
- P_m constant= 1 p.u.;
- constant wind speed = 1 p.u.;
- blades attack angle constant = 0 degrees.

The simulation time has been equal to 10 s, time much longer than the typical time constants of the voltage dips that abut the hundreds of milliseconds. Figure 2-25 shows a complete transient of the rotational frequency of the generator, expressed in p.u., with P_e = 0.8 p.u. and J=0.8 p.u. In Figure 2-26 the frequency variations is reported measured after 10 s, expressed in percentage points and obtained by varying these two parameters.

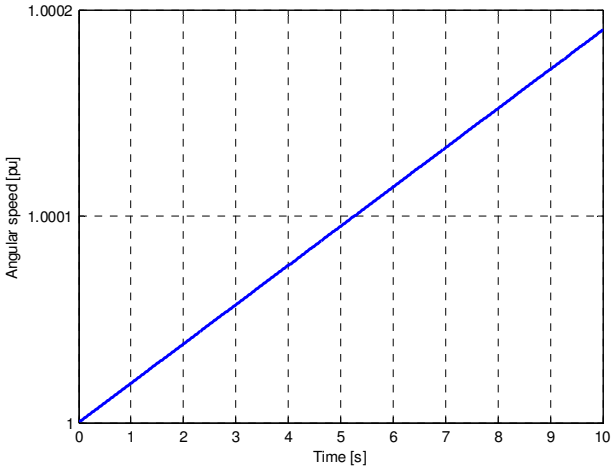

Figure 2-25: Transient variation of the rotation speed of the wind generator

The frequency variations are very limited, even for times longer than those typical of electrical disturbances for example the voltage dips. Therefore, the rotation speed of the generator on short periods can be considered constant, confirming the hypothesis to replace, for the type of phenomena under investigation, the wind generator complete model with a simplified model.
In addition, the choice of not model in detail the generator is also justified by the fact that, considering that to the aim of the activity is to study the interactions between wind power generation and distribution network, the presence of stages of power electronic makes independent the generator from electrical network, and vice versa. Therefore, disturbances in the operation of the wind generator does not have consequences on the network behavior, in a first approximation, and thus it's possible to simplify the model of the generator.

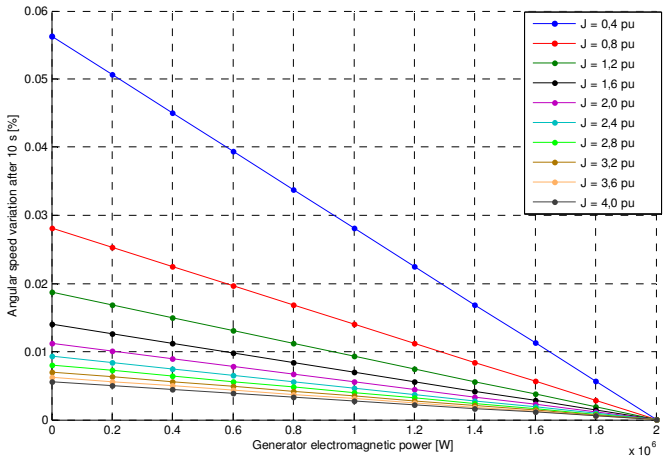

Figure 2-26: Percentage variation of the speed of rotation of the generator after 10 s

2.3.3 Converters and transformers for connection to the network of a wind generator

In the back-to-back configuration, the use of an intermediate section composed of electronic power circuits, as already said, allows to decouple the generator and the wind turbine from the distribution network. In particular, the system composed of the wind turbine and the generator can operate with a frequency different from the network one, allowing to not insert a reducer mechanical gear box between turbine and generator, which represents a criticality in terms of reliability and efficiency of the entire system. Furthermore, the presence of the connecting stage with rectification function allows to make insensitive, within the limits dictated by the control loops of the same circuits, the value of the inverter DC voltage from the turbine rotation speed, which ultimately depend on the speed of the wind and the blades pitch angle.

For the study, the same inverter used for the generator of photovoltaic type (§ 2.2.30) has been taken into consideration and in particular a three phase inverter based on the topology full-bridge controlled with pulse width modulation (Pulse Width Modulation - PWM) at a fixed frequency [49]. Both the generator side converter and the network side are designed for a rated power of 2 MVA. There is an isolation transformer for the connection to the MV network. For the purpose, a 3 MVA MV/LV transformer has been modeled, overdesigned to allow to manage power peaks during transients. The main parameters design of the two converters and the transformer are reported in Table 2-8.

Table 2-8: Main specification for the inverter and the transformer

DC Side inverter			
Rated Voltage	V_N	1100 V	
Maximum Voltage	V_{dcmax}	1400 V	Maximum reverse voltage of the valves
Capacitance	C_{dc}	100 mF	
Rectifier and Inverter			
Rated Power	A_{Ninv}	2.5 MVA	
Inductance switching	L_{inv}	7.64 μH	0.04 p.u.
Filter Resistance	$R_{filt,inv}$	10 mΩ	
Filter Capacitance	$C_{filt,inv}$	5 mF (f_r = 814 Hz)	
Switching Frequency	f_{sw}	1950 Hz	Fixed Frequency
AC voltage	V_{CAn}	400 V	
Nominal Current (@P_{nom})	I_N	3.6 kA	For each phase, in LV
Maximum switched current with continuity from valves	I_F	6 kA	
Maximum peak current that can be delivered by the valves	I_{FRM}	12 kA	
Transformer			
Rated Power	A_N	3 MVA	
Leakage Inductance	L_k	3.5 μH	0.07 p.u. [38]
Short Circuit Resistance	R_{dc}	0.16 mΩ	0.01 p.u.
Turns Ratio	N	20000/220	
Winding coupling		Dy11n	

Fixed the design, the inverter capability curves are shown in Figure 2-27 and Figure 2-28 respectively the nominal and the transient ones for different network voltage condition (0.9, 1 and 1.1 p.u.).

a) b)

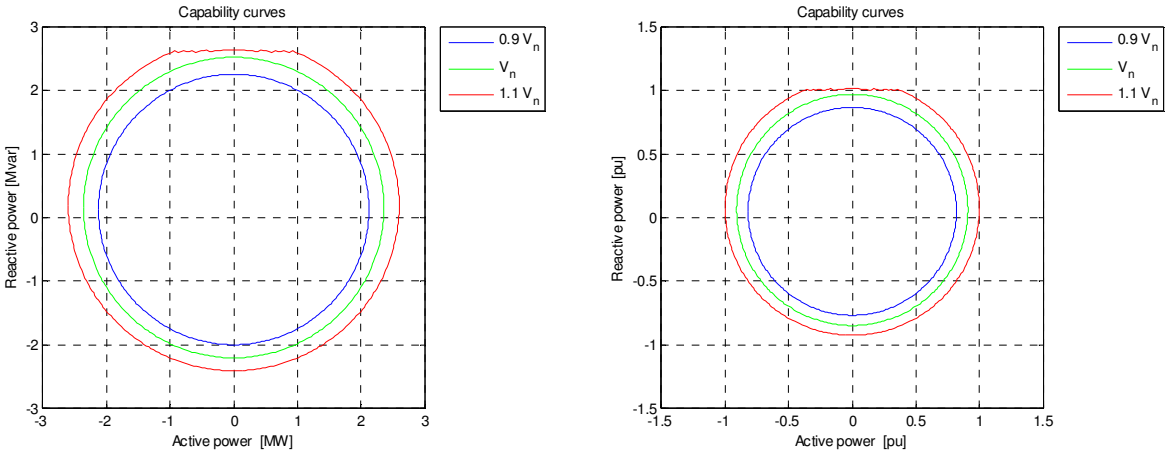

Figure 2-27: Inverter nominal capability: absolute values (a) and p.u. (b)

a) b)

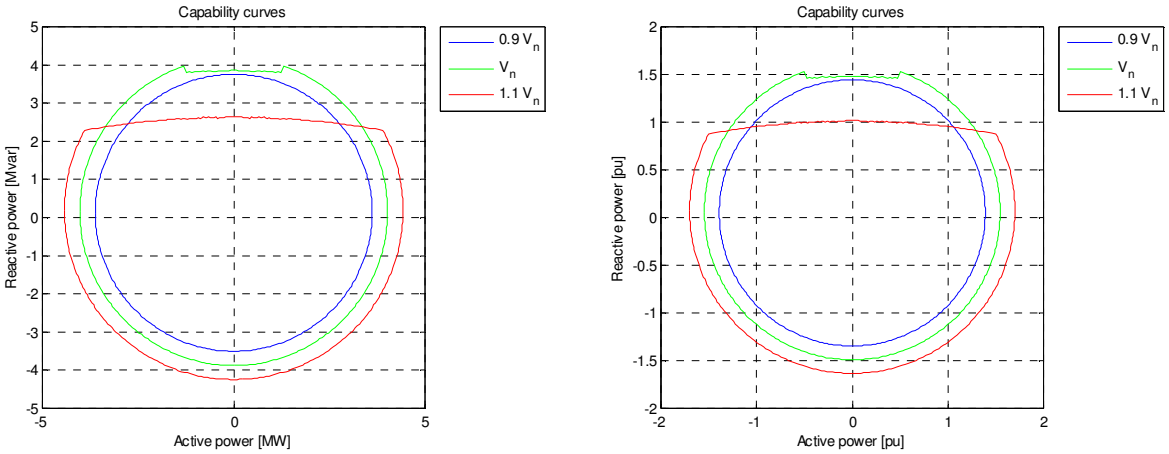

Figure 2-28: Inverter transient capability: absolute values (a) and p.u. (b)

2.3.4 Control and modulation strategies of the converters

2.3.4.1 *Control of the AC/DC generator side converter*

In [50], for the AC/DC converter, a field oriented control strategy is presented, which aims to maximize the power extracted from the generator and, therefore, is actually an extraction of the MPPT, as already mention in §2.3.2.2. The modulation is a Pulse Width Modulation (PWM). This type of control is characterized by a ring of current with references over rotating axis d-q and the adopted scheme is shown in Figure 2-29. The current reference over d-axis is chosen to extract from the generator its nominal active power, when it rotates at the angular speed rating. Variations in the speed of the wind turbine cause power variations proportional to the extracted one from the generator. In the simplified model of generator, represented by Thevenin equivalent, the variations in the speed of the turbine has been simulated with variations in the amplitude and frequency of the voltage of the equivalent generator. The active power exchanged by the generator is transferred to the capacitor DC and the voltage across its terminals would increase, in the absence of further systems connected to it.

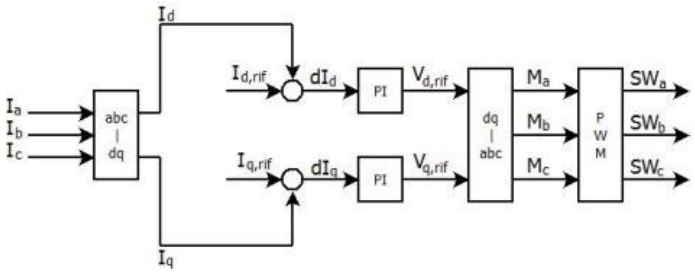

Figure 2-29: Simplified control scheme of the rectifier AC/DC

The PI regulator is designed to guarantee a dynamic stability according to the following specifications:

Table 2-9: Rectifier regulator features

Rectifier Control			Gain bandwidth product	Phase margin
PI regulator	$H_{PI,r}(s)$	$\frac{0{,}1s+2}{s}$	13kHz	90°

In order to test the effectiveness of the control that is used and validate the design compared to theoretical predictions, simulations in response to a step variation of the d-current reference have been carried out: Figure 2-30 shows the regulator step response.

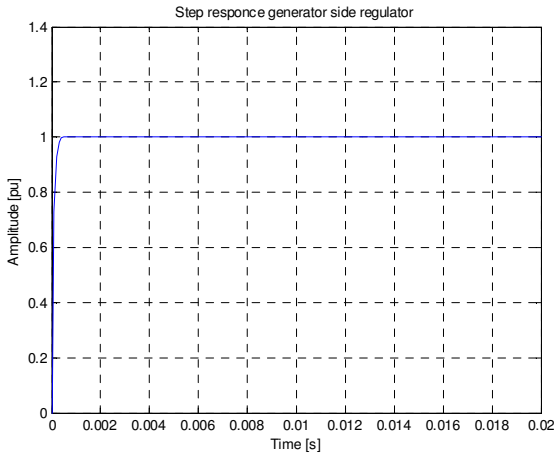

Figure 2-30: Regulator generator side converter: step response

2.3.4.2 Control of the DC/AC network side converter

The Voltage Source Inverter (VSI) topology employed is a three-legs bridge with IGBT switches. The control scheme for the VSI is represented in Figure 2-31, and it's the same used for the photovoltaic generator (§ 2.2.4.4).

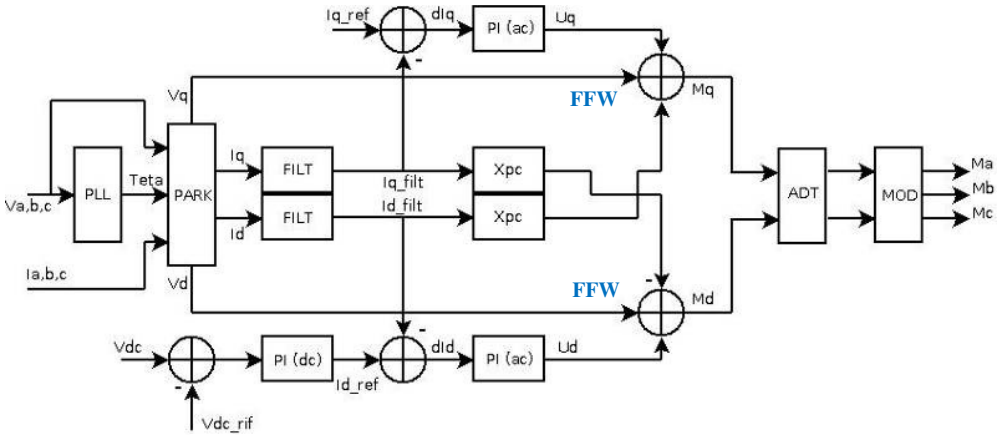

Figure 2-31: Block diagram of the control strategy base

Also in this case, the control aims to regulate the inverter currents represented over the rotating d-q axes. In this case, the rotating frame is synchronous to the grid voltages. In this way it's possible to control separately the inverter active power, proportional to the i_d current, and the inverter reactive power, proportional to the i_q current. The i_d reference value is calculated by an outer voltage loop processing with a PI regulator the difference between the DC-link voltage and a reference value. The DC-link voltage is maintained constant and all the active power coming from the rectifier is injected into the grid. In fact:

$$V_{dc} = \cos t \Rightarrow \frac{dV_{dc}}{dt} = 0 = \frac{I_c}{C} = \frac{1}{CV_{dc}}\left(P_{raddr} - P_{inv}\right) \Rightarrow P_{raddr} = P_{inv} \tag{2.24}$$

where V_{DC} is the DC-link voltage, i_C is the DC-link capacitor current, $i_{rect,DC}$ is the DC current of the rectifier, $i_{inv,DC}$ is the DC current of the inverter, P_{rect} is the active power of the rectifier and P_{inv} the active power of the inverter.

The q-axis current reference is usually set to zero in order to minimize conduction losses but different values can be possible in some cases, according to different National Standards. For instance the Italian Standard [3] requires that the inverter should exchange reactive power in case of grid under-voltage or over-voltage. For this reason, a suitable outer loop for the calculation of the i_q reference has been added to the control.

The PI regulators are designed to guarantee a dynamic stability according to the following specifications:

Table 2-10: Inverter regulators features

Inverter Control			Gain bandwidth product	Phase margin
DC voltage PI regulator	$H_{PI,vinv}(s)$	$\frac{0{,}0289s+1}{0{,}009s}$	40Hz	50°
Current PI regulator	$H_{PI,iinv}(s)$	$\frac{0{,}2769s+1}{0{,}0028s}$	2kHz	25°

In Figure 2-32 the inverter regulators step responses are shown.

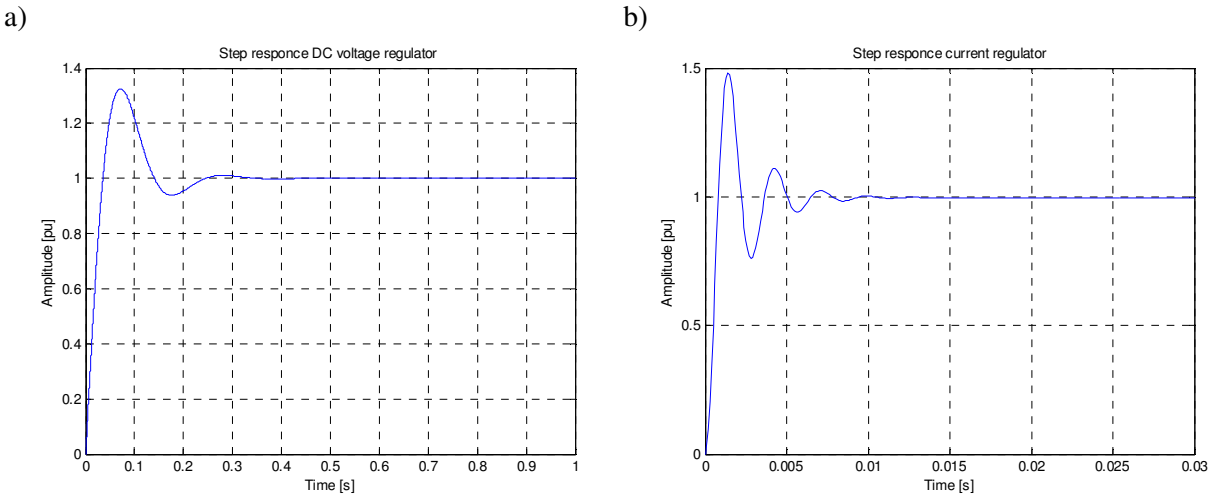

Figure 2-32: Step response of converter network side regulator: DC voltage (a) and current regulator (b)

2.3.5 Simulation in the absence of networks disturbances

The operation of the back-to-back wind generator has been simulated during steady state and transient condition, in order to verify the validity of the carried out design.

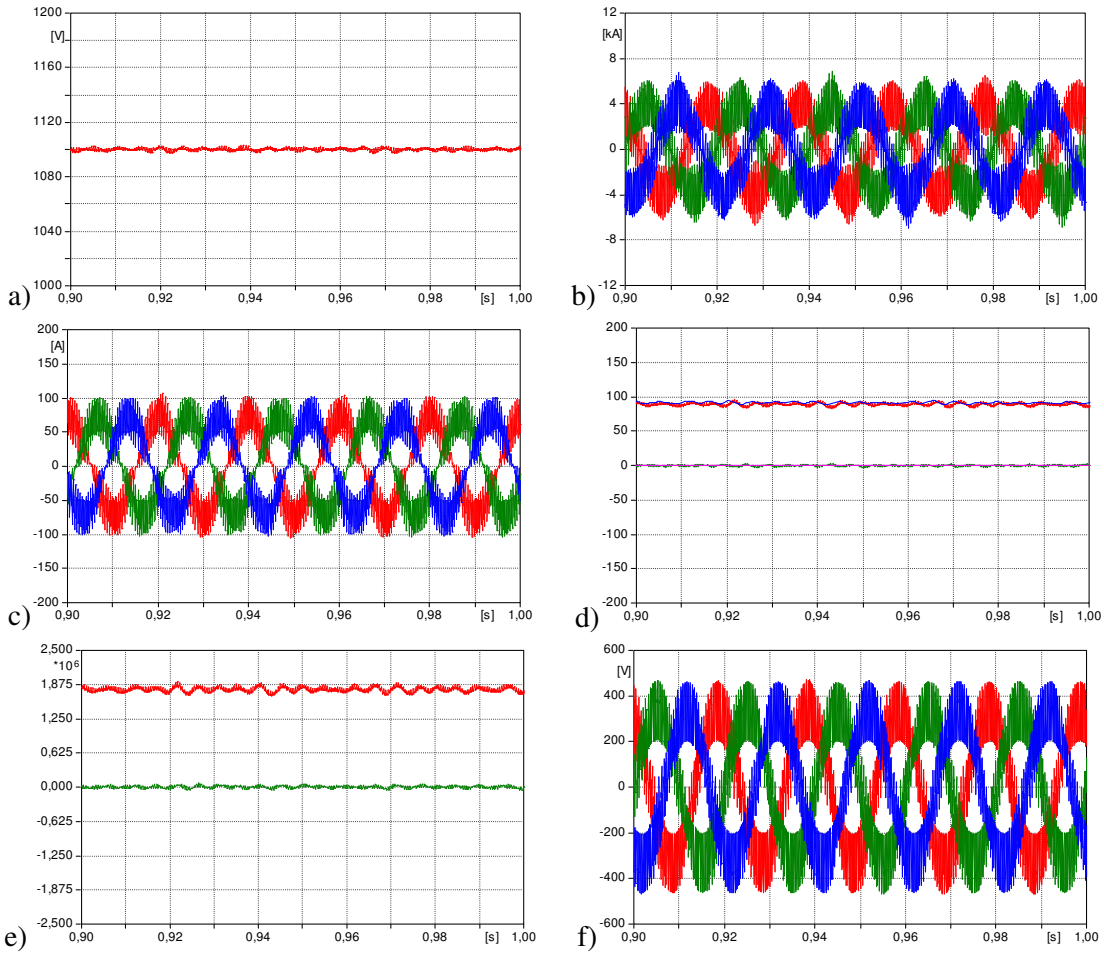

Figure 2-33: Steady state simulation: DC voltage (a), current inverter side (b) and network side (c), current axis d and q with reference values (d), active and reactive powers (e), phase voltages at the secondary of the transformer coupling (f)

It has been also simulated the behavior of the system in case of a step variation of the reference current over q-axis. Figure 2-34 shows the system response characterized by the same dynamics evaluated theoretically in Figure 2-32b.

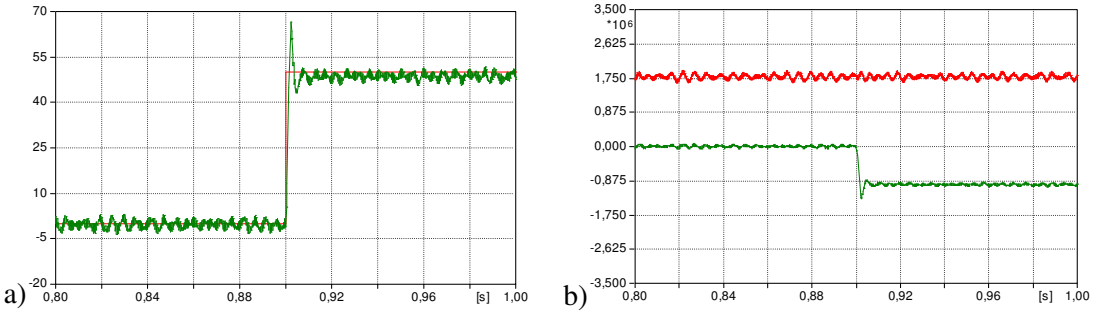

Figure 2-34: Transient behavior of the system back-to-back in case of a step of the q-axis reference current: q-axis current and its reference (a), evolution of active powers (red curve) and reactive (green curve) (b)

2.4 Final Considerations

The models developed in the course of the activities provide an adequate basis for a general methodology to study different control logics to connect Distributed Generators (DG) to the network. In the next Chapters the study results of the behaviour of these generators connected to the network through converters based on power electronics in case of voltage dips and unbalanced network conditions will be presented.

2.5 Structure simulated model in ATPDraw

Network model and control implemented in ATPDraw for the photovoltaic generator.

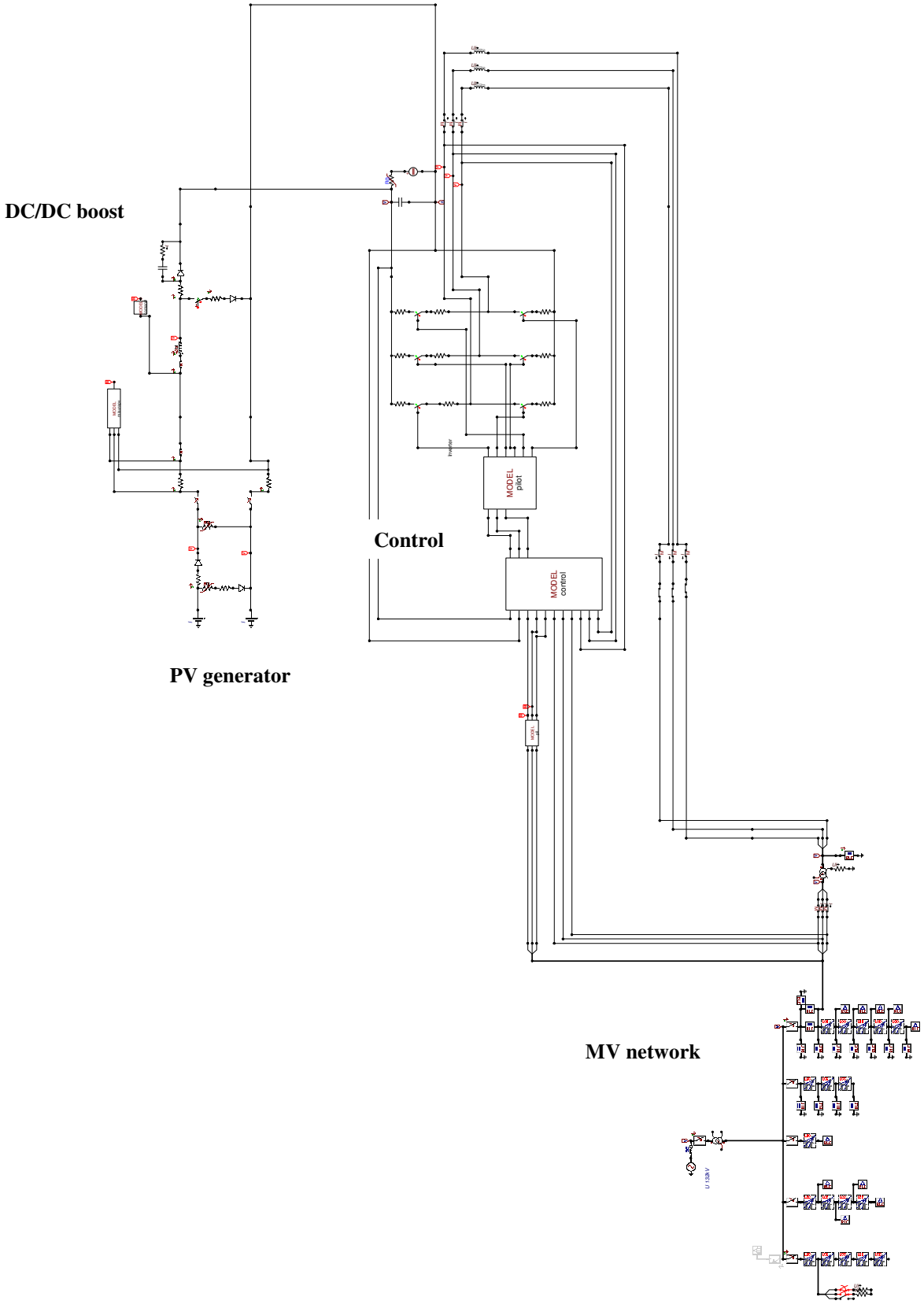

Network model and control implemented in ATPDraw for wind generator in a back-to-back configuration.

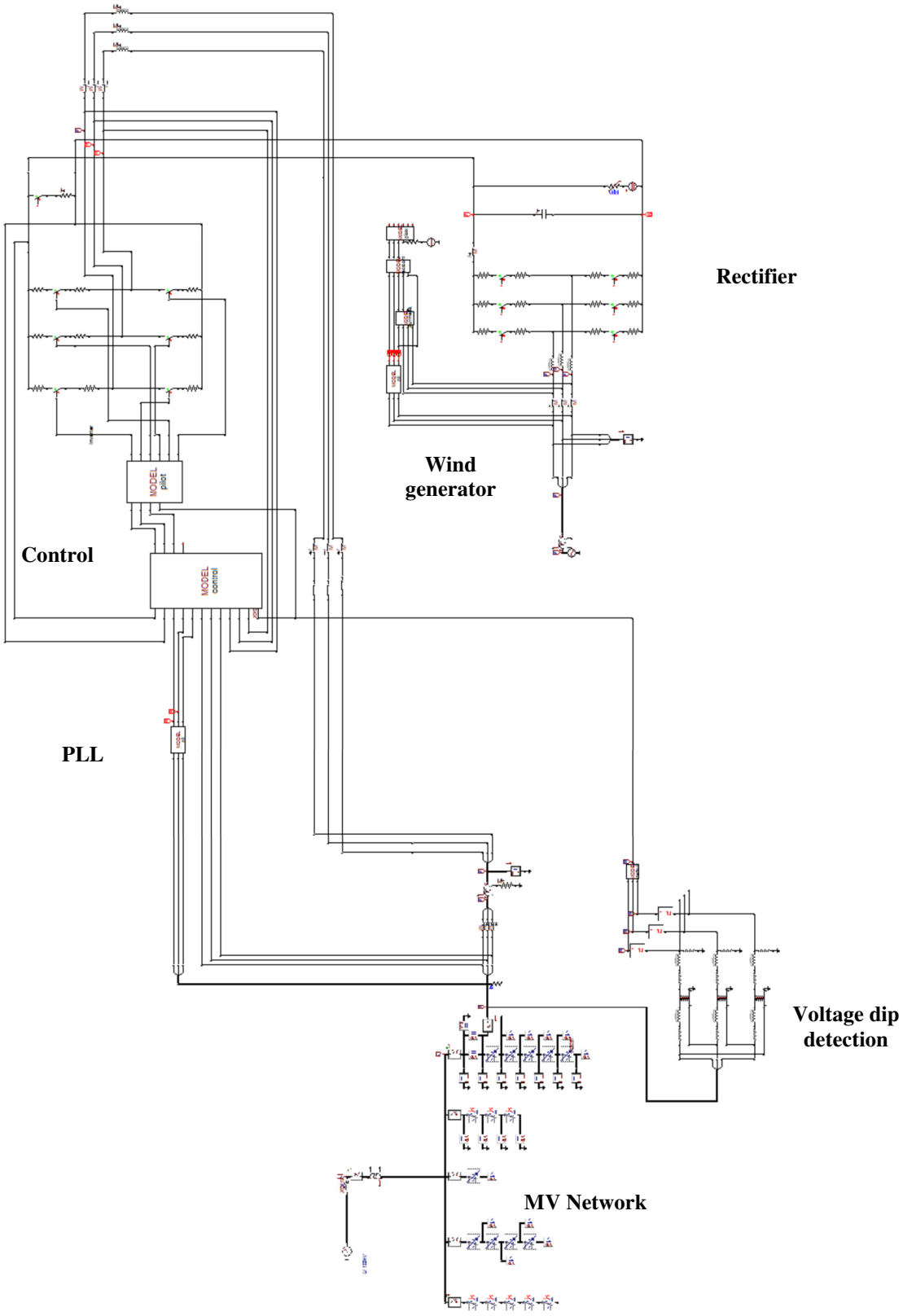

3 INTERACTION BETWEEN INVERTER AND ACTIVE NETWORKS: THE FAULT RIDE THROUGH

Once defined and analyzed typical configurations of Distributed Generators (DG) interfaced to the network through electronic converters (Chapter 2), their behavior in presence of network disturbance has been simulated.
In particular, the study presented in this Chapter has been focused on the capability of static generators of providing ancillary services to the network, in particular grid voltage support while remaining connected to the grid during voltage disturbances, f.i. voltage dips (*Fault Ride Through* - FRT).

Until today, the Standards had required that the DG, in response to a fault in the network (with the consequent opening of the line Circuit Breaker - CB), was disconnected from the network itself in the shortest possible time, as a result of the Interface Protections (IP) tripping, preventing the possible unwanted island operation. Recently however, at the national level, new Standards for connection of distributed generators to Low Voltage (CEI 0-21 [2]) and Medium Voltage (CEI 0-16 [3]) network have been approved together with a new network code[24] [51].

The recent Annex A. 70 of the Italian grid code [51] defines a series of new requirements for the DG plants to support the safe operation of the system:

- generators response to frequency variations;
- voltage dips immunity;
- voltage control regulating reactive power;
- regulation of the active power generated (under and over-frequency);
- automatic loads reconnection;
- voltage support during a short circuit.
- participation in the defense plans.

Generally, national Grid Codes prescribe that DG remains connected to the network if the voltage/duration profile of voltage dips are in compliance with given Fault Ride Through (FRT) requirements [51] ÷ [55].

Some example of FRT curves are reported in Figure 3-1 referred to wind generation plants connected to the distribution and transmission network. These diagrams define the boundaries between zones where generation shall remain connected and zones where shall be disconnected, automatically or selectively.

Grid Codes also define the time schedule to be respected to return to Standard operation after fault clearing. Similar FRT requirements are defined for PV plant, f.i. as requested in Italy for generators connect to Low Voltage networks [2].

[24] More detailed explanations will be provided in the Chapter 7.

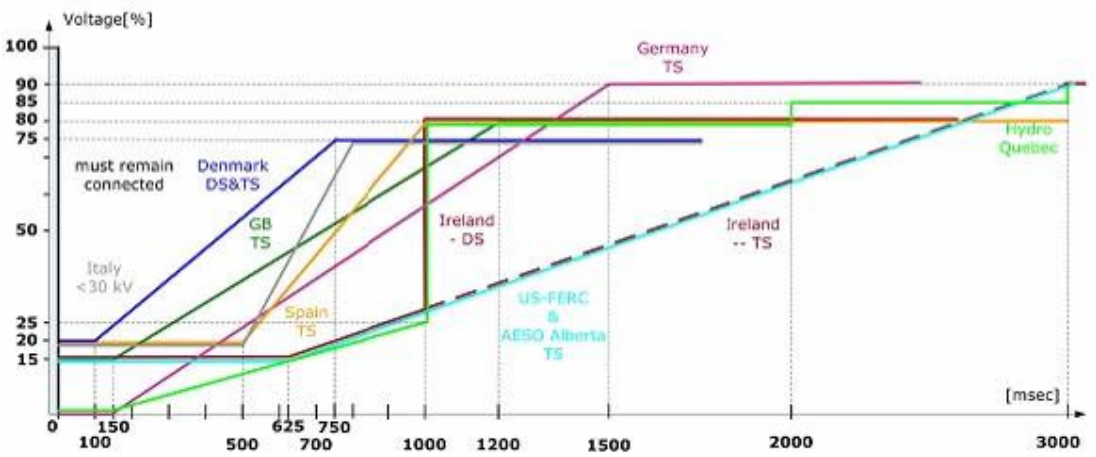

Figure 3-1: Wind generation FRT capabilities as reported in different national Grid Codes

Some grid codes also require that generating plants shall support the grid voltage also with additional reactive current during voltage dip. For example the German Grid Code [51] prescribes the generation unit connected to High Voltage (HV) and MV network remains connected during voltage dips and supplies a reactive current proportional to the network voltage variation in accordance with:

$$\frac{\Delta I_q}{I_N} = k\frac{\Delta V}{V_N} \tag{3.1}$$

where ΔI_q is the variation of q-axis current that the inverter should supply during the voltage dip, I_N is the inverter rated current, $k \geq 2$ is a constant, ΔV is the voltage variation and V_N is the rated grid voltage. The d-axis current reference value is reduced according to the q-axis reference to respect the device current capability. The graph in Figure 3-2 shows the specific requests contained in this network code.

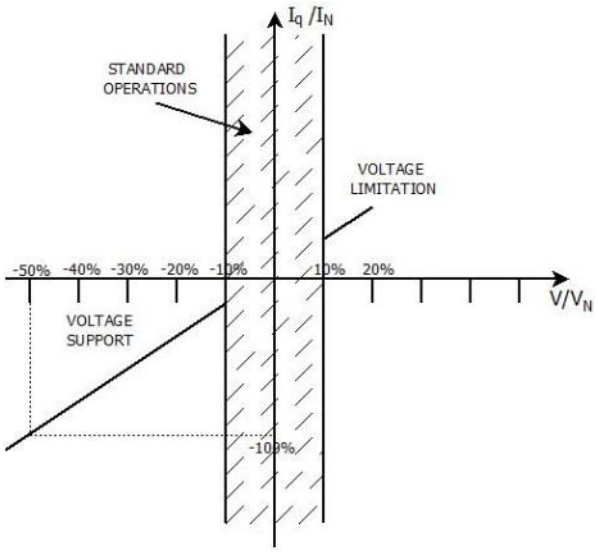

Figure 3-2: German grid code specification

3.1 FRT strategies

To study the DG power plant behaviour, different kind of voltage dips (different depth, inductive or resistive fault impedance) and different system configuration have been considered. The models presented in Chapter 2 for the photovoltaic/wind generators interfaced to the network through power electronics have been used.
The results of the study, which reasonably can be extended to any kind of distributed generator connected to the network through an inverter, have allowed to highlight three different items to be considered for the inverter design to overcome a network fault and in particular:

- limit the growth of the DC voltage using a special braking chopper;
- limit the maximum current value that flows through the inverter valves;
- provide control strategies activated only when a voltage dip occurs.

Regarding the last point, different control strategies for the FRT have been analyzed:

- the control is "frozen" in the steady state status;
- the inverter is forced to supply null active power;
- the inverter is switched to the stand-by mode.
- the inverter should supply a controlled current over q-axis.

3.2 External devices to overcome the voltage dips

The "natural" response of the modelled PV array (system behaviour without any external device or any special control strategy) to a voltage dip has been simulated, in order to understand if the generator can ride through the disturbance without disconnecting from the network.
The simulations have considered different types of network fault: two-phase and three phase, isolated and ground faults, with resistive or inductive impedances. In all the simulations it's assumed that the dynamics of the MPPT is slower than the phenomena subject of analysis, in agreement with Chapter 2.

In particular, the following two configurations have been taken into account:

- without any "external" device or control logic;
- with an "external" device or/and control logic acting during the voltage dip.

In the second configuration, the "external" device is a chopper introduced to limit the DC voltage. As "external" control logic, the voltage dip detection has been developed to regulate the DG active power flow (§3.4.1).
In these studies, it's important first to consider the V_{dc} reaction to the voltage dip. Every voltage dips induces an oscillation in the V_{dc}. During a voltage dip, the DG injects the same current as before, since the MPPT dynamic is slower. In this condition the network voltage is less and so there is an excess of active power injected that can't flow to the network and it's absorbed by the inverter capacitor resulting in an instantaneous increase of the DC voltage. The magnitude of this increase depends on the dip depth and on the fault impedance type. In the following simulations the "user convention" has been taken into account.
The analysis show that the "natural" response of the system to a voltage dip is not satisfactory in a view of FRT: the increase of the DC voltage appears to be excessive and can make the device protections tripping.
Figure 3-3 reports the inverter DC voltage growth in response to a voltage dip with residual voltage of 30% V_N and duration of 120 ms, caused by a three phase fault with resistive impedance in conditions of irradiation of the photovoltaic panel of 1000 W/m2. For this type of fault, being the most severe in terms of FRT among those simulated, the FRT requirements ask to the generator to remain connected to the network.

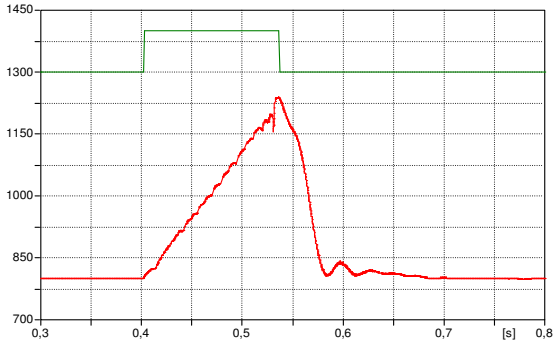

Figure 3-3: "Natural" DC voltage behavior of PV the inverter in case of a voltage dip

In case of network fault "less deep", the DG could overcome it, if the inverter valves are designed to support a temporary overcurrent. This is, for example, the case reported in Figure 3-4, in response to a voltage dip with a residual voltage of 70% V_n caused by a three phase inductive fault. The currents in Figure 3-4c and Figure 3-4d show an higher value during the voltage dip.

Figure 3-5 shows the DC voltages in case of the two different types of fault: with the same severity, in terms of residual voltage and duration. The different behavior in case of voltage dip caused by inductive impedance faults is due to the fact that these do not introduce phase shifts in the mains voltages, as the faults with resistive impedance that are the most critical in terms of FRT.

As anticipated before, there is the need to provide a system to dissipate the excess of the energy on the capacitors. A possible circuit solution is to use a "braking chopper" in parallel with the DC capacitors. Figure 3-6 shows its scheme: the devise is composed by a resistor and a static switch, whose closure is slaved to the overcoming of a voltage threshold. In order to avoid "continuous oscillations" at high frequency in the chopper operation, an appropriate hysteresis band has been provided to define the opening and closing signals for the device valves.

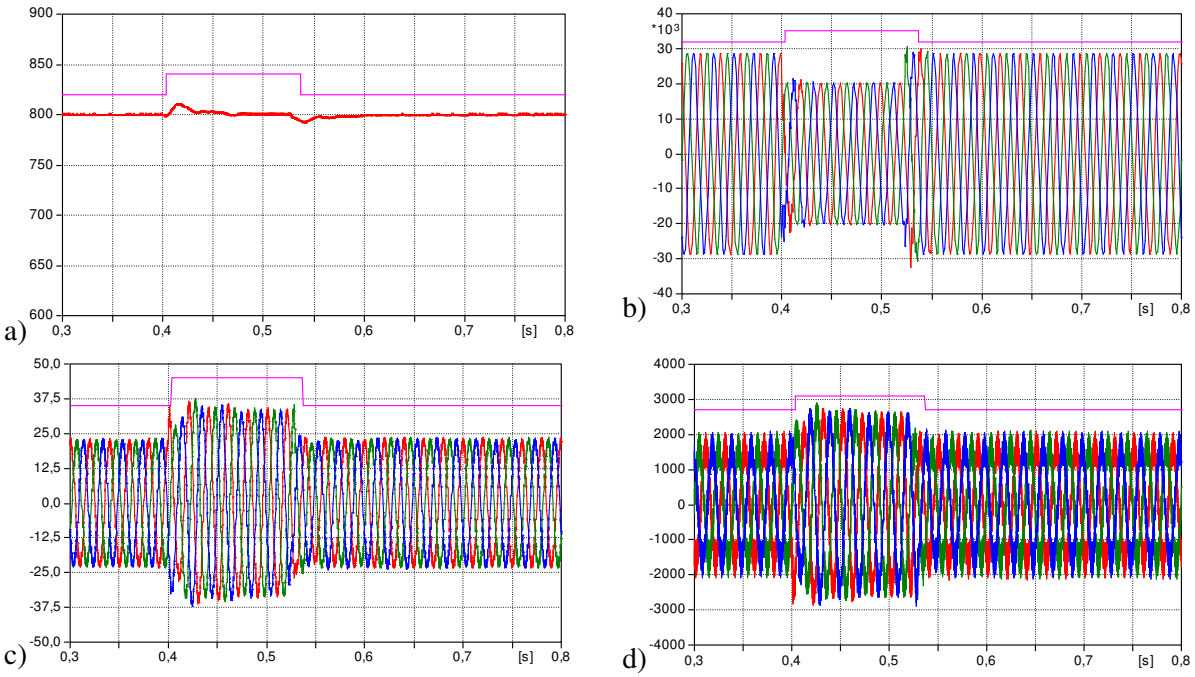

Figure 3-4: "Natural" behavior of the inverter PV in case of an inductive voltage dip: (a) DC voltage, (b) MV voltages, (c) currents in MV network and (d) inverter currents. In all the figures the voltage dip identification signal is shown (pink line).

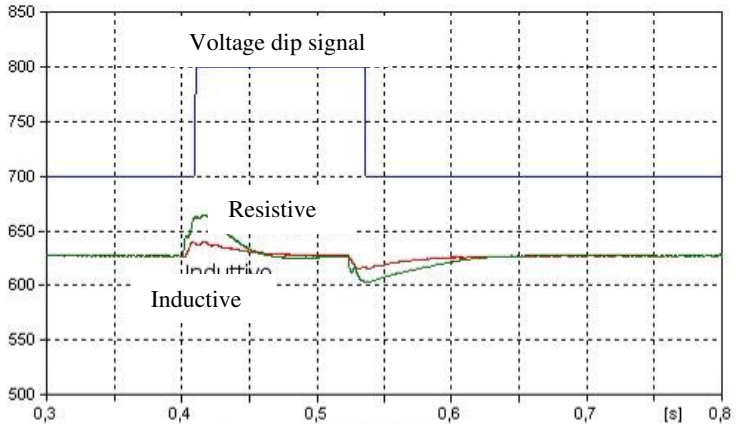

Figure 3-5: DC voltage magnitude in case of inductive and resistive voltage dips

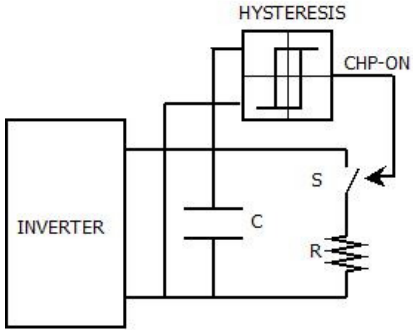

Figure 3-6: Braking chopper scheme

Figure 3-7 shows the DC voltage obtained by simulating the inverter response with braking chopper, in case of resistive three phase fault with residual voltage equal to 30% V_n. Comparing it with the Figure 3-3 it's possible to underline the effectiveness of the braking component in limiting the V_{dc} growth. The protection systems is simulated with the following characteristics:

- voltage threshold: 920 V (1.15 V_{dcn});
- hysteresis bandwidth: 70 V (7.5 % of the threshold).

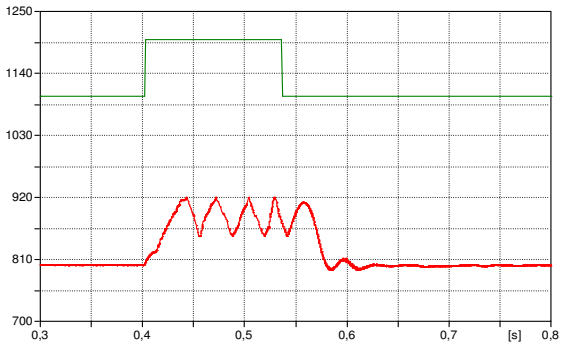

Figure 3-7: PV inverter DC voltage magnitude in the presence of braking chopper during a voltage dip

3.3 Inverter current limitation

The simulations showed that the inverter DC voltage limitation may not be enough to overcome the voltage disturbance. As can be seen from Figure 3-8, where the inverter currents in response to the voltage dip of the previous simulation are shown, even in presence of the braking chopper the currents supplied by the inverter reach "instantly" higher values than the valves capability. Generally the inverter valves would tend to "protect themselves" by passing to a block condition. In addition, as can be seen in Figure 3-8, the same situation can appear also during the transient at the end of the voltage dip.

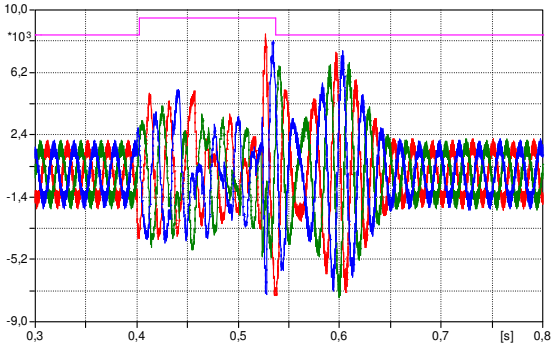

Figure 3-8: PV inverter currents waveform with braking chopper in case of a voltage dip

A limitation of the inverter currents should be implemented, in order to avoid damages to the valves allowing the transient operation of the device. This limitation acts directly and instantaneously on the ON/OFF commands of the IGBT whose status is changed when the current reaches the maximum instantaneous allowable value. In this way the peak value of the inverter output current is limited but the current limitation occurrence has also the side effect to worsen the harmonic distortion of the current waveforms supplied to the MV network[25] (in §3.4.3 some simulations show the effect of the instantaneous current inverter limitation).

Since the current limitation is transient, it has been necessary also to implement a slower current limitation that will reduce the direct axis current set-point, if the inverter current overcomes the maximum current value that can flow thought the switches with continuity.
The current value ($I_{threshold}$) at which this "slow" limitation starts is defined by the maximum current that can flow with continuity through the valves. This limitation has been implemented comparing the value of the current delivered to the network, over d-q axes, with the threshold value and then the ratio is calculated:

$$\alpha = \frac{I_{threshold}}{I_{meas}} \quad 0{,}2 \le \alpha \le 1 \tag{3.2}$$

where I_{meas} is the inverter output current appropriately filtered. In the control scheme over d-q axes this coefficient multiplies the current references.

Figure 3-9 shows the currents waveforms of the PV plant in case of a permanent three phase resistive fault with a voltage reduction of 60% V_n occurred at t = 0.4 s. The peak values reached by the device currents are not such as to justify the instantaneous current limitation intervention, but their RMS value is transitory greater than the current that can be delivered with continuity from the valves. The intervention of the "slow" limitation brings the currents within the maximum current that can be delivered with continuity from valves (whose expression over axis d-q represents the $I_{threshold}$). The

[25] This transient should be roughly of the order of a few hundred milliseconds, compatibly with the valves characteristics and with the overall duration of a voltage dip and the transient consequent to the restoration of the mains voltage.

transient that characterizes the action of the current "slow" limitation is linked to the dynamics of the filter used for the measurement of the inverter currents[26]. In this figure is also shown the behaviour of the corrective factor α[27].

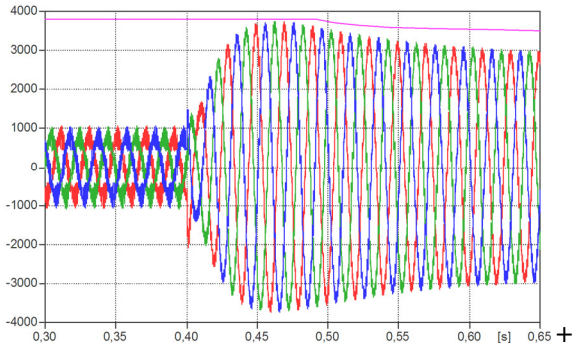

Figure 3-9: PV inverter currents waveform in presence of "slow" current limitation and corrective factor of the current reference (pink curve)

3.4 Control logics implementation

Special control strategy of the VSI, activated only during a voltage dip, should be implemented in order to guarantee the FRT requirements for the DG plants.
Each control strategy requires the voltage dip to be detected as fast as possible by a suitable voltage measurement apparatus and a logic signal has to be sent to the controller when the inverter the dip condition is detected. The upper limit for the dip detection time is 20 ms (equivalent to one period of the 50 Hz MV sinusoidal voltage). Then, the measuring device should be calibrated to send the voltage dip signal to the inverter only if the residual voltage is below a given threshold, since less severe disturbances can be overcome without special strategies.
The voltage dips detection system can be implemented internally in the converter control or as stand-alone system. In the second hypothesis it's necessary to provide a communication channel between the measuring device and the inverter.
Below the voltage dip detection method and the simulation results for different control strategies implemented are presented.

3.4.1 The voltage dip detection system

In general, the speed for the disturbance detection is an important issue to be considered and must be carried out in accordance with the device function. With reference to voltage dips and voltage interruption, between the possible detection criteria of the disturbances the following have been chosen [56] ÷ [58]:

- measurement of the RMS value on a quarter of a period of three line to line network voltages[28]: the criterion, unlike those based on the processing of the components αβ or d-q (Park vector) for the measurement of the RMS value, allows to treat separately and independently the three line to line voltages overcoming also the problem related to the presence of a possible unbalance in mains voltages that generates a 100 Hz component in the voltage signal over coordinates d-q;
- rectifier line to line network voltages: this criterion provides the comparison of the rectified voltages with an appropriate threshold and is faster than the previous one.

[26] The filter implemented is a first order filter (1/ (1+sT)) with T = 100 ms.
[27] To have more visibility on the scale of the graph, the corrective factor is represented with a width of 2800*α and an offset of 1000.
[28] The networks under study are MV primary distribution network and the monitored voltages for the dips interruption detection are the line to line ones.

The detection disturbance logic is exclusive type (logical OR), that is to say, it's sufficient that only one of the two criteria has being violated because it is detected the disturbance: in particular, therefore, it is sufficient that one of the RMS values of network line to line voltages or their rectified are less than the limit established because it is detected the fault. For the determination of the conditions of absence of disturbance is necessary that all the three RMS values of network line to line voltages and their rectified are above the limits. Below the two criteria are briefly illustrated.

Criterion based on the RMS value measurement on a quarter of a period

The criterion is based on the calculation of the RMS value on a quarter of period (1/4T, where T is the network period). This calculation is carried out starting from the sampling of the mains voltage, which is appropriately filtered to remove high frequency disturbance, and it's based on the identification, each half period, of the voltage zero-crossing.

With reference to Figure 3-10, at the first voltage zero-crossing (point A) the RMS value of the previous 1/4T (waves indicated in blue) is calculated. For the next 1/4T, between the zero-crossing and the minimum (the same applies to the 1/4T between the zero-crossing and maximum), the calculation is made when a number of samples equal to those used in the previous quarter of period are acquired (point B, RMS value relative to the waveform shown in green). The synchronization with the voltage is performed once again at the next zero-crossing (point C), when the calculation of the RMS value of the waveform shown in pink is done. In this way, the synchronization with the voltage is performed every half period, while the calculation of the RMS value is carried out every 1/4T and is always referred to the previous quarter of period; the value obtained is kept constant until the calculation of the next.

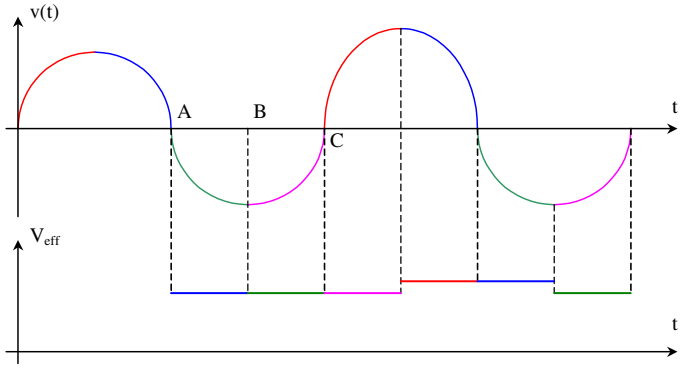

Figure 3-10: Schematic representation of the RMS value calculation

The zero-crossing point is determined by opposite sign of two successive samples: in the example (Figure 3-11) 5 samples for a quarter of period are considered and the voltage zero-crossing is identified from samples 6 and 7. The collected samples (1÷7 in the example) are then used to build another set of samples with the last takes the zero value. The method used is to determine from the last two samples (Figure 3-11b) the entity of the translation that allows to the new sample P6 to be zero.

$$ERRT = \Delta T \cdot \frac{Y_7}{Y_6} \tag{3.3}$$

where ERRT is the entity of the translation, ΔT is the sampling period (time between two successive samples), Y_6 and Y_7 are the last two samples values.

This translation is then applied to each of the other pairs of samples, to determine the new sample set P1÷P6. From these last samples the RMS value calculation is done.

For the quarters for the period that do not provide the zero-crossing identification (those that go from zero to maximum and from zero to minimum) the same samples translation procedure is followed using the same ERRT value used in the previous quarter of period.

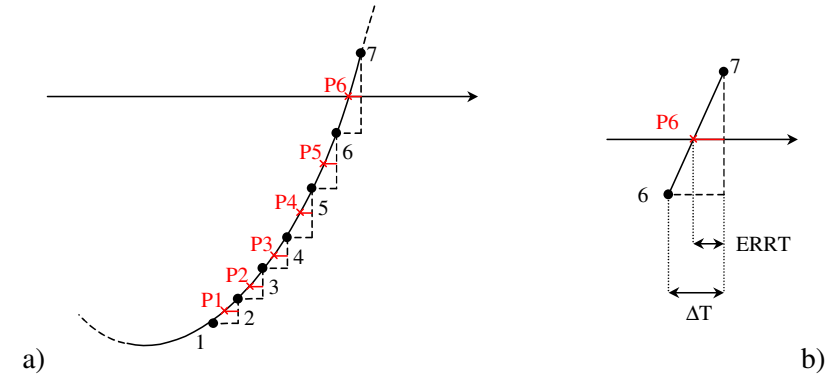

Figure 3-11: Acquisition of the samples for the calculation of the RMS value

The RMS value is then updated every quarter of period and is always relative to the voltage samples acquired in the quarter of previous period.
As an example, Figure 3-12 shows the filtered line to line V_{bc} voltage (red curve) measured by the secondary winding of the voltage transformers, connected phase to phase, and its RMS value calculated according to the method described (green line). It may be noted that, at the first zero-crossing (t~ 0.102 s), the RMS is calculated: the result obtained is lower than the previous one since in the previous quarter of period an under-voltage occurred due to the fault. During the next quarter of period, where all the samples are related to the reduced voltage, the RMS presents a further lower value.

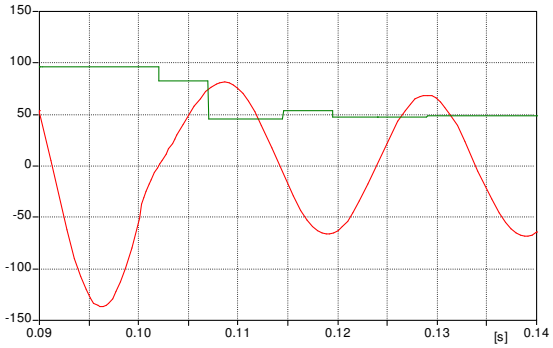

Figure 3-12: Line to line voltage V_{bc} at the secondary of the transformer connected between phase and phase: filtered (red) and RMS value (green)

A voltage dip is detected if at least one of the three RMS values falls below a limit, usually 90% of V_n. The disturbance detection rate with this criterion, according to the type of voltage dip and of its depth, can be considered in the order of a few milliseconds.

Criterion of the "rectified" voltage

Since the calculation of the voltages RMS value, as illustrated before, involves a certain amount of delay, due to the fact that the calculation is performed every quarter of period and refers to the previous quarter of period, another criterion has been implemented. This second logic is faster and is based on the processing of the line to line voltages, properly filtered to eliminate any high frequency disturbance, to obtain a signal equal to the voltages "rectified".
Also in this case the presence of the disturbance is detected if the voltages are lower than a limit. For the definition of the limit it's to be considered that the average value of the rectified value is linked to the voltages RMS value through this relationship:

$$V_{d0} = \sqrt{2} \cdot V \cdot \frac{q_v}{\pi} \cdot \sin \frac{\pi}{q_v} \tag{3.4}$$

where q_v indicates the number of pulses per period (in the case under examination is 6).

In this case, therefore, the ratio between the mean value of the rectified and the RMS value of the "reference" voltage is 1.35; the rectified has a variation around the mean value between a maximum and minimum, respectively 1.05 and 0.9 p.u. (such extremes expressed in p.u. of the voltage RMS value are approximately 1.35·1.05 =1.414 and 1.35·0.9 =1.22). Taking into account this variation, a threshold equal to 0,7 p.u. of the average value of the rectified has been chosen to detect the disturbance.
To avoid that the adoption of this very fast detection method would entail the identification of a disturbance even in the presence of network normal transient, a minimum permanence time of the rectified under the limit has been introduced. In this way it will degrade the performance from the point of view of speed but it avoids untimely interventions; the permanence time should then be suitably selected, and must not be lower than the typical delay of the criterion based on the RMS value. In the analysis conducted it has been set equal to 1 ms. The minimum permanence time required, in addition, influencing directly the voltage dip detection method speed, might be one of the elements to be modified for the coordination of more compensation devices connected in cascade.
As an example, Figure 3-13 shows the line to line measured by the secondary windings of the voltage transformers connected between phase and phase (red, green and blue curves), the same voltages filtered (pink, brown and grey curves) and the trends of the rectified voltage (light blue curve).

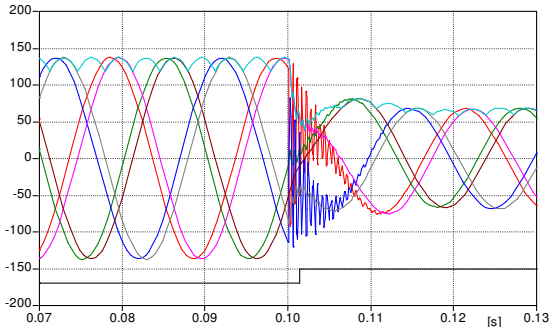

Figure 3-13: Line to line voltages at the secondary of the transformers connected between phase and phase (red, green and blue curves); same voltages filtered (pink, brown and grey curves); rectified voltage (light blue curve); voltage dip identification signal (brown line).

3.4.2 FRT control logics

In this section the simulation results of the behavior of the distributed generation, first photovoltaic and then wind, in presence of voltage dips are presented. Some logic for overcoming the voltage dip, activated by the signal of the disturbance detection, are taken into account, in particular the following will be presented:

1. the control is "frozen" in the steady state status;
2. the inverter is forced to supply null active power;
3. the inverter is switched to the stand-by mode.
4. the inverter should supply a controlled current over q-axis.

3.4.3 Simulation results for the implementation of control logics for PV generators

3.4.3.1 Control "freezing" in the steady state status

Thus strategy requires that, after the receiving of the fault detection signal, the regulators control state variables are forced to the values that they had before the abnormal situation (obtained averaging the

variables values for a time of 100ms before the occurrence of the voltage dip). It's therefor necessary to keep memory for a time long enough to ensure that the voltage dips detection system recognizes the event and communicate it to the controller of the inverter. The values of the variables are held constant for the entire duration of the event, and then they are released to proper mains voltage after the voltage restoration.

Below the simulation results of the system behavior in presence of phase to phase resistive ground fault (Figure 3-14 with voltage reduction of 70% V_n on the voltage more affected by the fault) and three phase resistive fault (Figure 3-16)[29]. Figure 3-15 and Figure 3-17 show the DC voltage, LV phase voltages, MV currents and inverter currents for these simulated events.

The simulations show that the inverter control "freezing" in the steady state status is useful to avoid that the control regulators reach the saturation condition, situation that can cause problems during the voltage dip extinction but it's not enough to satisfy the FRT requirements. This strategy doesn't present advantages in terms of inverter currents and voltages, since, during the voltage dip, the currents reach the limitation threshold limit (Figure 3-15d and Figure 3-17d) and the braking chopper is working to limit the DC voltages (Figure 3-15a and Figure 3-17a).

Phase to phase resistive ground fault with a voltage reduction of 70 %V_n

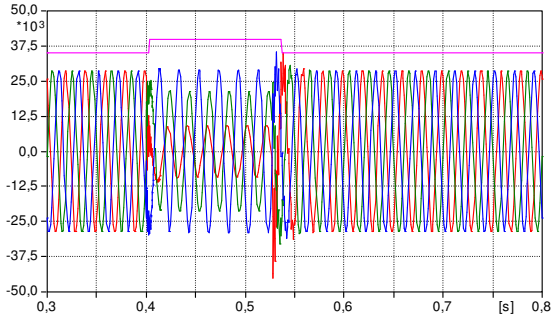

Figure 3-14: MV bus bar line to line voltages and voltage dip detection signal

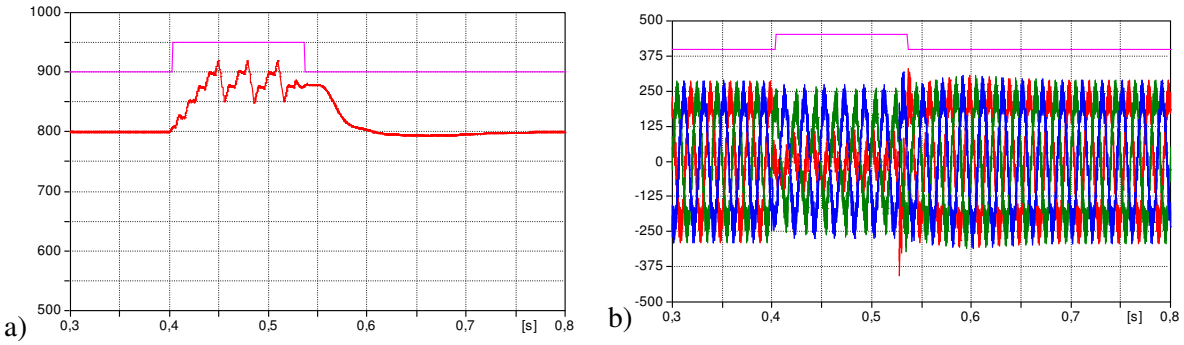

[29]In regards single phase ground faults, since in a MV distribution network does not cause any voltage dips on line to line voltages, have not be considered.

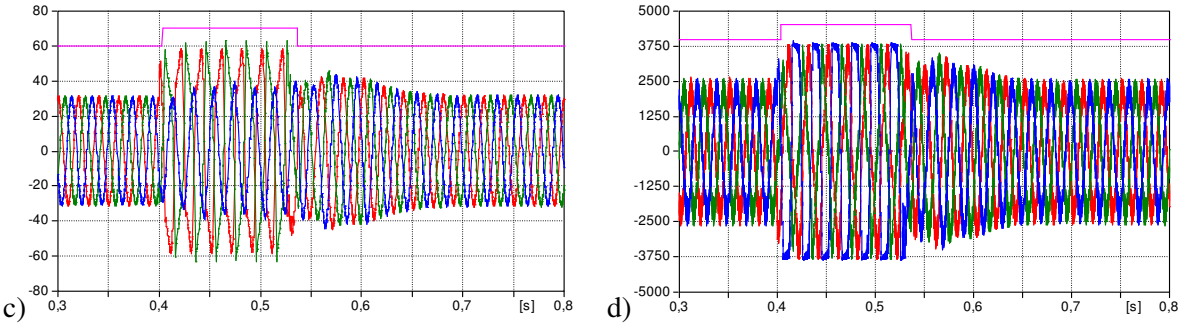

Figure 3-15: Response of the PV inverter: (a) DC voltage, (b) LV phase voltages, (c) MV currents, (d) inverter currents. In all the figures the voltage dip identification signal is shown (pink line).

Three phase resistive fault with a voltage reduction of 70 %V_n

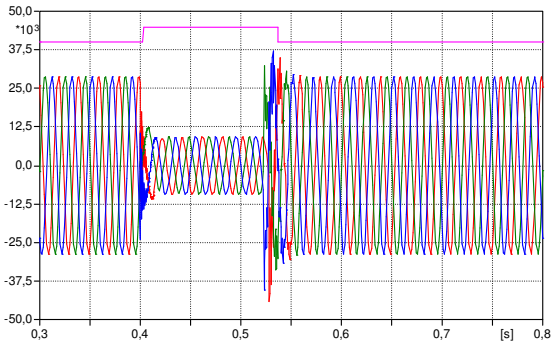

Figure 3-16: MV bus bar line to line voltages and voltage dip detection signal

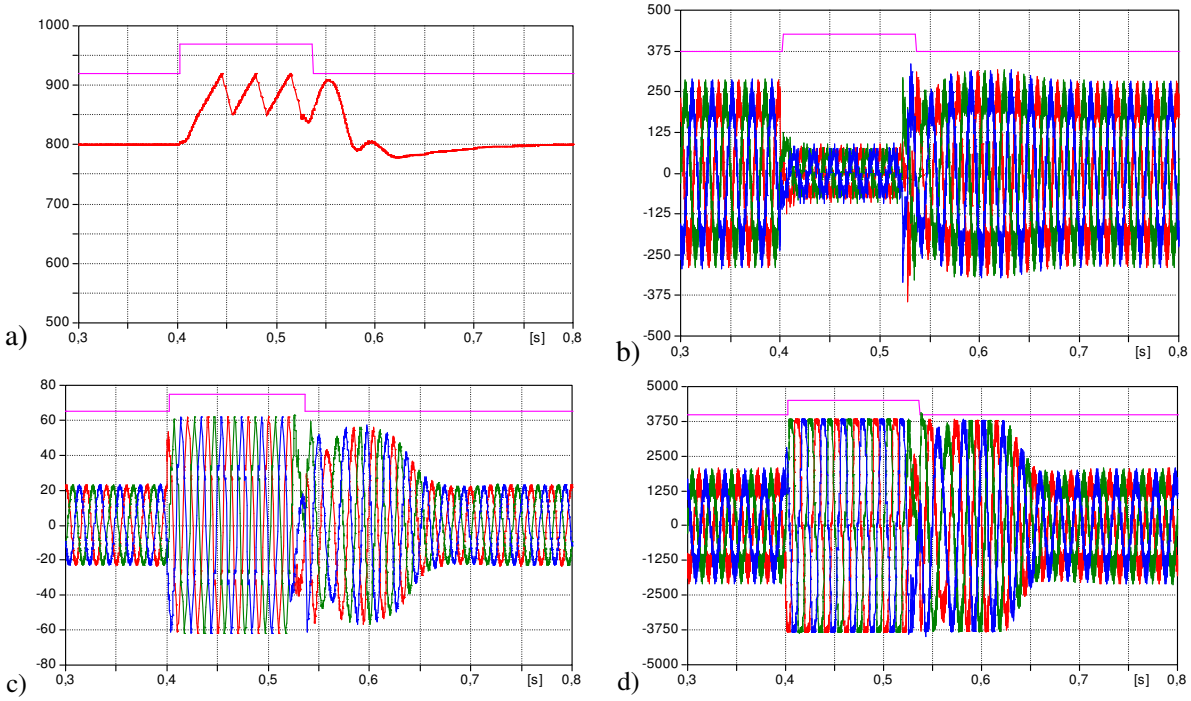

Figure 3-17: Response of the PV inverter: (a) DC voltage, (b) LV phase voltages, (c) currents in MV, (d) currents of inverter. In all the figures the voltage dip identification signal is shown (pink line).

3.4.3.2 *Supply null active power*

The control strategy has been implemented setting both the "d-axis" and "q-axis" current references (i.e. proportional to active and reactive powers) to zero values during the voltage dip. In addition all the control variables are fixed at the values necessary to inject null active power during the disturbance.

Figure 3-18, Figure 3-19 and Figure 20 show the system response to a three phase resistive fault that cause a voltage reduction of 30% V_n (Figure 3-14). In particular the results obtained using three different values of solar irradiation are reported. In each figure also the logic signal that identifies the voltage dip is shown.
Figure 3-18a, Figure 3-19a and Figure 20a show that the braking chopper is always necessary and the simulations with reduced solar irradiation have highlighted that the braking chopper, in these conditions, switches less frequently.
In terms of inverter current Figure 3-18d, Figure 3-19d and Figure 20d show that, with this control strategy, the current limitation is not active during the voltage dip.

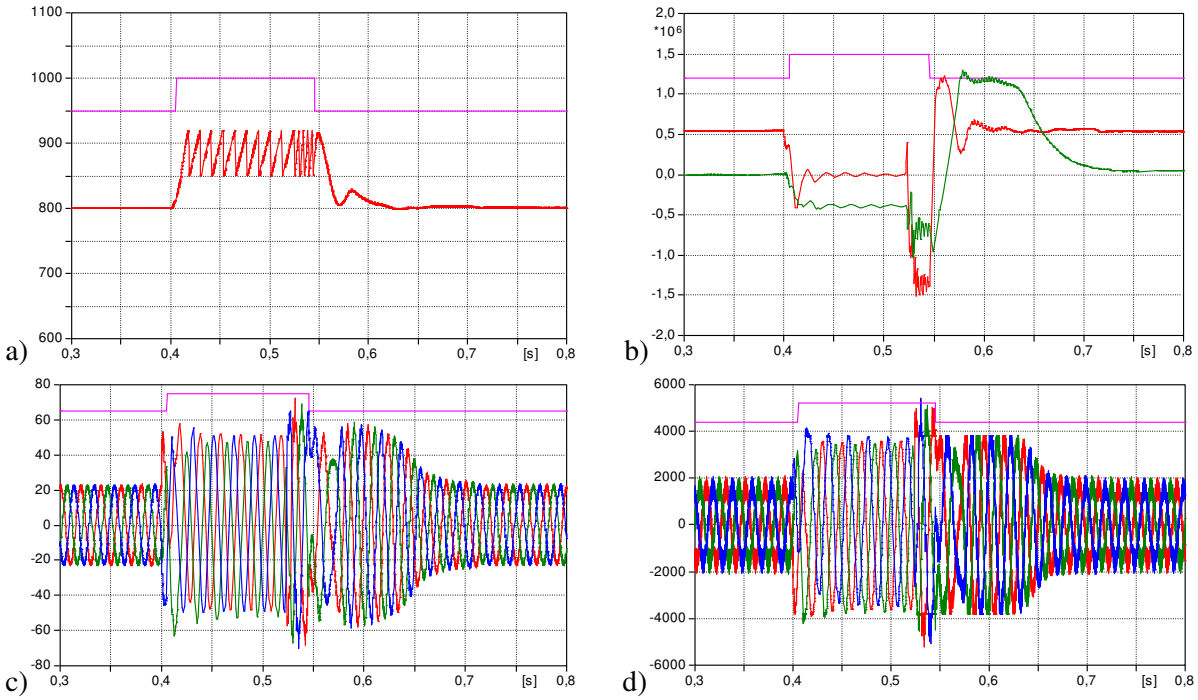

Figure 3-18: Response of the PV inverter with irradiation 1000Wm-2; (a) DC voltage, (b) active (red curve) and reactive (green curve) powers, (c) inverter currents, (d) MV currents.

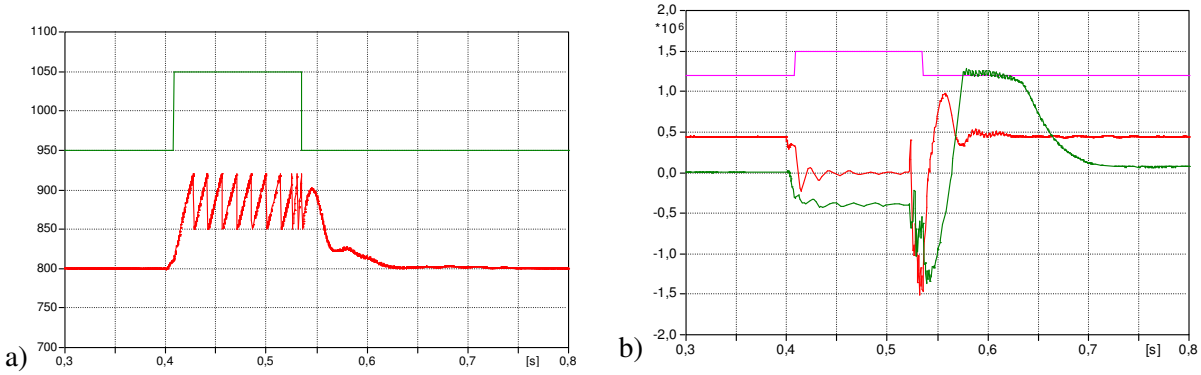

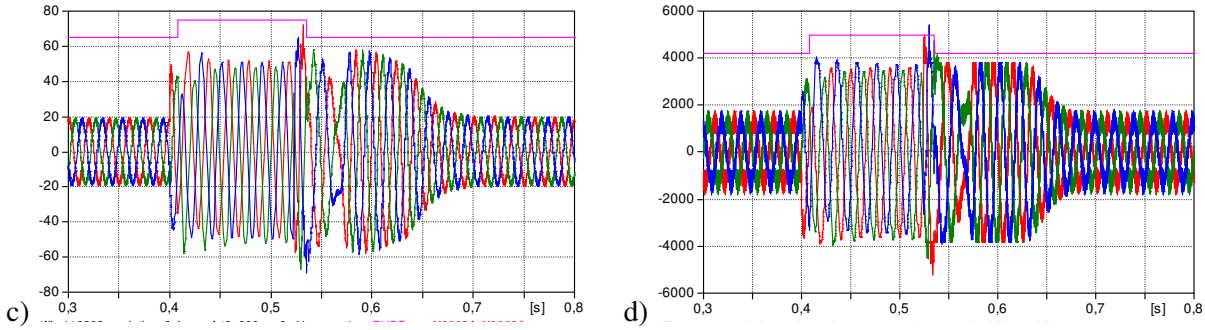

Figure 3-19: Response of the PV inverter with solar radiation 800 Wm-2: (a) DC voltage, (b) active (red curve) and reactive (green curve) powers, (c) MV currents, (d) inverter currents

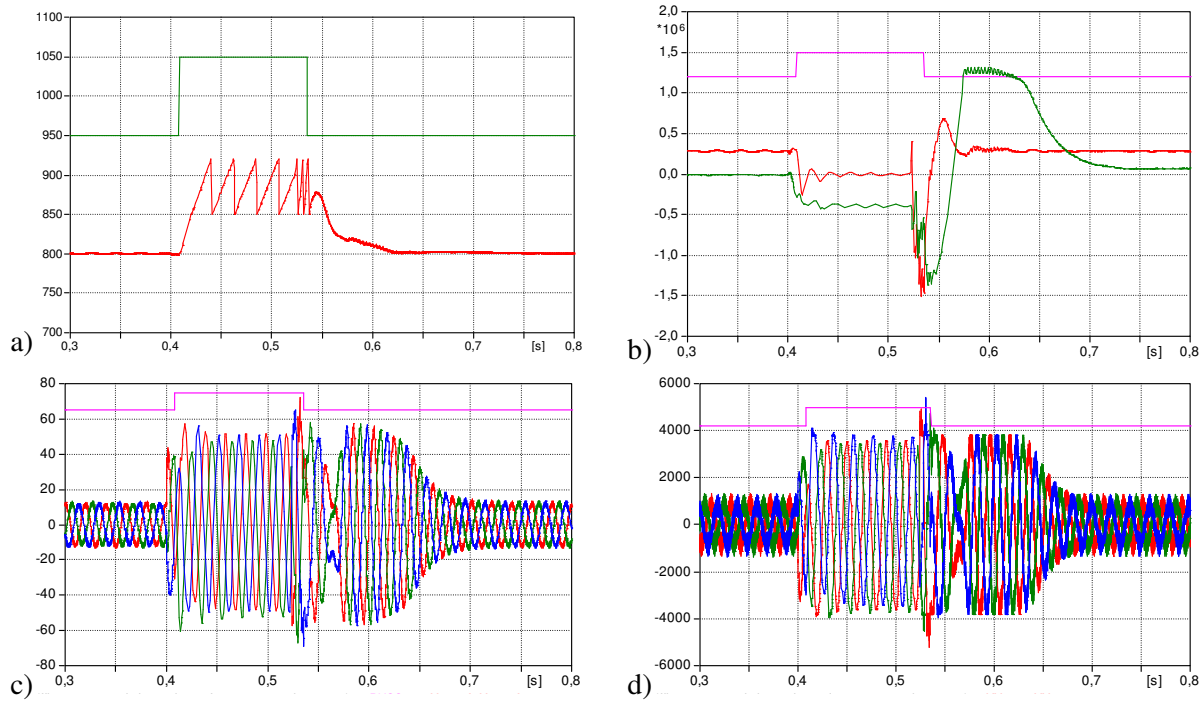

Figure 3-20: Response of the PV inverter with solar radiation 500 Wm-2: (a) DC voltage, (b) active (red curve) and reactive (green curve) powers, (c) MV currents, (d) inverter currents.

3.4.3.3 "Stand-by" mode

This strategy is characterized by the stand-by mode that could be activated in three different ways and each of them requires a careful evaluation in the design of the device:

- opening all the valves of the inverter; possible over-voltages across the IGBT should be taken into account during the design of the converter, f.i. including snubbers for limiting the spikes;
- maintaining in ON state all of the upper or the lower valves for each inverter leg, while the others are left in OFF state; in this case, over-currents through the short-circuited devices should be considered;
- adopt auxiliary static switches, turned on during the voltage dip in order to short-circuit the inductances by-passing the inverter switches.

Figure 3-21 shows the currents waveforms, with the lower valves of each inverter leg short-circuited, in case of a three phase resistive fault that causes a voltage dip with residual voltage of 30% V_n. The currents that flow through the inverter valves present, in correspondence with the restoration of the mains voltage with the inverter still in stand-by, a spike of 3.8 times the maximum switched current from the valves.

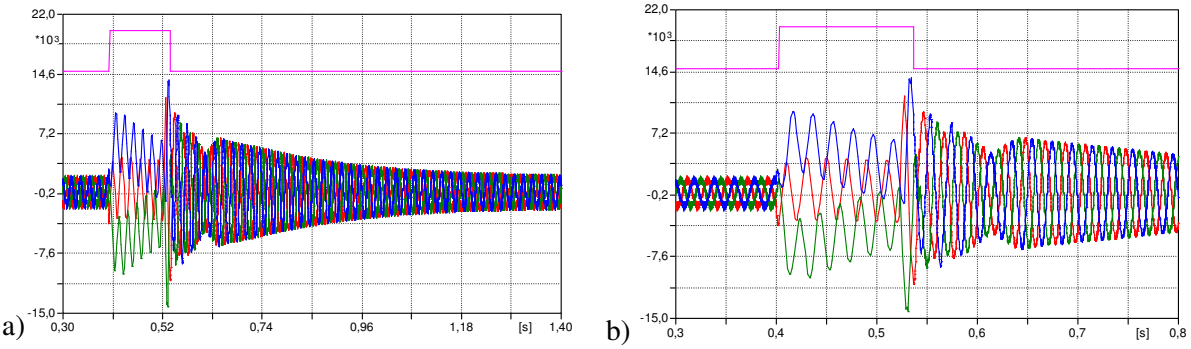

Figure 3-21: Stand-by condition: (a) inverter currents waveforms (b) detail. In all the figures the voltage dip identification signal is shown (pink line).

3.4.3.4 Supply a controlled reactive current

To implement the control strategy that allows reactive current injection in the network during the voltage dip, it's necessary to modify the PV plant design presented in § 1.2.4.3.
The request to supply an additional current than the designed one has requested to modify the inverter capability, so it can supply an higher power approximately 25% more than the one reported in Chapter 2. The new device design has also requested an adaptation of the transformer for the network connection equal to 900 kVA. The main new design parameters are summarized in Table 3-1 and the new capability curves are shown in Figure 3-22.

Table 3-1: Main design inverter and transformer parameters for the new PV plant

Inverter		
Rated Power	800 kW	
Capacitor DC	100 mF	
Inductance switching	18.68 µH	
Maximum current that can be delivered with continuity	48 A	RMS value referred to MV
Maximum instantaneous current	3800 A	
Switching Frequency	1950 Hz	
LV Voltage	162 V	
DC Voltage	800 V	
Transformer		
Rated Power	900 kVA	
Inductance	14.75 µH	
Turns Ratio	20000/162	
Winding coupling	Dyn11	

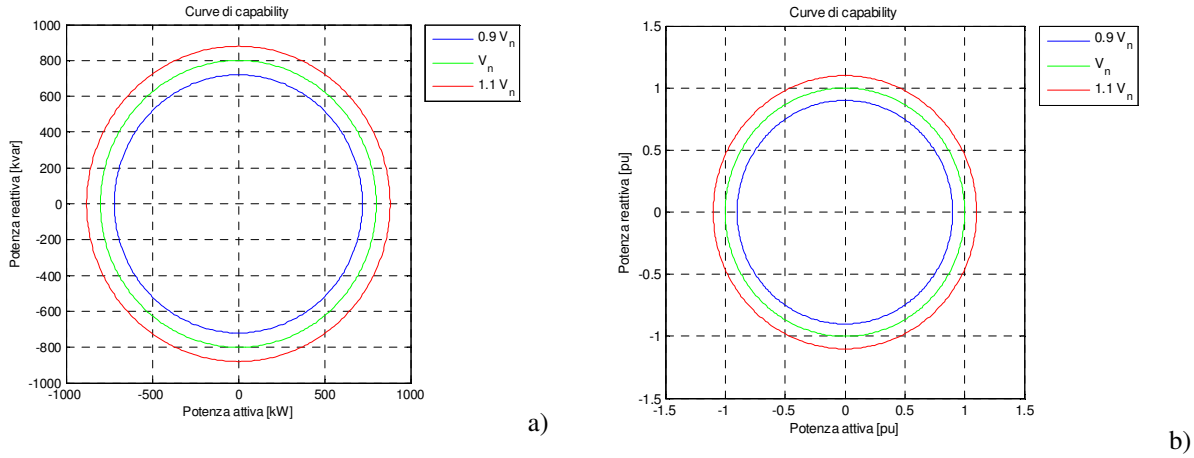

Figure 3-22: Inverter nominal capability for kW PV inverter: absolute values (a) and p.u. (b)

The inverter is designed with the external device (braking chopper § 3.2) and the current limitations (§ 3.3) to overcome the voltage dip, as presented before.
To allow the inverter operating out of the current limitation during the injection of both active and reactive current, the current reference value over d-axis has to be modified if it is verified that:

$$\sqrt{I_{d\_rif}^2 + I_{q\_rif}^2} > I_N \tag{3.5}$$

where I_{d_rif} is the reference current over d-axis, I_{q_rif} over q-axis and I_N is the inverter rated current.

In this case, the d-axis reference current is modified according to the law:

$$I'_{d\_rif} = \sqrt{I_N^2 - I_{q\_rif}^2} \tag{3.6}$$

The response of the system has been simulated in case of different types of fault on the network. The simulation results are reported in Figure 3-23 and Figure 3-24, respectively for:

- three phase resistive fault at t=0.4 s with a duration equal to Δt=0.2 s and residual voltage of 30 %V_N;
- three phase inductive fault at t=0.4 s with a duration equal to Δt=0.2 s and residual voltage of 70 %V_N.

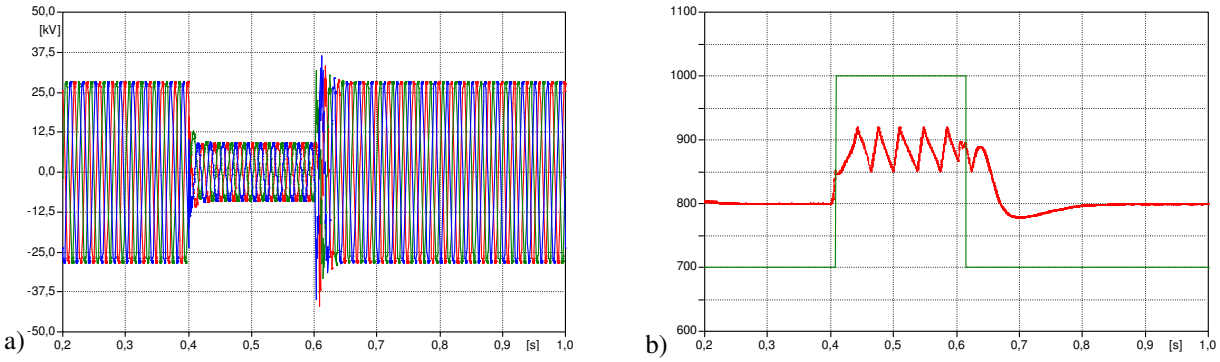

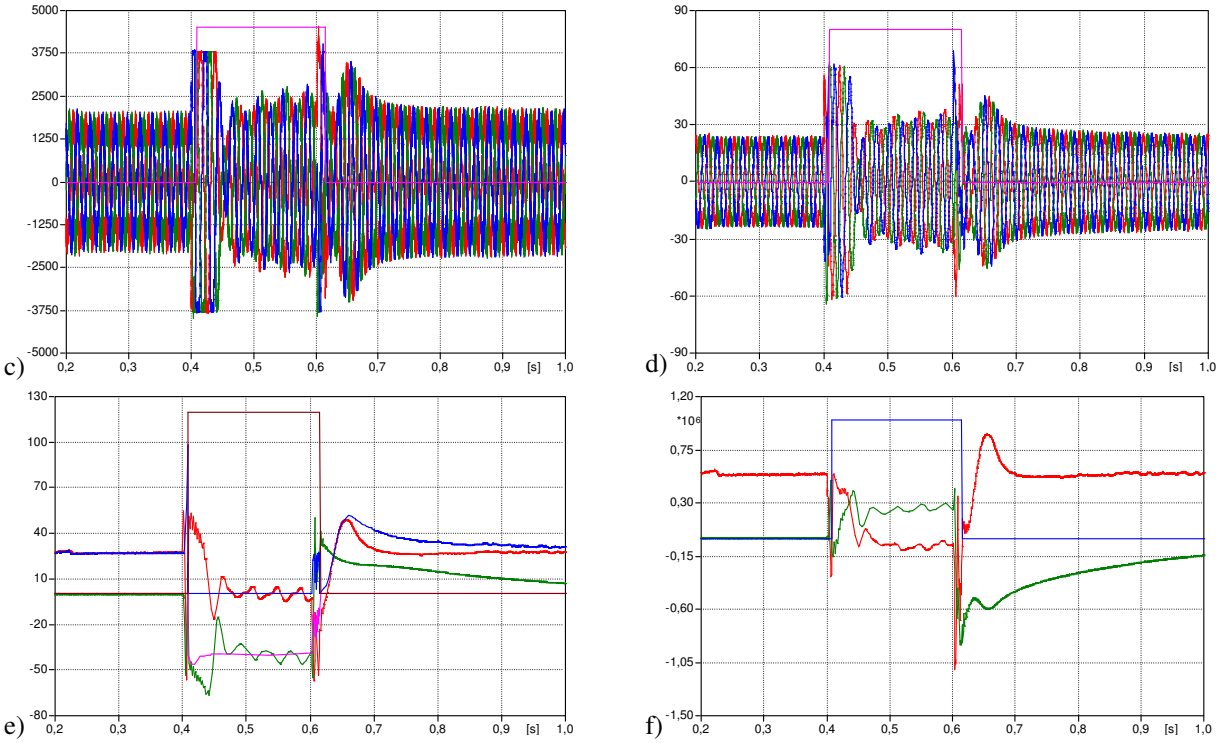

Figure 3-23: **Main waveforms (a) MV bus bar line to line voltages, (b) DC voltage, c) LV inverter currents, d) MV network currents, e) inverter currents over axis d (red) and q (green) and their references, f) active (red) and reactive (green) power. In all the figures the voltage dip identification signal is shown (pink line).**

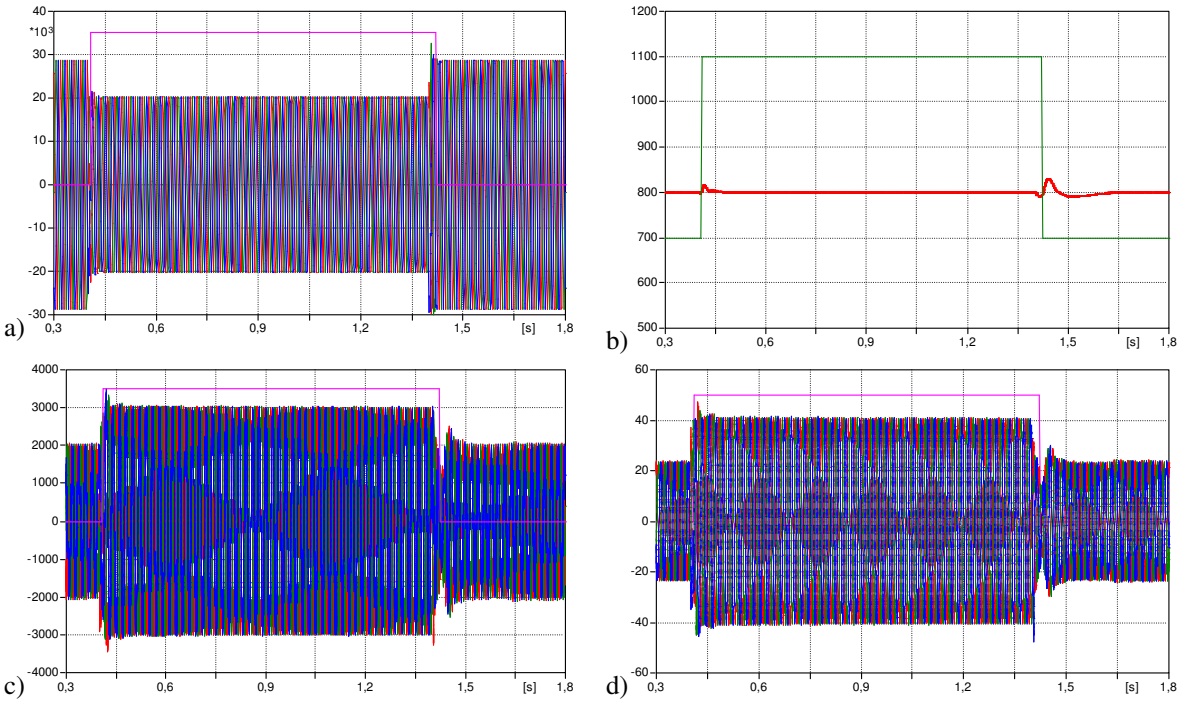

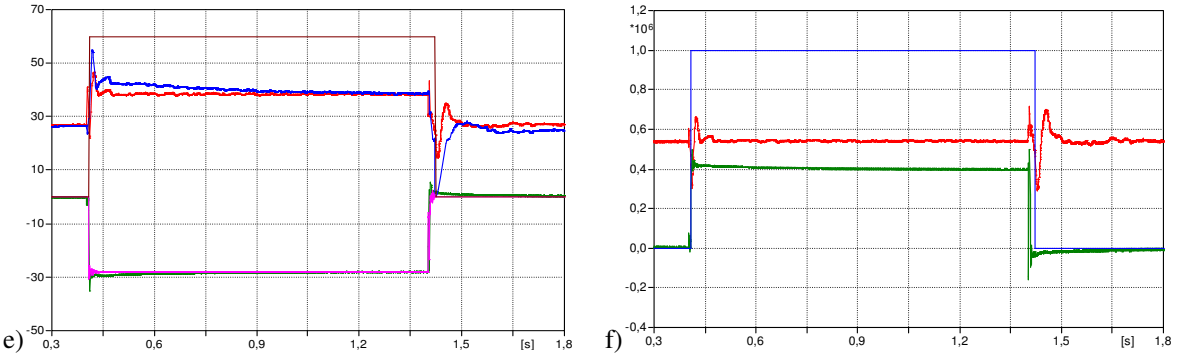

Figure 3-24: Main waveforms (a) MV bus bar line to line voltages, (b) DC voltage, c) LV inverter currents, d) MV network currents, e) inverter currents over axis d (red) and q (green) and their references, f) active (red) and reactive (green) power. In all the figures the voltage dip identification signal is shown (pink line).

The results have allowed to highlight that the control strategy to exchange a controlled reactive current allows to overcome voltage dips using the same methods already emerged for the other control strategies for the FRT (braking chopper, instantaneous and slow current limitation). However, the photovoltaic generator, being of limited power, does not provide any significant contribution to the sustenance of the mains voltage during the voltage dip. In the next this issue will be analyzed in presence of wind generators of greater power.

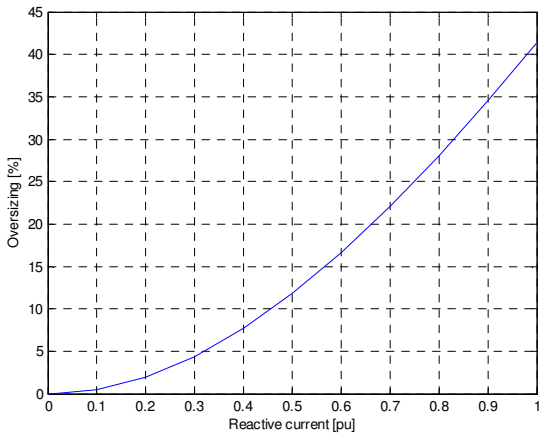

Figure 3-25: Percentage of overdesign of the inverter PV as a function of the share of reactive current that you are going to deliver, maintaining a constant delivery of active current

As said before, to allow the DG to supply an added reactive current it's necessary design power electronic stages and any connection network transformers for power ratings greater than those provided by primary source of energy. In this way, the system can supply a significant amount of active power even in case of voltage dip of a certain depth. Figure 3-25 shows the curve that describes the relationship between the overdesign percentage, in terms of currents that can be dispensed with continuity from the valves, and the reactive current that can be supplied without changing the d-axis reference (fixed to 1 p.u.).

3.4.4 Simulation results for the implementation of control logics for wind generators

From the study of the behavior of the wind generators in presence of voltage dips, the same results, as for the PV plants, have been obtained[30]. Figure 3-26 shows the DC voltage and the inverter currents in case of a three phase resistive fault that cause a voltage dip of duration Δt=500 ms, with residual voltage equal to 20% V_N, in presence of braking chopper and instantaneous current limitation.

The adoption of the methods described above allows the overcoming of voltage dips complying with the inverter capability. Despite this, the inverter operation during the voltage dip is still problematic. The frequency spectra of the inverter current during the steady-state operation and during the voltage dip are shown in Figure 3-26c,d. It's shown how the instantaneous current limitation causes low order harmonic components (5°, 7°, 11° and 13° mainly), that represent a disturbance for the network. This phenomenon can be considered acceptable in the hypothesis that remains only for the duration of the voltage dip (few hundreds of ms) and that it's the result of a necessary measure for the achievement of the FRT requirements. In addition, the braking chopper is subjected to a considerable heat stress. The resistance of the braking chopper must therefore be designed to withstand the thermal stress which can be costly both in design and economic terms.

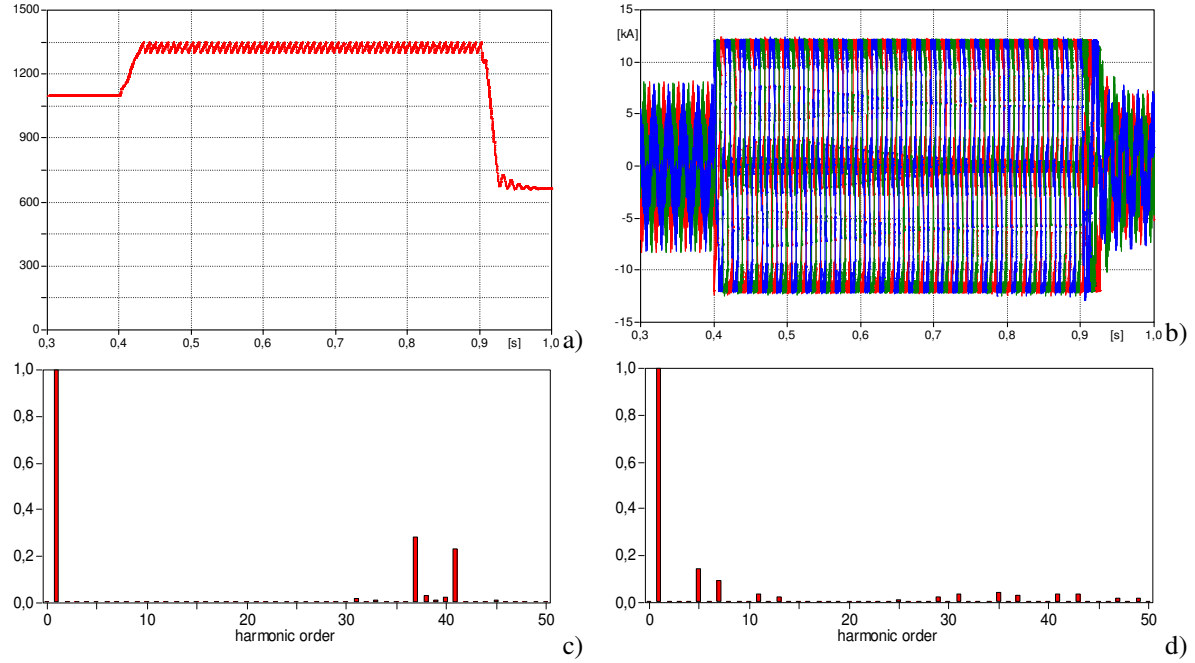

Figure 3-26: Natural response to a voltage dip of the wind generator with instant current limitation and braking chopper (a) DC voltage, (b) inverter currents (c) harmonic spectrum of the inverter current, d) harmonic spectrum of the inverter current with the current limitation active. The spectra are expressed in p.u. of component a 50 Hz

Also for wind generators FRT control strategies, seen before, have been analyzed. For simplicity only the most relevant results of the wind generator behavior for different control strategies will be presented. The simulated fault is a resistive three phase that occurs at t=0.4 s and causes a voltage dip with a residual voltage equal to 40% V_n.

[30] In case of real application of wind generators, the phenomenon of growth of the DC voltage can be restricted by the action of the pitch control that slows down the turbine rotation.

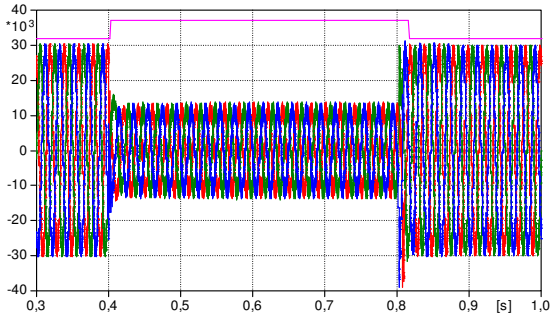

Figure 3-27: MV bus bar line to line voltages and voltage dip detection signal

Considering the control logic to supply *null active power* during the voltage dip, the digital simulations allow to conclude that in this case the inverter is able to overcome the voltage dip without current limitation. Only during the input and output transient from the disturbance, there is the current limitation (Figure 3-28).

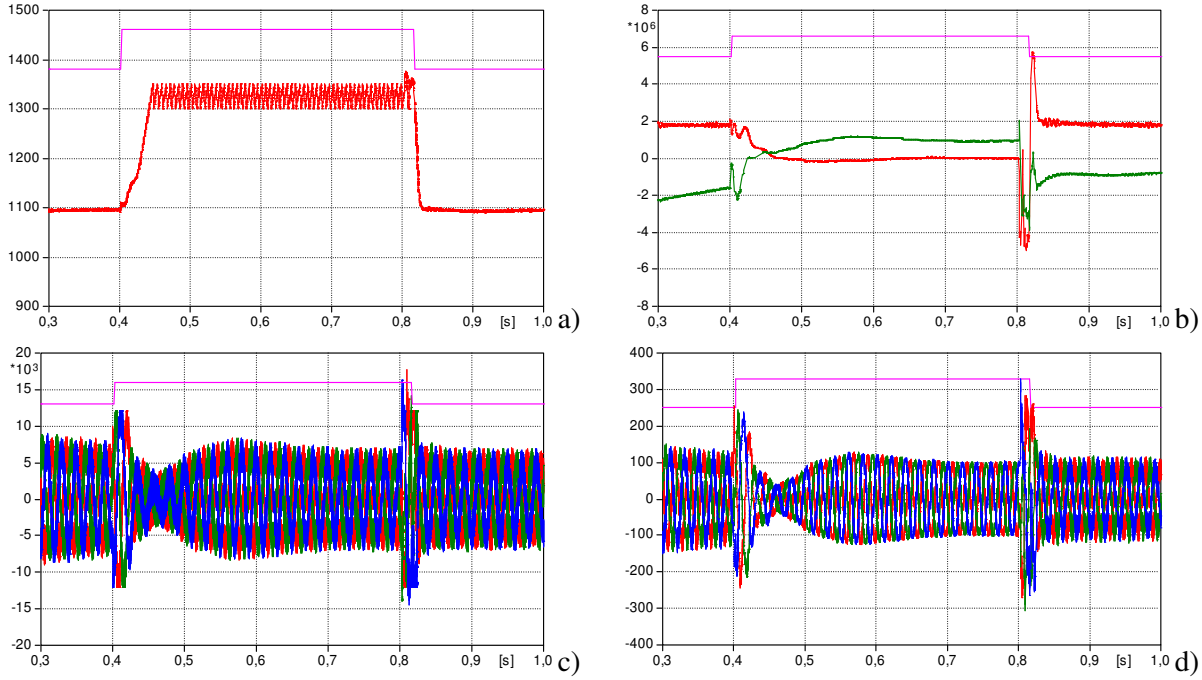

Figure 3-28: Response of the inverter with control P=0: (a) DC voltage, (b) active (red curve) and reactive (green curve) powers, (c) inverter currents, (d) MV currents.

Regarding the *stand-by mode* of the inverter, during the voltage dip, forcing the opening of all of its valves[31], the simulations show that it's necessary to pay special attention in the valves design for the inverter and snubber, since the forced opening of both valves of the same leg can cause surges potentially dangerous for the components. In addition, the stand-by condition implies that the inverter may not be used to provide any auxiliary services to the network (Figure 3-29).

[31] During this condition, the regulators are "frozen" to the steady state status to allow a faster restarting of the device when the mains voltage is within the nominal parameters.

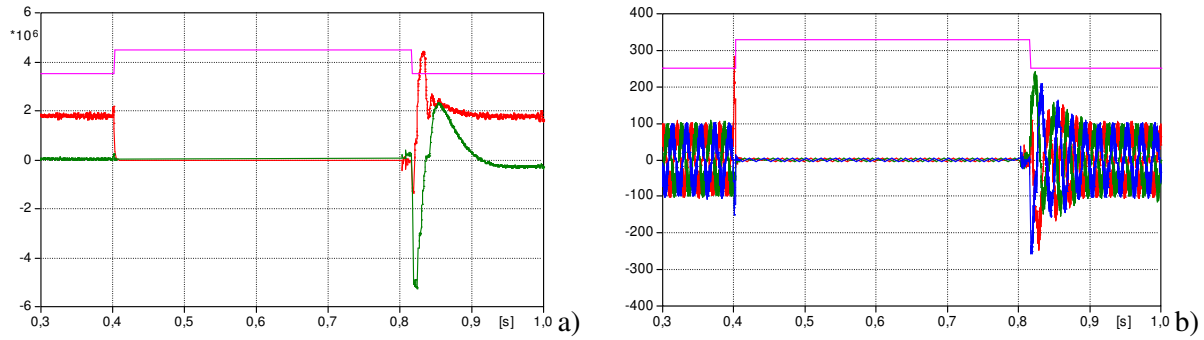

Figure 3-29: Stand-by condition: (a) active (red curve) and reactive (green curve) powers, (b) MV currents.

Finally, in the case of *supplying controlled reactive current*, proportional to the depth of the voltage dip, also for the wind generators there are problems with the inverter design, as already highlighted in case of PV generators. The need to over-design the device to allow the exchange of reactive power, which in some cases is added to the active power, has been already considered in the dimensioning of the wind generator reported in Chapter 2. The simulations show that, with an adequate inverter design and with the methods to limit voltages and currents described above, it's possible to exchange a controlled reactive current during voltage dips (Figure 3-30).

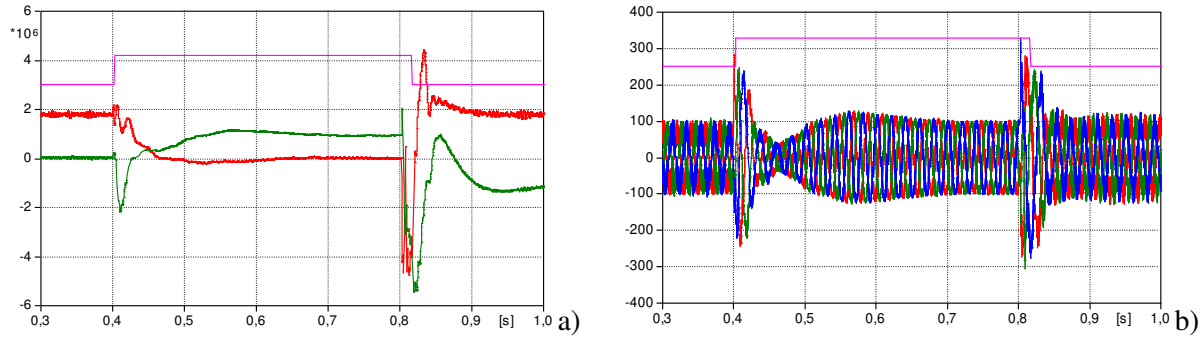

Figure 3-30: Inverter injecting reactive current: (a) active (red curve) and reactive (green curve) powers, (b) MV currents.

System response to a phase to phase voltage dip

It has been finally simulated the inverter behavior in case of voltage dips unbalanced. In particular has been simulated , initially, the response of the device to a two-phase fault with inductive impedance that causes a voltage dip with duration 1 s and residual voltage 50% V_N, referring to the phase voltage of lower amplitude.

The network voltages waveforms are shown in Figure 3-31, while the simulation results of the natural system response and the effect of the FRT strategies already analyzed are reported in Figure 3-32 ÷ Figure 3-35. In particular, only in case of reactive current supply the instantaneous current limitation is active during the voltage dips (Figure 3-34c). In the other simulations, this limitation is present only during the transient at the end of the voltage dip.

In all the simulations, except the stand-by operation mode, 100 Hz oscillations appear in powers and the inverter currents[32]. These phenomena, caused essentially by the voltages unbalance, may be, depending on the network short circuit power, further disturbing for the mains voltages, causing an impact in terms of Power Quality. The solution of forcing the inverter in stand-by operation condition avoids the generation of these disturbances and could therefore be the preferred in case of unbalanced

[32] For a detailed explanation of the causes of the phenomenon, see Chapter 5.

voltage dips. A possible alternative is adopt inverter control schemes specific to mitigate the effects of the unbalances of voltage network (Chapter 5).

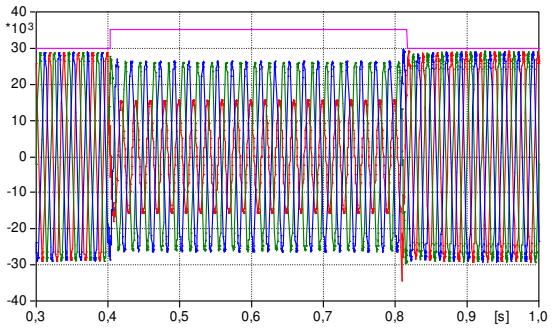

Figure 3-31: MV bus bar line to line voltages and voltage dip detection signal

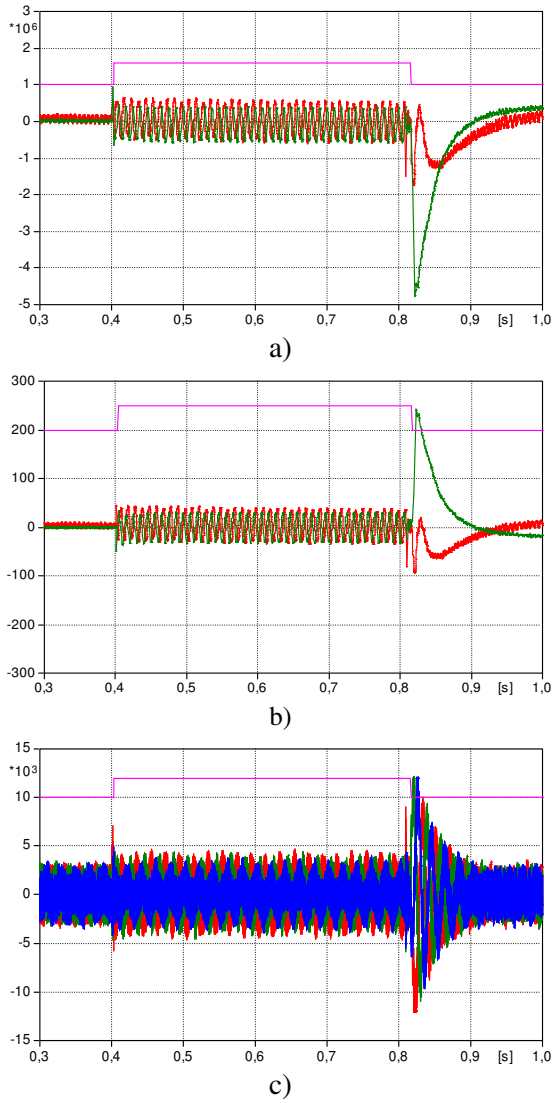

Figure 3-32: Natural response: (a) active (red) and reactive (green) power, (b) currents over axis d (red) and q (green), (c) LV inverter currents and voltage dip identification signal is shown (pink line)

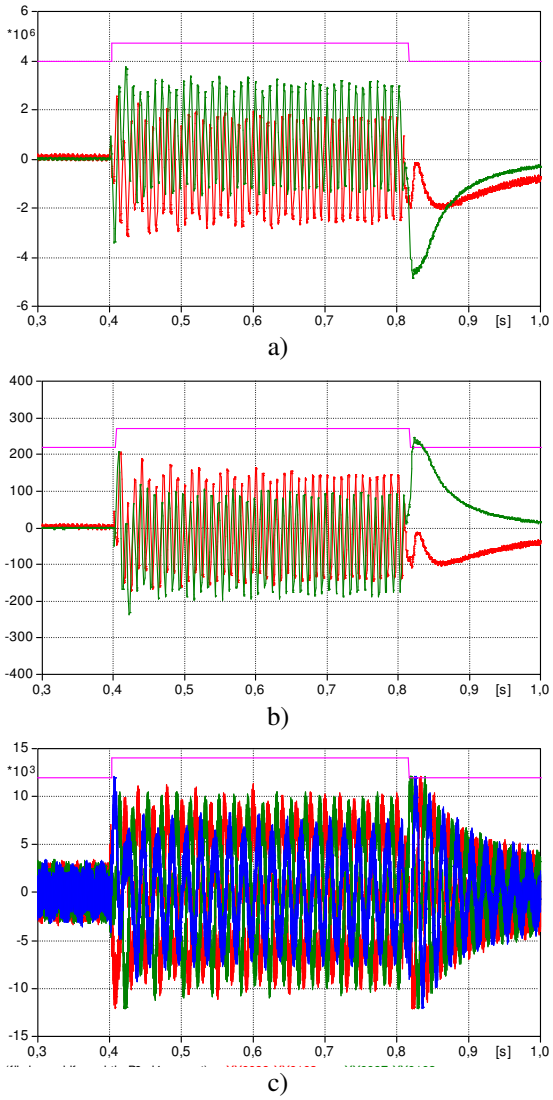

Figure 3-33: Inverter control P=0: (a) active (red) and reactive (green) power, (b) currents over axis d (red) and q (green), (c) LV inverter currents and voltage dip identification signal is shown (pink line)

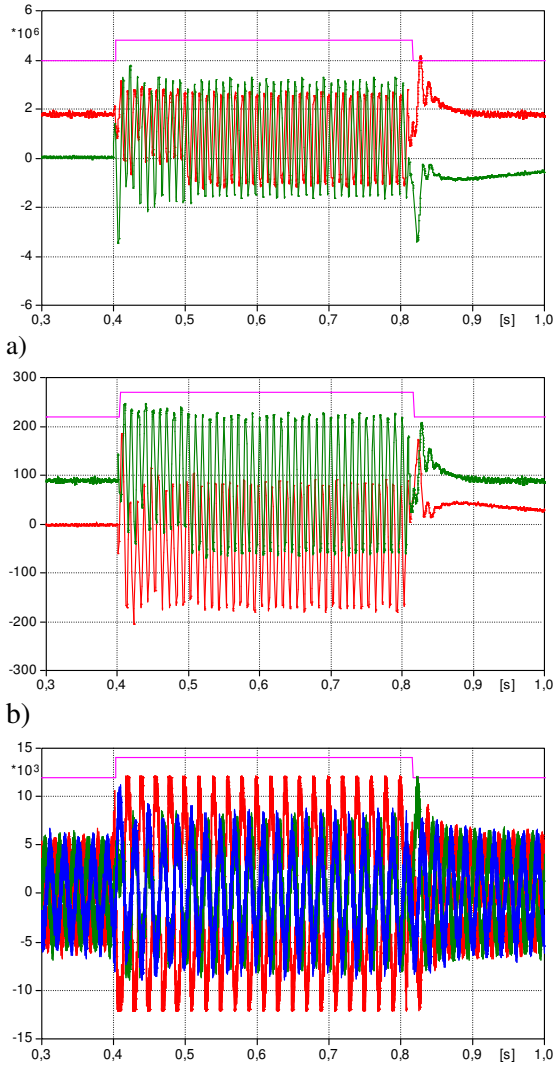

Figure 3-34: Inverter injecting reactive currents: ((a) active (red) and reactive (green) power, (b) currents over axis d (red) and q (green), (c) LV inverter currents and voltage dip identification signal is shown (pink line)

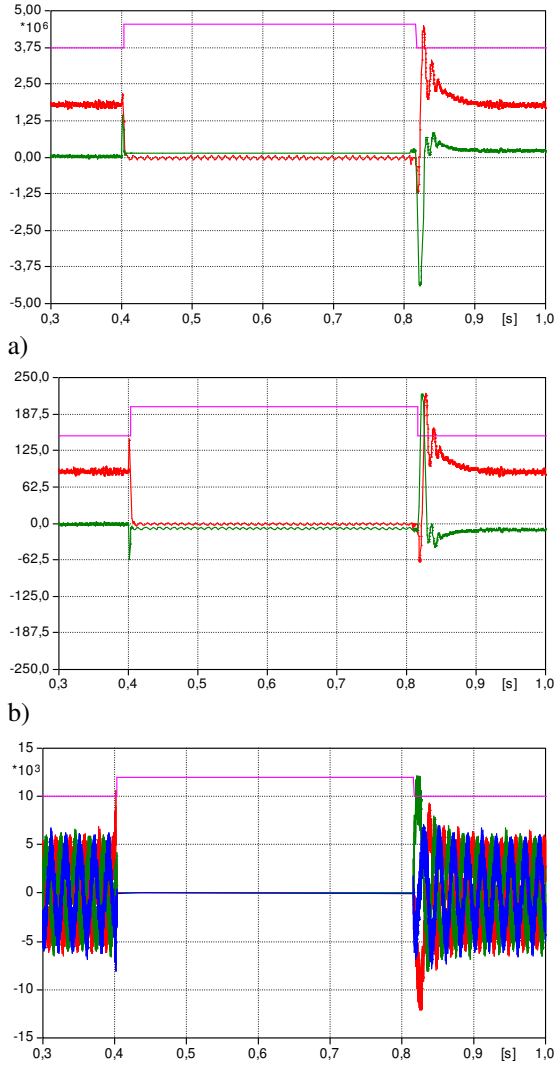

Figure 3-35: Stand-by inverter condition: (a) active (red) and reactive (green) power, (b) currents over axis d (red) and q (green), (c) LV inverter currents and voltage dip identification signal is shown (pink line)

3.5 Final Considerations

In this Chapter possible control strategies and circuit countermeasures to meet the new Fault Ride Through (FRT) requirements have been analyzed using digital simulation for photovoltaic (PV) and wind distributed generators.

In particular different control strategies, activated only during voltage dips, have been considered:

- the control is “frozen” in the steady state status;
- the inverter is forced to supply null active power;
- the inverter is switched to the stand-by mode.
- the inverter should supply a controlled q-axis current.

In general, the simulations showed that for all kind of control strategies, it's necessary to provide:

- a braking chopper to limit the voltage swell in the inverter DC link, due to an unbalance between the active power coming from the generator, practically constant, and the injected power, which decreases due to the decrease of the mains voltage;
- an instantaneous inverter current limitation.

The main results can be summarized in this way:

- the stand-by mode operating condition for the inverter, together with a "freezing" of the control variables to the pre-dip steady state condition, has the less impact on the network, however during the device design it must be considered that the currents can assume high transient values;
- the possibility for the inverter to exchange both active and controlled reactive power, implies an oversize of the system and, in case of faults with critical characteristics, can cause the instantaneous inverter current limitation, with consequent distortion of the output current and voltage waveforms.

The methodology applied for the study of the behaviour of PV and wind plants in case of voltage dips can be extended to any type of Distributed Generators connected to the distribution network through power electronic converters.

4 ANALYSIS OF THE IMPACT ON THE NETWORK OF MORE DISTRIBUTED GENERATORS: DIGSILENT SIMULATIONS

In this Chapter the model of a network for analysis of interactions between more distributed generators connected to the network through electronic converters in case of network disturbance is presented. In this case, the simulations have been carried out in environment DIgSILENT. Since the final aim is to analyze transiently the interactions of more devices to each other and with the network itself, in DIgSILENT a model has been developed, similar to that realized in ATPDraw, whose evaluation/validation has been conducted by comparing the simulation results (in DIgSILENT the transient simulations are defined EMV, Electromagnetics Transient). This step has been necessary due to the DIgSILENT characteristics, mostly oriented toward calculations of Load Flow, short circuit and simulations of electromechanical transients.
The advantage of carrying out simulations in DIgSILENT environment lies essentially in greater flexibility to analyse extended electrical systems that, especially for the detail used in the representation of the power electronic components, is not possible in the ATPDraw environment.

Initially, the model of the photovoltaic generator in DIgSILENT has been developed to assess the equivalence with the with the one modelled in ATPDraw and the capability of these generators to sustain the MV and LV network voltage has been evaluated.
Then the network has been expanded with the introduction of a portion of transmission network representative of the typical Italian configuration including traditional and wind generators (PMSG as those presented in Chapter 2). In the study the Distributed Generation effect on the network voltage support has been investigated.

4.1 Equivalence ATPDraw - DIgSILENT

In DIgSILENT the model of the photovoltaic system, presented in the Chapter 2, has been developed. Its validation has been carried out comparing its transient behavior, in case of a voltage dip, with the results obtained in ATPDraw environment.
The model of photovoltaic generator implemented in DIgSILENT has the same hardware and software structure: the component *ElmGenStat* which represents a controlled current generator capable of supplying active and reactive current setting two reference values has been used. In particular, several simulations of electromagnetic transient “EMT” have been done.

Figure 4-1 show some characteristic measures and control waveform of the “natural” behavior of the PV plant (in absence of Fault Ride Through logic) in case of a three phase inductive fault that cause a voltage dip with depth equal to 30% V_n. The differences in the behavior of the two systems are more attributable to the difficulty in DIgSILENT environment, to manage freely all the parameters relating to the three phase inverter.

The purpose of the simulations developed in DIgSILENT environment is to highlight the influence that a strong penetration of the DG would have on the voltage quality and to analyze the interactions between different distributed generators connected to the network. Therefore the differences between the two models are not considered significant, thus allowing the validation of the model of the photovoltaic generators connected to the network by using devices of power electronic developed in DIgSILENT.

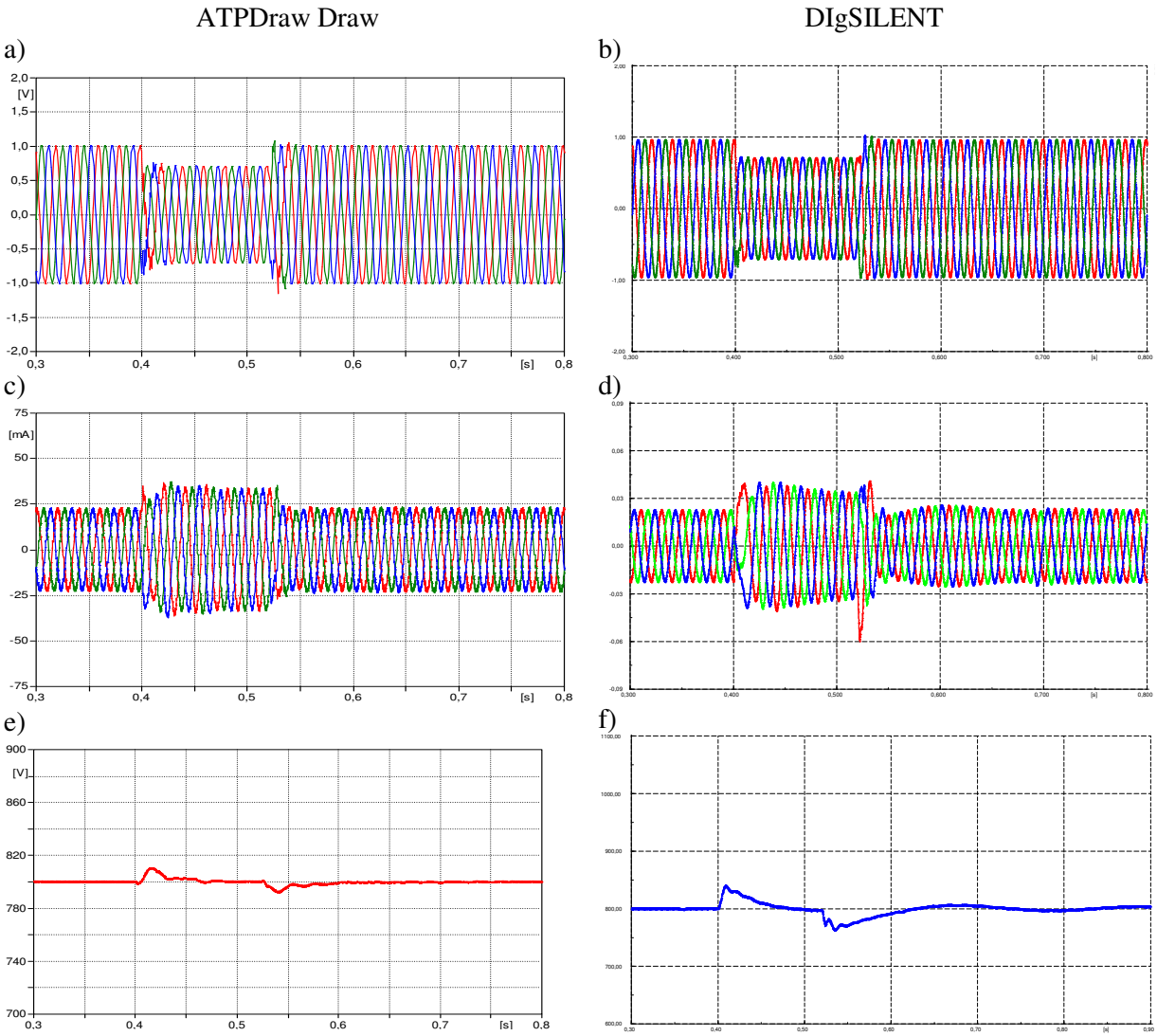

Figure 4-1: Simulations comparisons EMT in ATPDraw and in DIgSILENT: line to line voltages in p.u. (A) and (b); inverter currents MV side (c and d); DC voltage (e and f)

4.2 MV and LV network model

The network simulated in DIgSILENT, as done in ATPDraw, develops from a MV bus-bus of a Primary Substation (PS) supplied by the HV network (132 kV), represented with an equivalent impedance. In particular five MV feeders of different lengths, including both cable and overhead line sections have been considered, along which loads of different types are directly connected (passive loads and, in addition than the ATPDraw model, rotation and disturbing loads); some Secondary Substations (SS) and LV networks with installed the same kind loads as in MV are also detailed.
The PV plants are connected directly to MV and LV network; in particular 3 "sizes" with the following ratings have been considered:

- 630 kW - MV connection with coupling transformer;
- 60 kW - LV connection with a dedicated coupling transformer;
- 19 kW - direct LV connection without transformer.

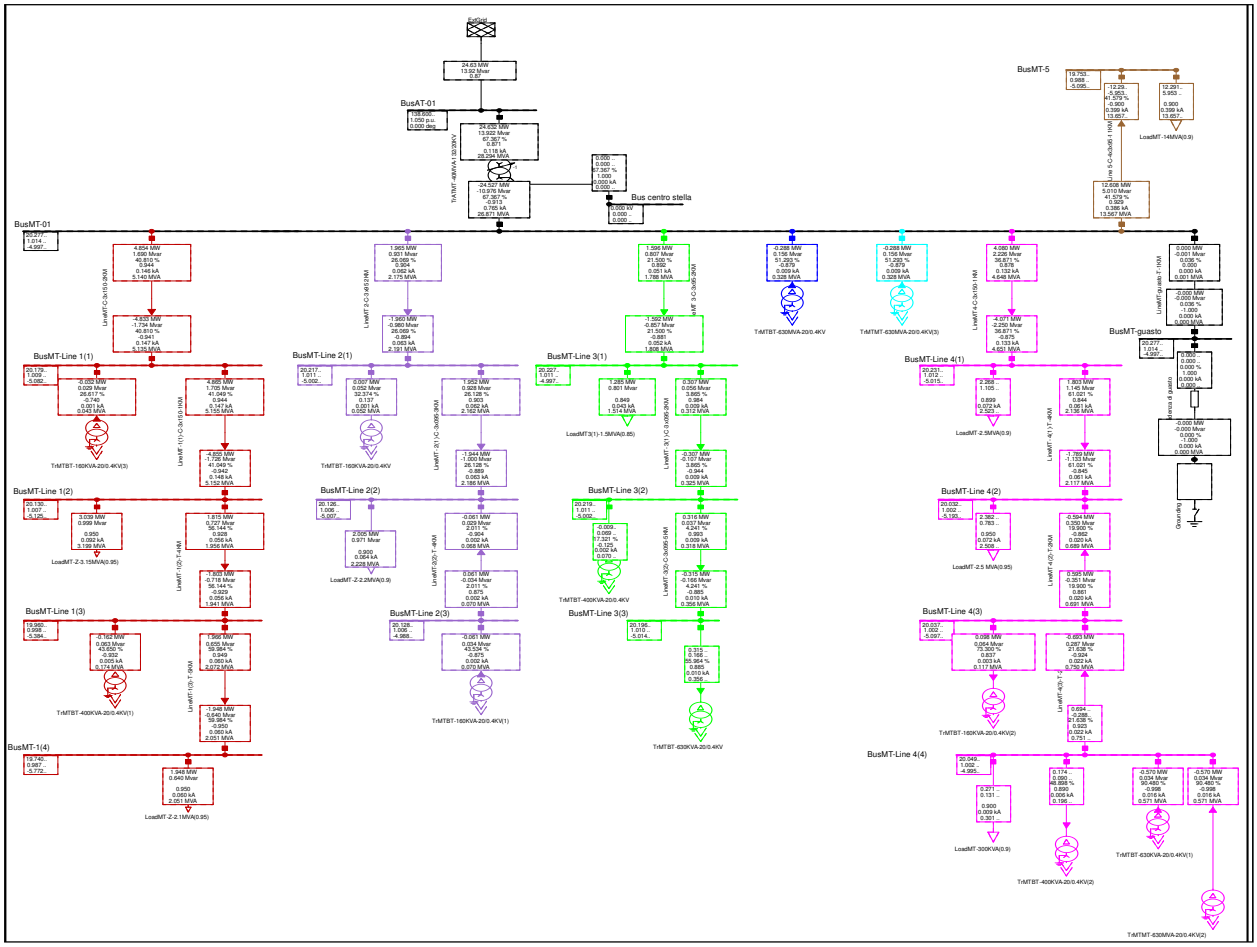

Figure 4-2: DIgSILENT MV network structure

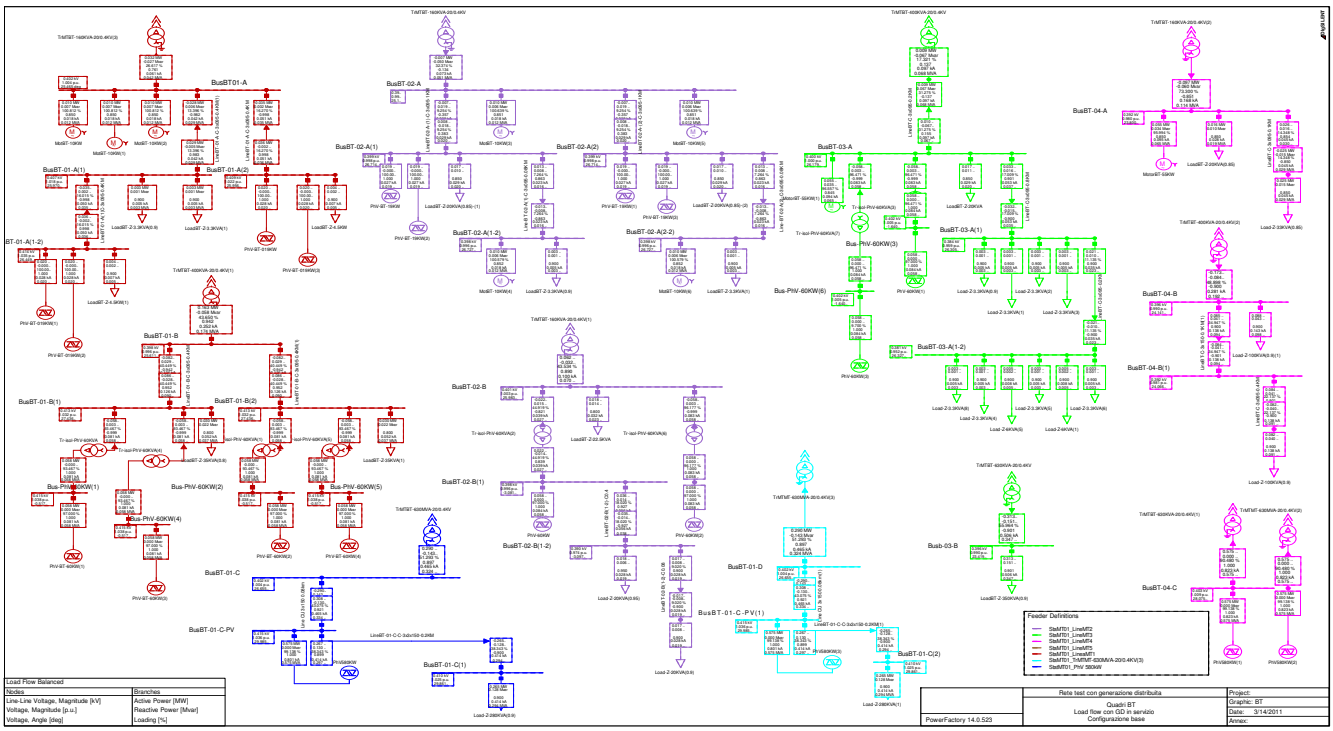

Figure 4-3: DIgSILENT LV network structure

4.2.1 Simulation results of LV and MV network voltage support from PV generation

The preliminary simulations have been developed starting with a base case with DG penetration equal to 10% of the total power consumption of the MV network (under the irradiation conditions 1000W/m2 and temperature 25C) and with a total load, representative of industrial utilities and residential, equal to 70% of the rated power of the PS transformer.
Since the first objective of the study is to check the network steady state condition (Load Flow) and the voltage profiles along the feeder using the phasor mode, some model simplifications have been done, for example in this case the switching of the valves are not represented[33].

Simulations in case of a transient and permanent network fault, simulating also the fast and slow logic of reclosing of the line Circuit Breaker (CB), have been done and different voltage dips have been considered (phase to phase, three phase, isolated or ground, resistive or inductive fault). These preliminary simulations have also been carried out for different network scenarios, such as:

- absence of the whole DG (to assess the behavior of the network completely passive);
- condition of passive load reduced and presence of the whole DG connected (to assess the impact of the DG on voltage profiles in the case of network "partially discharged").

Finally the configurations considered have been simulated in case of compensated network and isolated network.

For example, for a MV feeder (with a percentage of distributed generation of 7% of the passive load derived from feeder itself), Figure 4-4 shows the voltage profile in the case base, while Figure 4-5 highlights what happens without DG.

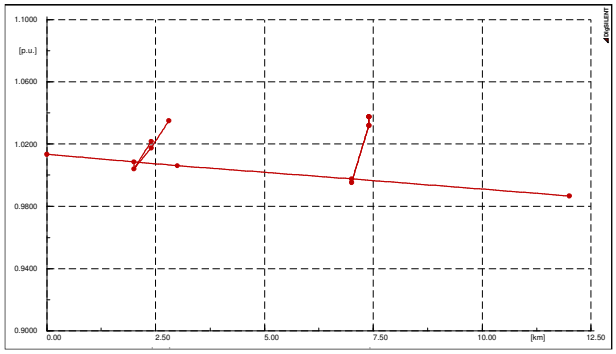

Figure 4-4: Voltage profile of a MV feeder base case

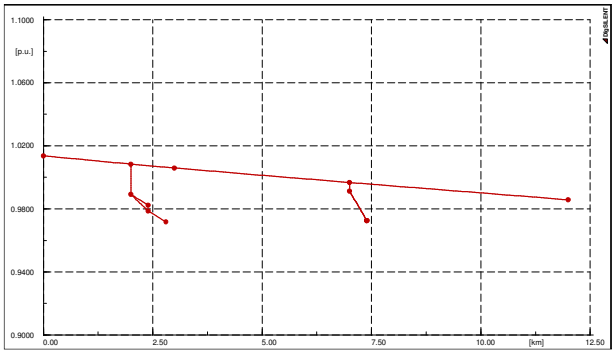

Figure 4-5: Voltage profile of a MV feeder without DG

In particular in Figure 4-6 the detail diagram of a LV feeder is reported with highlighted the nodes at which it is examined the voltage profile with the distributed generators connected (Figure 4-7): the generators (two 19 kW plants) are connected to the nodes C and D at the bottom of two different LV lines ("base case"). It is possible to verify that the presence of DG gives rise to an increase in the voltage in the connection node up to a value equal to about 2% of the LV bus-bar voltage in the SS (node A).

[33] While in the EMT validation simulation reported in § 4.1, this operation has been modeled.

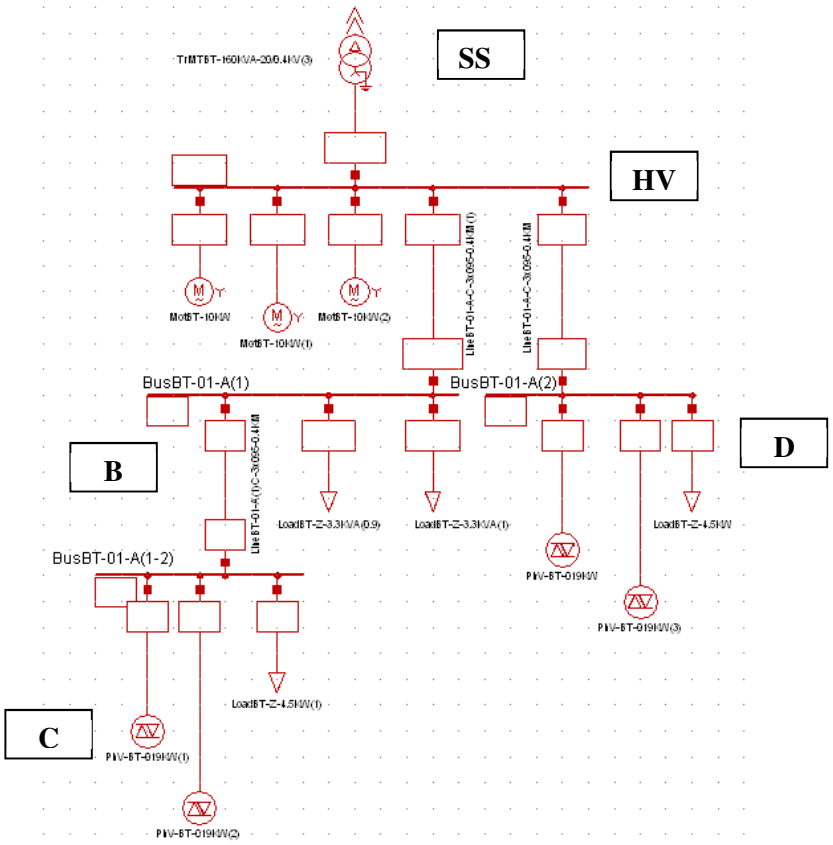

Figure 4-6: Zoom of a LV feeder with 19 kW photovoltaic generators

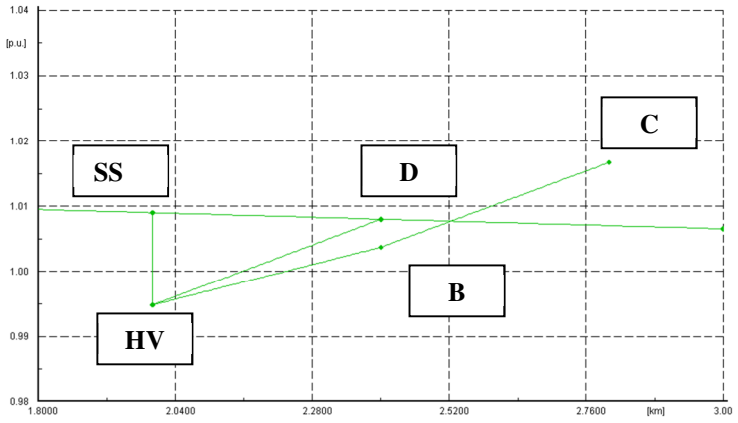

Figure 4-7: Voltages profile (in p.u.) LV feeder in the "base case"

Figure 4-8 and Figure 4-9 show the voltage profiles for the same feeder, respectively, without DG and with reduced load. The last case is the one that determines, as expected, the rise of higher voltages in the connection DG node; the voltage variation between the conditions "with DG" and "without DG" is about 3% for the node D and approximately 5% for the node C.

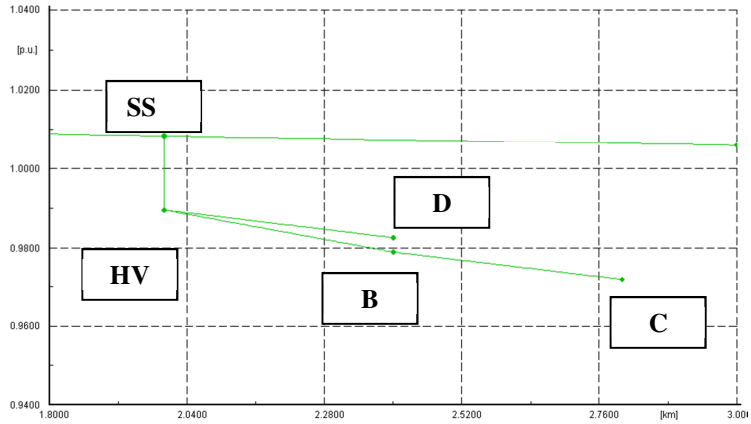

Figure 4-8: Voltages profile (in p.u.) LV feeder without DG

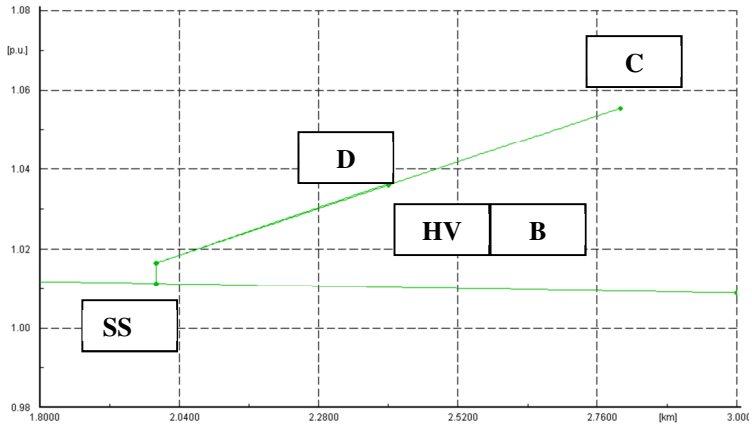

Figure 4-9: Voltages profile (in p.u.) LV feeder with DG and reduced load

Then in the presence of network faults, two different situations have been analyzed:

- transient fault with a typical sequence of fast reclosing;
- permanent fault with a typical sequence of fast + slow reclosing and subsequent permanent opening of the line circuit breaker.

The simulation results report the RMS values of the voltages at the connection node of two 19 kW generators (node C in Figure 4-6) in case of a three phase voltage dip, with a depth such that inverter valves current limitations aren't activated both in the "base case" and without DG.
In particular Figure 4-10 shows that during steady state condition the voltage in the "base case" is higher and in case of fault the voltage is supported by the DG causing an increase in the residual voltage equal about 10% compared with the case without DG. In each simulation the natural response of the distributed generation is considered (without FRT logic).

It should be noted that the RMS voltage value trend during and immediately after the disturbance is linked to the behavior of rotating loads, as confirmed by Figure 4-11, that shows the results of the same simulations in the presence of an "equivalent" static load.

Finally, from the analysis of the Figure 4-12, comparing the RMS values in p.u. of the MV bus-bar where the fault is located and the PV plant connection node in LV (node C in Figure 4-6), in case of a voltage dip with a depth of 40% V_n, the presence of the DG reduces the depth in its node of 5%, that is the depth of voltage dip becomes about 35% V_n.

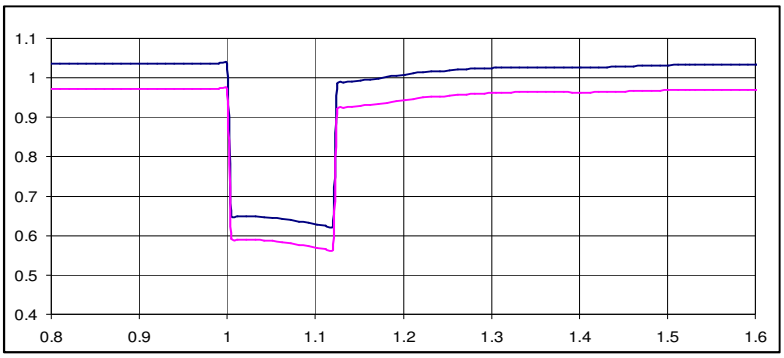

Figure 4-10: Voltage RMS (in p.u.) at two 19 kW PV generators connection point: "base case" (blue curve) and without DG (curve pink)

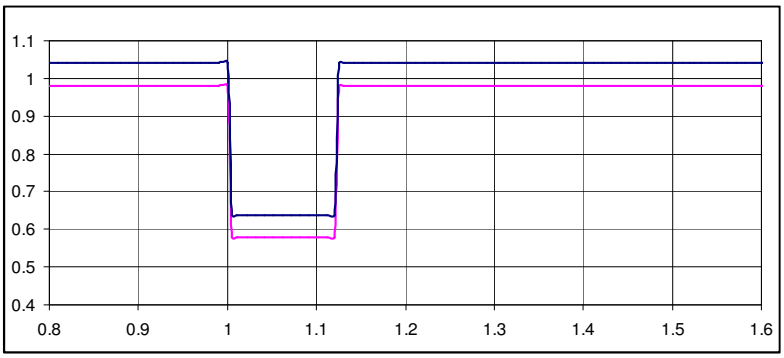

Figure 4-11: Voltage RMS (in p.u.) at two 19 kW PV generators connection point: "base case" (blue curve) and without DG (curve pink), with only static load

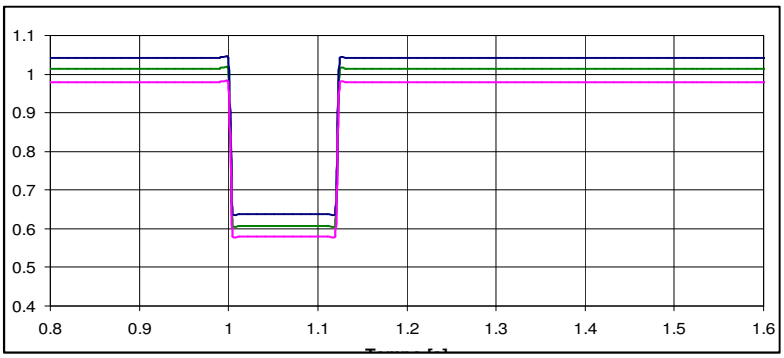

Figure 4-12: Voltage RMS (in p.u.) at two 19 kW PV generators connection point: "base case" (blue curve), without DG (curve pink) and to the MV bus- bar (green curve), with only static load

In general, these simulations have allowed to characterize the modeled network; below an extension of the network is presented with different placement of the DG to evaluate the mutual interactions of distributed generators, also wind generators, in presence of network disturbances considering the Fault Ride Through strategies presented in Chapter 3.

4.3 Network extension (HV)

The model of a portion of the HV network representative of the typical Italian configuration of transmission and sub-transmission including traditional and wind generators is presented in Figure 4-13.

The HV network model has been completed by implementing the models of typical protection used in the meshed transmission networks. These protections are essentially distance relays. The HV network

feds, in a PS, a bus-bar MV through a 40 MVA transformer with short circuit power equal to 11 %. The transformer has a tap changer. From this bus-bar, 5 feeder have been defined:

- Feeder 1: cable line with an overall length of 18 km. The modelled line is divided into 8 sections and on each section loads and power factor correction capacitors are connected: on this feeder is supposed to be installed the DG;
- Feeder 2: passive cable line with an overall length of 6 km, on the bottom there is installed a 800 kVA transformer for the supply of industrial loads at 690 V. Along the line loads and power factor correction capacitors are connected;
- Feeder 3: cable line of length equal to 10 km, with a load equivalent to 23.5 MVA and power factor of 0.85;
- Feeder 4: empty cable line with a length of 10 km, used to simulate network faults;
- Feeder 5: short line connected to a SS, to which 2 LV networks at 400V are connected. Each LV network is powered by a 630 kVA transformer and includes several residential loads, represented by an equivalent.

The DIgSILENT network model is represented in Figure 4-13. In general, in this network model, the faults can be simulated at every voltage level to evaluate different voltage dip conditions.

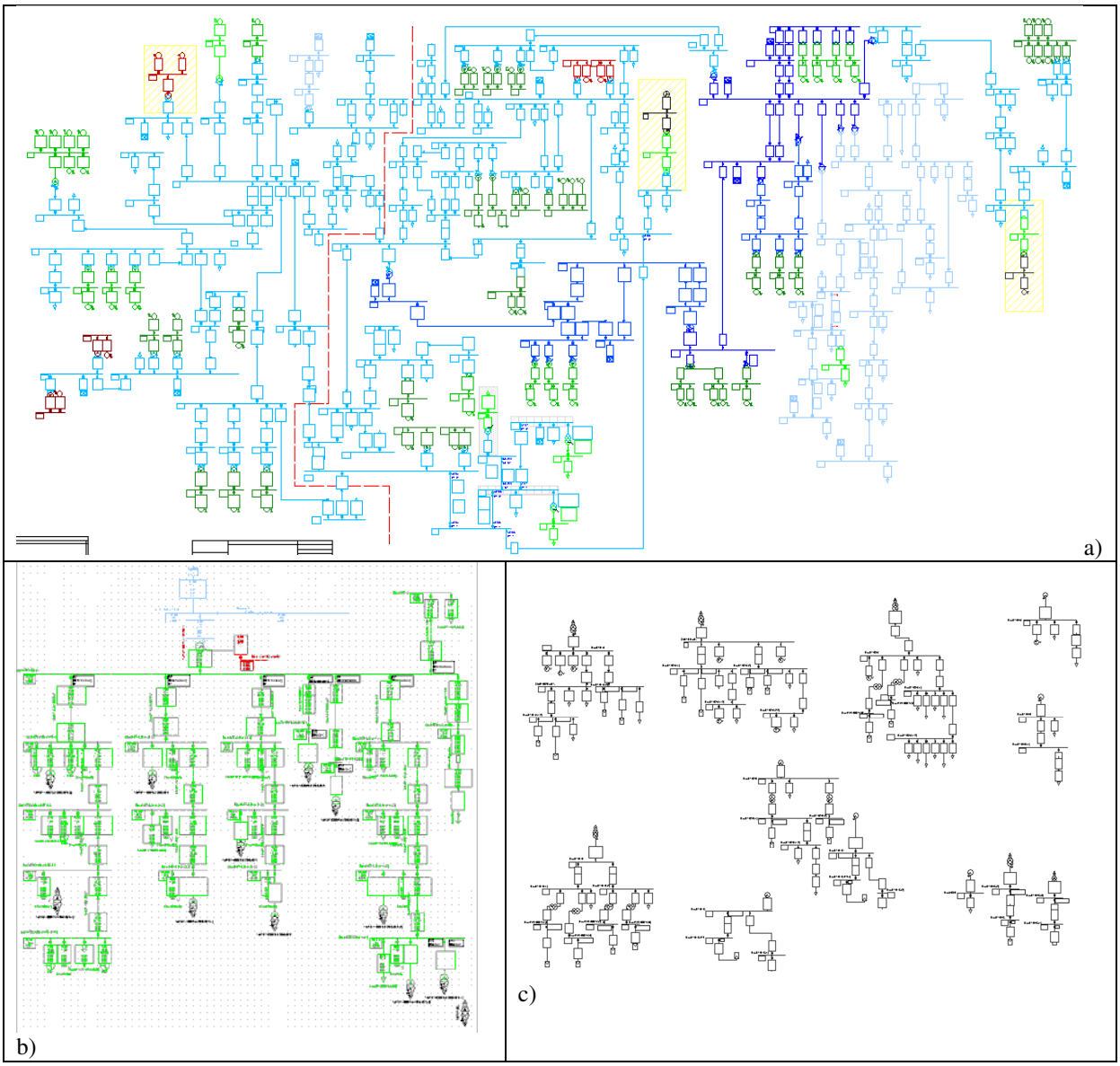

Figure 4-13: Network model developed in DIgSILENT. (a) section HV, (b) section MV, (c) sections LV

4.3.1 HV network protection model

Distance relay have been modeled as lines protections of the HV network. To reduce the simulation complexity, the protections are included only in certain sections of the network and in particular at the ends of the lines on which the faults are simulated. It's used a model of distance relay already available in the simulator libraries, referring to a commercial distance relay protection[34], calibrated according to the given indications summarized in Table 4-1.

Table 4-1: Typical settings for HV distance relay

	Tripping impedance	**Intentional Delay**
1st zone	$0.8 \cdot Z_L$	Basic Time
2nd zone	$0.8 \cdot (Z_L+0{,}8 \cdot Z_{LC})$	0.3 s
3rd zone	$1.2 \cdot (Z_L+Z_{LL})$	0.8 s
4th zone	Starting impedance $1.25 \cdot 1{,}2 \cdot (Z_L+Z_{LL})$	1.4 s ÷ 1.6 s at 132 kV and 150 kV 2.2 s at 220 kV 3.5 s at 380 kV
5th zone (if present)	As 4th	As 4th
where: • Z_L: impedance of the line to protect; • Z_{LC}: value of the line impedance with lower impedance subsequent to that to protect; • Z_{LL}: value of the line impedance with higher impedance subsequent to that to protect.		

The tripping impedance must be chosen in such a way that meets the criteria:

- greater than or equal to 125% of the value of the impedance of the 3th zone;
- less than or equal to 50% of the load impedance, in the most critical exercise condition;
- smaller than the minimum impedance seen on healthy phases in case of a single phase fault.

As an example, Figure 4-14 shows the areas of intervention of the relay place at the beginning of the feeder that feds the primary substation from which the MV network where the faults are simulated is derived. This PS is also fed by a second sub-transmission HV line that is healthy for the purposes of the simulations.

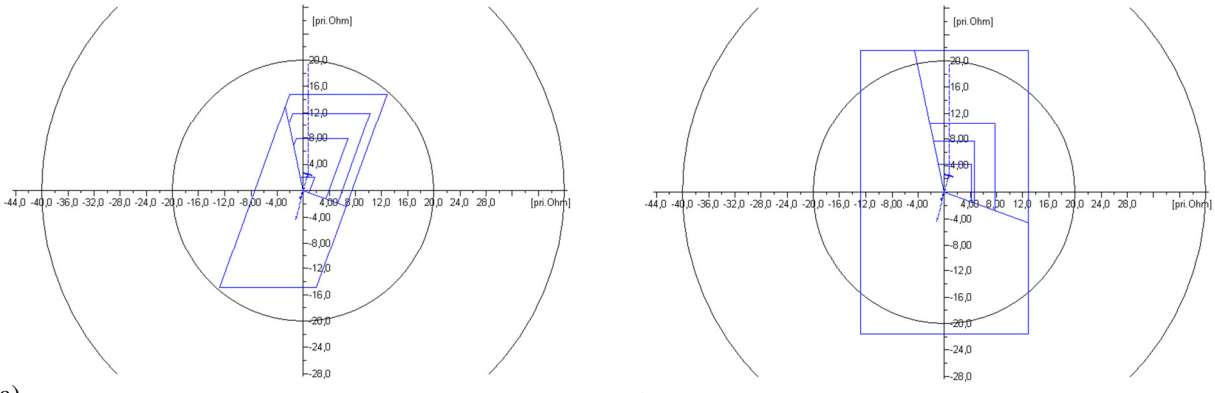

a) b)

Figure 4-14: HV distance relay intervention areas, diagram R-X a) settings for measurement of quantities between phase and phase, (b) settings for measurement between phase and earth

[34] The settings have been defined in accordance with the indications contained in the Italian Technical Guide GRTN "Criteri generali per la taratura delle protezioni delle reti a tensione uguale o superiore a 120kV", 2000.

The two graphs are shown on the plan R/X, where R is the resistive and X the reactive component of the impedance measured by the distance relay protection. The two graphs refer respectively to the impedance measured between phase and phase, which is used to recognize two-phase and three phase faults, and between phase and earth, used for the single phase to ground fault detection. If the impedance value measured by the protection, along the direction of the protected feeder, is included into one of the highlighted areas, the protection trips and causes the opening of the circuit breaker associated, after the intentional delay as reported in Table 4-1.

Figure 4-15 shows a simplified diagram of an HV line, placed between two HV bus-bars, at the ends of which are installed two distance relay protections R1 and R2, each is set according to the typical parameters. For each of the protections the intervention areas are shown in terms of line length and intentional delay (t1 for the first area of intervention and t2 for the second zone). If a direct fault to ground occurs at one of the two ends of the line, for example near R1, R1 starts in the first step and trips after t1, while R2 starts in the second step, tripping after t2 >t1.

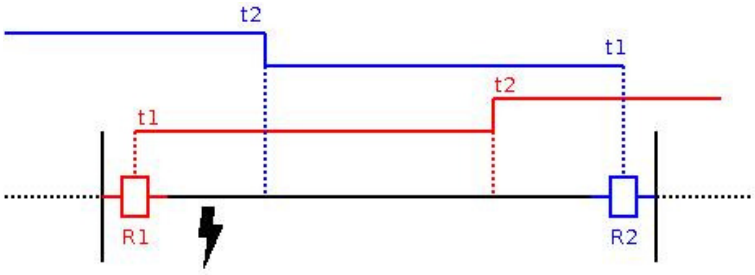

Figure 4-15: Typical intervention scheme of distance relays placed at the opposite side of the same line

Figure 4-16 shows an example of a three phase direct to ground fault in the HV network, in a location similar to that described in the previous example. This figure presents the comparison, for the purpose of validation of the model, between the result of the simulation (a) and a recording (b) of an event whose origin is found in a fault occurred in the HV network, provided by the Italian QuEEN[35] system for monitoring the voltage quality in MV network.

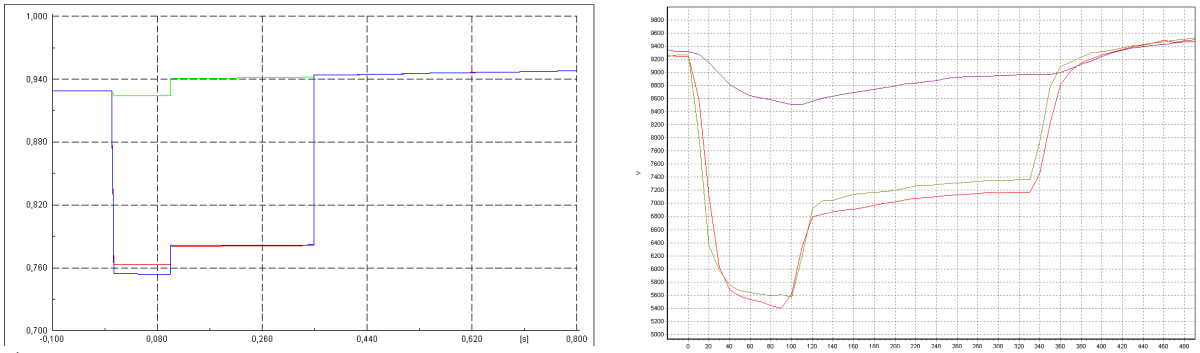

a) b)

Figure 4-16: MV bus-bar RMS voltages in case of a fault in the HV network: a) simulation result, b) values measured by the voltage quality monitoring system QuEEN

[35] Http://queen.rse-web.it/

4.4 Wind generators model

The model of wind generator connected to the Medium Voltage distribution network, implemented in DIgSILENT[36], has a rated power equal to 2 MVA, designed to exchange with the network the 110% of its power (according to the requirements included in the CEI 0-16 for voltage dips overcoming, Chapter3).

The Permanent Magnet Synchronous Generator (PMSG) is modeled using the native DIgSILENT component *static generator* ("ElmGenstat"). The block diagram which describes the functional parts of the generator and the connections between them is shown in Figure 4-17, where there are the electrical measurement stages, the control section and the power components of the generator.

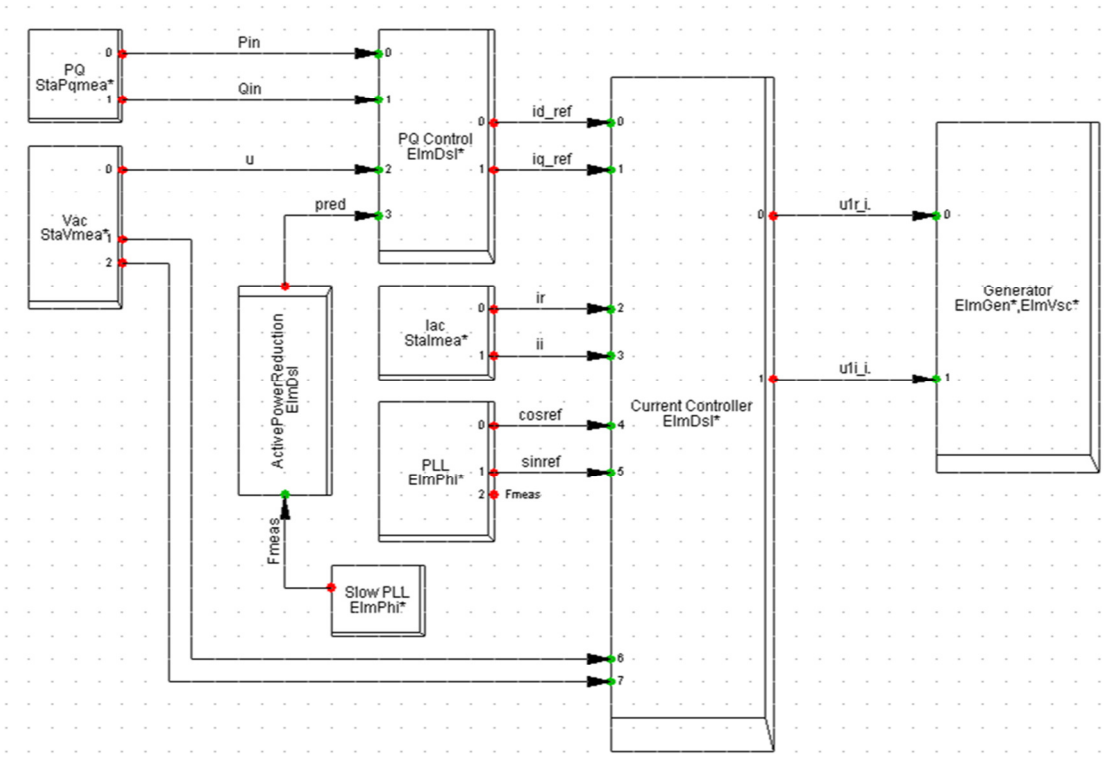

Figure 4-17: Block diagram of the wind PMSG

This model is essentially a controlled current source, it's possible to set independently the current references over direct and quadrature axes. The output current regulation is made with two Integral Proportional regulators. The models implemented allow to set the maximum current that can be exchanged by the generator, calculated on the basis of its maximum power and output voltage. The diagram of the control is similar to that developed in ATPDraw. The only difference, as a result of the reduced inverter model (the valves of the inverter are not modeled), is in the calculation of the direct-axis reference current, which in this case is fixed to allow the generator to inject its rated active power, while in the ATPDraw model the d-axis current reference is calculated to keep the inverter DC voltage at a constant value. A detailed diagram of the control is shown in Figure 4-18 and Figure 4-19. The distributed generator is equipped with a control system that is able to meet the FRT requirements and their impact on the voltage support has been evaluated.

[36] It has all the same features as the model implemented in ATPDraw.

The design parameters of the wind generator are the same used in ATPDraw except the parts relating to the control that are reported in Table 4-2[37].

Table 4-2: Wind generator design parameters

Inverter		
Rated Power	2 MW	
Rated output voltage	400 V	Line Voltage in LV
Current rating	2.9 kA	For each phase, in LV
Inductance switching	25.3 µH	10% V_{cc}

Table 4-3: Wind generator regulator parameters

	Gain bandwidth product	**Phase margin**
$H(s) = \frac{1+0{,}002s}{0{,}002s}$	90 Hz	5°

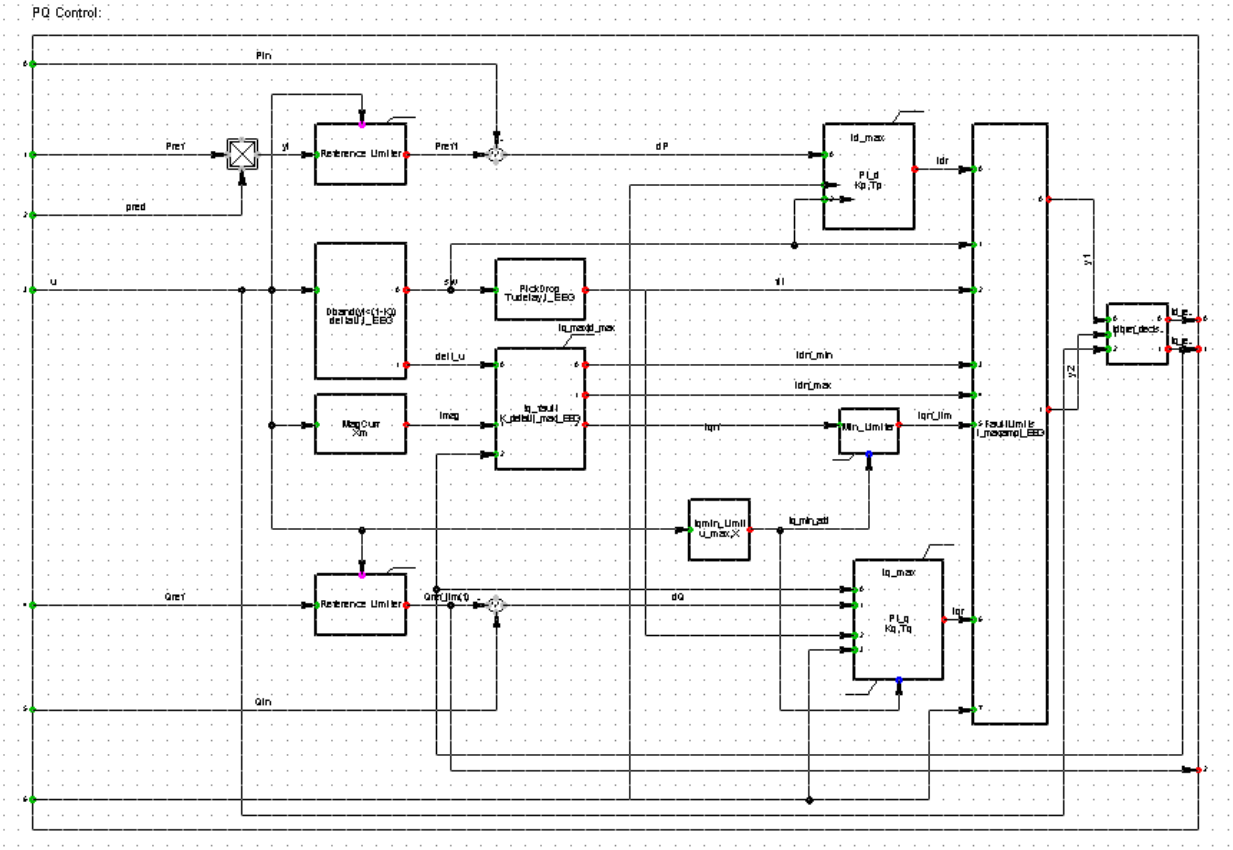

Figure 4-18: DIgSILENT Diagram of the control of the wind PMSG: current references calculation

[37] In any case, the performance in terms of step response are comparable to those calculated in Chapter 2.

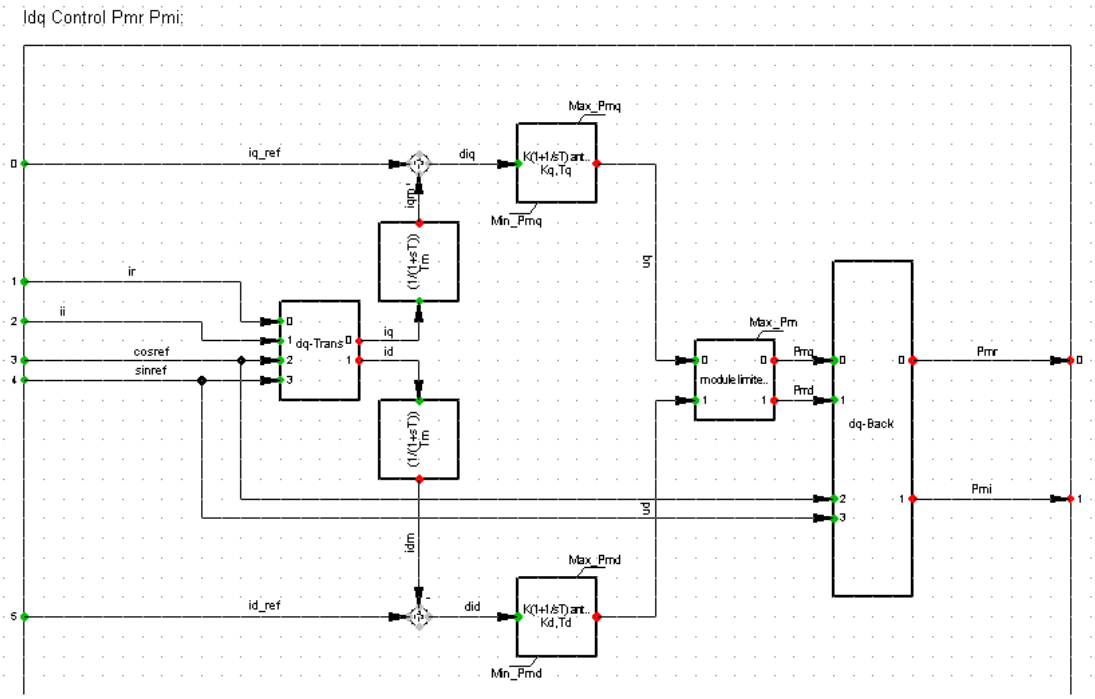

Figure 4-19: DIgSILENT Diagram of the control of the wind PMSG: adjustment of the d-q currents

4.5 Simulation results of LV and MV network voltage support from wind generator

In the simulation model, five wind turbines each equal to 1 MVA are introduced and connected to the MV network, in different locations of the same feeder as shown in Figure 4-20. For simplicity in the scheme the loads, those are connected to all the MV and LV network nodes, and other MV feeder are not shown.

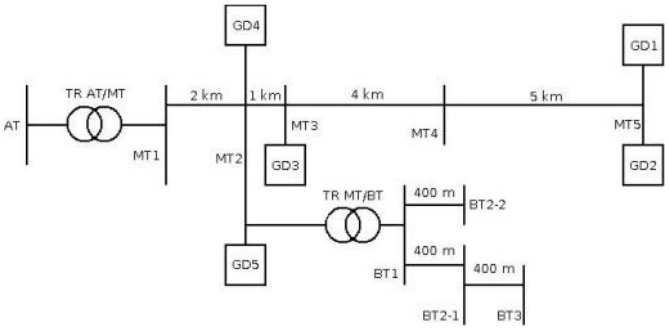

Figure 4-20: Schematic representation of the MV and LV network with wind generators

In order to evaluate the DG effect in terms of voltage support, the simulations have been carried out with the "EMT" of the environment DIgSILENT and different types of fault have been simulated, in particular:

- three phase fault direct to ground on the HV line close to the PS (residual voltage at the MV bus-bar:33 % V_N);
- resistive three phase fault with impedance (5 Ω) on the HV line close to the PS (residual voltage at the MV bus-bar: 82% V_N);
- three phase fault direct to ground on a line with a distance from PS of about 20 km (residual voltage at the MV bus-bar: 83% V_N);

- three phase fault direct to ground on one MV feeder (without DG installed), at a distance of 2.75 km from the MV bus-bar (residual voltage at the MV bus-bar: 53% V_N).

Figure 4-21 shows the simulation results concerning the DG behavior in case of three phase direct to ground fault away from the Primary Substation.

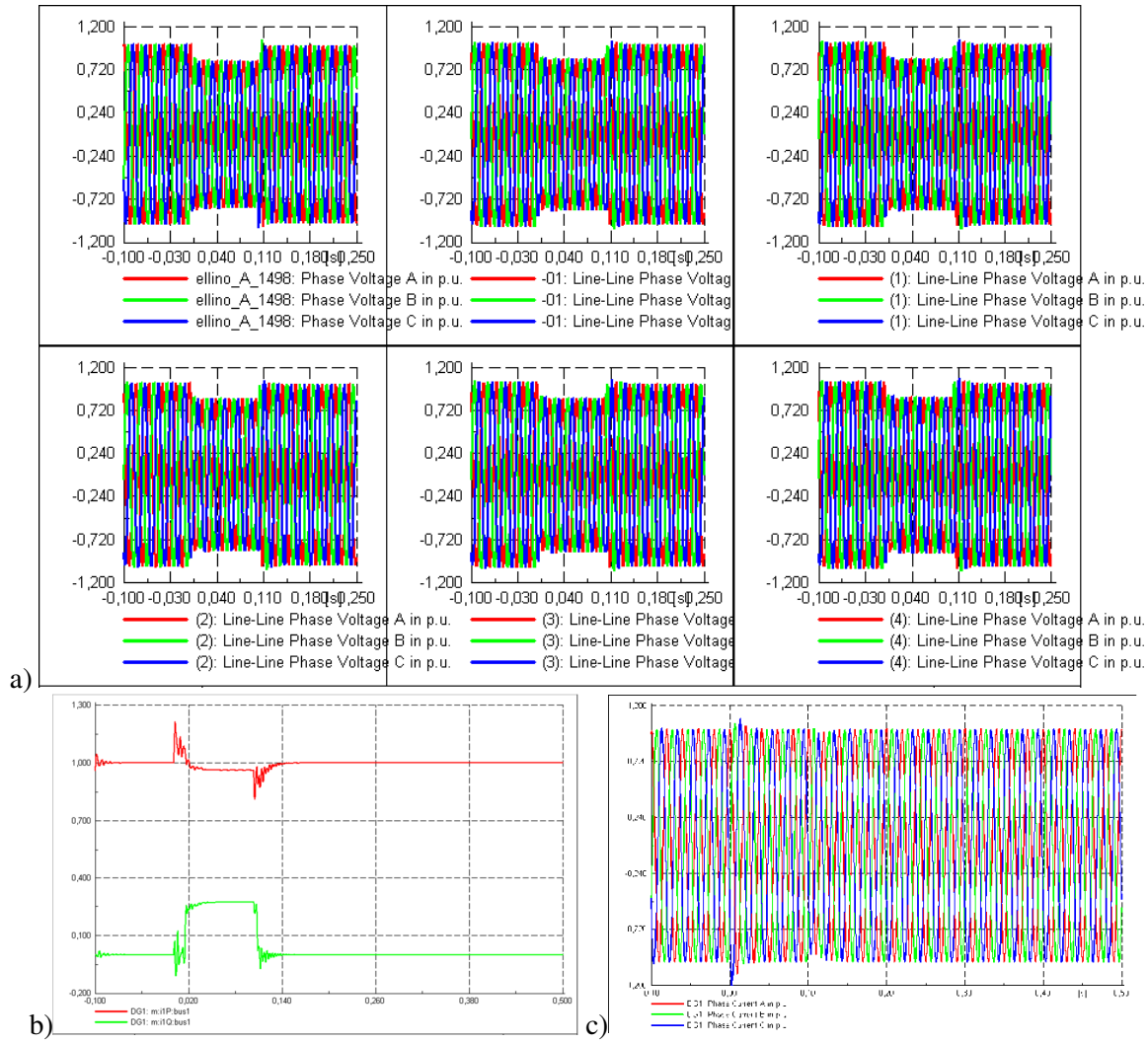

Figure 4-21: Simulation results in p.u.: a) HV (graphs above) and MV (lower graphs) voltages; b) direct (red) and quadrature (green) GD1 current, c) inverter currents of inverter.

In order to analyze the capability of distributed generators to support the network voltage during the voltage dip, for each type of fault, in any node of the MV or LV network, the response of the entire system without DG and the responses obtained by connecting the wind generators one by one, following the numbering order given in Figure 4-20, have been simulated. For each case, it has been detected the residual voltage during fault and at the end of the transient. The results are shown in Figure 4-22 ÷ Figure 4-25. The graphs show both the residual voltages at different network nodes (MV and LV) for different powers of DG installed along the MV line and the percentage variations of the network residual voltage with respect to the case of feeder purely passive. These percentages are:

- in the MV network in all cases below 6%;
- at LV network level under 3%;
- in the HV network there aren't significant voltage variations neither for the effect of the MV network faults nor for the effect of the DG.

Direct ground fault "close" to the PS

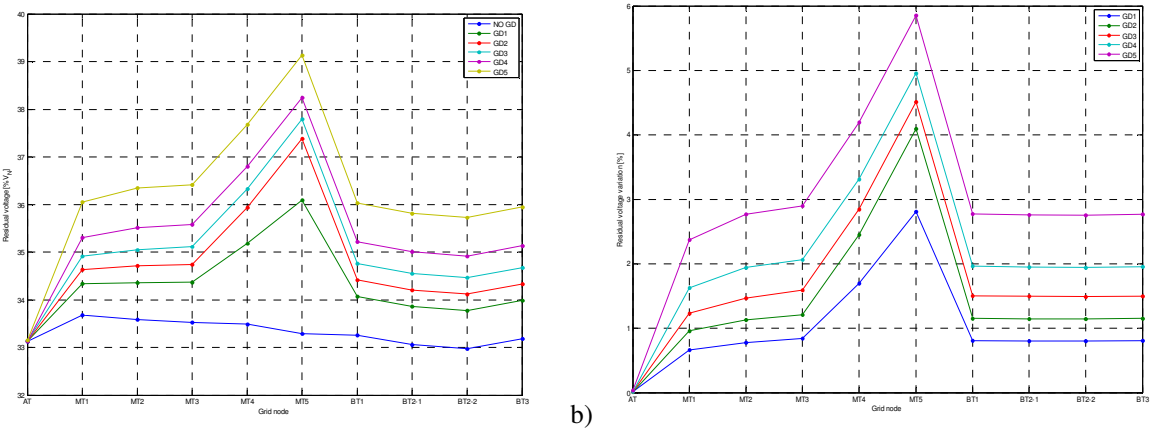

a) b)

Figure 4-22: For different DG powers installed: a) residual voltages at each node during voltage dip, b) residual voltage percentage variation respect to the case of passive feeder.

Resistive fault "close" to the PS

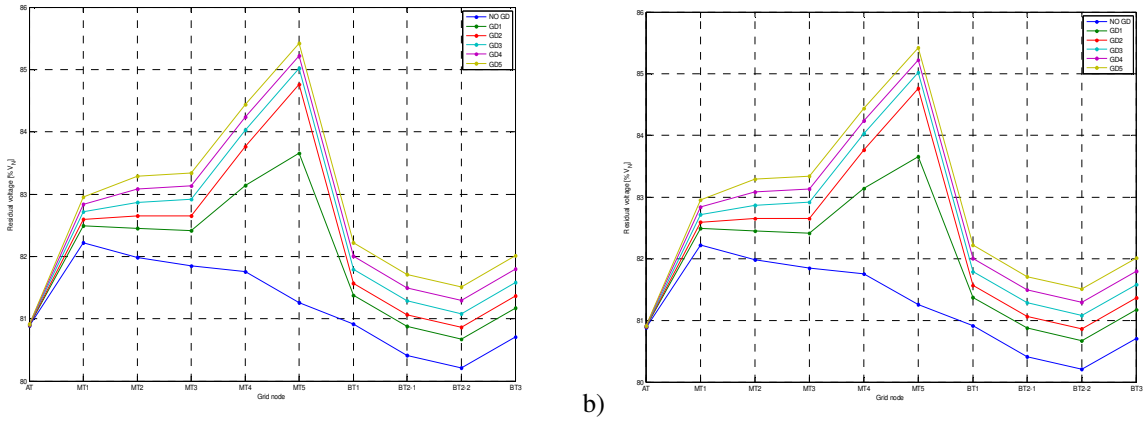

a) b)

Figure 4-23: For different DG powers installed: a) residual voltages at each node during voltage dip, b) residual voltage percentage variation respect to the case of passive feeder.

Direct ground fault "far away" by PS

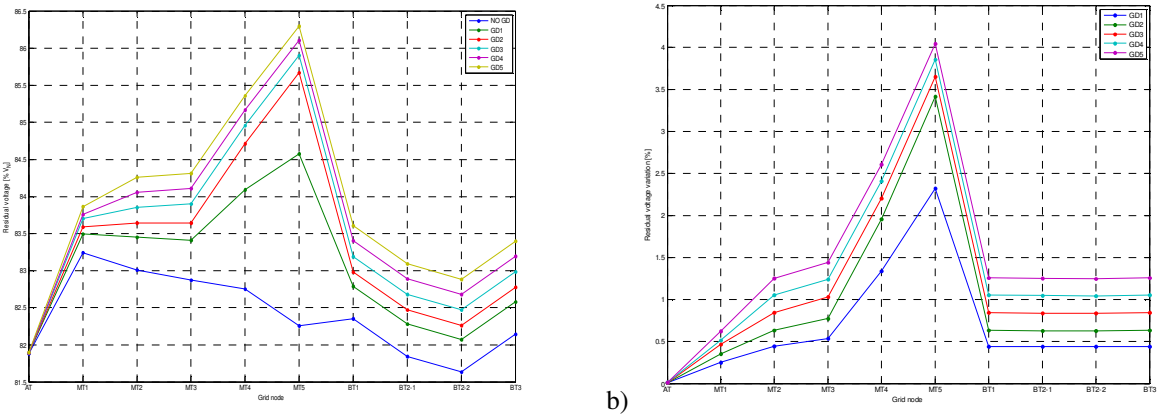

a) b)

Figure 4-24: For different DG powers installed: a) residual voltages at each node during voltage dip, b) residual voltage percentage variation respect to the case of passive feeder.

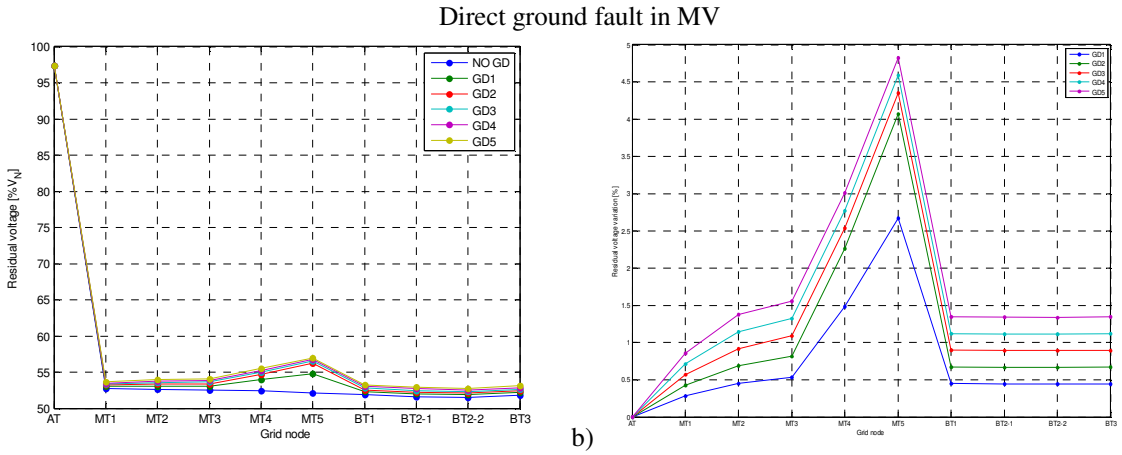

Figure 4-25: For different DG powers installed: a) residual voltages at each node during voltage dip, b) residual voltage percentage variation respect to the case of passive feeder.

4.6 FRT logic

Also for the generator modeled in DIgSILENT the following FRT strategies have been taken into account:

- the inverter is forced to supply null active power;
- the inverter should supply a controlled current over q-axis.

The two FRT strategies analyzed have been implemented by modifying the current references over the d-q axes, in accordance with the type of control adopted and verified by simulating a three phase fault direct to ground at a distance of about 26 km from the generator connection point. In particular, it has been simulated a fault that causes a voltage dip of residual voltage and duration, measured at the point of connection of the DG, equal to 25% of the rated voltage (150 kV) and a duration of 120 ms.

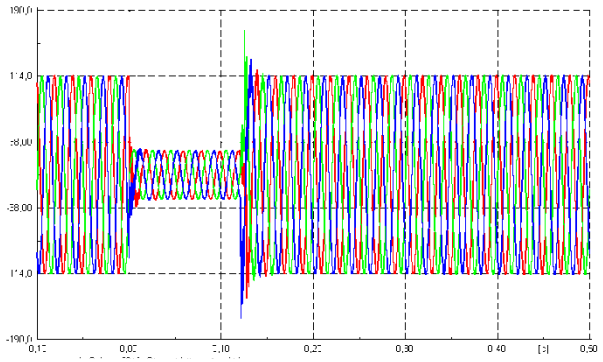

Figure 4-26: PMSG bus bar line to line voltages and voltage dip detection signal

FRT strategy to supply null active power

The strategy to supply null active power during the voltage dip has been implemented putting to zero the reference value of the current direct-axis, as already done in ATPDraw. The main waveforms obtained in simulation are shown in Figure 4-27. The simulation results show that there is no problem for the generator to implement this control strategy but obviously the generator cannot be used in any way to provide services to the network.

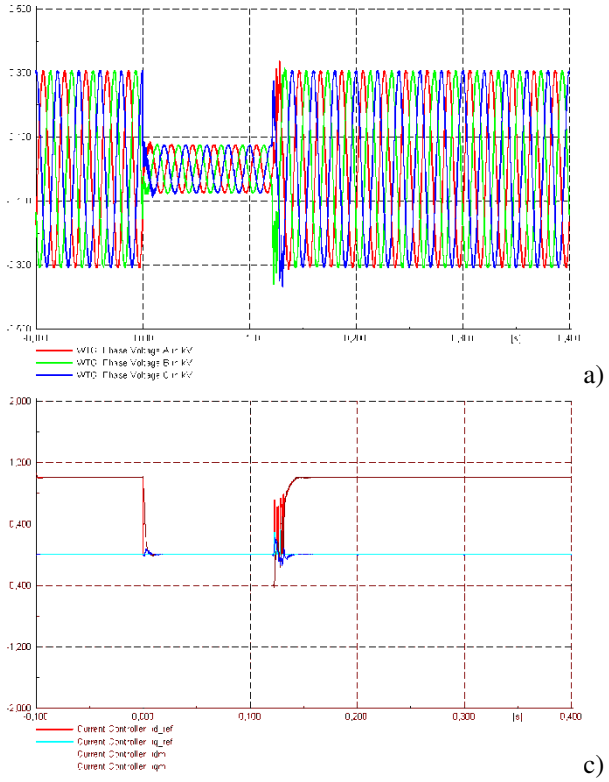

Figure 4-27: Response of the wind PMSG with control P=0 during voltage dip:
a) generator output voltages;
b) LV side current;
c) current d-axis (pink) and q-axis (blue) with their references.

FRT strategy to supply controlled reactive current

The implementation of the control strategy has been carried out in a way similar to that used for the model of ATPDraw wind generator: Figure 4-27 shows the simulation results. Also in this case, the simulations show how the control strategy allows the generator to remain connected to the network for the duration of the voltage dip. In contrast to the control strategy seen previously, thanks to this logic, in principle, the DG can support the mains through the provision of reactive power. In the next section the effect of more DG has been evaluated for the network voltage support.

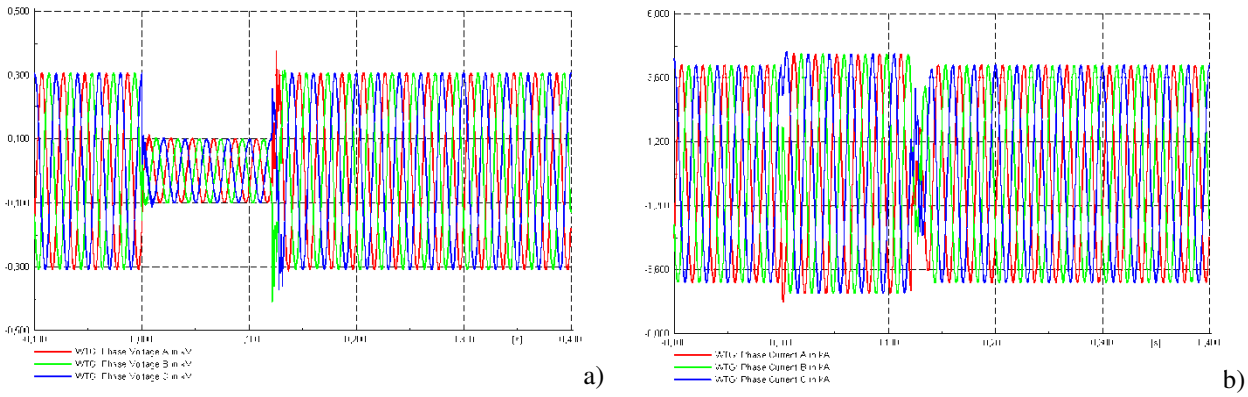

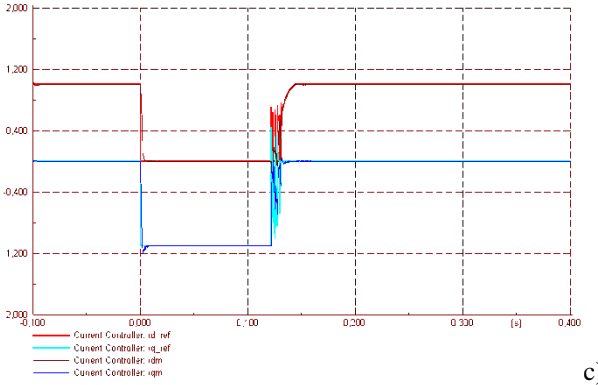

c)

Figure 4-28: Response of the wind PMSG with control to supply controlled reactive current during voltage dip:
a) generator output voltages;
b) LV side current;
c) current d-axis (pink) and q-axis (blue) with their references

4.7 Simulation results of HV network voltage support from wind generator

Using the wind PMSG presented in § 4.4 two wind farms, each having a power of 200 MVA, are modeled in the HV network. Figure 4-29 shows the portion of the network characterized by the connection of these wind farms, whose position is highlighted by boxes with red area. In red the bars on which is evaluated the residual voltage variation due to DG in case of voltage dip are also shown. A permanent three phase fault direct to ground has been simulated without the network protections tripping and the blue color shows the line on which fault is simulated. The same figure, part b), shows a schematic representation of the network portion under examination with indicated the HV lines lengths.

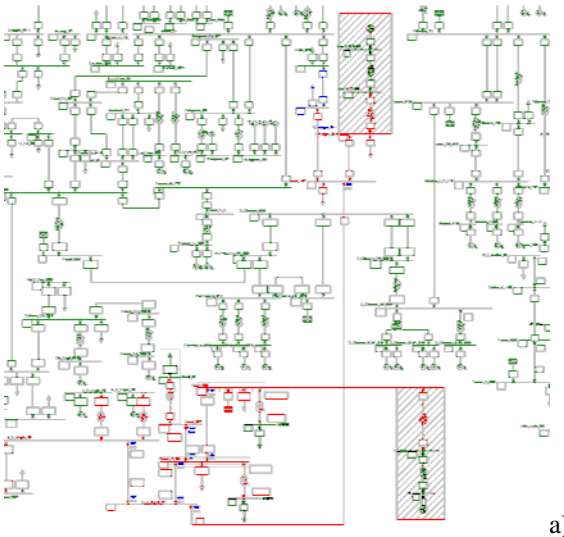

a)

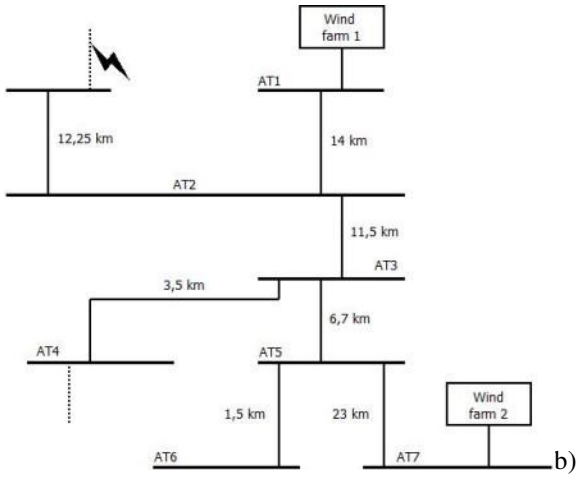

b)

Figure 4-29: Portion of the HV network (highlighted in red) to evaluate the DG voltage support

The study has been carried out varying independently the power generated by the two wind farms, during steady state and during the voltage dip, from zero up to 100% of their capability, according to the scheme shown in Figure 4-30.

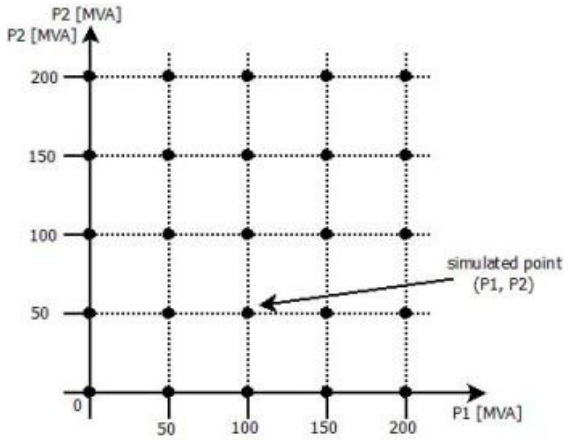

Figure 4-30: Grid of the powers pairs of generated by two wind farms

The residual voltage during the voltage dip has been evaluated after 250 ms from the fault occurrence, that is when all the transients related to voltage dip have been finished. The steady-state pre-dip voltage of the bars in the portion of the network under consideration has also been evaluated, always considering different power values generated by the two wind farms. The results of the simulations are shown in the graphs from Figure 4-31 to Figure 4-37.

The graphs show that:

- during the steady-state condition the amount of wind generation considered doesn't have a big effect on the network voltage: the variations are between 1.1% and 2.6 %;
- during the voltage dips the residual voltage rises with variations between 6% and 17%, depending on the node, thanks to the reactive current injected by the generators; these percentages highlight the contribution that these generators can provide to the support of the mains voltage during the voltage dips.

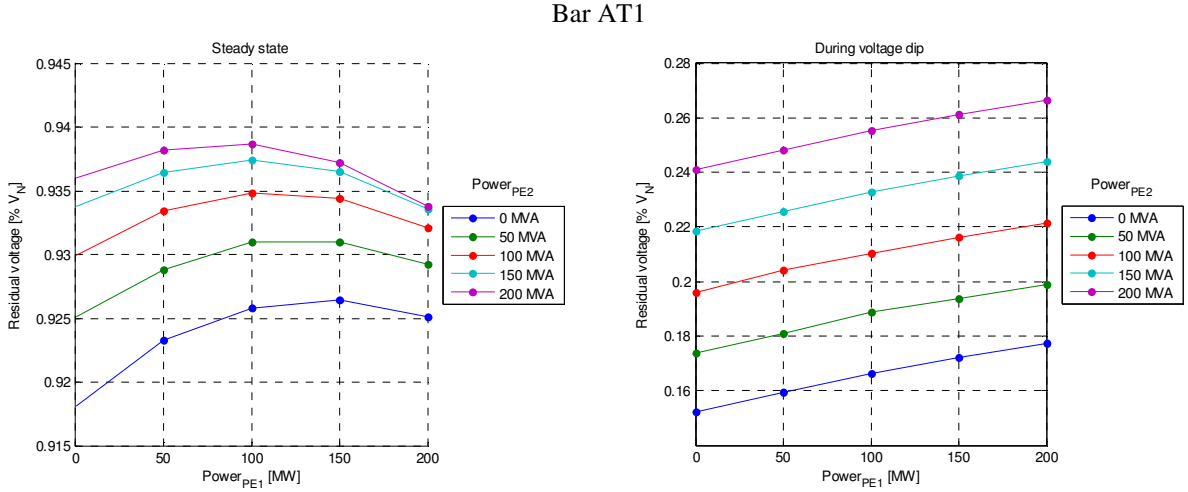

Figure 4-31: Steady state network voltages and residual values during the voltage dip

Bar AT2

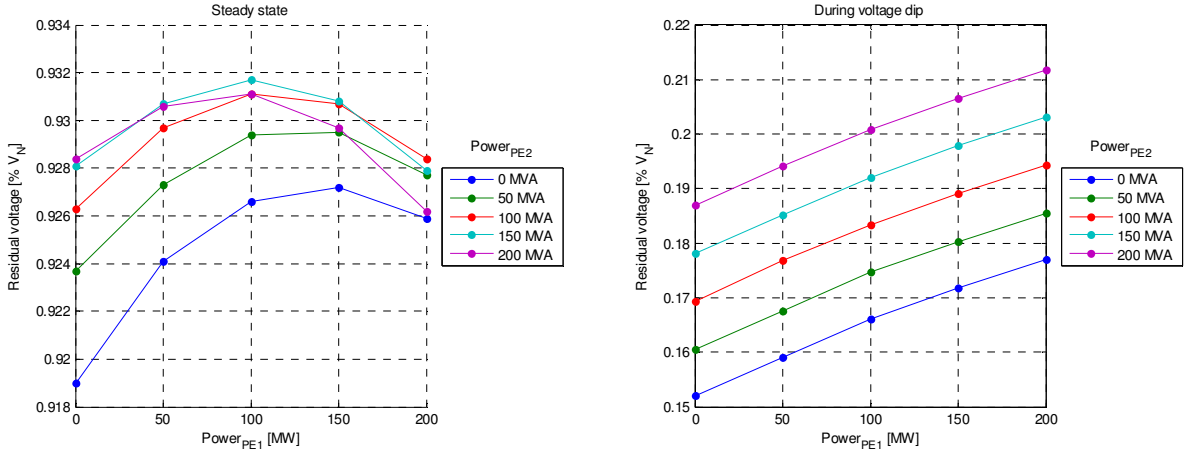

Figure 4-32: Steady state network voltages and residual values during the voltage dip

Bar AT3

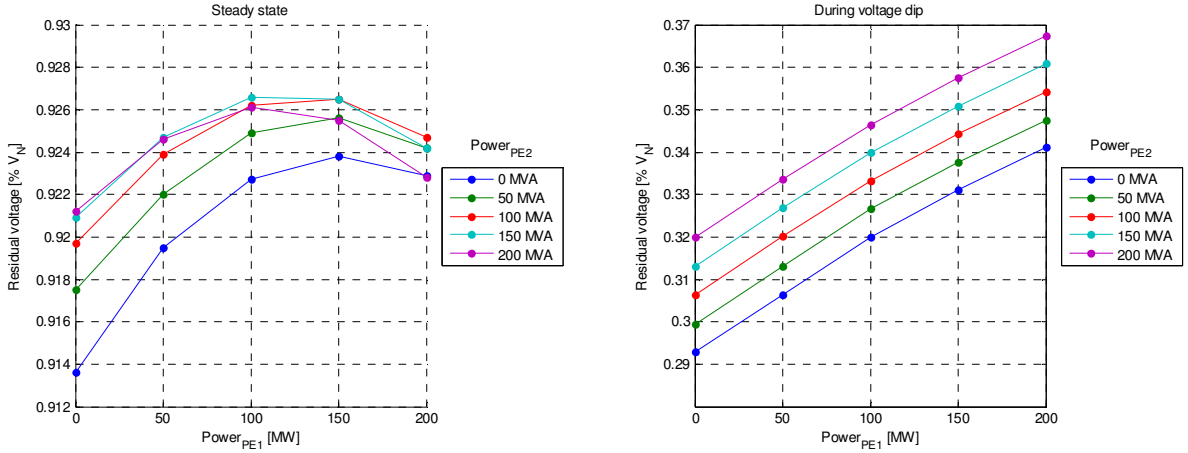

Figure 4-33: Steady state network voltages and residual values during the voltage dip

Bar AT4

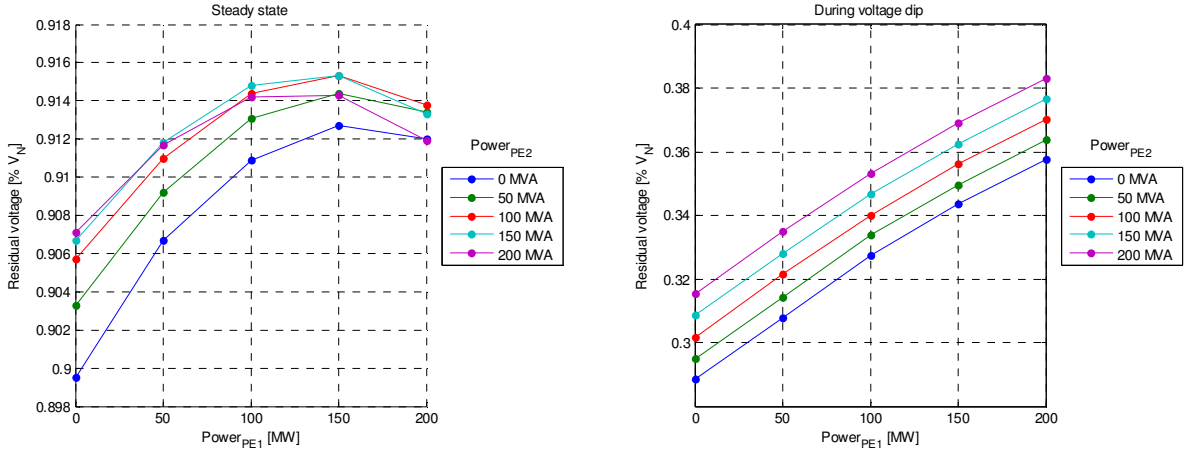

Figure 4-34: Steady state network voltages and residual values during the voltage dip

Bar AT5

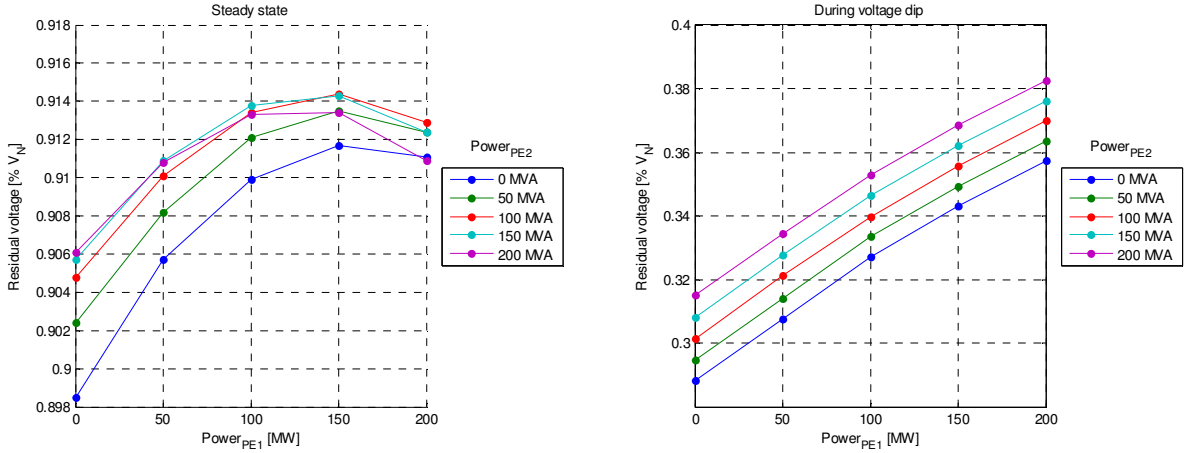

Figure 4-35: Steady state network voltages and residual values during the voltage dip

Bar AT6

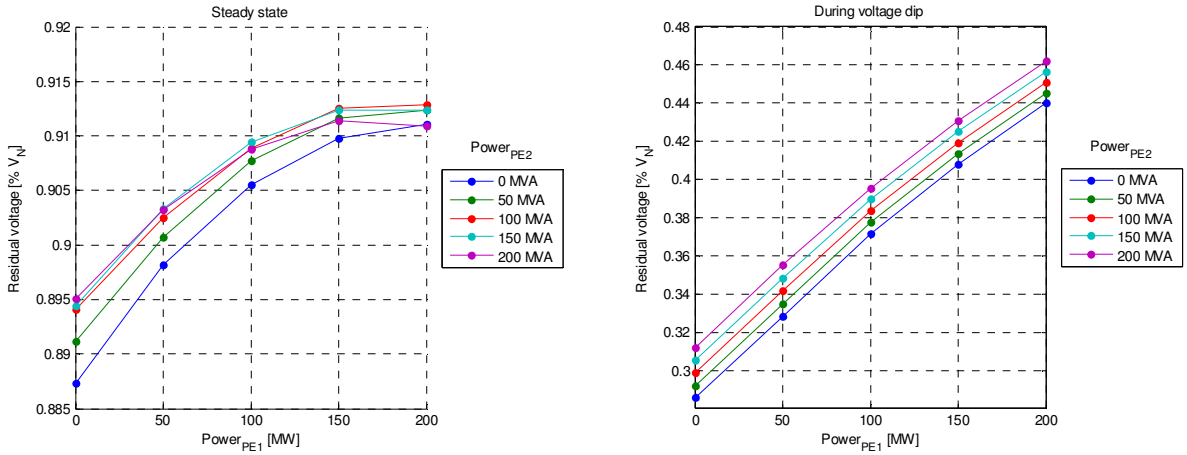

Figure 4-36: Steady state network voltages and residual values during the voltage dip

Bar AT7

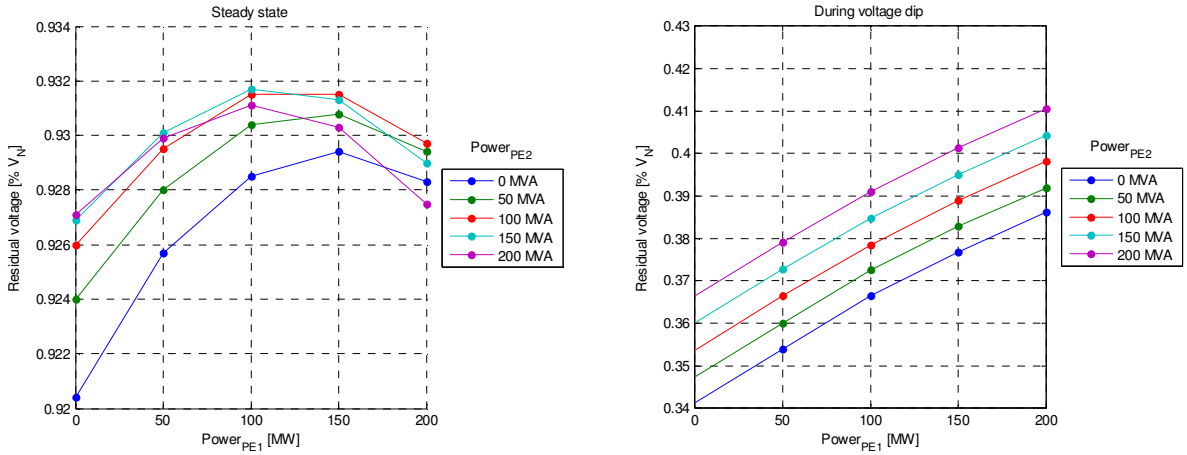

Figure 4-37: Steady state network voltages and residual values during the voltage dip

4.8 Final Considerations

After the validation of the model developed in DIgSILENT of an extended network (HV, MV and LV levels) with photovoltaic and wind Distributed Generators (DG) able to satisfy the Fault Ride Through requirements, with regard to the capability of the DG to support the voltage, it is possible to state that:

- the distributed generators connected to MV and LV distribution networks can support the voltage depending on the type of fault and on their rated power; in general, the percentage of voltage variation, during a voltage dip, is maintained below the 6% for the MV nodes and does not exceed 3% in case of LV nodes;

- the presence of wind generators connected to the HV network (and in general generators designed with higher rated power), during the steady-state condition does not give support to the various HV bars considered (the variations are between 1.1 % and 2.6 %). During the voltage dips, on the other hand, the residual voltage rises between 6% and 17% depending on the node considered and thanks to the reactive power injected by the plants, highlighting their contribution to the sustenance of the mains voltage during the voltage dips.

5 THE INVERTER BEHAVIUOR IN PRESENCE OF UNBALANCED NETWORKS AND VOLTAGE DIPS

The wind generator inverter control described in Chapter 2 represent one of the most frequently solutions adopted [36]. This type of control is based on the possibility to express the three phase voltages and currents in the d-q rotating frame using the transformation expressed in (5.1). In such a reference system, the sinusoidal balanced waveforms are transformed into continuous quantities. In this way, the inverter control becomes the control of two DC equivalent, one over the direct-axis and one over the quadrature-axis, making easier the regulators design.
However, the possible presence of unbalances and asymmetries in the network voltage after the transformation in the rotating frame introduce harmonic components with specific frequencies, usually multiple of the mains frequency. Such components are undesired since they downgrade the Power Quality and can affect other systems connected to the distribution network. The reasons of this behavior are explained in detail in the next paragraph.
One of the typical situations, which occurs in case of voltages unbalances, consists in the injection of active and reactive power affected by oscillating components with frequency double than the grid one. Depending on the network configuration, the network short circuit power at the generator connection point and the overall power delivered, this condition can lead to a deterioration in the voltage quality due to harmonics and unbalanced currents.
In this context, a study has been performed to evaluate different inverter control strategies which allow to mitigate power oscillating components injected into an unbalanced network, with digital simulation in ATPDraw and with the help of calculation programs (Matlab).
The discussion is related to the control of the inverters to interface distributed generators to the network and can be applied to every kind of system (for example wind generator connected to the network through rectifier + chopper boost elevator and inverter or back-to-back configuration or photovoltaic generator connected with chopper boost and inverter).

5.1 Inverter behavior with classical control over axis d-q in case of unbalanced network

Each three phase system can be composed into direct, reverse[38] and zero sequences, as shown in the vector diagram in Figure 5-1, where the three phasors (x_a, x_b, x_c) can be obtained by summing the phasors of the same color of three balanced phasor system.

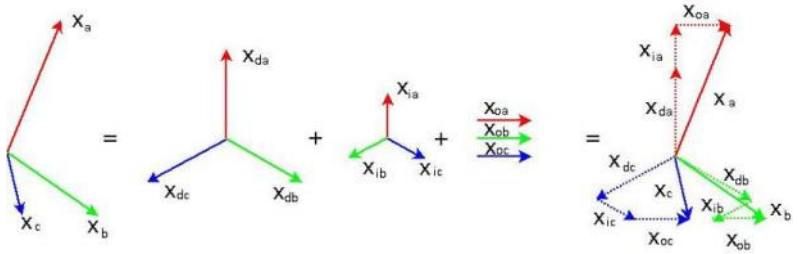

Figure 5-1: Three phase system represented as phasors: direct, reverse and zero sequence

Since the three phasor systems are balanced, i.e. $|x_{da}|=|x_{db}|=|x_{dc}|=|x_d|$, $|x_{ia}|=|x_{ib}|=|x_{ic}|=|x_i|$, $|x_{oa}|=|x_{ob}|=|x_{oc}|=|x_o|$, the original quantities can be written in the form:

$$\begin{aligned} x_a &= x_d\cos(\omega t)+x_i\cos(\omega t)+x_o\cos(\omega t)\\ x_b &= x_d\cos(\omega t-2\pi/3)+x_i\cos(\omega t+2\pi/3)+x_o\cos(\omega t)\\ x_c &= x_d\cos(\omega t+2\pi/3)+x_i\cos(\omega t-2\pi/3)+x_o\cos(\omega t) \end{aligned} \qquad (5.1)$$

[38] This reverse sequence can be called also negative sequence or quadrature sequence.

Expressing the magnitudes (x_a, x_b, x_c) in the rotating d-q frame, in case of voltage unbalance, it can be obtained that:

- the direct sequence is represented by continuous quantities;
- the reverse sequence presents oscillating magnitudes with angular frequency of 2ω;
- the zero sequence has null values.

Such transformations are shown in Figure 5-2 and Figure 5-3, that present respectively: the decomposition of an unbalanced sinusoidal system (a) into three balanced phasorial systems (b) (direct, reverse and zero sequence), and the transformation over d-q axes. The fact that the transformation over d-q axes of reverse sequences produces two sinusoidal signals with double frequency than the network one is an intuitive result. In fact, the reverse sequence can be viewed as a system that rotates with angular speed opposite to the network ($\vec{\omega}_{revers} = -\vec{\omega}_{network}$). By projecting such sequence on two axes rotating at the same network frequency, the magnitude obtained oscillates with angular frequency: $\vec{\omega}_{dq,revers} = \vec{\omega}_{network} - \vec{\omega}_{revers} = 2\vec{\omega}_{network}$.

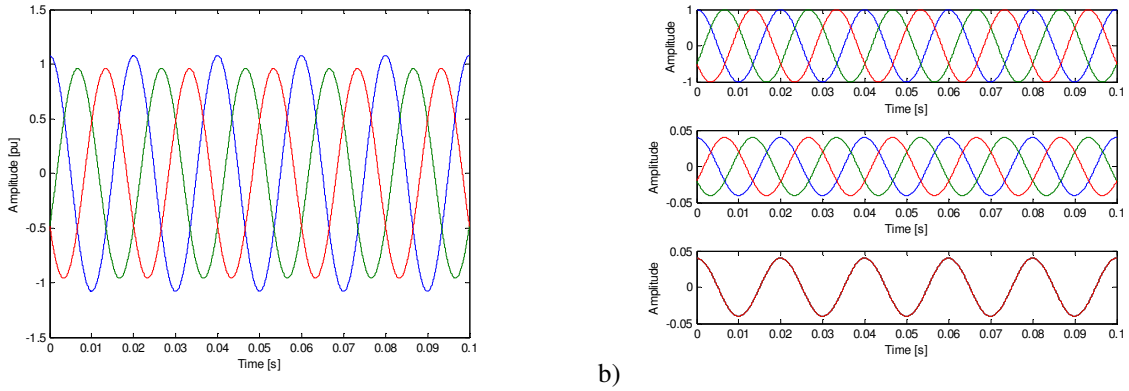

a) b)

Figure 5-2: Decomposition of an unbalanced system (a) into the phasorial balanced system: direct, reverse and zero sequences (b)

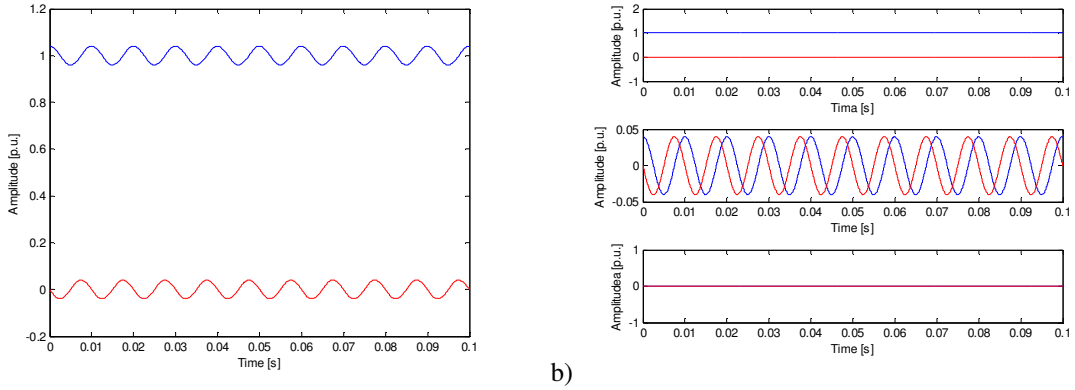

a) b)

Figure 5-3: Sinusoidal system over d-q-axis (a) and related transformations into direct, reverse and zero sequences (b)

As already pointed out in § 2.3.2.1, the inverter control of the wind PMSG is based on the transformation of the sinusoidal voltages and currents on rotating frame d-q, since this approach has the advantage of making continuous quantities processed by regulators. As already mentioned, in the presence of an unbalanced mains voltage, the voltages expressed over d-q-axis are characterized by 100 Hz component. Transforming the network voltages and currents over d-q-axis, it's possible to distinguish four different components:

$$
\begin{aligned}
v_d &= v_{dp} + v_{dp} \\
v_q &= v_{qp} + v_{qn} \\
i_d &= i_{dp} + i_{dp} \\
i_q &= i_{qp} + i_{qn}
\end{aligned}
\tag{5.2}
$$

where the v are voltages, i are currents, the first subscript indicates the rotating axis over which the magnitude is expressed (d direct-axis, q quadrature-axis) and the second subscript indicates if the amount is direct or reverse sequence (p direct sequence, n reverse sequence)[39].

In the example shown in Figure 5-4, the mains voltages, initially balanced, are unbalanced by the insertion at time t = 0.6 s of a 20 MVA load between two phases. As a result, there is a reverse sequence component of amplitude equal to 0.04 p.u., whereas it is not present the zero sequence. These oscillating components are processed by the control obtaining three modulating signals, which are used by PWM modulator. In general, the 100 Hz oscillations are propagated to all the control parameters, including the current references[40] and the output voltages of the regulators. This figure show the network voltages before and after the unbalance, their transformation over d-q axes, the inverter currents and their transformations over d-q axes, the modulation index and the calculated phase and the resulting powers injected into the grid. The unbalance of the PWM modulating waveforms results in an unbalance of the currents exchanged. It may be noted that after the occurrence of the disturbance in the network, the active and reactive power are affected by a 100 Hz oscillation (Figure 5-4g).

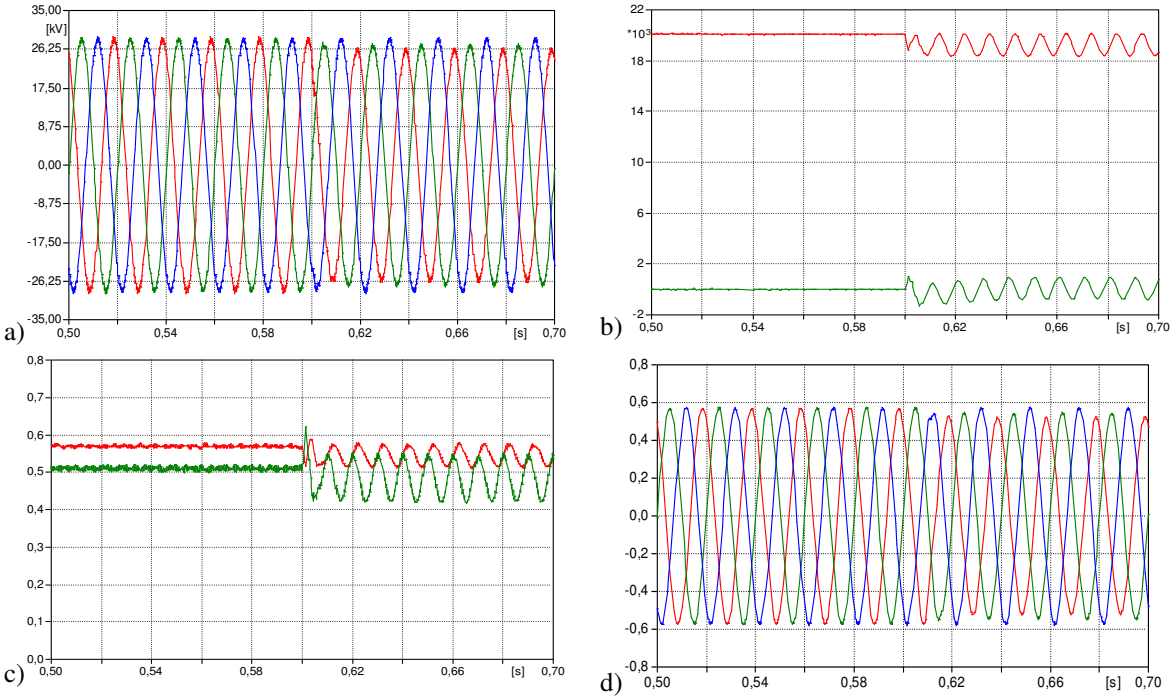

[39] p and n indicate respectively the direct and reverse sequence components and these are used to indicate in the English language *positive sequence* and *negative sequence*.

[40] The case where the current quadrature reference is fixed at the value zero does not have, obviously, oscillations on this reference value.

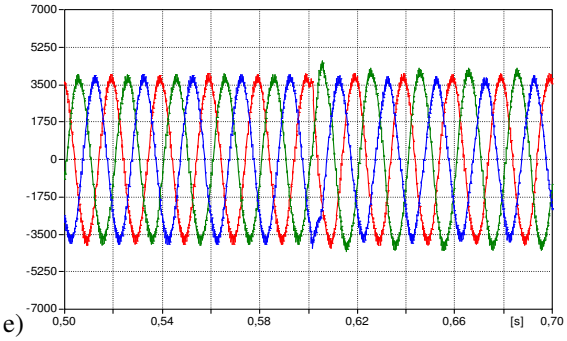

e)

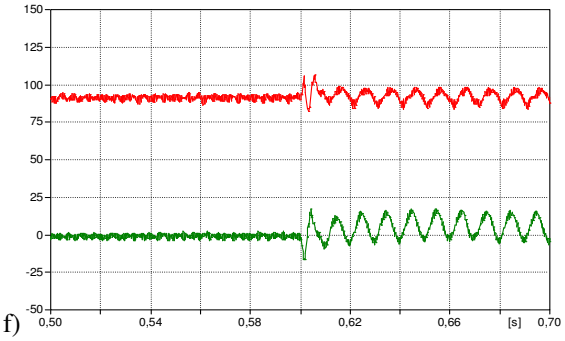

f)

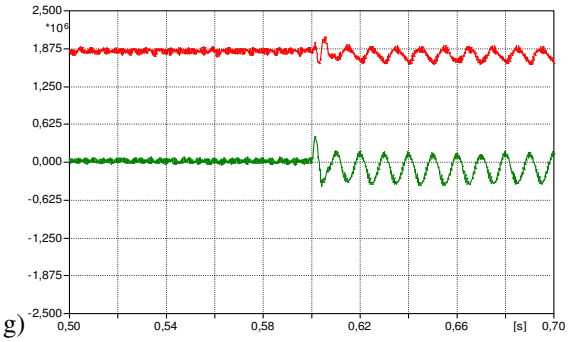

g)

Figure 5-4: Classical inverter control with unbalanced network:
a) network voltages;
b) mains voltages transformed over axis d (red) and q (green);
c) modulation index (red) and phase (green;
d) inverter modulating waveforms;
e) LV inverter currents;
f) transformation of the currents of inverter in MV on axis d(red) and q (green);
g) active (red) and reactive power (green).

In general, the powers injected into the network by the converter are expressed as:

$$\begin{aligned} A &= P + jQ = vi \\ P &= v_d i_d + v_q i_q \\ Q &= v_q i_d - v_d i_q \end{aligned} \tag{5.3}$$

In case of voltage unbalance it's necessary to consider the d-q axes components and therefore the power (5.16) can be rewritten as:

$$A = (v_{dqp} + v_{dqn} e^{-j2\omega t}) * (i_{dqp} + i_{dqn} e^{-j2\omega t}) \tag{5.4}$$

where ω is the angular frequency of the network.

Considering the definition of the active and reactive powers (5.16) and introducing the direct and reverse sequence components of voltages and currents (5.2) the following expressions is obtained [60]:

$$\begin{aligned} P &= P_0 + P_1 \cos(2\omega t) + P_2 \sin(2\omega t) \\ Q &= Q_0 + Q_1 \cos(2\omega t) + Q_2 \sin(2\omega t) \end{aligned} \tag{5.5}$$

Therefore, the active power injected into network is given by P_0 constant and two oscillating 100 Hz components. The expressions (5.5), can also be written as:

$$\begin{bmatrix} P_0 \\ P_1 \\ P_2 \\ Q_0 \\ Q_1 \\ Q_2 \end{bmatrix} = \begin{bmatrix} v_{dp} & v_{qp} & v_{dn} & v_{qn} \\ v_{qp} & -v_{dp} & v_{qn} & -v_{dn} \\ v_{dn} & v_{qn} & v_{dp} & v_{qp} \\ v_{qn} & -v_{dn} & -v_{qp} & v_{dp} \\ v_{qn} & -v_{dn} & v_{qp} & -v_{dp} \\ -v_{dn} & -v_{qn} & v_{dp} & v_{qp} \end{bmatrix} \cdot \begin{bmatrix} i_{dp} \\ i_{qp} \\ i_{dn} \\ i_{qn} \end{bmatrix} \tag{5.6}$$

As anticipated, the generation of unbalanced currents and, as a reflection, of oscillating power, can impact the voltage quality depending on the network short circuit power at the inverter connection point. These effects can be mitigated by using control schemes modified than the classical one over axis d-q, to take into account the presence of reverse sequences to mitigate the power oscillations and the currents unbalance, including in the control the regulation of the reverse sequence components of the inverter currents expressed over d-q-axis.

In particular, to cancel the 100Hz oscillations in the power is necessary to eliminate the power reverse components of the (5.6). The current references of negative sequence to use for the control of the converter are expressed according to the formula:

$$\begin{aligned} i_{dn\_ref} &= \frac{\left(v_{dn} i_{dp} + v_{qn} i_{qp}\right)}{v_{dp}} \\ i_{qn\_ref} &= \frac{\left(v_{qn} i_{dp} - v_{dn} i_{qp}\right)}{v_{dp}} \end{aligned} \tag{5.7}$$

If the converter is synchronized with the mains voltage the following condition is verified $v_q=0$, therefore the active power in (5.3) can be rewritten as follows:

$$P_0 = v_d i_d \tag{5.8}$$

During network unbalance power exchanged is expressed as:

$$P = v_{dp} i_d = v_{dp} i_d \frac{v_d}{v_d} = P_0 \frac{v_{dp}}{v_d} \tag{5.9}$$

from which it follows that in case of asymmetric network as a result of a single phase fault, of an unbalanced load or unbalanced network, the power injected by the converter decreases according to the ratio between the voltage positive sequence component and the nominal voltage [62].

Below, two special inverter control strategies, devoted to the management of grid voltage unbalances are proposed, analyzed, and compared.

5.2 Dq-axes control with negative sequence compensation

This control is similar to the previous one, with the main difference that also the currents and voltages negative sequence components, calculated on the dq-axes, are taken into account. The positive sequences components of each quantity (x_{dp} and x_{qp}, where x represents current or voltage) are calculated with the usual Park transformation, the zero component indicated by "0" is neglected and the magnitudes on axes α and β, indicated as x_α and x_β, can be expressed in the two references rotating dq_p and dq_n, by the following formulas:

$$\begin{aligned} \begin{bmatrix} x_{dp} \\ x_{qp} \end{bmatrix} &= \begin{bmatrix} \cos(2\pi f t) & \sin(2\pi f t) \\ -\sin(2\pi f t) & \cos(2\pi f t) \end{bmatrix} \cdot \begin{bmatrix} x_\alpha \\ x_\beta \end{bmatrix} \\ \begin{bmatrix} x_{dn} \\ x_{qn} \end{bmatrix} &= \begin{bmatrix} \cos(-2\pi f t) & \sin(-2\pi f t) \\ -\sin(-2\pi f t) & \cos(-2\pi f t) \end{bmatrix} \cdot \begin{bmatrix} x_\alpha \\ x_\beta \end{bmatrix} = \begin{bmatrix} \cos(2\pi f t) & -\sin(2\pi f t) \\ \sin(2\pi f t) & \cos(2\pi f t) \end{bmatrix} \cdot \begin{bmatrix} x_\alpha \\ x_\beta \end{bmatrix} \end{aligned} \tag{5.10}$$

Since the only amount of interest are the voltages and currents continuous components expressed over d-q axes, the oscillating components can be eliminated by an ideal integrator filter. Therefore, for the purposes the main value of each quantity is given by[41]:

$$\begin{aligned} < x_{dp} > &= \frac{1}{\tau}\int_0^\tau x_{dp}dt \\ < x_{qp} > &= \frac{1}{\tau}\int_0^\tau x_{qp}dt \\ < x_{dn} > &= \frac{1}{\tau}\int_0^\tau x_{dn}dt \\ < x_{qn} > &= \frac{1}{\tau}\int_0^\tau x_{qn}dt \end{aligned} \tag{5.11}$$

where τ is the current time, then used in the control for noise filtering.

Once calculated the d-axis and q-axis components of the grid voltages and of the inverter currents, it's possible to apply the equations (5.7) for the calculation of reverse current references, while the direct sequence current references are obtained according to the scheme of classic control described in § 2.2.4.4. The total references current are obtained by adding together, separately on the two axis, the direct sequence and reverse sequence references, and then compared with the inverter currents.
Since voltage and current unbalances are represented as components with double frequency in the dq-axes decomposition of the respective quantities, current PI regulators should be modified into Proportional-Integral-Resonant (PIR) regulators with resonant frequency equal to 2*f* [60] [61]:

$$H_{PIR}(s) = k_p + \frac{k_i}{s} + k_r \frac{s}{s^2 + 2\alpha s + (2\cdot 2\pi f)^2} \tag{5.12}$$

where k_p and k_i have the usual meaning, k_r is the resonant gain and α is a damping factor used to widen the resonant zone across 2*f* and to maintain the controller gain at a finite value.

These PIR regulators have an high gain in the neighborhood of the resonance frequency and eliminate the error between the measured signal and the reference.

In absence of grid voltages unbalances, however, the control here described, at least during steady state, has a behavior similar to the classic one, since the reverse sequence components have zero amplitude, and, therefore, also their transformations on d-q axes are null [62].

For the simulations, the following values of the parameters: f= 50 Hz, α=2π, k_r=104 are used to mitigate the 100Hz components, while the other parts of the regulators are the same presented in § 2.2.4.4. The block diagram of the control described here (Modified Park control) is shown in Figure 5-5, where in red the additional parts than the "classic" approach are highlighted.

[41] For simplicity of notation, in the following to indicate the medium components of direct and inverse sequence it will be used the notation without the "angle brackets" < >.

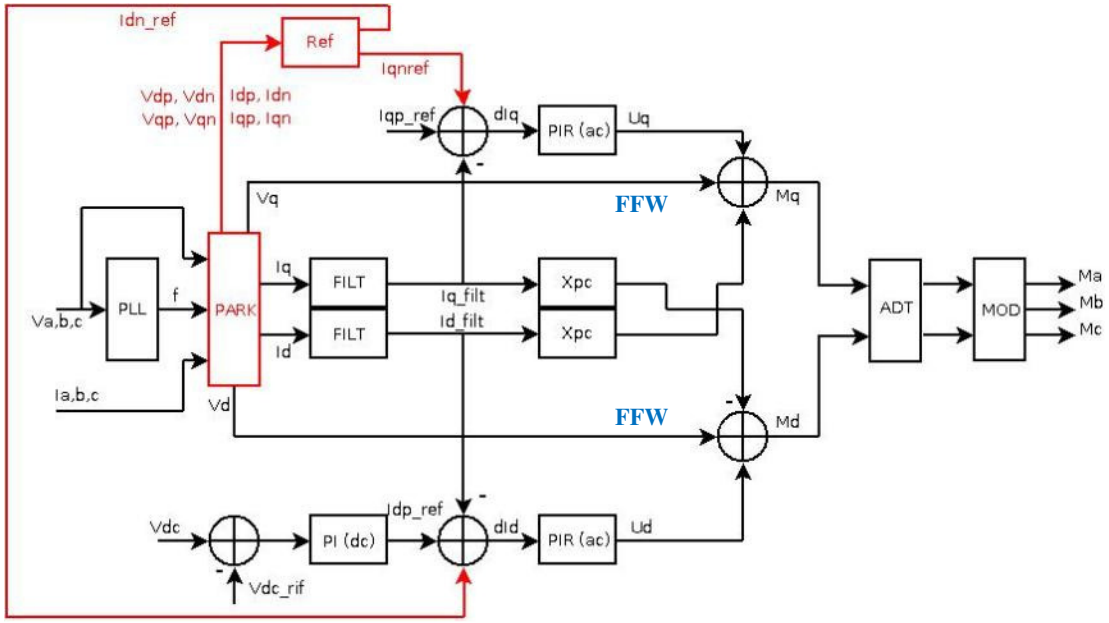

Figure 5-5: Scheme of a dq-axes control with compensation of negative sequences components with modified Park transformation

5.3 Second Order Generalized Integral (SOGI) control

A second method for the calculation of the components over dq-axes of the reverse sequence components is proposed in [63] and is applied to the static compensator current control. The main difference than the dq-axes control with negative sequences compensation consists in the calculation of the positive and negative sequences of the currents and voltages dq-axes components, which are calculated starting from the αβ components:

$$x_\alpha = \frac{1}{2}(x_\alpha - x_\beta e^{-j90})$$
$$x_\beta = \frac{1}{2}(x_\alpha e^{-j90} + x_\beta) \quad (5.13)$$

The block diagram of the algorithm on the Second Order Generalized Integrator filter - SOGI is represented in Figure 5-6, where f(t), d(t) and q(t) are time signals and h and ω' are two gains.

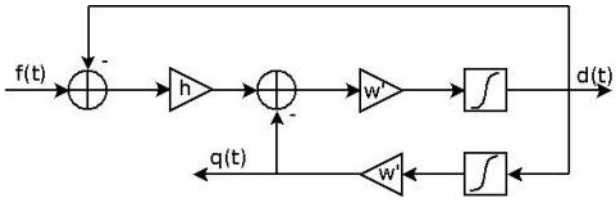

Figure 5-6: Block diagram of a filter SOGI

The major filter transfer functions are the following:

$$H_d(s) = \frac{D(s)}{F(s)} = \frac{h\omega' s}{s^2 + h\omega' s + \omega'^2}$$
$$H_q(s) = \frac{Q(s)}{F(s)} = \frac{h\omega'^2}{s^2 + h\omega' s + \omega'^2} \quad (5.14)$$

where D(s), Q(s) and F(s) are the Laplace transform of the signals d(t), q(t) and f(t).

If f(t) is a signal with fundamental component at a frequency equal to the one around which the SOGI filter is centered (ω'/2π), the signal d(t) presents the fundamental component at the same frequency and in phase with the fundamental component of f(t) (but with different harmonic components because of the filter); q(t) is, instead, a signal perpendicular to d(t). The situation is shown in the Bode diagrams of the two transfer functions $H_d(s)$ and $H_q(s)$, reported in Figure 5-7, and referred to a SOGI filter centered around 50 Hz, then ω' =2π50 and for example h=2[42].
The graphs show in red that at 50 Hz the two transfer functions have gain equal to 0 dB, while they have lower gains at higher frequencies (the two phases, evaluated at the fundamental frequency, are respectively 0° and 90°). The two signals d(t) and q(t), essentially sinusoidal, mutually orthogonal and synchronized with the 50 Hz component of the signal f(t). The result of applying the SOGI filter to a sinusoidal 50 Hz signal is shown in Figure 5-8.

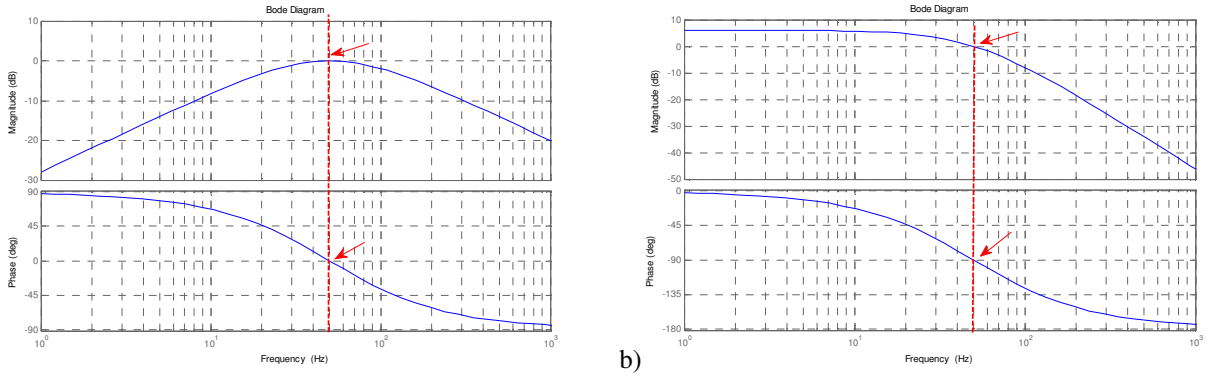

a) b)

Figure 5-7: Bode diagrams of the SOGI filter transfer functions: (a) amplitude and phase related to H_d, b) diagrams relating to H_q

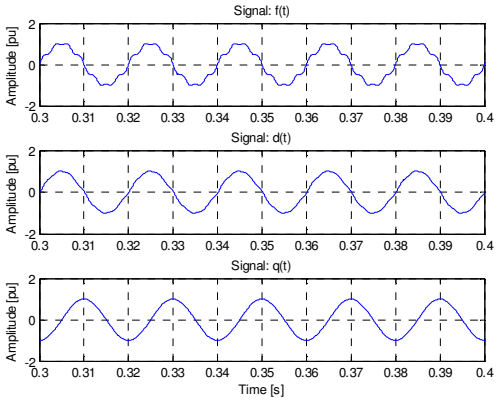

Harmonic 50 Hz: 1 p.u.
5th harmonic: 0.05 p.u.
7th harmonic: 0.10 p.u.

Harmonic 50 Hz: 1 p.u.
5th harmonic: 0.03 p.u.
7th harmonic: 0.05 p.u.

Harmonic 50 Hz: 1 p.u.
5th harmonic: 0.03 p.u.
7th harmonic: 0.05 p.u.

Figure 5-8: Example of calculation of d(t) and q(t) signals with SOGI filter, starting from a 50 Hz signal f(t)

Exploiting the SOGI filter characteristic to synchronize with the component of the signal at a frequency equal to the one around which the filter is centered and combining suitably the two output signals d(t) and q(t), it's possible to generate two pairs of signals, which are the αβ components of direct and reverse sequences of the electrical quantities involved in the inverter control. Starting with the αβ components of a generic three phase system (5.13), the SOGI filtering stage is adopted for extracting the positive and negative sequences in this way:

[42] The *h* value regulates the damping factor of the filter poles and, therefore, with a value decrease the filter module is described by a bell-shaped curve more closely and the phase transitions are speeder.

$$
\begin{aligned}
x_{\alpha p} &= \frac{1}{2}\frac{x_\alpha k\omega s - x_\beta k\omega^2}{s^2 + k\omega s + \omega^2} \\
x_{\alpha n} &= \frac{1}{2}\frac{x_\alpha k\omega s + x_\beta k\omega^2}{s^2 + k\omega s + \omega^2} \\
x_{\beta p} &= \frac{1}{2}\frac{x_\alpha k\omega^2 + x_\beta k\omega s}{s^2 + k\omega s + \omega^2} \\
x_{\beta n} &= \frac{1}{2}\frac{-x_\alpha k\omega^2 + x_\beta k\omega s}{s^2 + k\omega s + \omega^2}
\end{aligned}
\tag{5.15}
$$

where $k = \sqrt{2}$ is a parameter to ensure the filter unity-gain at the frequency $\omega/2\pi$, and p and n indicates the direct and reverse sequences.

The values expressed in the fixed frame $\alpha\beta$ are then transformed over rotating frame d-q. In particular, the positive sequences are processed with an angular frequency equal to that of the mains voltage (ω) while for the negative sequences an opposite angular frequency is used:

$$
\begin{aligned}
\begin{bmatrix} x_{dp} \\ x_{qp} \end{bmatrix} &= \begin{bmatrix} \cos(\omega t) & \sin(\omega t) \\ -\sin(\omega t) & \cos(\omega t) \end{bmatrix} \cdot \begin{bmatrix} x_{\alpha p} \\ x_{\beta p} \end{bmatrix} \\
\begin{bmatrix} x_{dn} \\ x_{qn} \end{bmatrix} &= \begin{bmatrix} \cos(\omega t) & -\sin(\omega t) \\ \sin(\omega t) & \cos(\omega t) \end{bmatrix} \cdot \begin{bmatrix} x_{\alpha n} \\ x_{\beta n} \end{bmatrix}
\end{aligned}
\tag{5.16}
$$

Once obtained the magnitudes over dq-axes, they are compared with the references calculated as described in §5.2 and processed by PIR controllers, whose outputs are added independently on the two axes. The control scheme requires the usual decoupling stages and the setting of the signals for the calculation of PWM modulating waveforms. Figure 5-9 shows a block control diagram with the additional parts and/or modified than the version presented in Chapter 2 highlighted in red. The parameters of PIR regulators have the same values used for the control described in the previous section.

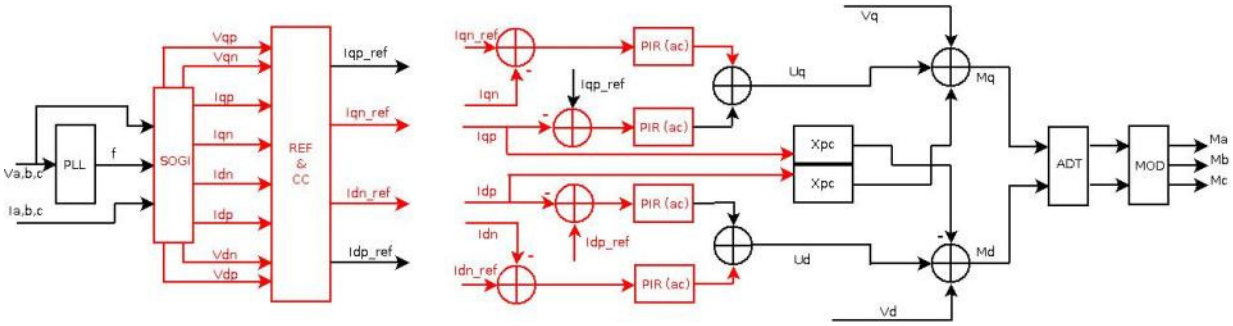

Figure 5-9: Block scheme of the SOGI control

5.4 Simulation results in presence of unbalanced network

These control schemes are implemented in the ATPDraw model of the wind PMSG (Chapter 2) and simulation results have been compared in two different situations:

- unbalanced network (due to the insertion of an unbalanced load);
- transient two-phase to ground grid fault.

The faults simulated are the same presented in Chapter 3 for the analysis of the FRT strategies.

5.4.1 *Unbalanced Network during steady state*

The network unbalance has been simulated, as for the case described in §5.1, generating an unbalance of 4% due to the connection of a load between two phases of the MV line where the wind generator is connected at time t= 0.6s. The generator behavior is reported in Figure 5-10 ÷ Figure 5-13. For the results comparison, it's used the convention that, in each figure in this section:

- letter (a) - indicates the results with the classic control;
- letter (b) - indicates the results with the dq-axes control with negative sequence compensation (modified Park);
- letter (c) - indicates the results with control filter-based SOGI.

From the simulations it's possible to underline that, while the network voltages are balanced, the three controls have the same behavior, while, in case of unbalance, the two modified controls offer higher performance than the classic one in the reduction of the active and reactive power 100 Hz oscillations (in terms of amplitude as can be seen in Figure 5-10 a, b, c) and of the currents unbalance (Figure 5-11 and Figure 5-12 a, b, c). Figure 5-13 shows the unbalanced modulating waveforms.

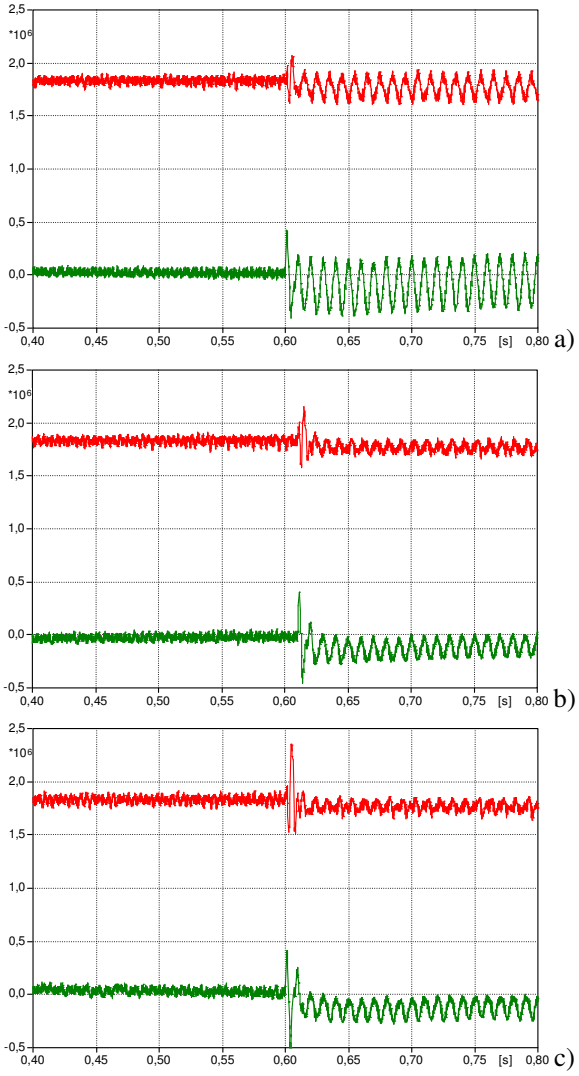

Figure 5-10: Active (red) and reactive power (green)

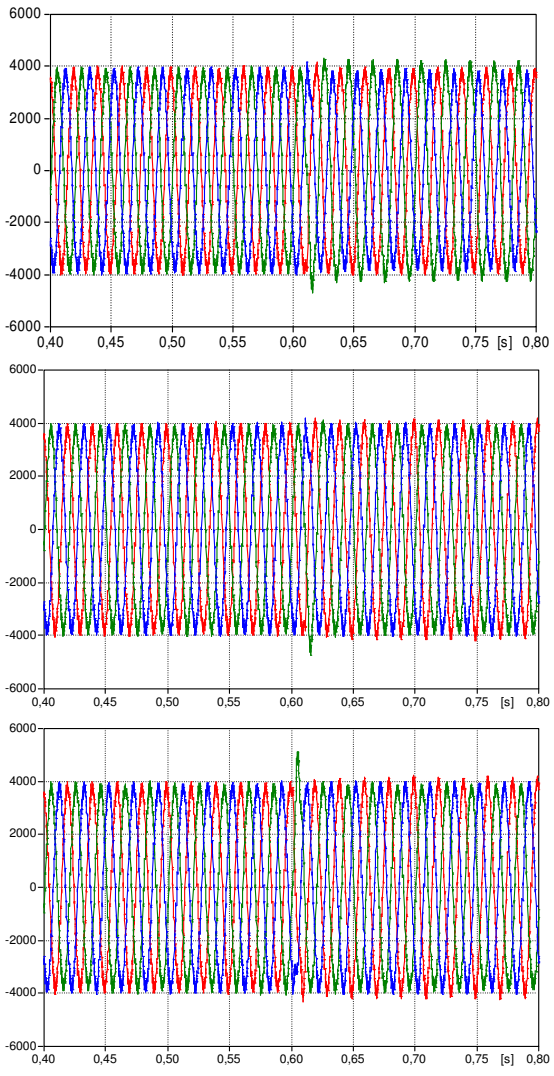

Figure 5-11: MV side filtered inverter currents

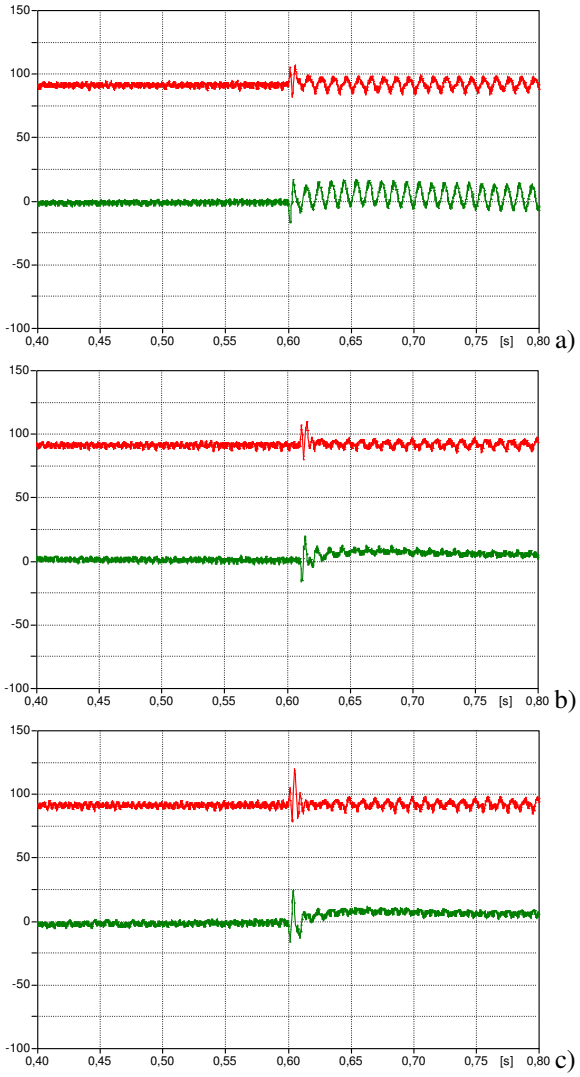

Figure 5-12: MV side inverter currents d-axis (red) and q-axis (green)

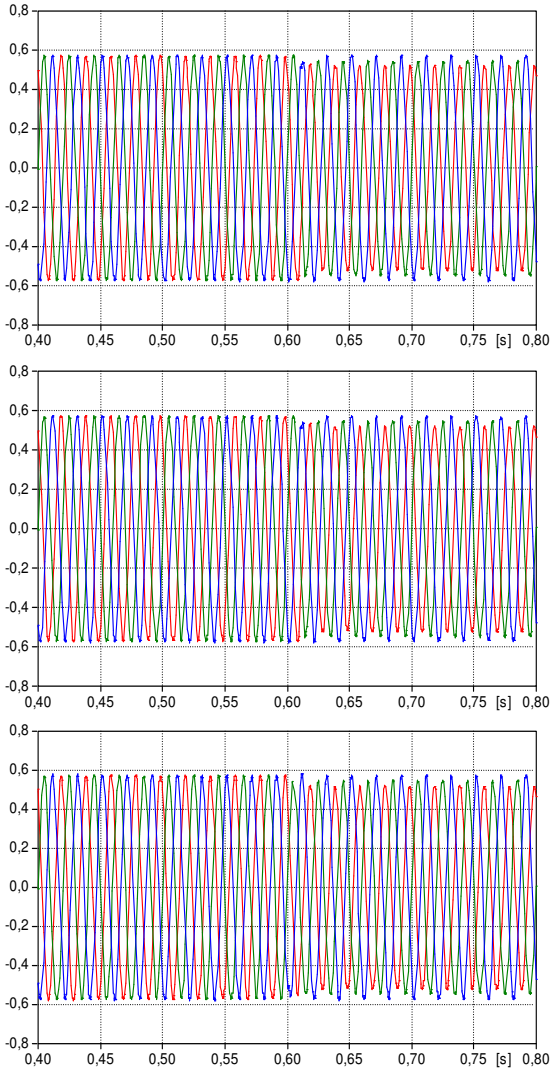

Figure 5-13: Inverter modulating waveforms

Figure 5-14 shows the active power and the d-axis current obtained with the different types of control. The reduction of the amplitudes of the 100 Hz oscillations is evident especially comparing the powers. Analytically, a comparison can be done calculating the spectrum of the active power and d-axis current for the three types of control and then expressing the relative amplitude of the 100 Hz component than the direct component for each magnitude. The obtained values are summarized in Table 5-1. The results of Table 5-1 show, in addition, a behavior substantially of the two modified methods similar in terms of reduction of the disturbance.

Table 5-1: Comparison between the performance of the three different control strategies

	Classic Control	Negative sequence compensation	SOGI filter
$100P_{rms}^{100}/\lvert S_0\rvert$	4.32 %	1.60 %	1.57 %
$100Q_{rms}^{100}/\lvert S_0\rvert$	8.88 %	3.68 %	3.50 %
$100I_n/I_p$	3.33 %	1.9 %	1.97 %

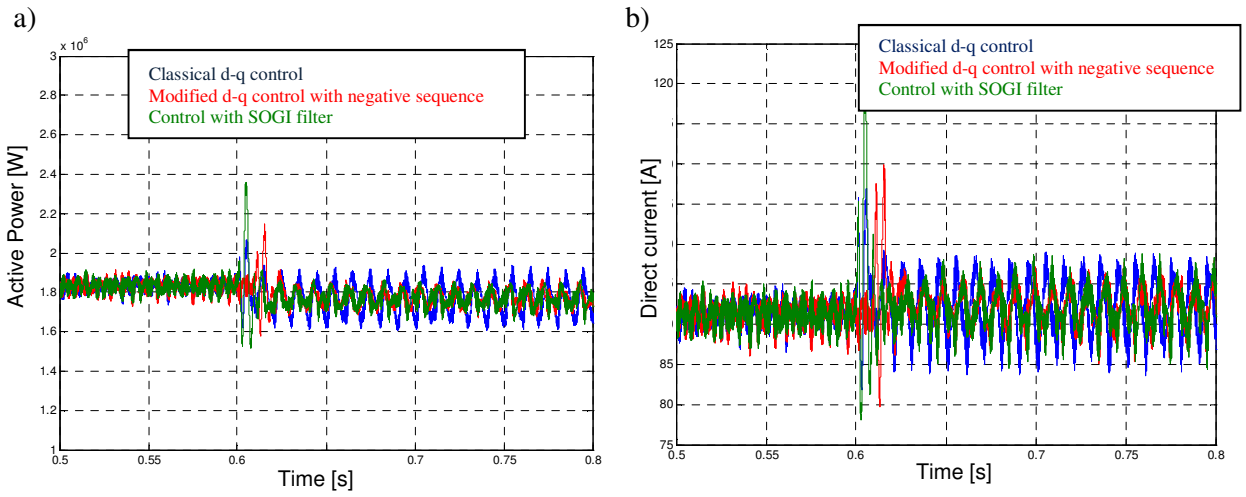

Figure 5-14: Active power (a) and d-axis current (b) applying the different control strategies

5.4.2 Phase to phase inductive fault

The responses to an unbalanced voltage dip of the three control approaches in the dq-axes frame have been also simulated in order to compare their performances. The voltage disturbance is caused by a two-phase to ground fault occurring at *t*=0,6 s and the network voltages at the inverter connection point are shown in Figure 5-15. The voltage dip presents a residual voltage of 70% V_n (referred to the lowest voltage) and finishes after 120 ms by the opening of the faulty line circuit breaker, as a consequence of the tripping of the over-current relays.

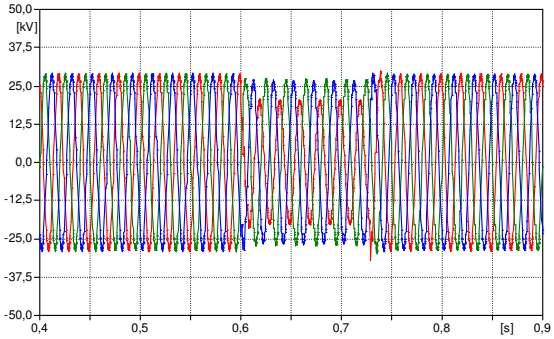

Figure 5-15: Line to line network voltages during two-phase inductive fault

The responses of the three control schemes are reported in Figure 5-16 ÷ Figure 5-19. In these simulations, in order to evaluate only the behavior of the controls, the FRT strategies are not implemented and then the generator remains connected to the network, in accordance with its capability.

A significant reduction of the 100 Hz oscillating components of the power is achieved with the improved versions of the control. In this case, also a reduction of the current distortion and unbalance are visible in Figures 17b,c in respect to Figures 17a. For instance, the current unbalances, calculated as the ratio between the amplitudes of the negative sequence and of the positive sequence of the currents injected into the grid, are: 9,6% for the basic control and about 3,2% for both the improved versions (Table 5-2).

Table 5-2: Comparison between the performance of the three different control strategies in case of two-phase fault

	Classic Control	Negative sequence compensation	SOGI filter
$100P_{rms}^{100}/\lvert S_0\rvert$	13.28 %	6.04 %	5.65 %
$100Q_{rms}^{100}/\lvert S_0\rvert$	27.58 %	11.64 %	11.95 %
$100I_n/I_p$	9.6 %	3.2 %	3.2 %

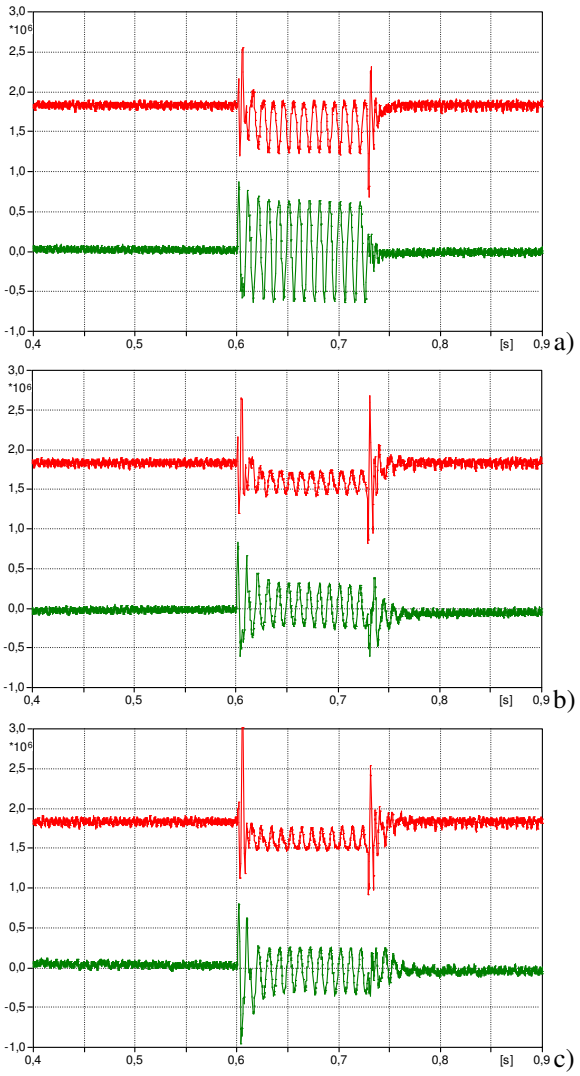

Figure 5-16: Active (red) and reactive power (green)

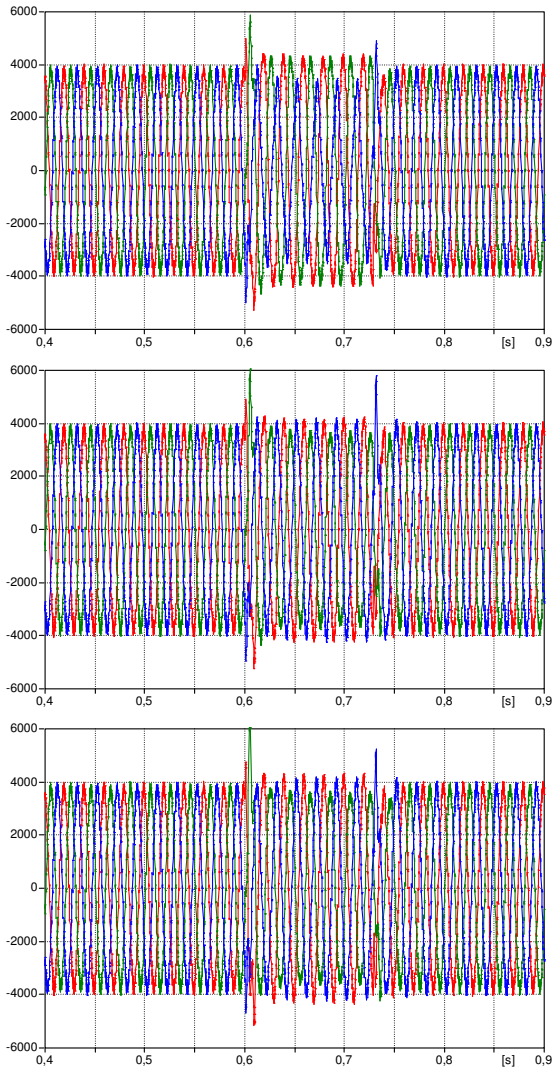

Figure 5-17: MV side filtered inverter currents

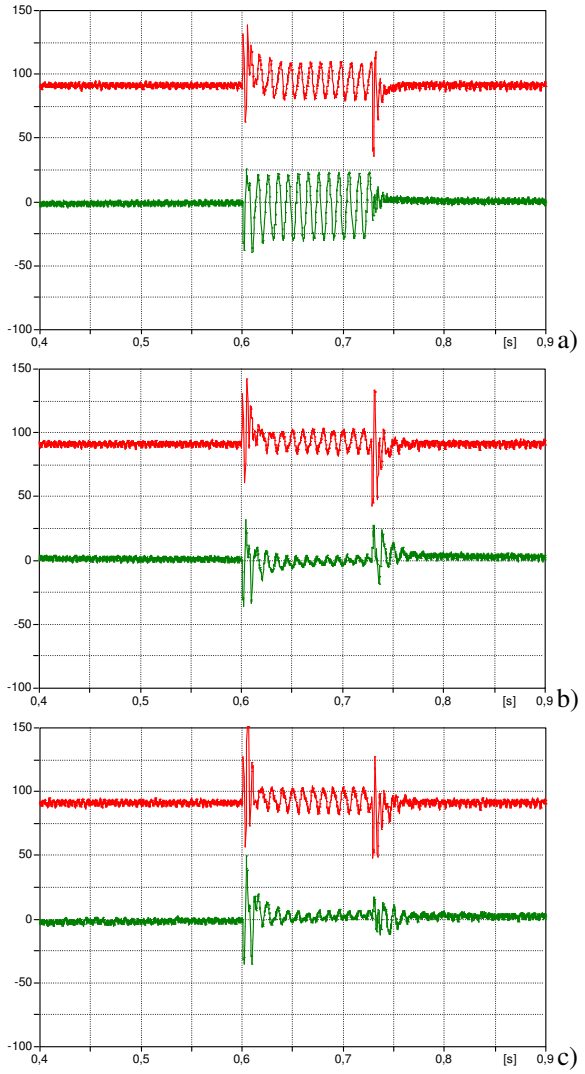

Figure 5-18: MV side inverter currents d-axis (red) and q-axis (green)

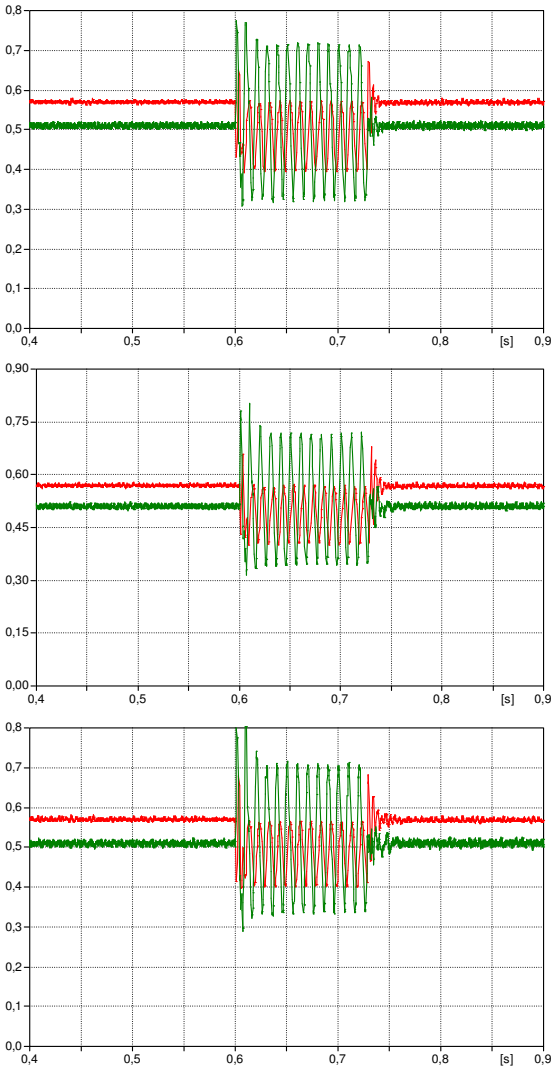

Figure 5-19: Modulation Index (red) and phase (green)

5.4.3 Three phase inductive fault

In this case the fault simulated is a three phase inductive one, such that the residual voltage at inverter connection point is the 70% of the nominal value. The fault occurs at t= 0.4s, and is terminated after 200 ms, thanks to the opening of the line circuit breaker. In Figure 5-20 the mains voltage are shown.

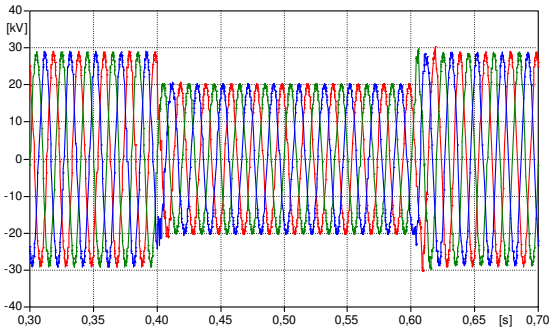

Figure 5-20: Line to line network voltages during three phase resistive fault

Figure 5-21 shows the behavior of active and reactive power and of the currents injected into the MV network from wind generator in case of classical control and filter-based SOGI control. The results obtained with the negative sequence compensation control are not reported because similar to those obtained with the SOGI filter.
As anticipated, the modified controls have a response quite similar to the classic control, when voltages are balanced.
The presence of the second-order generalized integrator filters or of the calculation of the mean values in case of control with modified Park transformation, instead, has an effect during the input and output transient of the voltage disturbance, these transients are characterized by the greatest number of oscillations in active and reactive power (Figure 5-21a, c).

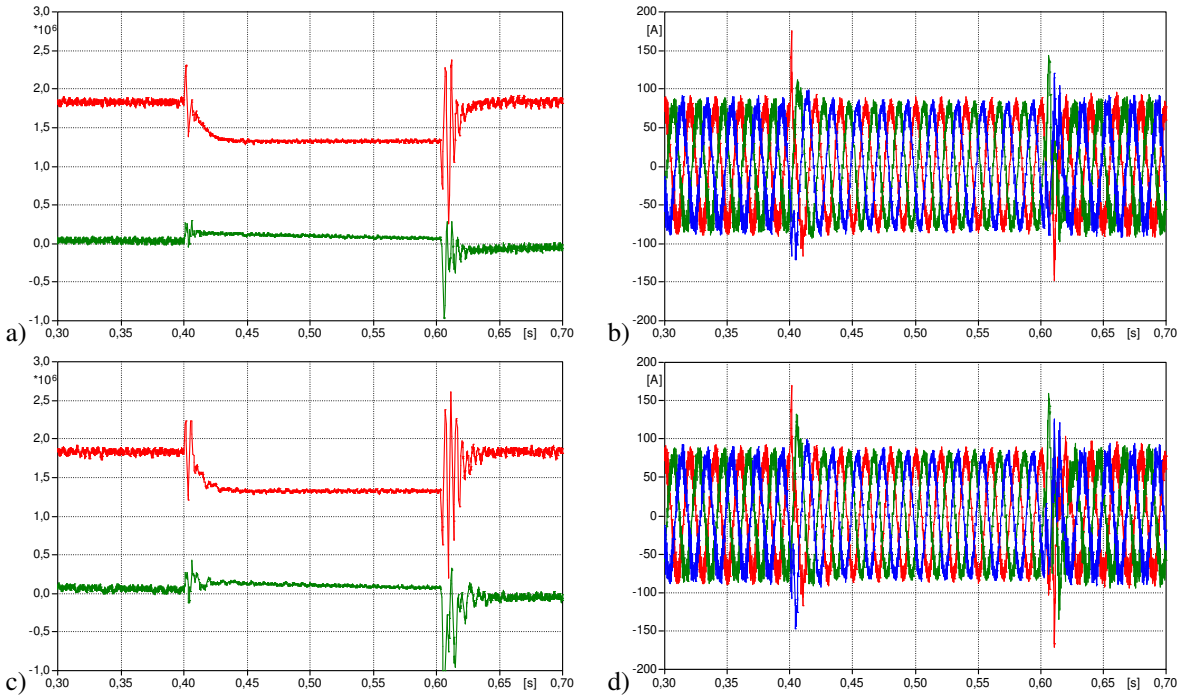

Figure 5-21: Inverter response to a balanced voltage dip: active (red) and reactive (green) power and inverter current with classic control ("a", "b") and with control SOGI ("c", "d")

5.4.4 Three phase resistive fault and FRT strategies

The control strategies described in this Chapter ensure the reduction of the network unbalances effects only if there aren't limitations for the inverter current or the DC voltage, introduced to safeguard the components in case of voltage dip. If these limitations are activated independently from the general control logic, the control operation can be modified, as already illustrated in § 3.4.3.
Now the FRT strategies, necessary for the overcoming of the network disturbance without the DG disconnection are implemented in the modified control schemes. The control schemes here analyzed have the feature, as well as the original one from which they derive, of being able to implement in a very simple way the control strategies to overcome voltage dips. As for the classic control all the possible control strategies for the FRT, have been implemented, in particular here only these will be presented:

- the inverter is forced to supply null active power;
- the inverter should supply a controlled current over q-axis.

The behavior of the inverter controlled with the different control schemes and with the different FRT strategies has been simulated in case of a voltage dip with residual voltage 20% V_N, generated by a three phase network fault with duration of 500 ms. Figure 5-22 shows the active and reactive power exchanged by the inverter for the different combinations control scheme-FRT strategy The results related to stand-by operation condition are not reported, because in that state the device behavior does not depend on the type of control selected. In addition to the FRT strategies, in all the simulations, the DC voltage braking chopper and the fast and slow current limitation are implemented (§ 3.4).

Since the network voltages remain balanced during the disturbance, there aren't, as expected, any substantial differences in the inverter responses with the different control solutions. Therefore the capability to apply FRT strategies to the inverter remains valid, even using the modified control schemes, including the possibility of providing support to network voltages by the injection of reactive power.

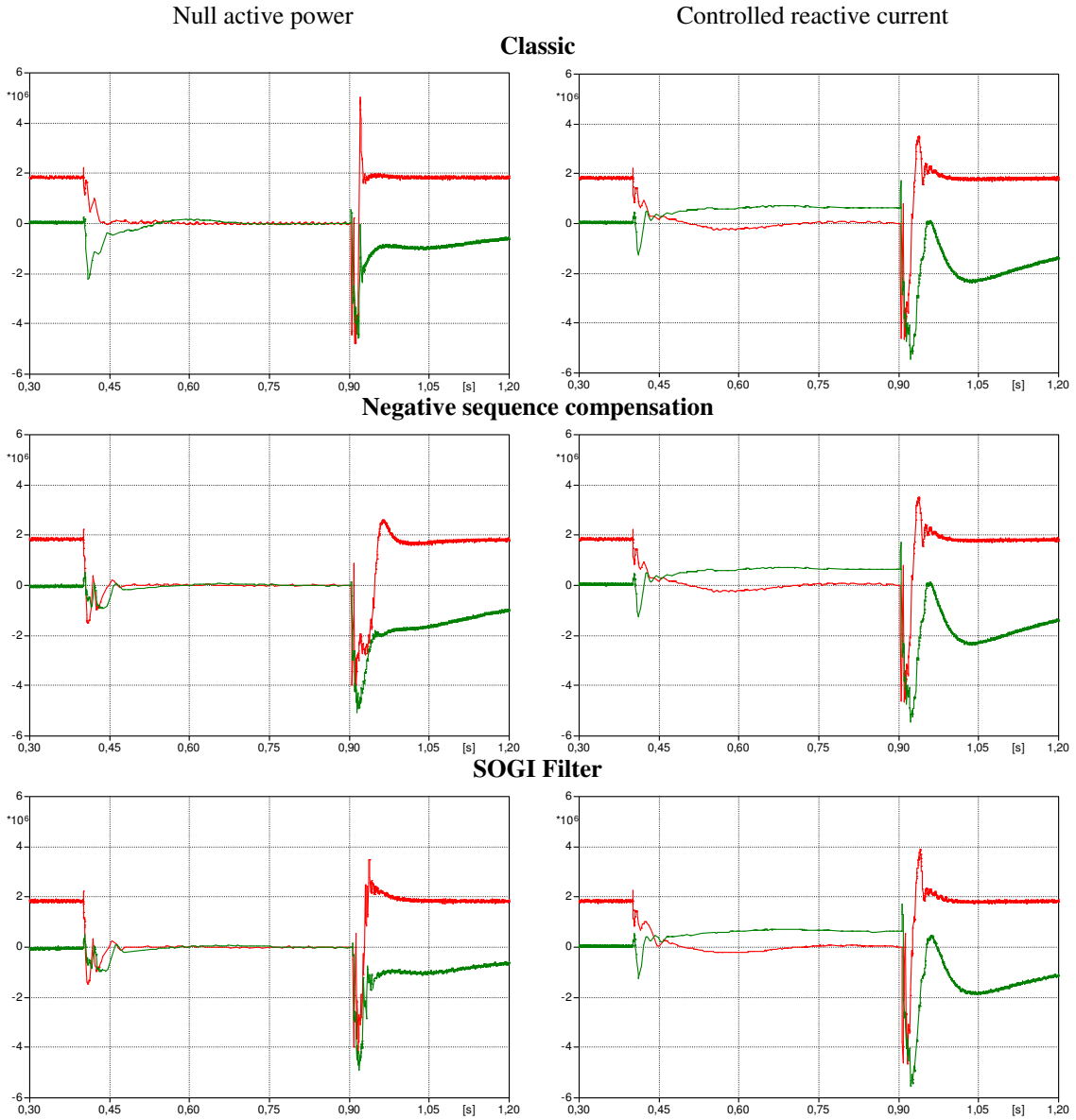

Figure 5-22: Active (red) and reactive power (green) during voltage dip, inverter controlled with different control schemes and FRT strategies

5.4.5 *Phase to phase resistive fault with current limitations*

A special inverter operation condition is when a two-phase fault occurs in the network. In this case, the inverter control variables over dq-axes present oscillating components at 100 Hz and the current waveforms injected into network and DC voltage are distorted for the limitation action.
Figure 5-23 reports active and reactive powers generated by the inverter in case of classic control and in case of control based on SOGI filter, obtained by applying the FRT strategy to supply zero active power during the voltage dip. The simulated fault is a phase to phase resistive fault, resulting in an unbalanced voltage dip with residual voltage 20% V_N (referred to the phase voltage with smaller value) and duration of 500 ms.

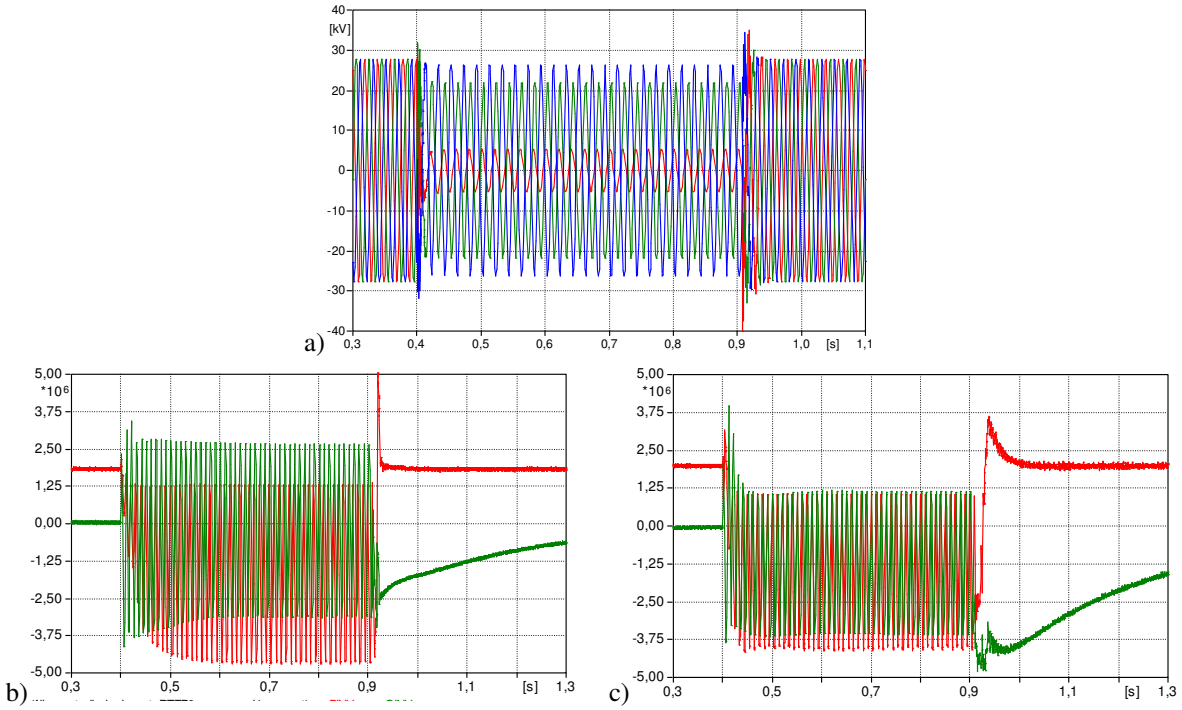

Figure 5-23: Inverter response to an unbalanced voltage dip (a) line to line network voltages at the inverter connection point, (b) active (red) and reactive (green) with classic control, c) powers with control filter-based SOGI

As shown by the figures, using specific control schemes to improve the inverter responses in the event of unbalanced voltages allows to reduce the 100 Hz oscillations in the power generated in the event of both two-phase voltage dip and intervention of some limitations. In particular, the powers oscillating components show a significant degradation of the performance of the modified control, mainly due to the intervention of the limitations.

The presence of a SOGI filter control is clearly visible in the active power behavior when the network returns to the pre-dip operating condition: the steady state condition is reached after 100ms, a time longer than the case of control d-q (20 ms) but more stable (less oscillation). As already described for the classic control, also in this case the device stand-by condition could be the best solution in presence of an unbalanced voltage dip and with inverter current limitation active, to avoid the possible voltage quality deterioration dependent on the network short circuit power at the DG connection point.

5.5 Final Considerations

In this Chapter two inverter control strategies optimized for operation with unbalanced voltages have been analyzed and verified by digital simulations.

These control schemes have been already proposed in the literature and substantially are based on a control of all components (direct and reverse sequence) of the current. Thanks to the simulations, these methods have established their positive effect on reducing the 100 Hz oscillations in power output and the unbalances of the inverter currents in case of an unbalanced network or two-phase voltage dip. This positive effect is present if the inverter current limitations aren't active.
Instead, in case of balanced voltages, the "modified" control schemes present performance similar to the "classic" control even during the input and output transient of the voltage dips.

For these two modified control schemes the possibility of implementing FRT strategies has been analyzed. The results show the same positive aspects and the same issues already highlighted in the previous Chapters, in terms of need to limit the inverter currents and the DC voltage. In general an optimum FRT strategy can be to impose the stand-by condition to the inverter during the voltage dip, so it can be ready to resume the standard operation at the end of the network disturbance as soon as possible.

6 LABORATORY TESTS OF INNOVATIVE INVERTER CAPABILITIES

The recent, and already cited, Standard in terms of energy sources interfaced through inverter to the distribution networks establishes that the distributed generators have not only to inject the maximum active power extracted from primary source to the network but they should be able to provide auxiliary services or implement additional functionality on the basis of a remote control or local conditions. Examples of these requests, which are contained in CEI 0-21 [2] and CEI 0-16 [3], related respectively to the LV and MV connections, are:

- operation at an arbitrary power factor, within a certain capability;
- overcoming voltage dips;
- sustenance/limitation network voltage;
- supply a controlled reactive power to support (or limit) the mains voltage, both in steady state and in transient condition;
- reduction of the active power exchanged if the mains frequency increases or due to an external control.

Main objectives of the laboratory activities, focused on the requirements of CEI 0-21, carried out in the RSE spa Laboratory in Piacenza, have been both the verification of feasibility of such new functionalities and to make the tests on commercial inverters to gain a better understanding of the issues and solutions adopted to implement the functionalities.

This Chapter is focused on the illustration of the types of tests performed in the laboratory and the conclusions that can be drawn from it.

6.1 Test bed description

The system represented in Figure 6-1 (picture) and Figure 6-2 (block diagram) has been implemented at the RSE laboratory in Piacenza (Italy). It consists of:

- a single/three phase connection to the public LV grid (alternatively, a 12 kVA grid simulator is available); in particular the linear programmable network simulator has the possibility to fed single-, two- or three -phase systems (Figure 6-3);
- a DC source with PV array VI characteristic emulation feature (P=20 kW, V_{max}=500 V) (Figure 6-4);
- an adjustable parallel RLC load (single or three phase) with overall power capability up to 18 kW and ±18 kVAr (inductive and capacitive);
- a data acquisition system which monitors AC and DC measurements and allows on-line calculations of active, reactive power and RMS values; the Supervision system offers some visual tool to easily check the magnitudes; an example of the Man to Machine visual Interface (MMI) of the data acquisition system is shown in Figure 6-5.

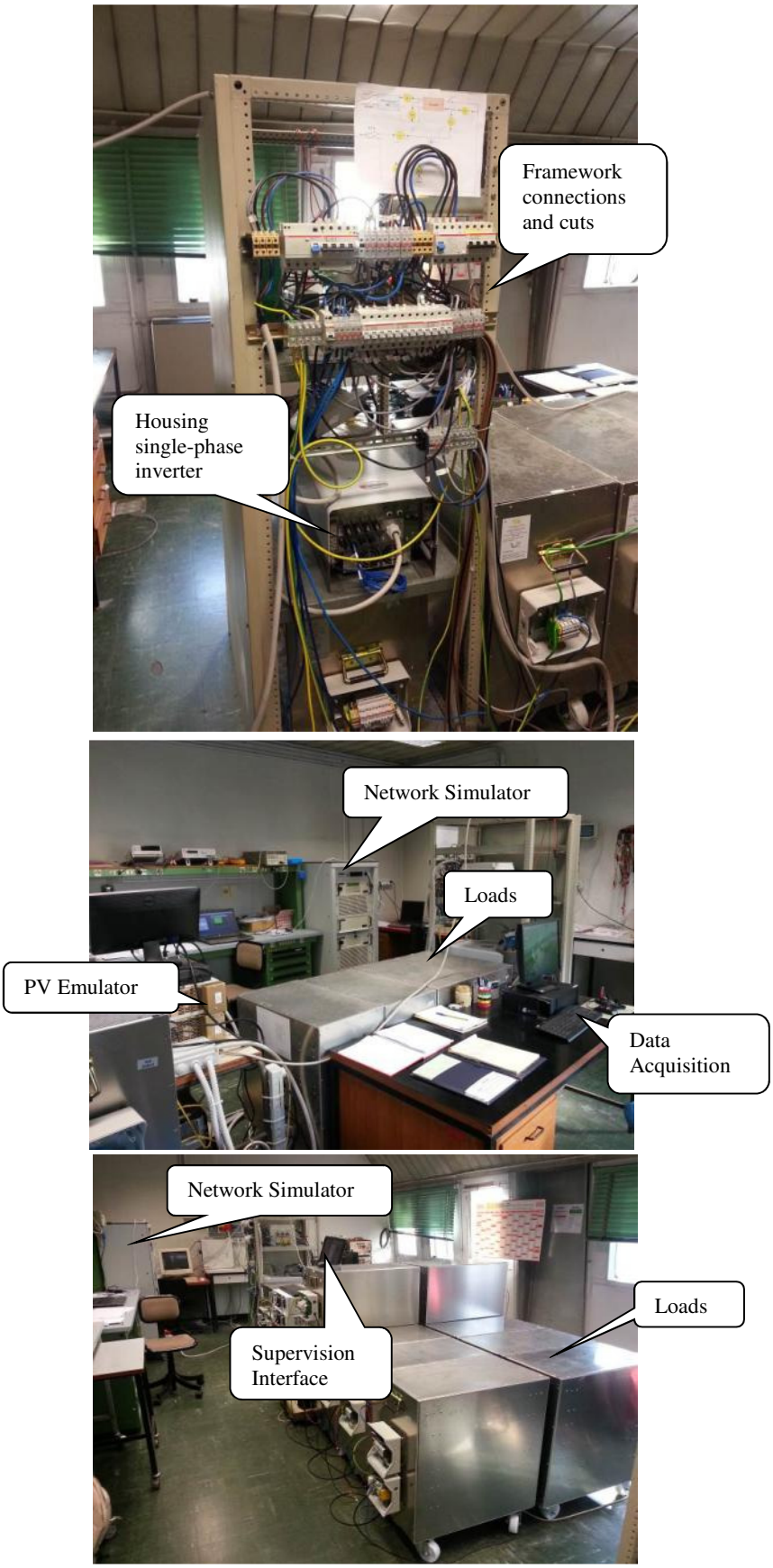

Figure 6-1: Picture of the laboratory filed and instrumentation

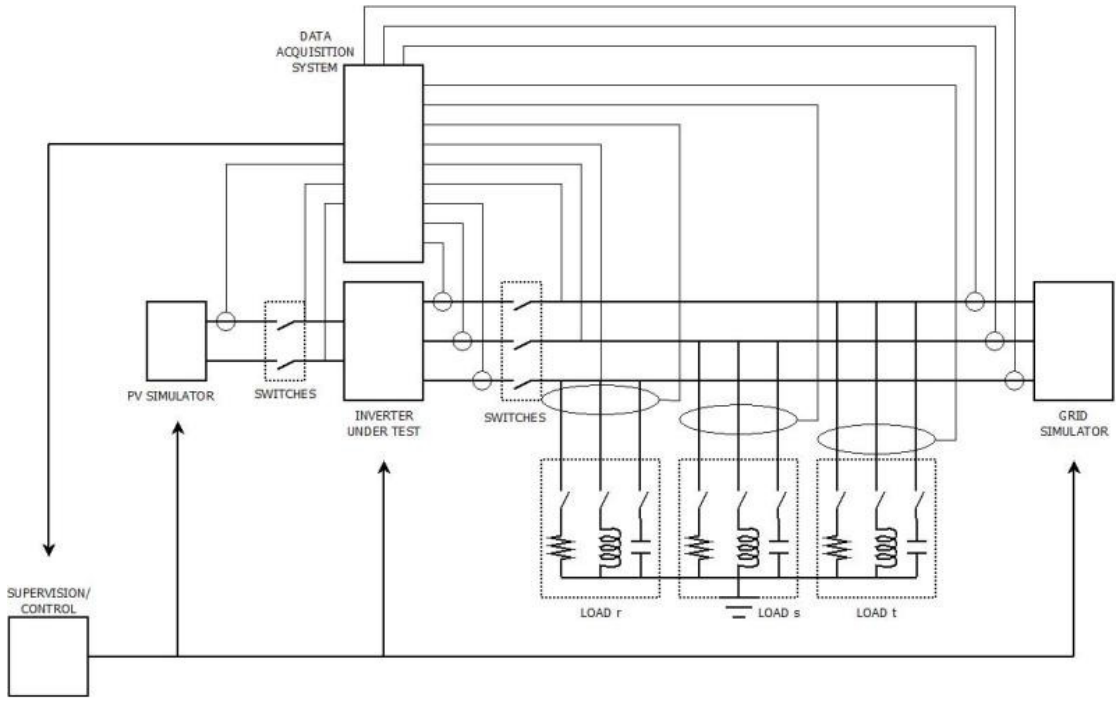

Figure 6-2: Schematic diagram of the test circuit

6.1.1 Linear programmable network simulator

A linear programmable network simulator is essential for the implementation of the functional tests on inverter, because it is necessary to modify voltage and frequency level of the AC network and to program network transients. The simulator, programmable through a graphical remote interface shown in Figure 6-3, works on four quadrants and has a maximum power of 12kVA in feeding and about 4 kVA in absorption, with the possibility of a 10% overload for limited periods of time. The simulator allows to realize single-, two- or three-phase connections with an independent voltage control of each phase, to be able to simulate voltage unbalances.

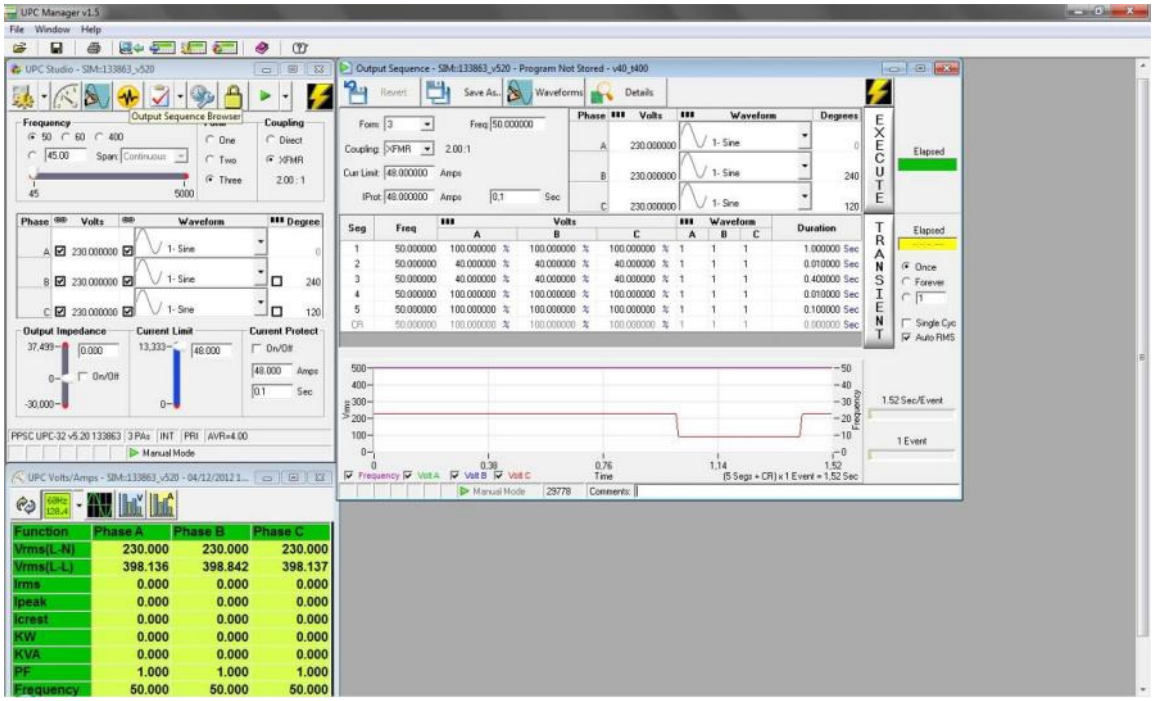

Figure 6-3: User Interface for programming the network simulator

6.1.2 DC source with PV characteristic curves emulation

The 20 kW DC power supply consists of two equal 10 kW modules which can be connected, in "master-slave mode", in series to increase the maximum voltage level supplied or in parallel to double the maximum current that can be generated. The source can be remotely programmed via a graphical user interface (Figure 6-4).

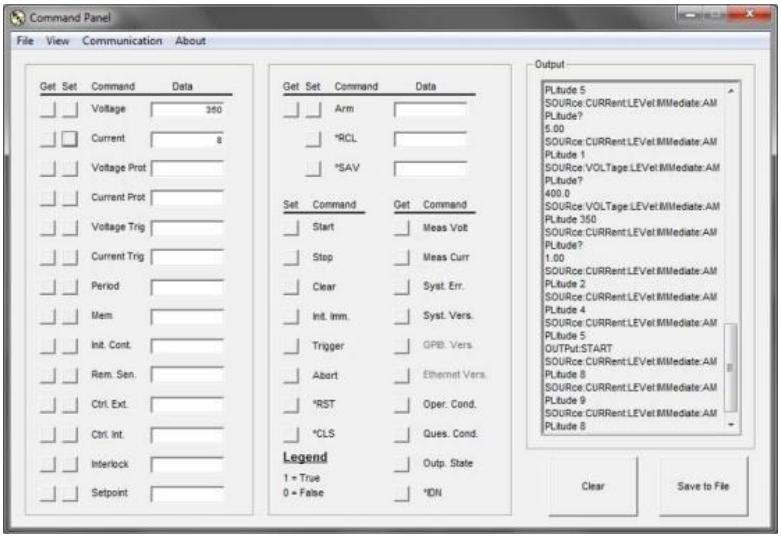

Figure 6-4: Graphical User Interface for remote control of the DC power supply

6.1.3 RLC variables loads

The available loads allow to reach a maximum active power of 18 kW and 18 kVAr reactive power, both inductive and capacitive. Each component is divided into three modules of the same maximum power and each module is configurable to achieve single- or three-phase loads.

6.1.4 The inverter under test

The experimental activities have focused on two different inverter for interfacing of photovoltaic generators.

The first inverter is a single-phase device with a DC power of 6 kW (INVERTER 1), while the second is a three phase device with DC power of 10 kW (INVERTER 2). This second device is equipped with some of the advanced features that can be set remotely, such as provision of reactive power and a limitation of active power according to various criteria ("advanced features"). Since the INVERTER 1 has been designed before the new Standard publication in the following it's considered as an "old conception" device.

The choice of these two types of inverter has been carried out to highlight the different design/control characteristics between the devices.

In addition, the tests carried out on the INVERTER 1 also had the purpose to establish how and if the "old conception" inverters could provide advanced features and services to the network, even if they are not designed for this purpose.

6.1.5 Data acquisition system

The AC and DC voltages and currents are directly acquired. The system allows the visualization of the quantities measured and some quantities "calculated" by a visual interface as shown in Figure 6-5:

- *oscilloscope:* view of the waveforms in time and their RMS values;
- *topological*: view of the powers, RMS voltages and currents of the network simulator, of the inverter and loads separated;
- *vector V/I :*view of the phasors of the voltage and current of inverter, loads and network simulator;
- *vector P/Q*: vector view of active, reactive and apparent powers of the different sub-components of the system.

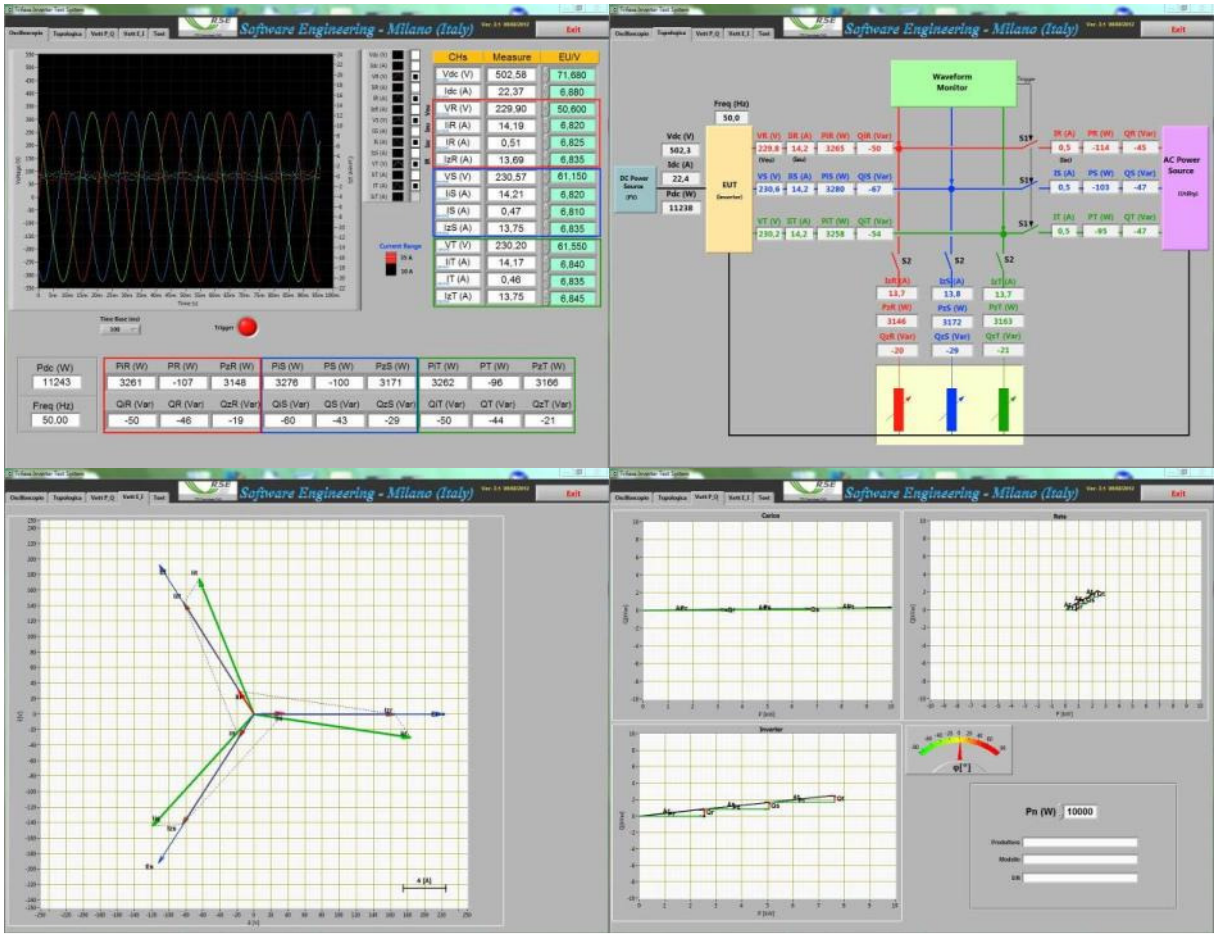

Figure 6-5: Data acquisition system visual user interface

6.2 Innovative capabilities required to the inverter

The new Standards impose to the generators, in particular those interfaced by an inverter, a series of new functional requirements. These requirements are focused, on one hand, to the improvement of the voltage quality and, on the other hand, to increase the number of DG connected to the network. The specific Standard requirements may vary for the different voltage level, LV or MV, but, in general, the required functions can be divided into the following macro-areas:

1. overcoming network disturbances;
2. supply controlled reactive power;

3. active power regulation.

The laboratory activity has been addressed to functional tests relating to the requirements included in CEI 0-21, the following is a brief overview of the requirements in relation to the earlier macro-areas.

6.2.1 Overcoming network disturbances

Voltage Dips - Low Voltage Fault Ride Through (LVFRT)

The CEI 0-21 establishes that the distributed generators have to remain connected to the network when there are voltage dips with characteristics of time/residual voltage within a given mask, shown in Figure 6-6.

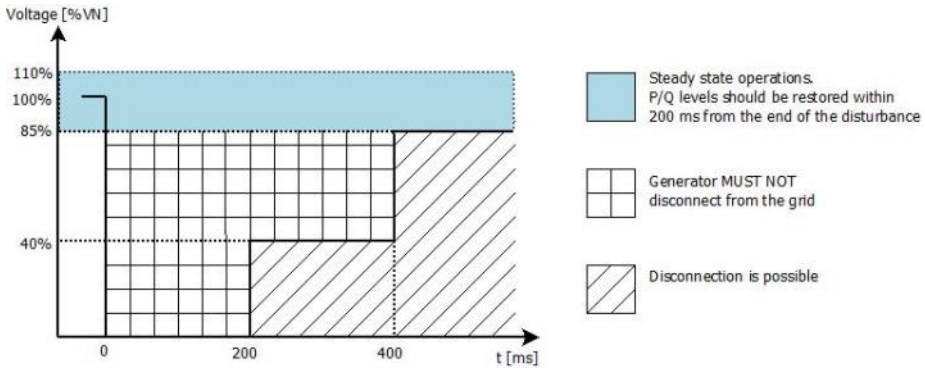

Figure 6-6: LVFRT according to CEI 0-21

It's not required to the inverter a particular behavior during the voltage dip, but it has to remain electrically connected to the network and to restart the injection of active power, at least 90% of the value pre-dip, within 200 ms after the RMS voltage return between 85% V_N and 110% V_N. For voltage dips that are under the LVFRT curve, the inverter is disconnected from the network by the interface protection tripping; the protection settings have been modified in accordance with the requests of overcoming the voltage dips.

The Standard also requires the types of proof to verify this requirement. The inverter behavior should be tested in case of symmetrical and unbalanced voltage dips.

During the experimental activities different voltage dips have been analyzed, not only the which ones included in the Standard, since the tests aim is not only to check the voltage dips overcoming indicated in CEI 0-21 but also to explore the real inverter capability to stay connected during the event, beyond what is required by the Standard.

6.2.2 Supply controlled reactive power

The requests for the supply of controlled reactive power included in CEI 0-21 foresee different modes of power exchange:

- with fixed power factor;
- according to a Q=Q(V) characteristic curve;
- on external remote control;
- according to a cos(φ) =f(P) characteristic curve.

Supply reactive power with fixed power factor

It's required that the generator is able to deliver power with a given power factor cos(φ) according to one of the two capability curves reported in Figure 6-7, respectively white area and grey area.

During the nominal operation (generation of active power P_N) can be requested to the inverter to provide a controlled reactive power (capacitive or reactive) with a power factor included in the range $0{,}9_{lagging} \leq \cos(\varphi) \leq 0{,}9_{leading}$.

This implies that the device should be over-sized to supply at least a nominal power $S_N = 1.11\ P_N$.

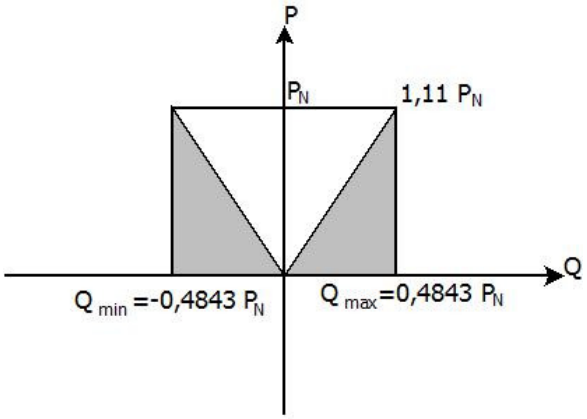

Figure 6-7: DG capability curves (white and grey areas) connected to LV networks, according to CEI 0-21

Supply reactive power according to a Q=Q(V) characteristic curve

The Standard requires that, in order to support the mains voltage (or to limit its growth), the inverter should supply reactive power as a function of the mains voltage, according to one of the two characteristics curves shown in Figure 6-8. These characteristic curves are in accordance with the limits defined by both the capability of Figure 6-7.

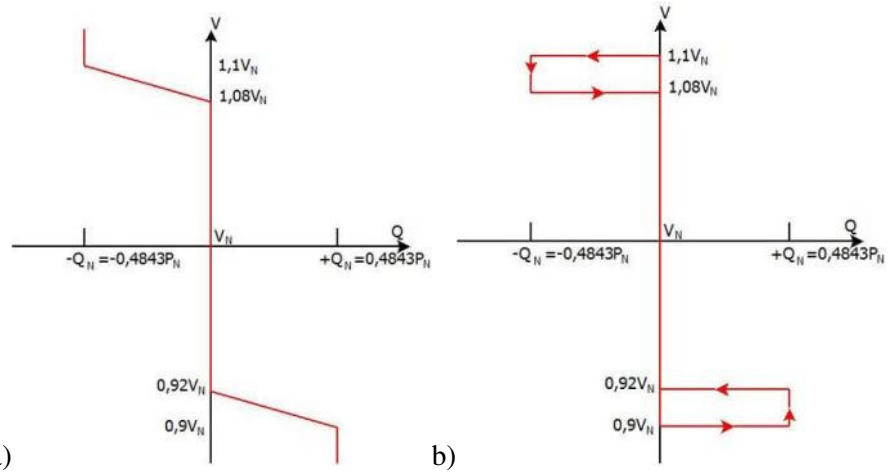

Figure 6-8: Q=Q(V) characteristic curves feature with "dead-band" a); with hysteresis b)

Supply reactive power on external control

The Standard requires that the generation system should be able to exchange reactive power according to a value assigned by an external remote control. Also in this case, the reactive power supplied must be in accordance with the inverter capability, and so the maximum reactive power available is equal to 0.4843 P_N. The Standard requires also that the achievement of the reactive power value, assigned by the external remote control, which takes place in less than 10 s.

Supply reactive power according to a cos(φ) =f(P) characteristic curve

Again, in accordance with the inverter capabilities shown in Figure 6-7, it's required to the inverter to inject reactive power with a power factor that depends on the active power. The characteristic reference curve is shown in Figure 6-9.

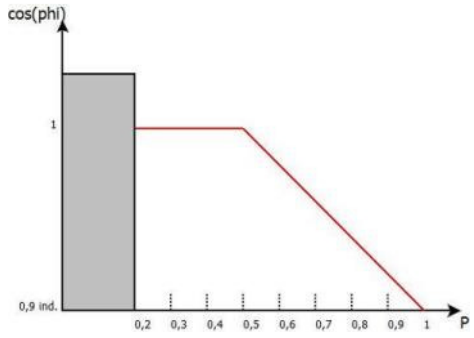

Figure 6-9: Power factor characteristic curve depending on active power

6.2.3 Active power regulation

The Standard requires the active power limitation in two different ways described in the following:

- on external remote control;
- in case of transients on the transmission grid.

Active power limitation on external control

It's expected the possibility to limit the active power delivered by the inverter with an external command. The power set-point can be set in the range 100% P_N ÷ 0% P_N. The power value requested must be reached with an accuracy of ±2.5 % P_N.

Active power limitation in case of transients on transmission network

The use of double frequency threshold for the generators interface protection, as required by CEI 0-21, CEI 0-16 and the national Grid Code, has the aim of keeping connected the distributed generators in case of network frequency variation as a result of a fault occurred in the transmission grid. In particular, there may be two situations:

1. frequency decreasing: when the power generated is less than that absorbed by the loads;
2. frequency increasing: when the power generated is greater than that absorbed from the loads.

In the first case, the Standards require that the distributed generators must remain connected to the network continuing to supply their full power, in accordance with the primary source availability, in order to avoid further unbalance between generation and load.

In the second case, however, the Standards require a gradual reduction of the DG power generated, to obtain gradually a rebalance between generation and power consumption. In this situation, the CEI 0-21 provides a P=P(f) curve of the active power supply decrease as reported in Figure 6-10.

The power delivered during the transient network is kept constant until the return of the mains frequency to the nominal value.

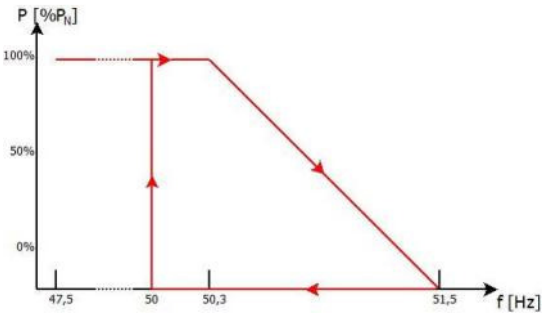

Figure 6-10: P=P(f) characteristic curve

6.3 Test Procedure

The first part of the activity has provided the identification of test procedures that would allow the implementation of the functional tests. In spite of the individual tests have specific topics in their execution, it has been possible to identify a series of general operations necessary to be performed for all types of test. In particular three main steps have been identified:

1. start of the test bed and of the inverter;
2. test execution;
3. results analysis.

The following table shows the specific procedure adopted for the test relating to overcoming voltage dips capability. It's not described the phase of start of the test bed, since it does not have specific issues related to the function under test.

Inverter 1: "old conception"	*Inverter 2*: "advanced features"
Test execution	
There aren't any inverter configurations to be modified.	Set the desired pre-dip active and reactive power supplied. It's necessary to modify the PWM modulator block setting for under-voltage, decreasing the threshold value to the minimum allowed by the settings of the device.
The Interface Protection (IP) can't be disabled and it's not possible to change the default settings, that define the minimum voltage tripping if the voltage is less than 80% V_N with intentional delay 50 ms. Therefor the tests have been carried out changing the nominal voltage setting at 200 V for which the IP would be triggered for a value V_{trip}=0,8*200V=160V corresponding to 70% of the voltage referred to 230V. With this setting, it's excluded the maximum voltage tripping, which has a threshold of intervention of 1.2 V_N.	The IP can't be disabled, but it's possible to change the trigger thresholds at the following new values: V_{trip} = 0.2 V_N T_{delay} > 2 s
The network simulator is programmed to generate the desired transient, setting for each voltage step the residual voltage, the duration of the voltage dip and the voltage restore conditions. An example of the graphical interface for controlling the network simulator used to generate a symmetrical three phase voltage dip with residual voltage equal to 60% V_N and duration 500 ms is shown in Figure 6-11.	
The data acquisition system is set to be able to record data for a time window enough to measure the whole transient; typically, for the evidence of overcoming voltage dip a window of 7 s is enough.	
The voltage transient runs in the network simulator.	
Results analysis	
It is verified that the steady state inverter operation before and after the transient, corresponds to the settled inverter configuration.	
It' verified that the network simulator has reproduced the desired voltage dip and that the inverter has	

remained connected to the network; this last operation may be carried out by displaying the current of the inverter measured at the network side. In particular: • if the inverter keeps the power delivery, the current increase of amplitude, possibly up to a limit value; • if, on the contrary, there is a passage in stand-by mode, the currents are reduced to those absorbed by the inverter output filters.
The data acquired (AC and DC voltages and currents) are saved in a data file.
The saved data are processed with a numerical software to obtain useful information, such as: • the active and reactive power waveforms and the DC power during all the transient state. • any distortions and unbalances of network or inverter currents and voltages during the voltage dip or at the normal network conditions restoration; • the recovery time for the rated power exchange of the inverter; • the inverter current limitation values.

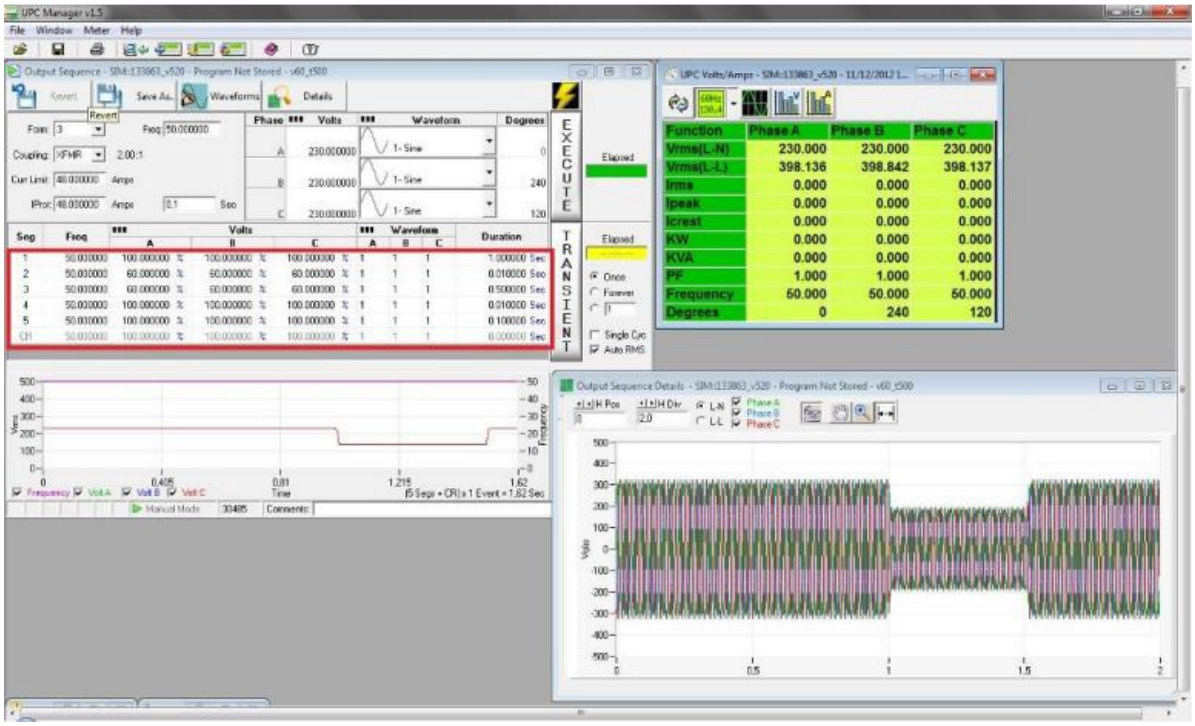

Figure 6-11: Graphical Interface for controlling the network simulator in case of voltage dip

6.4 Experimental activities results

During the experimental activities on the two mentioned inverters both the functionality of operation in the range of frequency/voltage extended and the LVRT capabilities have been tested.
Initially the continuous device operation during steady state is verified in the following voltage and frequency ranges required by the CEI 0-21:

$85\%\ V_N \leq V \leq 110\%\ V_N$
$47.5\ Hz \leq f < 51.5\ Hz$
where V_N is the nominal voltage.

6.4.1 6 kW single phase inverter

For the INVERTER 1 "old conception", since it's not possible to disable the Interface Protection (IP), it's not possible to test its continuous operation during steady state in the frequency range required by the Standard. The IP, set according to the Standard before the CEI 0-21 new edition, requires the inverter disconnection for network frequency values outside the range 49.7 Hz ÷ 50.3 Hz.
The validation of the proper inverter operation has been conducted by measuring the active power delivered toward the linear network simulator in different frequency conditions in the range of allowable variation imposed by the internal IP. It has been possible to check that before the IP tripping there are no significant alterations of the inverter behavior, as shown in Figure 6-12. The IP trip occurs at 49.71 Hz (under-frequency) and 50.31 Hz (over-frequency): the trip is visible in Figure 6-12 when the measured power becomes zero. The accuracy of the intervention threshold (10 mHz) is compatible with the CEI 0-21 requirements (±20 mHz). A similar result has been obtained measuring the power supplied when the voltage varies in the range 85% $V_N \leq V \leq$ 110% V_N, where V_N is the nominal voltage.

For the check of the operation under the 90% V_N, not being able to change the IP setting, the inverter nominal voltage value has been reduced up to a value equal to 77% V_N, through the machine user interface. In this way, the interface protection does not trip even for network voltages up to 70% V_N. The same approach has been used to test the device in case of voltage dips. All the tests have been carried out by starting the inverter at the frequency/voltage rated values, varying then the parameters to the desired values and measuring the waveforms after the achievement of new stable condition.

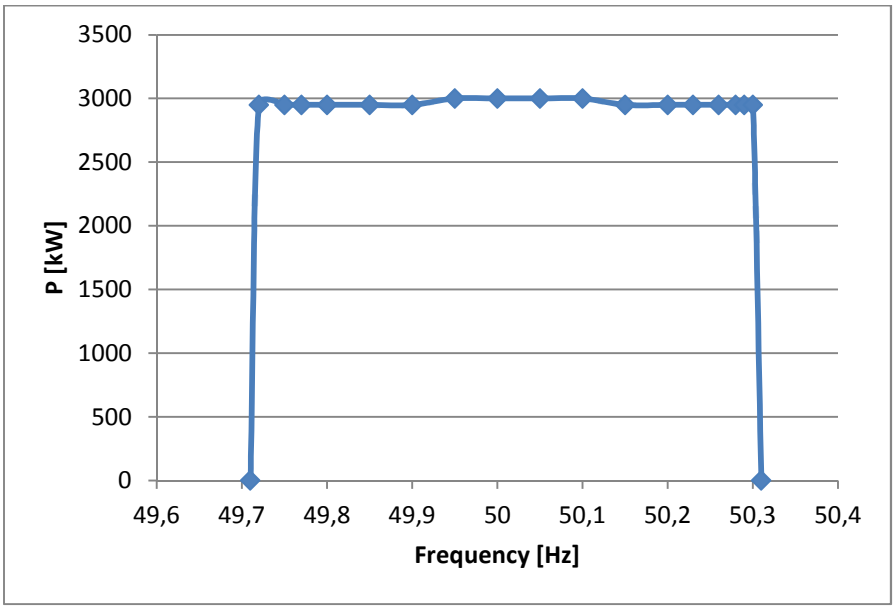

Figure 6-12: Measurement of the power generated by INVERTER 1 for different frequency values

Overcoming voltage dips

The inverter has showed a capability to overcome voltage dips of arbitrary duration, even greater than that required by the Standard, within the limit of residual voltage equal to 70% V_N (threshold for the interface protection tripping). Figure 6-13a shows the current injected by the inverter during a voltage dip with residual voltage 75% V_N and duration 1 s (Figure 6-13b).

The device has not shown any capability to provide network services, such as delivery/absorption of reactive or active power in particular network conditions. These features must be obtained both with the device and control design.

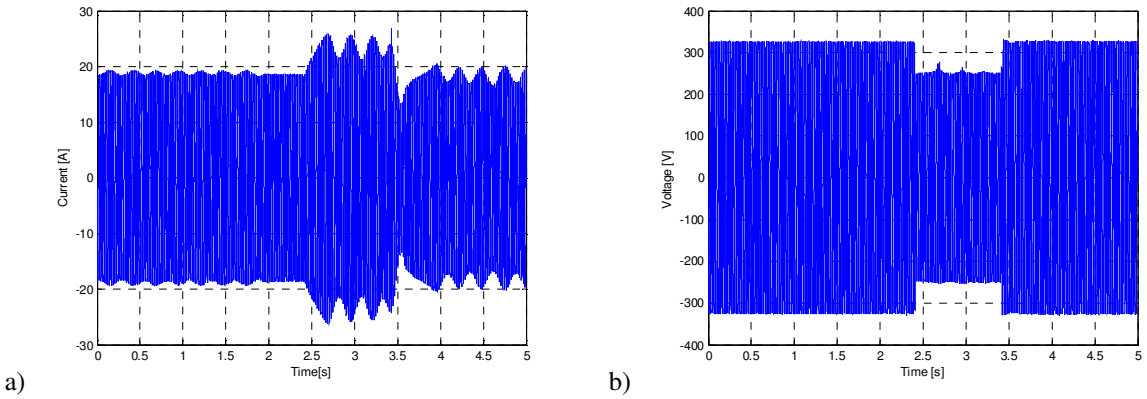

a) b)

Figure 6-13: Inverter response to a voltage dip: a) current injected, b) mains voltage

6.4.2 10 kW three phase inverter

Also for the INVERTER 2 "advanced features", the first test is the evaluation of the continuous operation during steady state in the frequency and voltages ranges defined by CEI 0-21. In this case it's possible to change the Interface Protection (IP) tripping thresholds to implement the required tests (essentially the IP is disabled in the voltage/frequency ranges under test).

Figure 6-14 shows the active power delivered for different network frequency values, with the active power reduction over 50.3 Hz.

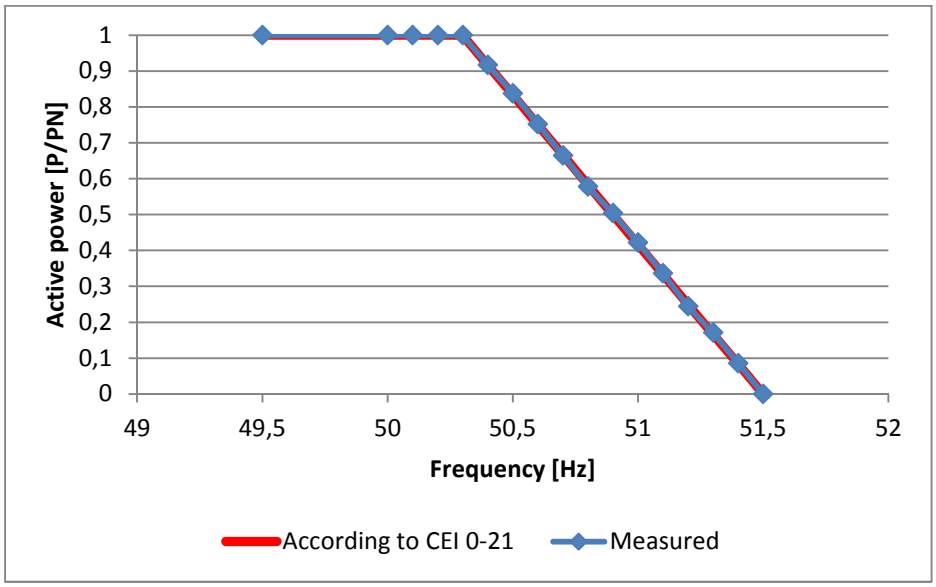

Figure 6-14: Inverter behavior for different network frequency values

Overcoming voltage dips

The inverter behavior has also been tested in case of voltage dips. It has been possible to verify the capability of overcoming the events of any duration and characterized by any residual voltage. This capability, for mains voltages below a certain value, occurs with the inverter stand-by operation. The recovery time to have the power exchange as during the pre-dip conditions depends on the voltage dip characteristics and for this inverter it's not in accordance with the Standard requirements.

Figure 6-15b shows the inverter current in response to a symmetrical three phase voltage dip with residual voltage 30% V_N and duration 400 ms (Figure 6-15a). During this test, the inverter is configured to inject only active power.

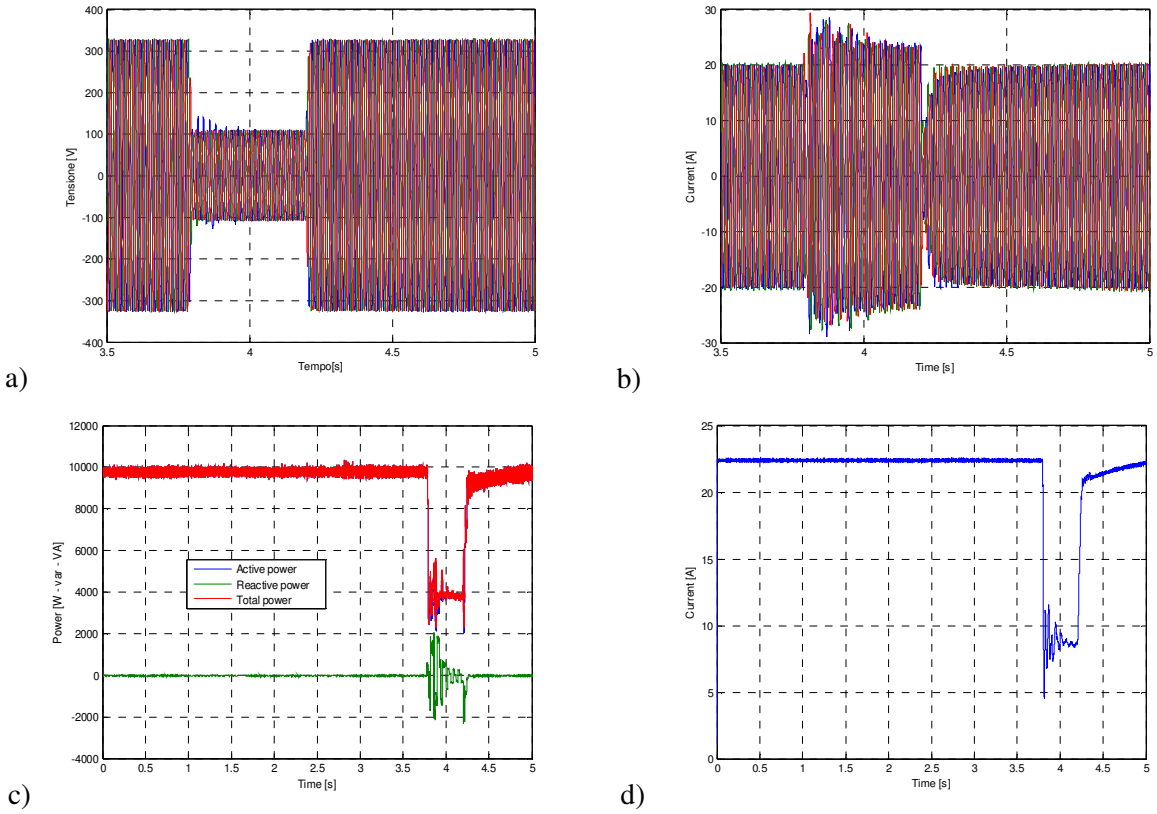

Figure 6-15: Waves recorded from data acquisition system for a symmetrical three phase voltage dip (a) AC output network simulator voltage; b) inverter currents; c) active, reactive and apparent power; d) DC power absorbed by the inverter

The response to an asymmetric voltage dip has shown more critical behavior, since both during and after the event the inverter injects three phases unbalanced currents. The inverter response in case of a phase to phase voltage dip (with residual voltages equal to 45%V_N, 45%V_N and 100 %V_N) of duration 500 ms is shown in Figure 6-16. Although the inverter is able to remain connected during the network disturbance, the restoration of symmetrical current occurs only after several seconds from the end of the event. In this case, the possibility to put the device in stand-by mode during the voltage dip, by suitably adjusting the thresholds for intervention of this functionality, it is preferable because it allows a restoration of normal operating condition without unbalanced currents.

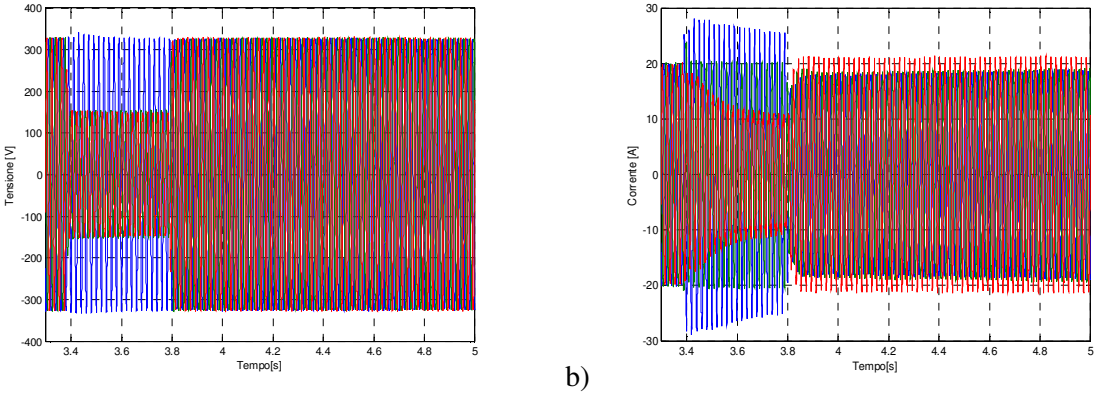

Figure 6-16: Currents supplied by the inverter (b) in response to a phase to phase voltage dip (a)

Active and reactive power exchanges

It has been also verified the possibility to exchange reactive power, according to the CEI 0-21 requirements.

This inverter is not able to satisfy, for size reasons, the active/reactive power capability prescribed in the Standard, but the tests show that is able to supply reactive power if there is a reduction in the delivered active power. The inverter P/Q capability measured during the laboratory tests and compared with the Standard requirements is shown in Figure 6-17.

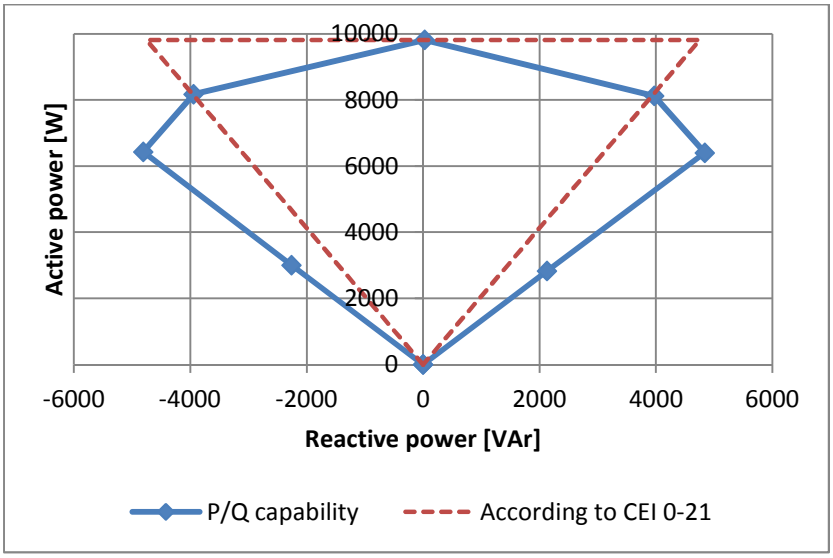

Figure 6-17: Tested P/Q capability of the three phase inverter

Figure 6-18 shows the active and reactive power generated in presence of network voltage variation, for a Q=Q(V) reactive power delivering.

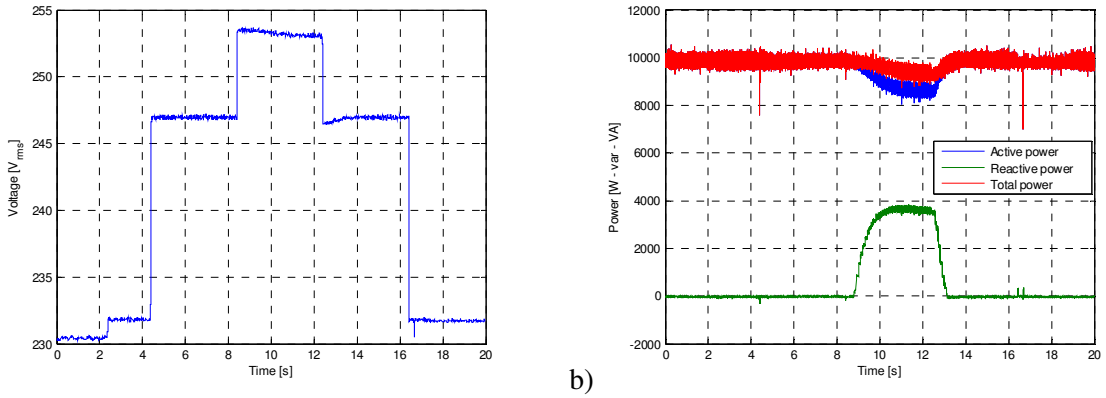

a) b)

Figure 6-18: Voltage transient network (a), inverter active and reactive power (b). A reactive power of positive sign corrisponds to the absorption by the device, this convention is used only for this figure

Finally Figure 6-19 shows the different reactive power (blue curve) measured for different values of the mains voltage during steady state conditions, compared with the Standard required operating curve (red curve).

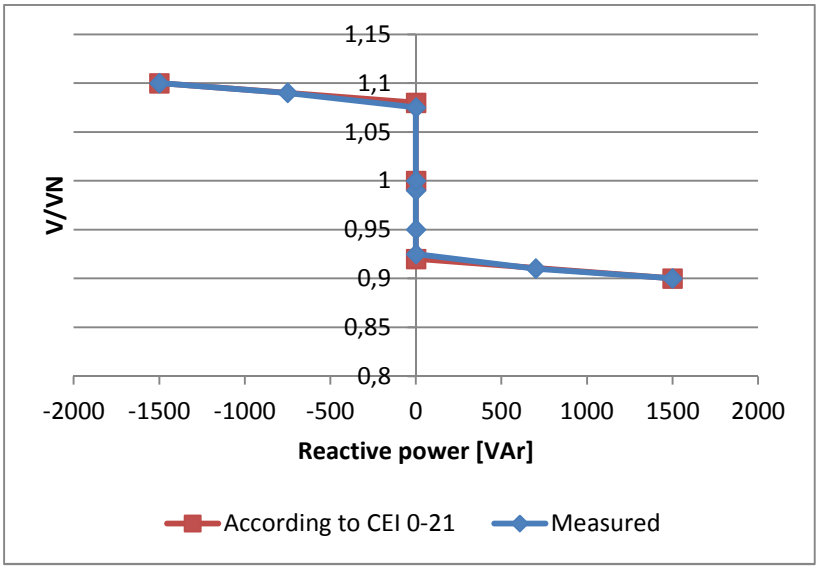

Figure 6-19: Q=Q(V) curve "dead band" measured for INVERTER 2 compared with the CEI 0-21 required

6.5 Final Considerations

The experimental activities, supported by theoretical analysis/modeling, have been oriented to the analysis of the functional tests for the photovoltaic interface inverter, included in the recent national Standards. The tests have been focused on three types of functionality required to LV inverter by the CEI 0-21:

- voltage dips overcoming;
- supply controlled reactive power;
- active power regulation.

The main purpose of the laboratory tests has been the deepening of issues that may arise in the implementation of these new inverters capabilities, through a critical analysis of the test results performed on both "old conception" inverter (designed according to the previous Standard) and on "advanced" inverter (designed to provide the required functionalities even if not completely compliant with the new Standard). Analysis of the two types of devices has allowed to highlight what is the evolution, in terms of design and control, requested to the inverters to meet the Standard requirements.

The aim of the activity has not been to perform the tests exactly as prescribed by the Standard, but to analyze which are the fundamental aspects to take into account when it's necessary to test the capabilities listed above.

In detail the experimental activities have provided the following results.

Voltage dips overcoming: the device is required to limit the maximum current delivered to a value less than or equal to the maximum switched current with continuity from the valves. This feature is already implemented, as a protective measure, even in the inverters of old conception, that offer in principle a "natural" Fault Ride Through (FRT) capability. The presence of an Interface Protection integrated in

the device that can't be disabled, or which is not possible to change the settings, may hide this capability.
A PWM modulator for under-voltage block, if required, represents a real obstacle for the overcoming of voltage dips. The recovery time to reach the pre-dip conditions depends mainly on the inverter control. The most critical situation is in case of unbalanced voltage dips. In these cases, in fact, the inverter currents are unbalanced and distorted, making impossible the regulation of the devices (Chapter 5). It has also been verified that the inverter offers capability to overcome heavier events in terms of durations than the ones required by Standard CEI 0-21.

Supply controlled reactive power: this function, required by the Standard CEI 0-21 with different execution modes, essentially foresees a redesign of the inverter control, which must include the provision of a quadrature current reference in accordance with the voltages transient. This additional current must be taken into consideration during the design of the device so that it can be able to exchange an apparent power of at least 1.11 P_N.

Active power regulation: the implementation of this functionality is mainly to limit, through the inverter control, the power absorbed by primary source and, in consequence, injected into the network.

In general, it can be concluded that the implementation of new features is, in the majority of cases, a problem related to the inverter control, as long as it is designed to supply a reactive power in addition to the active one, without incurring in its capability limits. Also the "old conception" inverter can satisfy the latest Standards with a firmware update and a revision of the capability curves.

7 ANALYSIS OF THE INTERACTION BEETWEEN INVERTERS WITH FRT STRATEGIES AND NETWORK PROTECTIONS

In this Chapter the main Medium Voltage (MV from 1 kV to 60 kV) and Low Voltage (LV less than 1 kV) distribution networks characteristics and the possible types of network faults management are described presenting the structural measures and the different network exercise choices implemented to improve the quality of electrical service.
In particular, to improve the continuity, in regards to actions for the network operation, it's highlighted, from the experience of the exercise of the MV network in two possible configurations: isolated and compensated, a significant reduction in case of compensated neutral of the number of interruptions, a lower stress for the insulation of the network components and a decreasing of the single phase fault to ground currents.
In terms of structural measures, a further contribution to the reduction of both the number of long interruptions and their duration, is related to the remote control and, as evolution, to the network automation.
Further reductions in the cumulative interruption duration are obtained thanks to the automatic procedures for the faulty line section selection. This measure, which is an evolution of the "simple remote control", allows the identification of the line segment affected by the fault and the restoration of the "healthy" line sections without the operator intervention, having a clear advantage in cases of faults that occur simultaneously in multiple network locations.
In the next these measures and the network evolution toward an active network will be shortly presented.

7.1 Distribution networks description

In general, the structure and the extension of MV and LV distribution networks are rather heterogeneous, even if the main difference is between urban networks (typically short and underground cable) and rural networks (typically long but not necessarily overhead type).
From a structural point of view the distribution networks are predominantly radial, so that each network node is fed from a single source of supply.
The electric energy distribution in the MV distribution networks takes place through lines that depart from HV/MV Primary Substations and which fed MV users and MV/LV Secondary Substations, from which the low voltage distribution develops.

Primary substations (PS)
The HV/MV PS are equipped with a number of transformers that can generally vary from 1 to 4 (typically 2 transformers) and a number of MV lines which can vary from 4 to 20 (with a typical value of 10). The trend, as regards the number of primary stations, is very different depending on the network and/or Distributor System Operator (DSO) needs in the different European countries.

Medium voltage feeders
The Medium Voltage (MV) lines are different in rural or urban areas, with a prevalence of cable lines in urban areas. In regard to the MV lines length, the average values of 10-35 km in rural areas and 3-10 km in urban areas. About the loads there isn't any difference between urban areas and rural areas; in Europe the situation is so much various, that some DSO are designing the rural lines to connect more loads than in the urban areas, others operate in the opposite way and others tend to load the MV network regardless of the type of area that supply. However, typical values of load installed in "rural" MV lines can be 1 ÷8 MVA, while in MV "urban" lines 1 ÷ 10 MVA.
In case of need, as a result of the occurrence of a fault in the network, the greater part of the MV distribution lines can be fed from other adjacent lines, through the closing of circuit breakers operating

normally open. Almost all MV networks in Europe are three phase systems, two-phase are used in France to supply rural areas with low energy consumption.

Secondary Substations (SS) and LV network

The average number of secondary substations (MV/LV) fed by MV lines depends on the type of area:

- from 5 to 15 SS for each urban areas MV line;
- from 15 to 50 SS for each rural areas MV lines.

In regards the typology of LV lines, these are mainly underground cable for an average number of LV users that varies from 40 to 100 for each secondary substation.
Unlike MV lines, the probability to have LV lines fed by adjacent lines is much lower with a percentage that varies between 0% and 30%.

MV networks neutral connection type

Relatively to the distribution networks neutral management, with particular reference to MV, it's possible to have different solutions:

- Isolated Network without any point connected to earth (in this definition the connections to ground through high impedance for the purpose of measures or security are not included). This management is used in Italy, Finland and some distribution networks in Switzerland, Austria and Belgium.
- Compensated Network with a Petersen coil connected between the star point of the transformer and earth with reactance or impedance (resistance and reactance). This type of system management is widespread in Austria, Germany, Switzerland, Finland. Relatively to Italy, historically the MV network has been neutral isolated and now is partially converted to compensated system.
- Network connected directly to earth via negligible impedance. In case of single phase fault to ground, the fault currents have a magnitude such that activating for sure the automatic tripping of the maximum current protection relays. This type of management is widespread in Belgium, France, Portugal and Spain.

7.2 The Italian protection philosophy

In the distribution network the fault is defined as an abnormal operating condition resulting from a malfunction of a circuit, a plant, of an apparatus or from a contact at low impedance between network parts with different voltage, which causes an abnormal current (fault current).
This current may occur between two or more phases (said poly-phase fault or short circuit fault) or between a phase and earth (single phase fault or ground fault).
Under fault conditions, the feeder "segment" affected by the fault should be immediately disconnected from the network in order to eliminate the fault current, to ensure safety to people and facilities, to maintaining the network stability and to preventing the deterioration of the network components.
To obtain the detection of the faulty network section, it is necessary to adopt protection devices able to recognize an abnormal operating condition (fault condition) by comparing one or more signals at their inputs, for example the currents, with preset threshold values that represent short circuit and ground fault currents.
The protection device operates in a very short time if the fault condition is detected and it controls the circuit breaker opening. In general, higher values of fault currents correspond to a shorter tripping time. Typically two or more tripping thresholds associated with different response times are set: for example "no delay" for high levels current and "time delayed" for below current values. For a correct operation of the protection devices, they should operate mutually coordinated to turn off the minimum possible network portion.
For this purpose it's frequent the presence of protection devices installed in "cascade" whose coordinated operation, in order to be effective, must be such that those near to the fault point trip in shorter time than the devices installed in farther points, whose intervention is exclusively for backup.

A not coordinated operation would cause the disconnection of network sections (and therefore of users connected to itself) does not directly affected by the fault.
An example of protections in "cascade" is that of MV protection relay installed on the primary substation HV/MV transformer (upstream protection) and the line protections installed on the same MV bus-bar of the transformer (downstream protections). In case of not-coordinated operation between the downstream and upstream protection relays, any fault with origin in a MV line would cause the transformer protection tripping and the consequent opening of all MV feeders (also the healthy ones) and all users connected.
Normally, selectivity criteria are based on current selectivity (based on the fault current values) or chronometric selectivity (by setting, for the same fault current, response times shorter in the downstream equipment than those upstream).

7.3 Actions on MV distribution networks to improve quality of service

The actions on MV networks to improve the quality of service can be distinguished into two main categories:

- improvement in terms of structure, components, remote control and network automation;
- operation and maintenance activities (on inspection and programmed).

The first category actions have to be considered useful for the purposes of strengthening the network capacitance to limit the disturbance effect to a limited number of users and to reduce the interruption time, while the measures included in the second category are methodologies and procedures designed to optimize operation and maintenance of the plants through prevention. A reduction of the fault probability is possible in many cases by operating network maintenance through preventive scheduled measures or with frequent inspections.

The structural actions to improve the continuity of the service are primarily oriented to a reduction of the times of power outage. Below the main structural solutions are analysed. In particular the first is the installation at the head of the MV lines of a circuit breaker with protection and automatic reclosing device, that lead to an evolution represented by the installation along the line of devices called reclosers and development of remote control and MV network automation for the faulty line segment selection.

MV network operation: from isolated to compensated
The neutral isolated networks ensure a certain simplicity of network operation and limit the fault to ground currents, proportional to the extension of the network itself, within relatively low values of the order of hundreds of amps, but there are some issues, such as the greater insulation stress and the phenomenon of the intermittent earth arc to be considered [64] ÷ [66].
The compensated system is implemented installing an iron-cored reactor connected between the star point of the substation transformer and earth, the so-called Petersen coil, and a resistor connected in parallel (Figure 7-1a). The impedance connection to the "neutral conductor", in this case, is made through a motorized isolator, which can be operated only with the HV and MV transformer circuit breakers in the open position.

The passage to a compensated network gives several advantages:

- limitation of the single phase to ground fault current, due to the compensation of the feeders capacitance to earth thanks to the "coil", allowing to maintain in service line during the fault research;
- the Petersen coil may be considered an Arc Suppression Coil (Reducing the intermittent arc risk);
- the probability of self-extinguishing single phase faults increases.

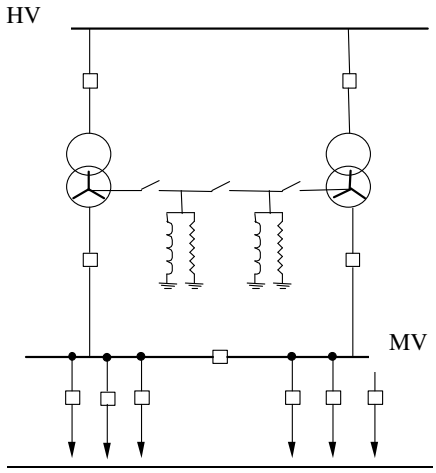

Figure 7-1: Petersen coil insertion scheme: connection between the HV/MV transformer star and the primary substation earth system

Some advantages in terms of improvement of the continuity of service are:

- avoided opening of the line circuit breaker in case of single phase faults, with a reduction in the number of outages and consequently of the cumulative total of interruption for LV user;
- less stress on network components insulation with reduction of their fault probability and consequent reduction of permanent fault rates and of the number of long interruptions (> 180 s).

The ground fault current limitation (theoretically up to the cancellation, on the assumption of full compensation by Petersen coil) also allows to keep in service the faulty line during the fault research (not otherwise applicable in an isolated network) [65]. In addition, it should be noted that these automatic procedures, based on the chronometric coordination of the circuit breakers installed along the lines, are also feasible thanks to the current earth limitation, that stresses less the earth systems in relation to the safety requirements associated with the values of the step and contact voltages.

Installation at the MV line head of circuit breaker and automatic reclosing device

Referring mainly to the MV distribution network, but in general to every radial network, in the hypothesis of passive network, a fault on a distribution line causes a fault current only in the line section upstream the faulty point.

Consequently, each MV line at its beginning is equipped with a circuit breaker controlled by a protection device able to:

- detect the short circuit and poly-phase ground fault currents caused by events originated in the under part of the network;
- eliminate the fault currents controlling the circuit breaker opening.

In some cases, in order to "eliminate" transient faults to allow better continuity of service, the MV line circuit breaker is associated with an automatic reclosing device, able to perform a sequence of fast and slow reclosing of the circuit breaker.

In order to better understand the automatic reclosing device importance for the continuity, it is necessary to consider the type of faults that can occur in a MV line: semi-permanent transients and permanent. In fact, apart from the faults that spontaneously are extinguished for natural arc extinction before the protections operation, the operating cycles of MV line circuit breaker allow:

- the transient faults extinction during the fast reclosing waiting time;
- the semi-permanent faults extinction during the slow reclosing waiting time.

In this way, only the permanent faults cause long interruptions in the power supply with the intervention of the operating personnel.

In detail, the logic of a reclosing cycle, shown schematically in Figure 7-2, requires:

- when a fault occurs along the MV line (single phase to ground or short circuit between the phases), the protection relays associated with the circuit breaker of the MV line detect the fault and controls the circuit breaker opening;
- after a certain time interval, which usually ranges from 0.3 s to 1 s (in Italy is generally 0.4 s)[43] there is the first reclosing, said fast reclosing. After that it's possible to verify that:
  - in case of self-extinguished fault, the MV line is resupplied, and there is a transient interruption;
  - in case of the fault permanence in the network, the line circuit breaker reopens for a period of time between 20 s and 3 min (in Italy 30 s) causing a short interruption;
- after the slow reclosing waiting time, the automatic reclosing device controls the line circuit breaker closing; this closure can be permanent or followed by a permanent opening in case of fault permanence.

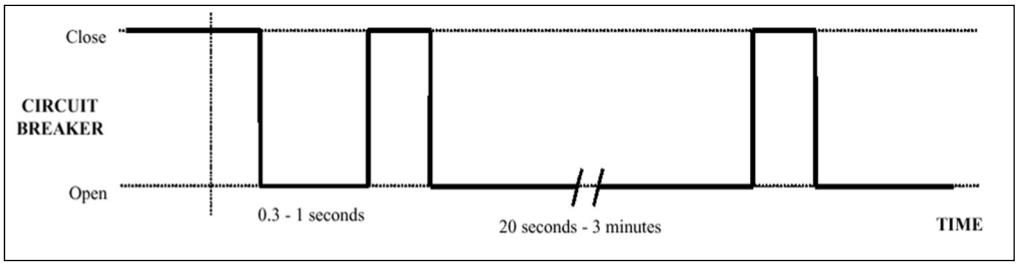

Figure 7-2: PS circuit breakers automatic reclosing in presence of a permanent fault

Remote control and MV network automation

In order to reduce both the number of long interruptions and the duration of them, other possible actions are those related to MV network remote control and its "automation". This means the adoption of procedures for the faulty line segment selection with the disconnection line segment affected by fault. After that the service restoration of the "healthy" line portions occur automatically, without operator intervention.

7.4 Protection issues for active networks exercise

The growing trend of installed power from Distributed Generators (DG) in distribution networks is giving rise to new issues to be considered for grid operations. In particular, the interaction between DG and network protection relays can cause:

- nuisance trips;
- unwanted island operations [64];
- worsening of Power Quality (Chapter 1);
- new interaction between distribution and transmission networks;
- DG interface protection settings revision to be in accordance with the Fault Ride Through requirements (Chapter 3).

The first phenomenon consists in nuisance network protection relays tripping in case of fault, and is due to the fact that the presence of DG can cause reversal power flow along the power lines[44]. The classic distribution networks protection system has been realized in the hypothesis of radial and passive distribution network, i.e. without generating units present or, if any, without any significant power level. An high level of DG penetration could cause problems with the selectivity causing nuisance tripping and therefore lead the need of a protection system revision. In particular, this issue is

[43] In some cases MV network with substantial DG presence this time has been brought to 0.6 s ÷ 0.8 s.

[44] In a radial passive network distribution the power flows from primary substation to the loads and to the secondary cabins along the line.

relevant for the over- current protection relays placed at the MV lines departures. In fact, these protections are not able to distinguish the measured current direction: the protections selectivity is obtained by adjusting the starting time as a function of the setting current values. If there are DG units near faulty lines, these can fed the fault, with reference to Figure 7-3. The contribution to the fault current from the local generation, if the protection setting value I_1 is exceeded, could cause the nuisance protection relay trip with consequent disconnection of the healthy line. This problem is more critical in presence of DG with rotating machines (synchronous/asynchronous), which can give an important contribution to the short circuit current. The case is different for DG interfaced to the network by electronic converters, whose contribution to short circuit current is limited, and it may cause problems only if the power of the plant is relevant.

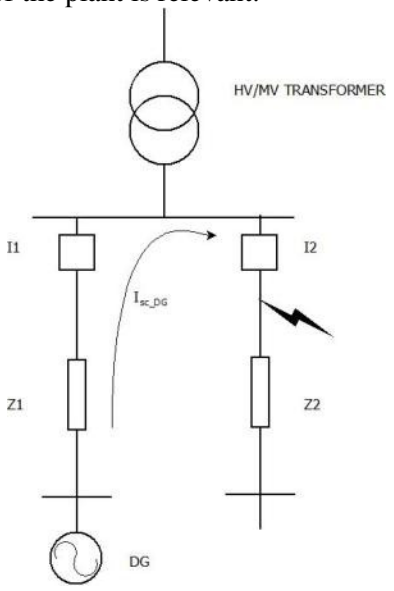

Figure 7-3: Nuisance MV lines maximum current protections tripping in presence of DG

The second possible phenomenon due to DG presence in the network is that these local generators can sustain voltage in a feeder disconnected from the main grid (f.i. for maintenance or after a fault) giving rise to an island network condition, if there is an equivalence between the active and reactive powers produced by generators and those absorbed from the loads. Unwanted island, whose voltage and frequency are not under the control of the main grid, could, in fact, represent a major harm for loads and people (§ 7.7.5).

The last issue linked to the massive presence of DG comes from the interactions between the HV transmission and MV distribution network. In particular, the transmission network frequency may vary for the occurrence of an unbalance between generation and loads: for example, if the power absorbed by the loads is greater than that delivered to the network by the generators, the network frequency decreases involving all the voltage levels (HV, MV and LV). If the frequency falls under the DG Interface Protection (IP) tripping threshold (§ 7.5.1 and 7.5.2), the generation would see a further power reduction due to the DG disconnection. This phenomenon would further affect the network frequency decreasing making necessary measures such as the loads disconnection. The opportunity to extend the IP settings for the frequency range could decrease the risk of such event, the importance is to maintain the protection relays themselves selective to avoid undesired island network operation.

Then, considering the new Fault Ride Through (FRT) requirements (Chapter 3), it's necessary a redefinition of the interface protections settings also in terms of voltage thresholds. Figure 7-4b, for example, shows the simulation results of the DG inverter behavior, equipped with an IP with default settings[45], in case of a three phase voltage dip with residual voltage equal to 45% V_N and duration 120

[45] In this case the settings are not redefined to ensure the voltage dips overcoming according to the CEI 0-16 ed. 2012.

ms. Even if the inverter is controlled with a FRT strategies (supply null active power during the event) and it's equipped with all the necessary devices (§ 3.2), the interface protection trips[46] and the relative circuit breaker opens, so the DG is disconnected from the network preventing the new Standard requirements fulfillment.

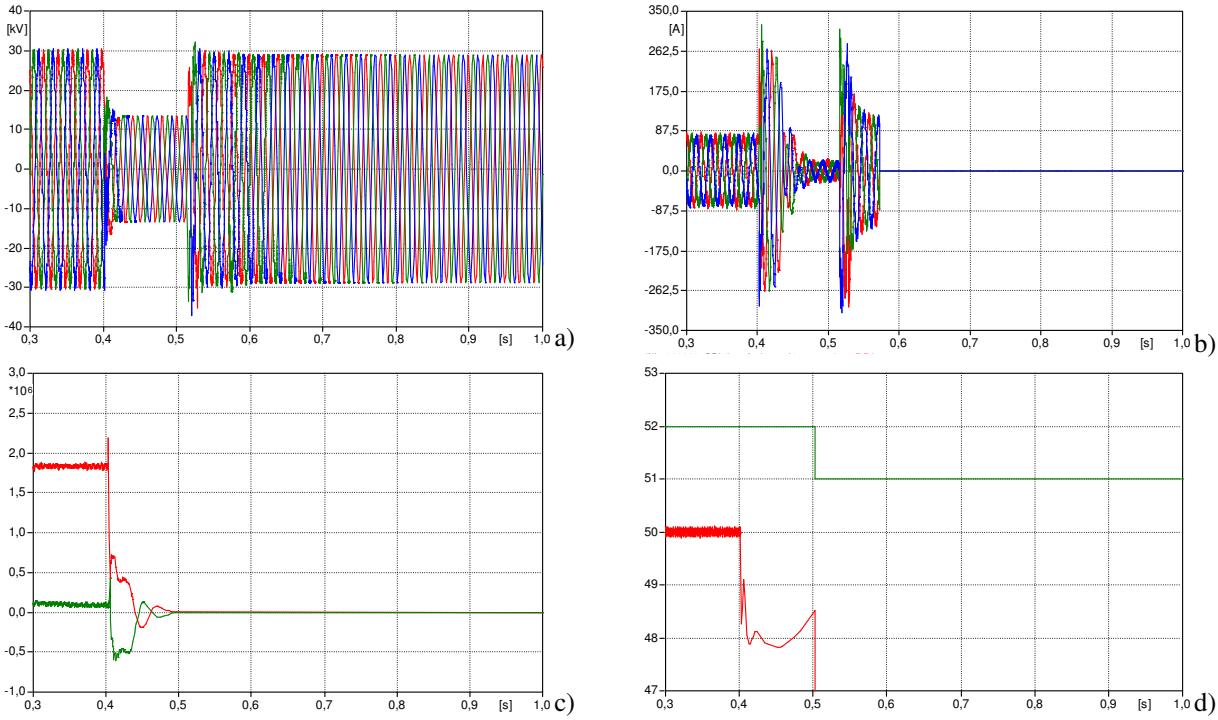

Figure 7-4: Simulation of the inverter response with "standard" IP settings: a) line to line voltages at the connection point (b) inverter current MV side, active (red) and reactive (green) power, (d) frequency measured by the IP relay (red) and tripping signal (green)

The problems described, in a scenario of gradual increase of the DG connected to distribution network, therefore leads to consider new settings for the relays and new protection schemes for active networks that include, for example, protection along the line able to communicate among them to coordinate the operations and the circuit breakers opening (logic selectivity). In this regard in § 7.8 a proposal for a protection network coordination based on logic selectivity will be presented.

7.5 Italian Standards: brief description

Relatively to the Italian system, the Standards that define the technical rules for the generators connection to the network are:

- CEI 0-16, "Regola tecnica di riferimento per la connessione di Utenti attivi e passivi alle reti AT e MT delle imprese distributrici di energia elettrica", Ed. 3, V1, December 2013, Italian language;
- CEI 0-21, " Regola tecnica di riferimento per la connessione di Utenti attivi e passivi alle reti BT delle imprese distributrici di energia elettrica ", Ed. 2, V2, December 2013, Italian language.

In these documents it's indicated the general active user plant configuration connected to the network, characterized by the following components according to the diagram of Figure 7-5:

[46] In particular, in this case the relay minimum frequency trips at first, then also the minimum voltage relay trips in accordance with the time delay setting, presented in Table 7-1.

- *General device*: protection, maneuvering and disconnection device which opening is controlled by a dedicated protection relay system that ensures the user line separation from the rest of the network;
- *Interface Protection (IP)*: one or more switching equipment whose opening (controlled by a special protection system) ensures the separation of the facility from the network, allowing island operation for privileged loads;
- *Generator protection*: it has the purpose to disconnect an active user from the network in case of a fault within its system. In particular the tripping thresholds must be selective with those of the interface protection to avoid early generators disconnection with respect to the active plant separation from the network.

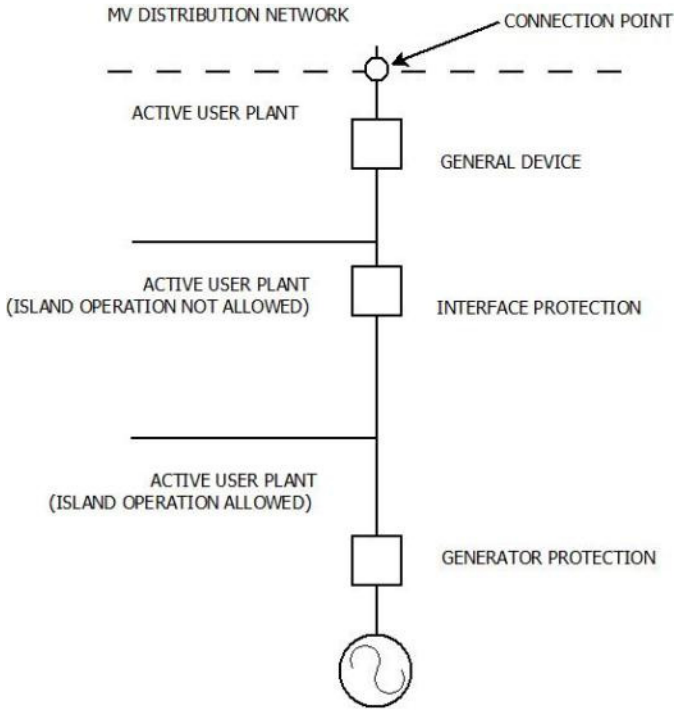

Figure 7-5: General configuration of the active user plant

Below, the main Interface Protection characteristics will be described.

7.5.1 Interface Protection for generators connected to MV and HV networks

The main function of the Interface Protection System is to disconnect the DG if network voltage and/or frequency are out of the thresholds, in order to avoid unwanted islands operation. The CEI 0-16 requires that the interface protection is made by:

- over/under frequency relay with two thresholds: wide band and narrow band;
- over/under voltage relay with two thresholds.

If the distributed generator is connected to the MV distribution network, Table 7-1 shows the interface protections settings as defined in CEI 0-16.

Table 7-1: IP settings in MV network

Protection	Abbreviation	Threshold	Intentional Delay
Maximum voltage (10 min)	59.S1	1.1 V_N	3 s
Maximum voltage	59.S2	1.15 V_N	0.2 s
Minimum voltage	27.S1	0.85 V_N	0.4 s
Minimum voltage	27.S2	0.4 V_N	0.2 s
Maximum frequency	81 > .S1	50.3 Hz	0.1 s
Maximum frequency	81 > .S2	51.5 Hz	0.1 s ÷5 s
Minimum frequency	81 < .S1	49.7 Hz	0.1 s
Minimum frequency	81 < .S2	47.5 Hz	0.1 s ÷5 s÷

Over/under frequency relay with two thresholds

As seen in Table 7-1, for the frequency relays, two intervals of intervention are required, in accordance with Annex A70 of the Terna Grid Code[47]. The wider range (S2) represents the standard setting while the activation of the narrow threshold (S1) occurs in case of a fault in MV network.

The need to distinguish a frequency variation caused by a phenomenon occurred in the HV network due to a fault in the distribution network where the DG is installed, derives from the opportunity, for events with origin in HV network, to maintain the distributed generators connected. In this way it's avoided a "sudden" reduction of the power generated in the network, that causes a further system frequency variation with the consequent possibility of making impossible to recovery the frequency by the dedicated systems for this purpose (for example by the programmed load disconnection).

On the other hand, in case of event with origin in MV the activation of the narrow thresholds allows a more rapid detection of fault conditions in order to prevent unwanted islands operation, favoring the DG disconnection. To achieve these target, the Standards prescribe that the interface protection could be tripped also through an external signal (remote control).

Over/under voltage relay with two thresholds

An important aspect to consider during the definition of the interface protection settings, in particular with regard to the minimum voltage relay, is the Fault Ride Through requirement (FRT) presented in Chapter 3. In fact, the DG has to be able to overcome, without disconnection, voltage dips with residual voltages even lower than 0.8 p.u. and durations greater than 200 ms; apparently these data aren't in accordance with the settings of the interface protection relay as can be seen graphically in Figure 7-6. In this context, it should be noted that the FRT Standard requires that the device has to be able to remain connected to the network in given conditions, even if the protections settings don't allow it.

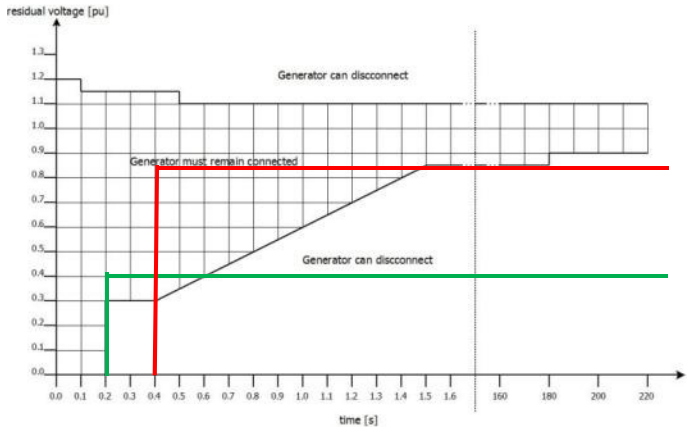

Figure 7-6: Overlap between the FRT curve and IP voltage relay intervention lines (red curve threshold S1 and green curve threshold S2 of Table 7-1)

7.5.2 Interface Protection for generators connected to LV networks

Relatively to the connection of static generators to LV network, the Standard CEI 0-21 provides the possibility that the interface protection is integrated in the inverter control for plants up to 6 kVA; vice versa, for power plants greater than or equal to 6 kVA the interface protection is expected to be realized by a dedicated device, external to the inverter. This Standard indicates as mandatory the following relays:

- over/under voltage;
- over/under frequency.

[47] A. A. V. V., "Codice di trasmissione, dispacciamento, sviluppo e sicurezza della rete", available on the web site: http://www.terna.it/, Italian language.

In addition, it must be provided the possibility to trip the interface device by an external signal, coming from the network controller or by other protection relays. The settings and tripping time of the interface protections are summarized in Table 7-2.

Table 7-2: IP settings in LV network

Protection	Abbreviation	Threshold	Intentional Delay
Maximum voltage (10 min)	59.S1	1.1 V_N	3 s
Maximum voltage	59.S2	1.15 V_N	0.2 s
Minimum voltage**	27.S1	0.85 V_N	0.4 s
Minimum voltage***	27.S1	0.4 V_N	0.2 s
Maximum frequency*◊	81 > .S1	50.5 Hz	0.1 s
Maximum frequency◊	81 > .S2	51.5 Hz	0.1 s ÷5 s
Minimum frequency*◊	81 < .S1	49.5 Hz	0.1 s
Minimum frequency◊	81 < .S2	47.5 Hz	0.1 s ÷ 5 s

Notes:
* Enabled threshold in the absence of communication;

** In the case of traditional generators, the value specified for the tripping time must be adopted when the overall power is greater than 6 kW, while for less powers, optionally, an intervention time without intentional delay can be used;

*** Threshold compulsory only for static generators with total installed power more than 6 kW;

◊For voltage values below 0.2 V_N, the maximum/minimum frequency protection must be inhibited.

7.6 Simulation Models

In order to investigate possible coordination strategies for network protection, the MV distribution network model in ATPDraw, shown in the previous Chapters, has been upgraded enriched with the models of some protection relays and of the relevant instrument transformers (Voltage Transformers or VTs and Current Transformers or CTs). For these instrument transformers, the saturation phenomena that have an impact on the behavior of protection relays during fault conditions have been modeled.

Below are presented in detail the characteristics of the instrument transformers and the relevant models that have been implemented; moreover, the results of the fault simulations are shown.

7.6.1 The instrument transformers

Usually the protection relays in use in the AC electricity networks are not directly supplied from voltages and currents of the primary system but from signals having magnitudes proportional to the primary ones, by means of current and voltage transformers. For the detection of zero sequence current is often used a toroidal CT that embraces the three phases of the system.
Each of these components complies with the requirements of the relevant Standards[48]; moreover, the revision of CEI 0-16 requires the verification of the characteristics of each single component, in order

[48] The current transformers to step and zero sequence must conform to the following Standards of product:
- CEI EN 60044-1: Instrument Transformers, Part 1:Current Transformers, valid until 2015-10-23 and substituted by CEI EN 61869-2:2012;
- CEI EN 60044-6: Instrument Transformers, Part 6: Requirements for protective current transformers for transient performance;
- CEI EN 60044-8: Instrument Transformers, Part 8: Electronic current transformers.

to ensure the functionality of the system protection as a whole. The specification of the characteristics and the test procedure, if any, are considered as compulsory, due to the significant need of reliability and intervention speed of the protection system.

In the following, inductive instrument transformers have been modeled with ratings and behavior typical of those used in MV distribution networks, and considered in CEI 0-16. In addition, the transformer models include the saturation phenomena, due to their impact on the measures provided by protection under fault conditions. Below the procedures used for the characterization of the transducers are detailed.

Current instrument transformers
The Current Transformer (CT) characteristics are:

- rated transformation ratio: 300/5
- accuracy class: 5P
- accuracy limit factor: 30
- rated burden: 10 VA[49]

Figure 7-7 shows the CT circuit diagram for the model implemented in ATPDraw: the magnetic core saturation is represented by a non-linear inductor connected to the secondary of the transformer. Here a resistive load equal to the rated burden for the measurement of the rms value of the current is also connected (this measure is assessed over a period of 20 ms and is updated every 10 ms[50]).

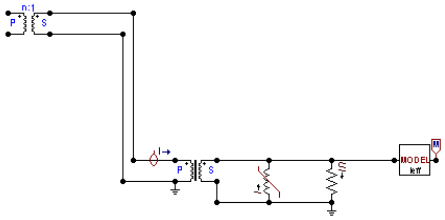

Figure 7-7: Current transformer scheme

The magnetization curve of the CT, shown in Figure 7-8, is specified for pairs of peak values of current and flux of the magnetic field, both in p.u. and in actual values, and is calculated as follows:

- the RMS voltage is calculated as the ratio of the rated burden of the CT to the rated secondary current: $V_{rms} = \frac{10VA}{5A} = 2V$;

The VT must conform to the following Standards of product:

- CEI EN 60044-2: Instrument Transformers, Part 2: Inductive voltage transformers, valid until 2014-08-17 and substituted by Norma CEI EN 61869-3.
- CEI EN 60044-5: Instrument Transformers, Part 5: Capacitive voltage transformers, valid until 2014-08-17 and substituted by CEI EN 61869-5.
- CEI EN 60044-7: Instrument Transformers, Part 7: Electronic voltage transformers.

It must be noted that CEI EN 61869-2, -3 and -5 have to be read jointly with CEI EN 61869-1 which gives the general requirements for the whole product family.

[49] From the ratings it is possible to calculate the resistance (R_N) that represents the rated burden through the relations: $V_N=A_N/I_N=10$ VA/5 A=2 V; $R_N=V_N/I_N=2$ V/ 5A=0.4 Ω. This resistance is represented in the model.

[50] The sampling period of the measuring instrument is 1 ms.

- the saturation knee point is linked to the voltage peak value $V_{pk} = \sqrt{2}V_{rms}$, and the flux value is therefore calculated as $\phi = \frac{V_{pk} * accuracyfactor}{2\pi f} = \frac{\sqrt{2} * 2 * 30}{2\pi * 50} = 0{,}26Wb$ (Point A in Figure 7-8b);
- to calculate the current value at which saturation knee point occurs it's used the composite error (5P) which is due to the current flowing in the saturation branch: $I = \frac{error}{100} I_{\sec} = \frac{5}{100} * 5 = 0{,}25A$ (Point A in Figure 7-8b);
- to find the curve slope after the saturation knee, a ratio equal to 1/1000 in relation to the slope of the linear segment is assumed; moreover, also the air and the iron permeabilities are taken into account.

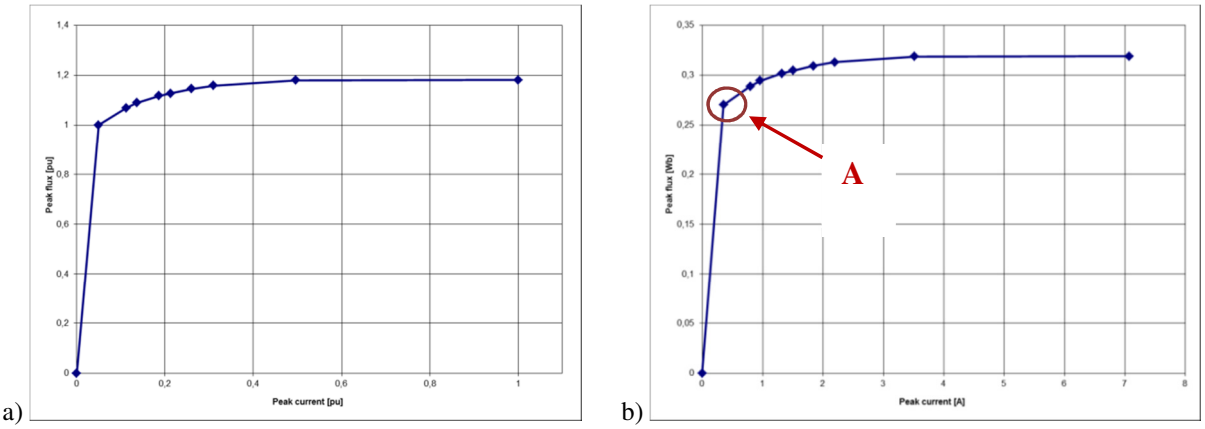

Figure 7-8: Line current transformer characteristic curve: a) currents and peak flux expressed in p.u., b) expressed in Weber and Ampere

In order to ensure an "homogeneous" response of the transformers installed in different plants, the CEI 0-16 standard prescribes a series of tests for the transducers, to verify their suitability for application in protection systems and to characterize their behavior. In a preliminary stage, some simulations in accordance with the Standard have been performed[51] in order to verify the conformity of the implemented model to a typical CT protection. Such simulations are also aimed at pointing out the situations where the saturation of the transformer has visible effects on the current measurement and, in this case, which is the behavior of the CT.
By following the CEI 0-16, the CT behavior has been verified, by supplying the primary terminals with a sinusoidal current at power frequency, having an amplitude equal to the rated current of the device:

$$i(t) = 300 \cdot \sqrt{2} \cdot \sin(2\pi 50t) \tag{7.1}$$

The results of the simulation are shown in Figure 7-9: the device is not affected by any saturation phenomenon and it measures correctly the RMS value of the secondary current.

[51] In fact, the Standard specifies what should be the behavior of the whole protection system, composed by protection relay and transformer, when the last one works in saturation conditions. In this case, the Standard requires that the protection recognizes the fault and trips within a limited time interval, according to given amplitudes of the measured current.

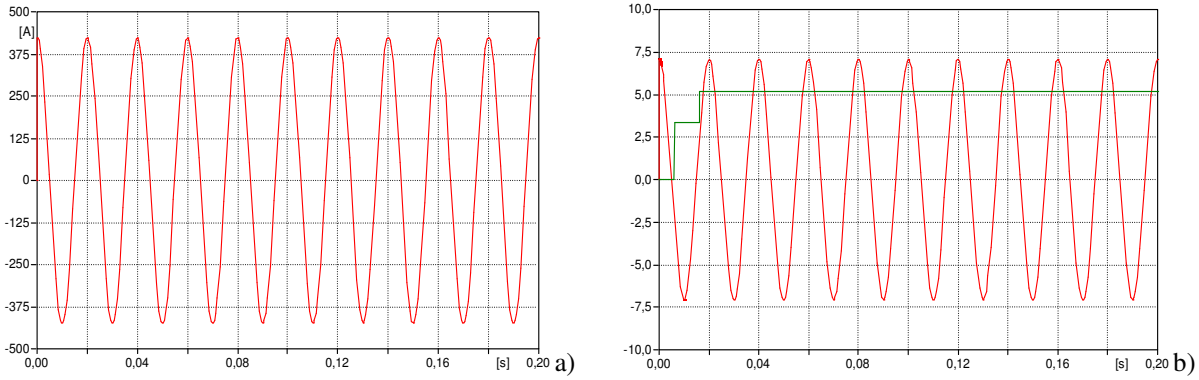

Figure 7-9: CT stationary test simulation results (a) primary current, (b) secondary current and its RMS value

Subsequently, the transformer behaviour is simulated in response to a power frequency current signal affected by unidirectional components (Figure 7-10):

$$i(t) = 600 \cdot \sqrt{2} e^{-50t} + 600 \cdot \sqrt{2} \sin(2\pi 50 t) \tag{7.2}$$

Despite the presence in the current of an unidirectional component having non-negligible width, the CT is not affected by saturation phenomena, as shown in Figure 7-11.

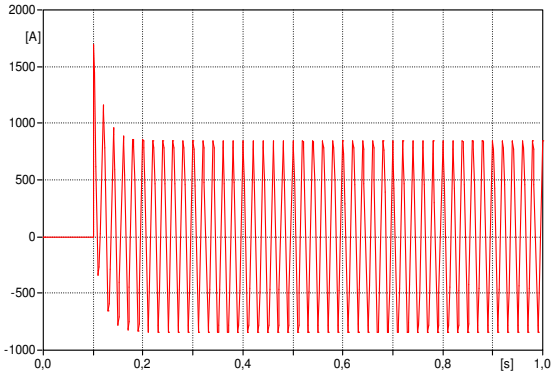

Figure 7-10: Current signal with unidirectional component for test of the CT

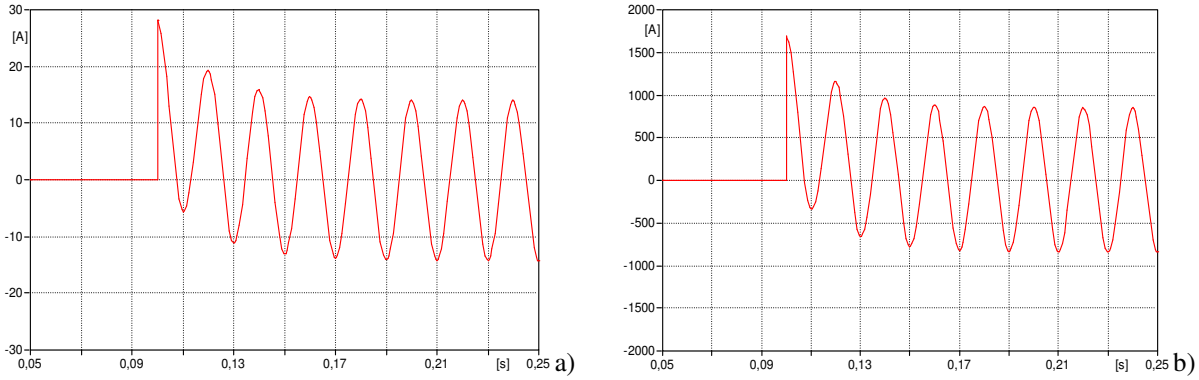

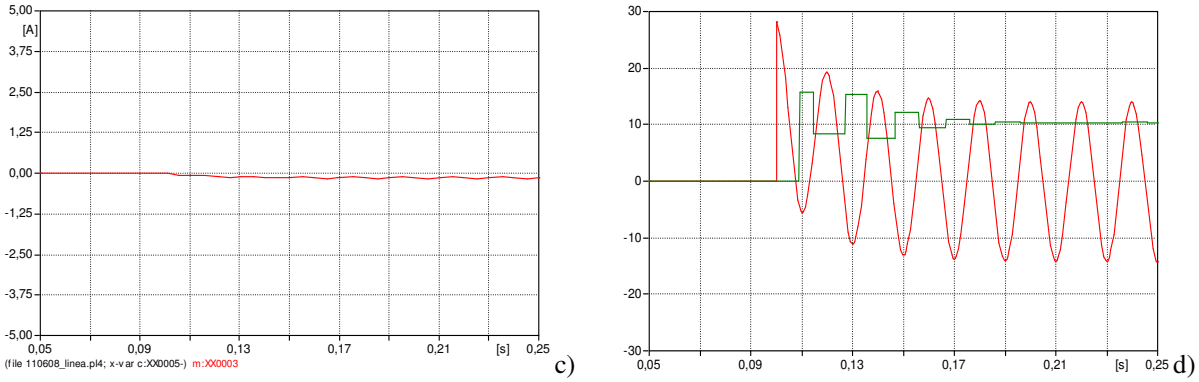

Figure 7-11: Line CT simulation test results a) secondary current, (b) primary current, (c) CT magnetizing current, (d) secondary current RMS value

Another test required by CEI 0-16 is performed in order to verify the transformer behavior in the event of a solid three phase to ground short circuit of duration 400 ms that occurs in the feeder where the CT is connected. For the simulation, a simplified network model composed by an equivalent prevalent HV network (150 kV) and a 40 MVA primary substation transformer 150 kV/20 kV with v_{cc}= 16% has been used. From the MV bus-bar a single feeder is provided having length 1 km; the short circuit has been simulated at the end of that feeder (Figure 7-12). The CT has been connected at the beginning of the feeder. Figure 7-13 shows the simulation results.

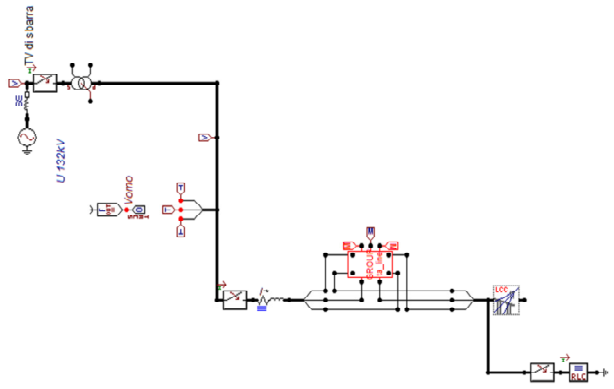

Figure 7-12: Network simplified model to verify CT

The simulation results show that the CT saturation causes a distortion of the secondary currents and this causes a time delay of the instant when the RMS meter measures the achievement of the steady-state values. Nevertheless, if the transducer is used just to measure the thresholds current, the presence of at least one phase correctly measured allows a quick enough measurement of the short-circuit current. Once the short circuit is terminated, the CT current value measured should return to zero because the line is in no-load conditions: nevertheless, the simulations show a different behavior: this is due to the particular implementation of the algorithm for calculating the effective values that is activated by the zero crossing of the voltages read on the load of the CT (§3.4.1). Since the CT current after the fault extinction decreases exponentially without zero crossing, as shown in Figure 7-14, there isn't the right RMS calculation. In this figure, the secondary currents development is due to discharge through the CT load resistance, branch that includes the saturation characteristic.

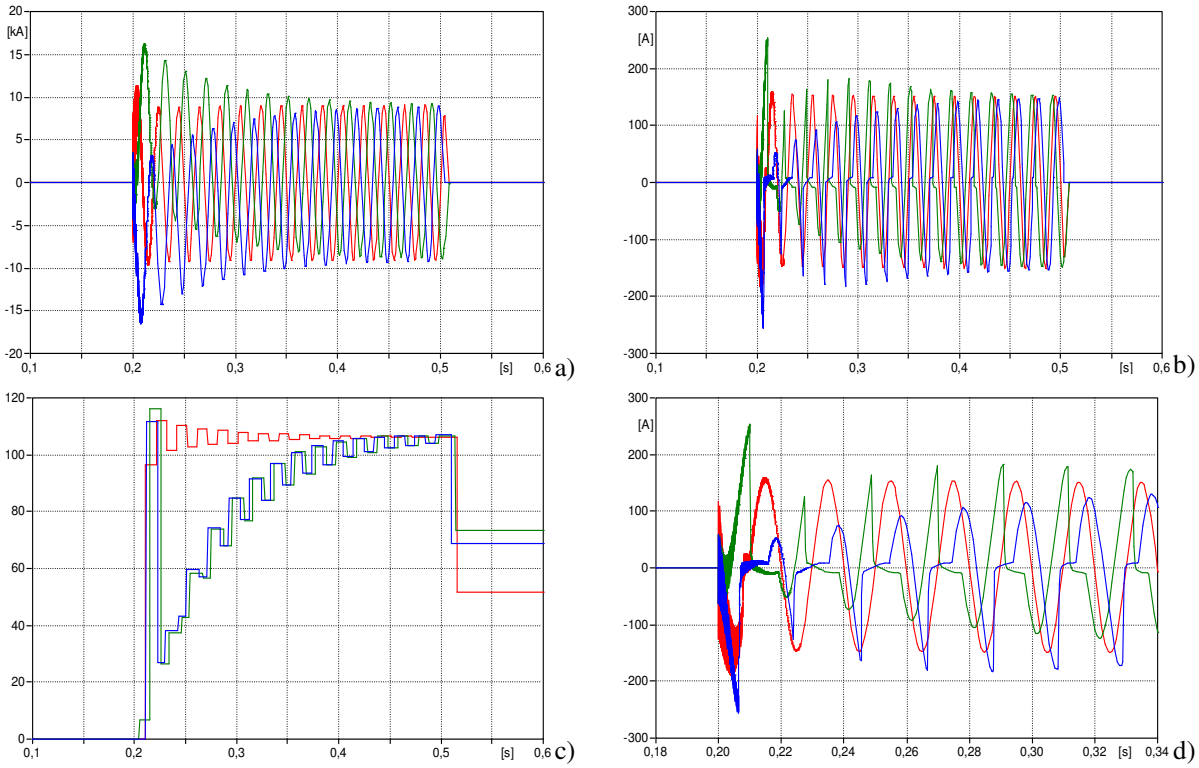

Figure 7-13: CT short circuit test simulation results a) short circuit currents (b) CT secondary current, (c) RMS secondary currents, (d) detail of b)

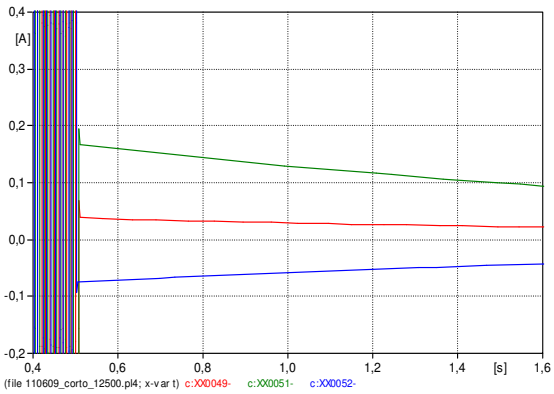

Figure 7-14: CT secondary currents during the fault extinction

Zero sequence current transformer

The electrical model of the zero sequence current transformer[52] is shown in Figure 7-15, where the different parameters have the same meaning as in the line CT model[53].

The implemented model provides three ideal transformers, with unitary transformation ratio, which measure the current on each phase and report them to the secondary circuits connected in parallel giving in this way their sum. A zero sequence current transformer is usually based on a toroidal

[52] In general, it's possible the use of three CT for the measurement of the zero sequence current, however the use as a single toroid simplifies the configuration.

[53] The transformer primary and secondary resistances have negligible values and are inserted in the model only to prevent an error message given back by the simulation program for the direct connection of transformers in parallel.

ferromagnetic core, where the primary circuit is made by the three line conductors inserted through its window. The transformer secondary winding is wound around the toroidal core. In this way (according to Ampere's law[54]) the magnetic field flux produced by the single line currents that pass through the toroid, induces a secondary current proportional to the sum of the primary currents.
In the simulations the sum of the currents is performed by three ideal transformers and then transferred to the secondary circuit by a saturable transformer. These two methods are equivalent and give the same results.

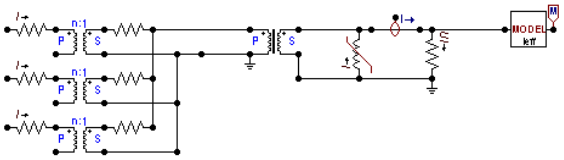

Figure 7-15: Electrical model of the zero sequence transducer

The following ratings of the toroidal CT are identified in Annex C of the CEI 0-16 Standard as those that automatically make suitable these devices for the protection system application:

- rated transformation ratio 100/1;
- rated burden 2 VA (corresponding to a 2 Ω load);
- current error equal to 5% for $I/I_n = 20$.

The magnetic field curve flux/current is shown in Figure 7-16 and it has been calculated using the same methods used for the line current transformer.

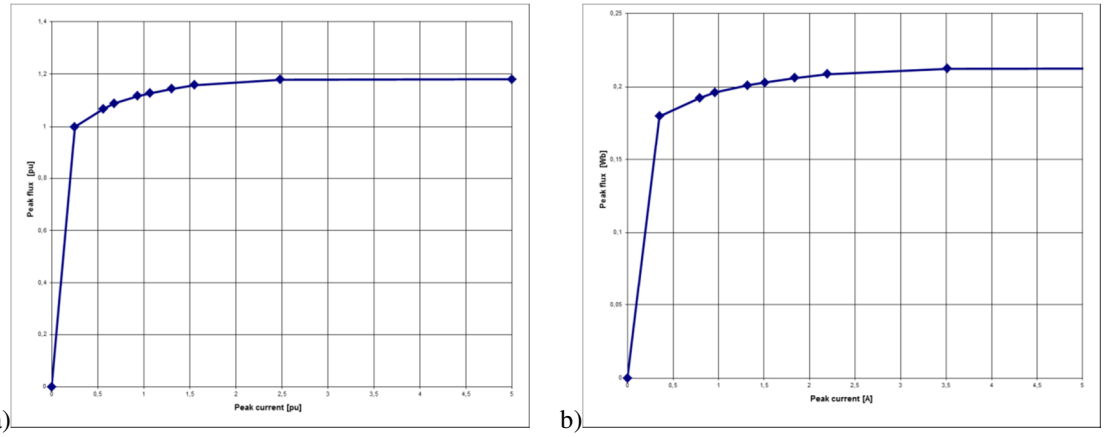

a) b)

Figure 7-16: Zero-sequence current transformer characteristic curve: currents and peak flux expressed in p.u. a), expressed in Weber and Ampere b)

The secondary current given by the toroidal CT is equal to the sum of the three line currents $I_s = I_a + I_b + I_c$, considering the transformation ratio, and is proportional to the zero sequence current.
Also in this case, the transformer operation has been verified by performing a simulation of some tests included in CEI 0-16. Figure 7-17 shows the simulation results without saturation phenomenon, at rated voltage, and, as required by the Standard, at a current equal to:

$$i(t) = 100 \cdot \sqrt{2} \sin(2\pi 50 t) \tag{7.3}$$

[54] The Ampere's law says that the magnetic field B along a closed line C is equal to the sum of the currents that pass through the surface defined within this closed line, multiplied by the vacuum magnetic permeability: $\oint_C \vec{B} \cdot d\vec{s} = \mu_0 \sum I_{conc}$.

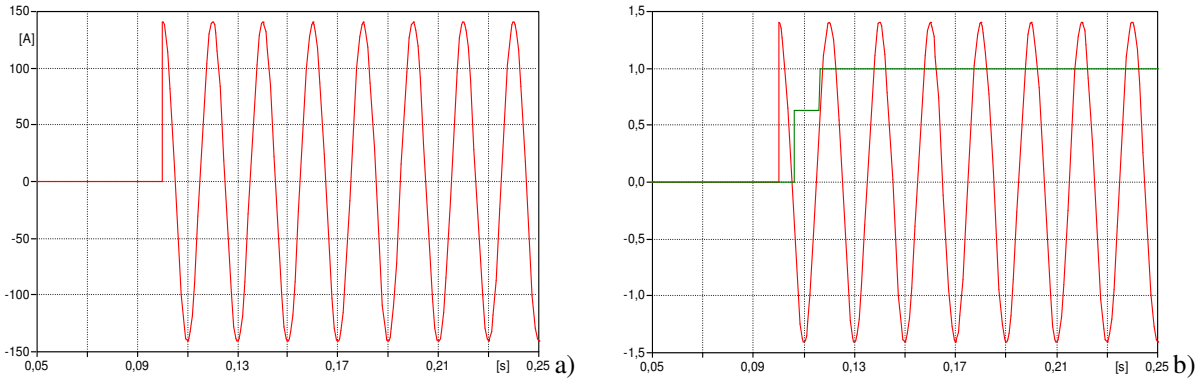

Figure 7-17: Zero-sequence current transformer steady-state test simulation (a) primary current (b) secondary current and its RMS value

In compliance with the Standard, the transducer has also been tested with a current signal characterized by a power frequency component and an unidirectional one, as in (7.2) but with different values:

$$i(t) = 500 \cdot \sqrt{2} e^{-t/0.15} + 50 \cdot \sqrt{2} \sin(2\pi 50 t) \tag{7.4}$$

and the simulation results are shown in Figure 7-18.

In this case, the zero sequence transducer saturation effect is not negligible. Nevertheless, the function of detection of a current exceeding the threshold can be carried out in a time interval compatible with the Standard requirements, that prescribe a maximum tripping time for the directional protection relay equal to 530 ms.

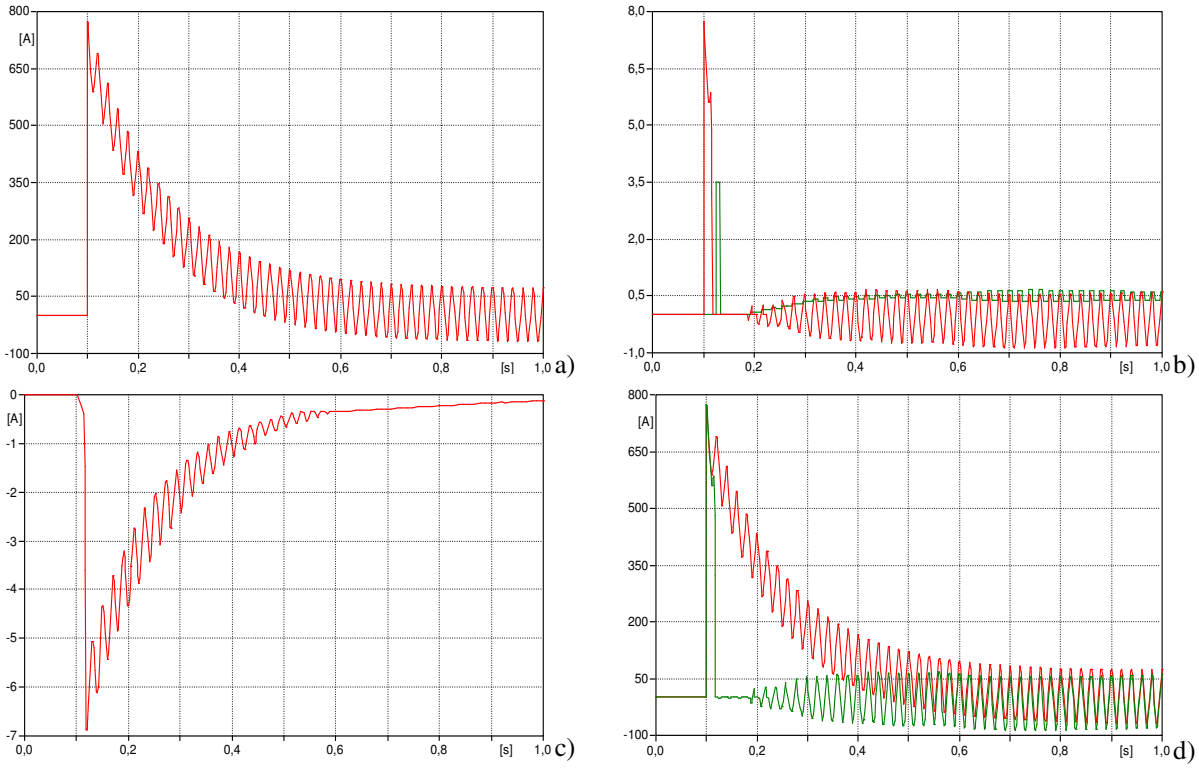

Figure 7-18: Zero sequence current transformer test simulation results (a) test signal, (b) secondary current and its RMS value, c) magnetizing current, d) comparison between test signal and secondary current, reported on the primary current scale

The model has been validated also in the simplified network described above (Figure 7-12), by adding a second feeder and the relevant capacitance to earth, simulating a single phase to ground fault (phase "A"). The test was carried out both for isolated and compensated network (in this last configuration compensation it's assumed 100%). The Petersen coil simulated is shown in Figure 7-20, it consists of a inductance designed in accordance with the network capacitance (in this case of 281.47 mH) with a resistor in parallel of the value of 460 Ω[55] and a resistance to earth of 1.8 Ω[56].

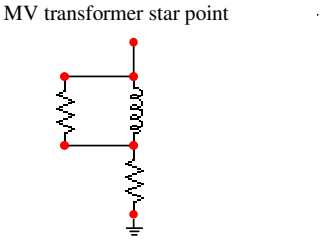

Figure 7-19: Petersen coil scheme modeled in ATPDraw

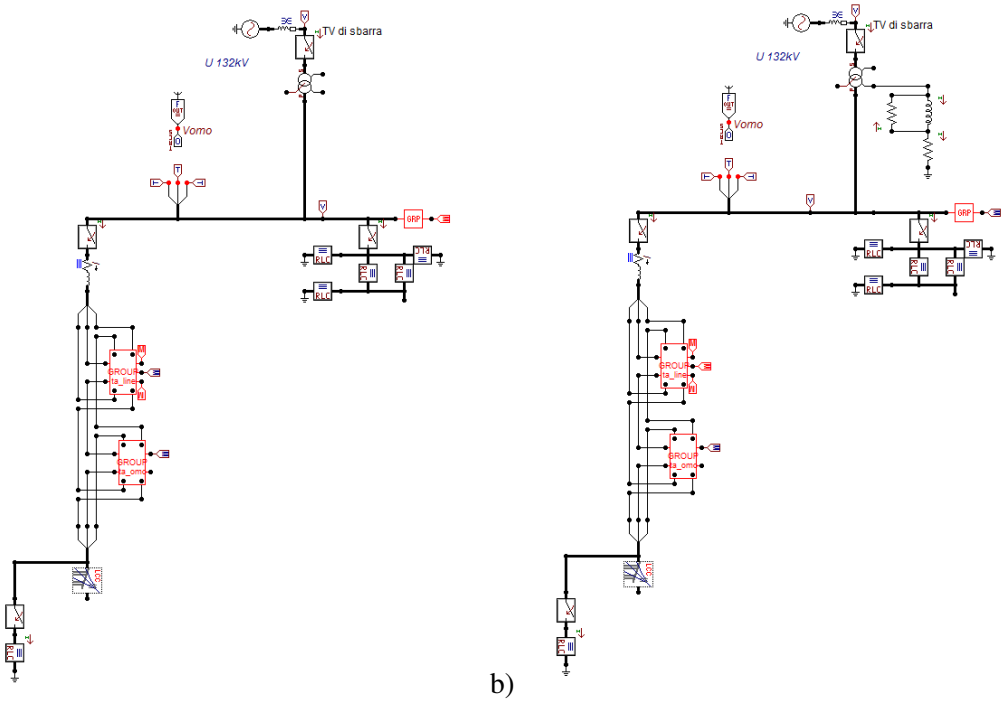

a) b)

Figure 7-20: Simplified network model for zero sequence current transformer verification in case of isolated (a) and compensated network (b)

Figure 7-21 shows the simulation results for the verification of the model of the transducer and Figure 7-22 show the simulation results obtained for compensated network.

[55] This resistance has the task to circulate in the ground circuit a "resistive" component of the fault current to allow the identification of the faulty line by the directional protections. The typical value of this resistance is included between 400 Ω and 500 Ω and complies with to the requirement to have a fault current limited enough to encourage the self-extinguishing of the fault (principle at the base of the compensated system) but with a value able to guarantee the protection selectivity.

[56] The value of this resistor is typically chosen so that the damping of the unidirectional component of the zero sequence current due to the faulty line (when the fault starts) lasts no more than a given time interval (up to 150 ms) to limit saturation phenomenon of the toroidal transformers, allowing the protections operation.

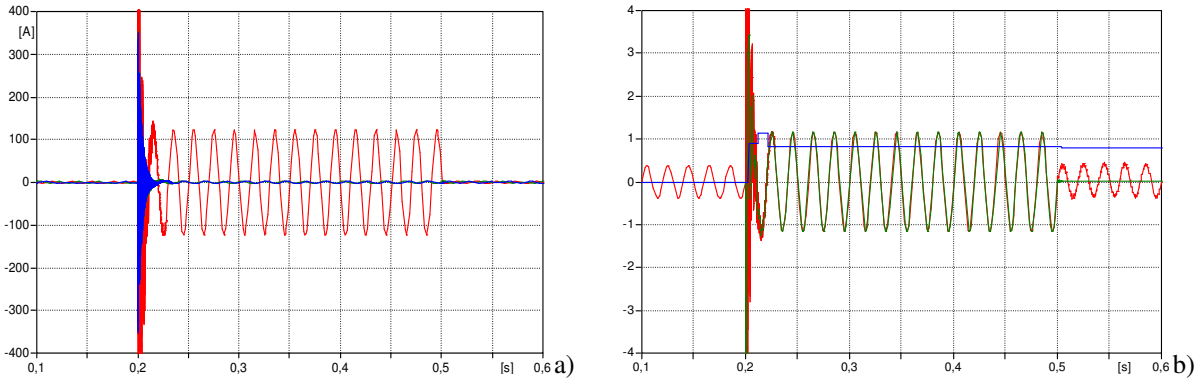

Figure 7-21: Zero sequence current transformer test during single phase fault (a) phase currents of the feeder fault, b) the sum of capacitive currents on the healthy phases compared with the secondary current and its RMS value

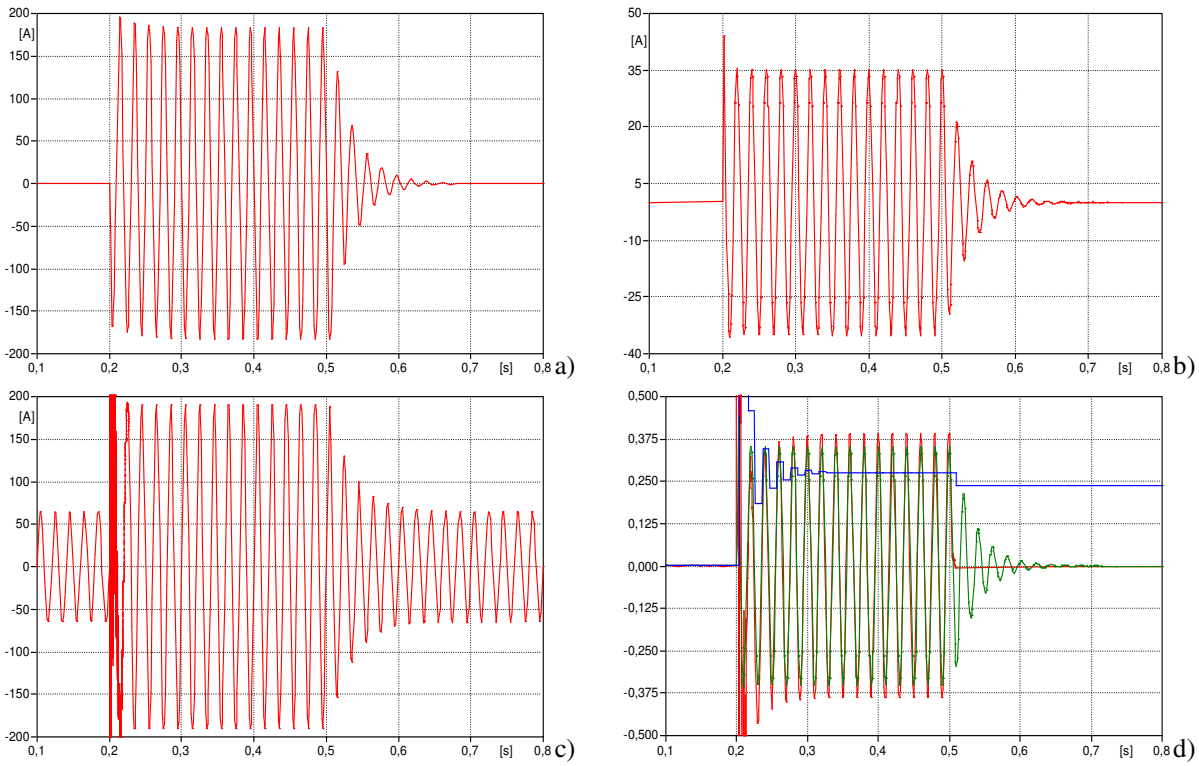

Figure 7-22: Zero sequence current transformer test during single phase fault with compensated network (a) Petersen impedance inductive current, (b) resistive component, c) total capacitive current healthy feeder, d) secondary current and its RMS value compared with the Petersen coil resistive current rescaled by a factor 1/100

Instrument Voltage Transformer (VT)

The Voltage Transformers (VT) electric models are shown in Figure 7-23: VT phase-to-ground connection (a), for the phase voltage measurement, and phase-to-phase (b) for the line to line voltage have been implemented. The main features are respectively reported in Table 7-3 and Table 7-4.

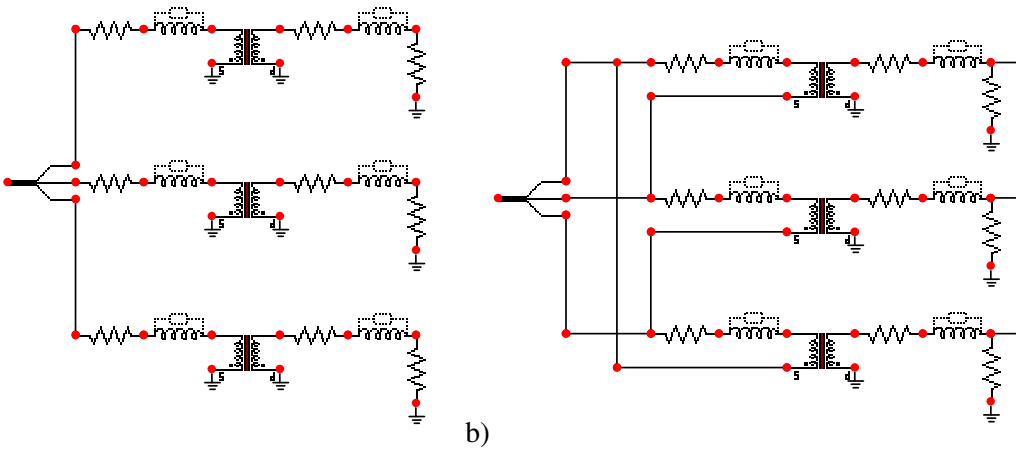

a) b)

Figure 7-23: Circuit diagram for connecting the VT phase-to-ground (a) and phase-to-phase (b)

Table 7-3: VT phase-to-ground main characteristics

Rated burned	50 VA	Magnetization characteristic	
V1n	$\frac{20000}{\sqrt{3}}$ V		
V2n	$\frac{100}{\sqrt{3}}$ V	Imax [A]	$\Phi_{Max\ [}$ Wb]
R1	2667 Ω	0	0
L1	12,758 H	0.297547	0.486011
R2	0.067 Ω	0.408954	0.543189
L2	0.3189 MH	0.554584	0.557483
Rated Load	66.67 Ω	0.878593	0.566060
		1.279403	0.571778
		36.742346	0.580056

Table 7-4: VT phase-to-phase main characteristics

Rated burned	50 VA	Magnetization characteristic	
V1n	20000 V		
V2n	100 V	Imax [A]	$\Phi_{Max\ [}$Wb]
R1	8000 Ω	0	0
L1	38,274 H	0.171685	0.601224
R2	0.2 Ω	0.235966	0.730303
L2	0.9568 MH	0.319995	0.819329
Rated Load	200 Ω	0.506948	0.905267
		0.738215	0.947036
		1.115109	0.990433
		21.213203	1.004507

Since the main problems for the voltage measurement with inductive voltage transformers are essentially linked to the saturation phenomenon, particular attention is paid to this aspect. Different magnetization characteristics are, therefore, considered, with reference to the slope of the various sections (initial segment, linear portion corresponding to the saturation operation) and to the knee voltage values. The transformer behavior has been examined, both supplied with voltages higher than the rated ones or in presence of unidirectional components; these conditions may occur in case of fault. The saturation curves implemented are shown in Figure 7-24 and Figure 7-25.

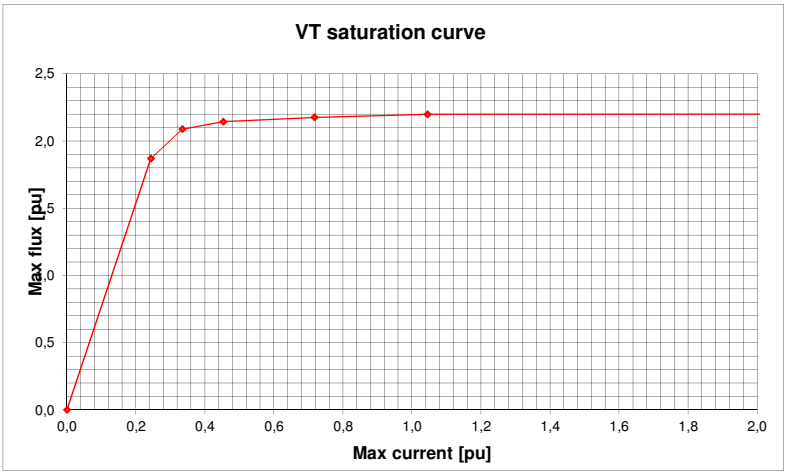

Figure 7-24: VT phase-to-ground characteristic curve: currents and peak flux expressed in p.u.

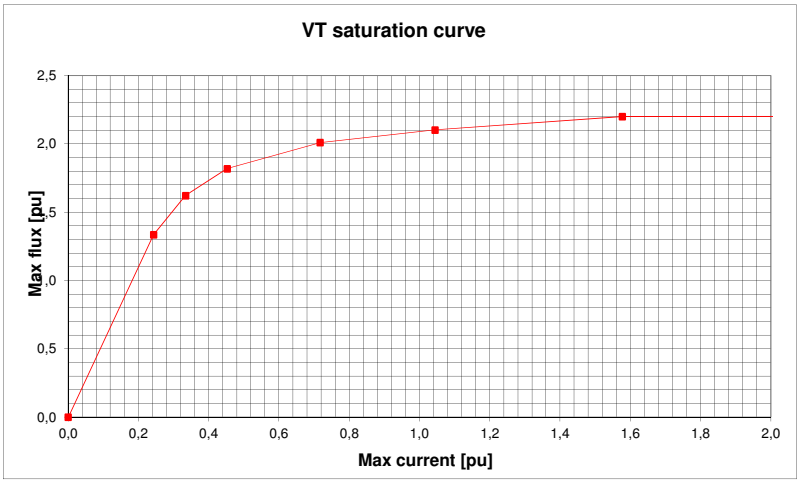

Figure 7-25: VT phase-to-phase characteristic curve: currents and peak flux expressed in p.u.

In the following analysis, the VT phase-to-phase connection for measuring the line to line voltage will be considered, since this magnitude is the input for both the over/under voltage and for the over/under frequency protection relays.

Zero sequence voltage instrument transformer

The scheme of the zero sequence voltage transformer model developed in ATPDraw environment is reported in Figure 7-26. The model includes three single-phase transformers with primary windings phase-to-ground connected and secondary windings open delta connected .

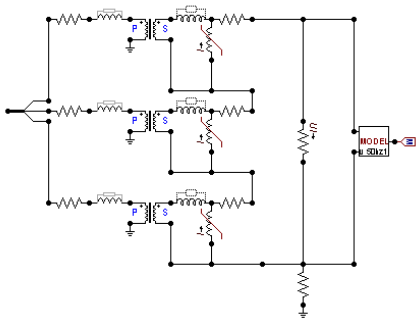

Figure 7-26: Zero sequence VT scheme

The ratings are:

- rated ratio[57] (20000/$\sqrt{3}$) V/(100/3)V;
- accuracy class 0.5 3P .
- rated burden 50 VA;
- rated burden (resistive) 22 Ω;

The circuit elements used have the same meaning as in the models shown above. The RMS meter measures in this case the VT burden voltage drop. The resistance that connects the secondary circuit to earth is included for reasons of simulations convergence; it's a high value resistance (1 GΩ) in which flows a negligible current. The VT magnetic characteristics curves are shown in Figure 7-27.

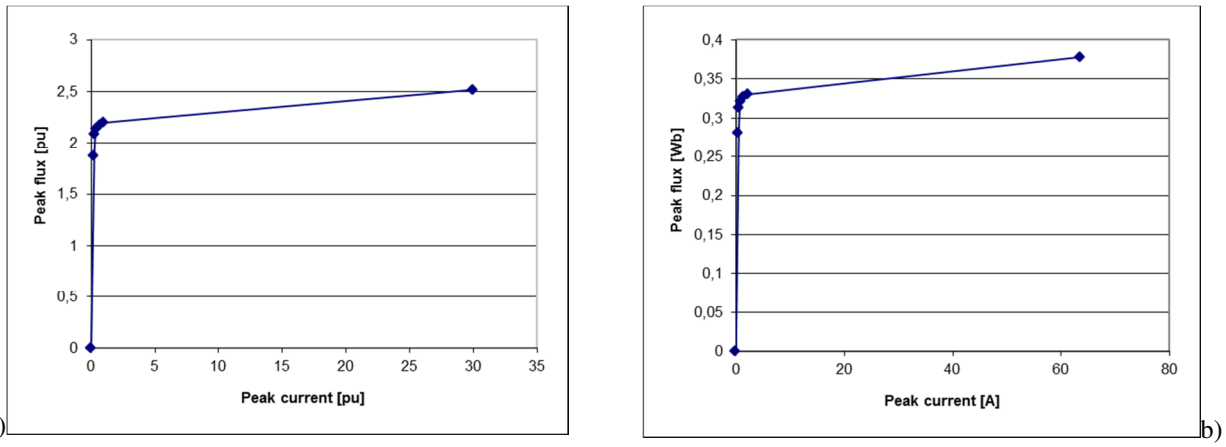

a) b)

Figure 7-27: VT characteristic curves: peak currents and flux expressed in p.u. (a) and expressed in Weber and Ampere (b)

The device has been tested in the both isolated and compensated simplified network previously used; the case of a 400 ms single phase to ground fault has been simulated, according to what is described in CEI 0-16. The results of the two simulations are shown respectively in Figure 7-28 for the isolated network and in Figure 7-29 for the compensated one. The small differences in the zero sequence voltage measurement are due to the different fault current values, influenced by the presence of the Petersen compensation coil. In this case, there aren't saturation phenomena, since the zero sequence VT is designed to operate in the linear range at the voltage value obtained during the fault and allows the right zero sequence voltages identification both in case of isolated and compensated network.

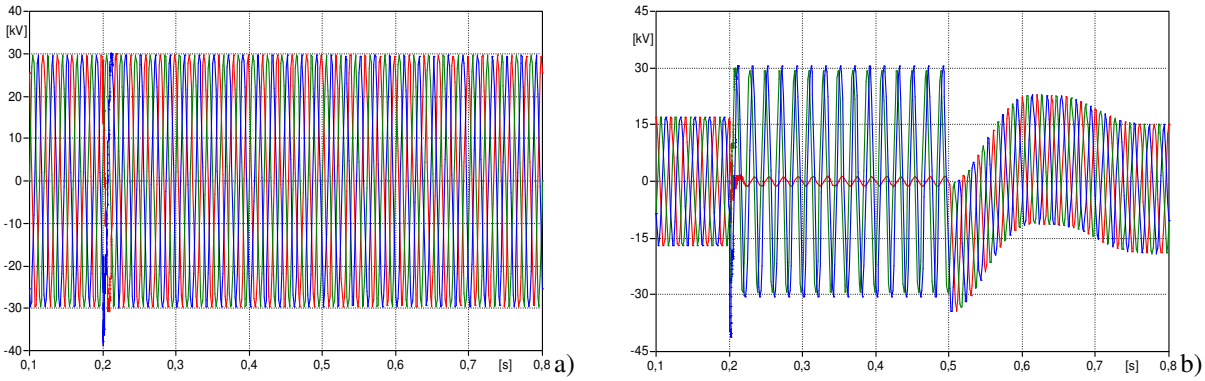

a) b)

[57] Such a relation between the voltages is defined to have in case of a single phase direct to ground fault, the line to line MV voltage measured across the open triangle is equal to 100 V, as required by CEI 0-16.

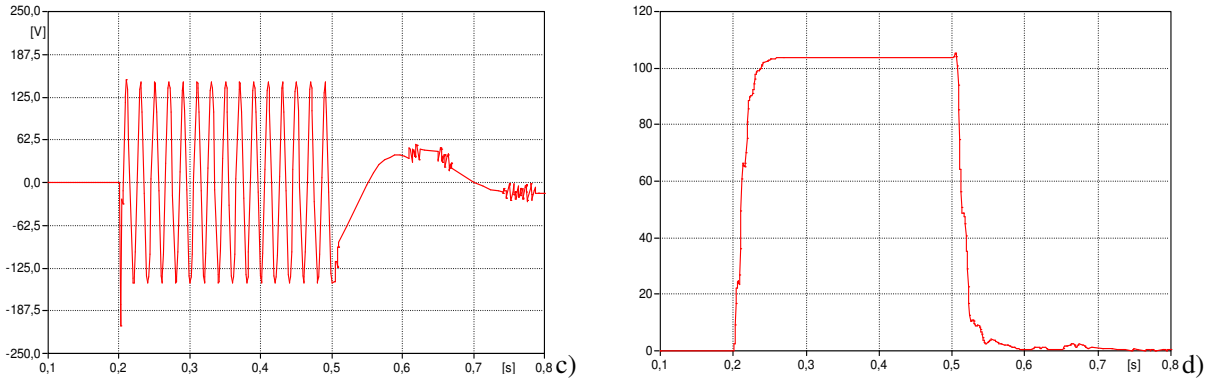

Figure 7-28: Zero sequence VT single phase fault test with isolated network (a) MV bus-bar line to line voltages, (b) MV bus-bar phase voltages, c) zero sequence VT load voltage, (d) RMS value of the zero sequence voltage calculated at the output of the VT

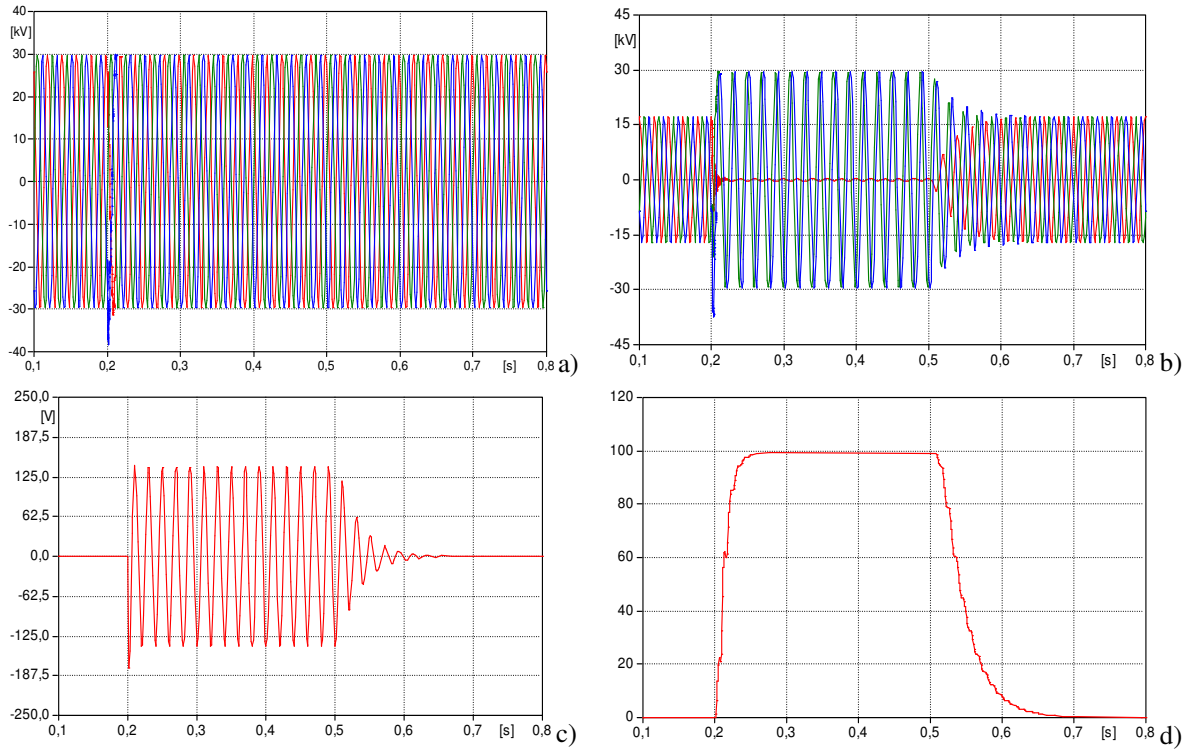

Figure 7-29: Zero sequence VT single phase fault test with compensated network (a) MV bus-bar line to line voltages, (b) MV bus-bar phase voltages, c) zero sequence VT load voltage, (d) RMS value of the zero sequence voltage calculated at the output of the VT

7.6.2 Protection relays: models and settings

Once the transducers have been modeled, the "basic" protection models, described below, have been developed; in the next section (§ 7.7) these devices will be modified with functionalities to allow the logic selectivity protection coordination.

For all the relay models it's provided the automatic reclosing control of the associated circuit breaker, subject to receipt of a logic signal as an input of the *model*[58] that implements the relay itself. This signal is generated by a further functional block, said reclosers, which, received as input the relay output signals, waits a given time before controlling the circuit breaker reclosing. After the reclosing, if the fault has been extinguished, the system resumes its normal operation. If protection is associated

[58] The *model* in ATPDraw is an algorithm that processes, in accordance with the equations written inside, input that can come from the network or from other model thus obtaining the signals/quantities required.

with a distributed generator its automatic restarting has been provided in case of successful reclosing[59]. After the reclosing if the fault isn't extinguished the protection may trip again. The events sequence that occur from the fault occurrence until the first circuit breaker reclosing are shown in Figure 7-30.

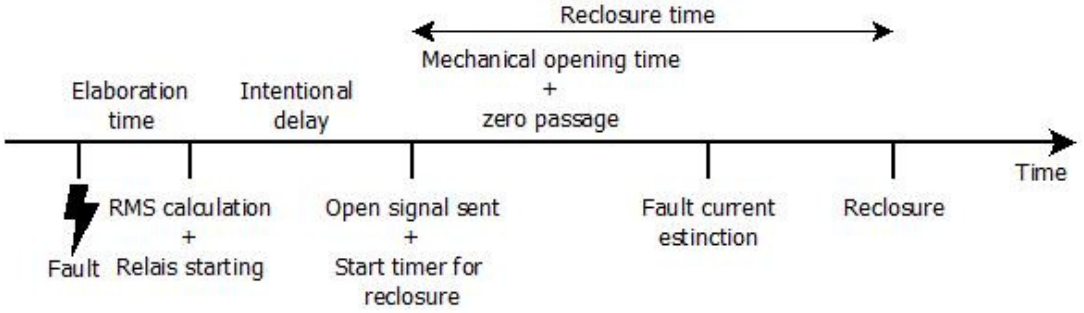

Figure 7-30: Protections intervention events sequence

The modeled protections are:

- over-current (51);
- directional maximum zero sequence current (67N);
- over/under frequency (81);
- over/under voltage (27).

7.6.2.1 Over-current protection relay (51)

This protection has been implemented by an ATPDraw *model* which detects if at least one of the three RMS network current measured by the CT secondary side are upper than the threshold values. The model produces an output signal, after an intentional delay time, dependent on the detected current value, used to control the circuit breaker opening. In the implemented model, it's possible to set the three current threshold values and three intentional intentional delays. The protection is not directional, i.e. it trips regardless the voltage and current phase relationships

The effective circuit breaker opening takes place after a delay of at least 70 ms once the command signal is sent by the relay. This delay is used to model the mechanical circuit breaker opening times, the current through the circuit breaker stops only at its passage to the zero value.

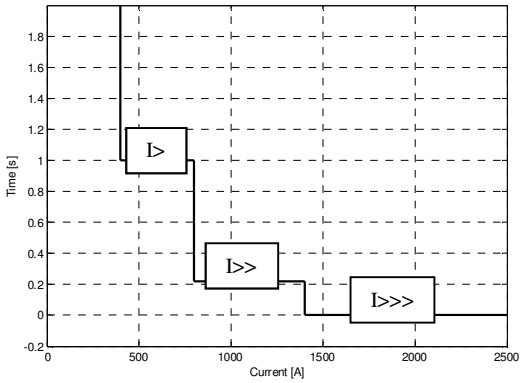

Figure 7-31: Over-current protection settings, with the respective intentional delays

[59] The automatic distributed generators restart is not provided in the models, because not of primary interest for simulations of the protection coordination.

7.6.2.2 Maximum zero sequence directional current protection relay (67N)

In order to detect the ground faults this protection has been implemented so that it's based on the processing (both module and phase) of the magnitudes present due to the earth involvement as a circuit fault current return.

For example, Figure 7-32 shows a schematic representation of compensated network with included the feeders capacitance to earth. The faulty line is highlighted in red, and the "healthy" lines have been combined into a single three phase equivalent line. For simplicity single phase direct to ground fault is considered[60].

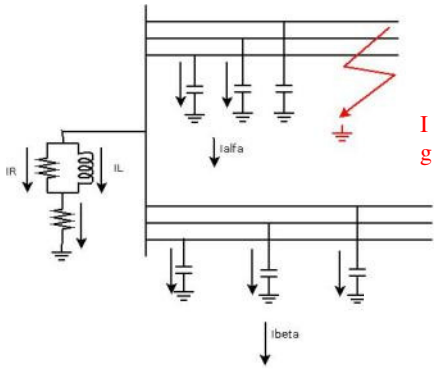

Figure 7-32: Network scheme in case of single phase fault to ground

The vector diagram of the electrical quantities involved is shown in Figure 7-33.

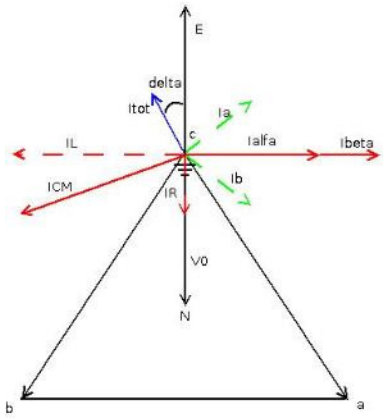

Figure 7-33: Voltages and currents vector representation in case of single phase fault to ground with compensated network

In particular, for the single phase to ground fault the following conditions occur[61]:

- the zero sequence currents measured in the faulty line have, with respect to the zero sequence voltage, a phase difference of:
  - 90° in delay in case of isolated network;
  - a delay angle between 90° and 180°if the network is compensated with a resistance;
  - a delay angle between 90° and 270° in case of compensated network.

[60] The series resistance with the Petersen coil has been neglected since its values is very less compared to the other parameters of the impedance to earth (§ 7.6.1).

[61] For the double single phase fault to ground, the zero sequence current measurable on the two faulty lines are practically in phase opposition between them, regardless the neutral network management and a precise phase relationship does not exist with the zero sequence voltage, it depends more on fault resistance and on the relative cyclic direction of the two faulty phases.

- the zero sequence currents measured in healthy lines are offset by 90° leading with respect to the zero sequence voltage regardless the neutral network management.

Furthermore it's shown that these phase relationships are independent from the fault resistance, since the presence of this resistance determines a zero sequence voltage vector rotation with respect to the reference axis (Figure 7-33) but does not vary the relative phase shifts with the zero sequence current.

From these considerations the concept of directional protections *intervention sector* is defined, i.e. a particular angular relationship between the zero sequence voltage and current phasors, which makes it possible to discriminate the fault location (upstream or downstream) from the measurement point (that is the protection controlled circuit breaker installation point).
Therefore the protection relay measures the zero sequence voltage and the zero sequence current values and evaluates the phase angle[62] between them, considering the zero sequence voltage as a reference. The protection relay starts if the following conditions are met:

- the zero sequence current exceeds a threshold value;
- the zero sequence voltage exceeds a threshold value;
- the angle between them is contained in a given angular sector.

With regard to the setting of the zero sequence voltage and current thresholds, it should be noted that these values are function of the fault resistance and this linear dependence generally is linked to the network design and the network compensation degree.

With regard to the sector of intervention, the phase angle between the zero sequence voltage and current does not depend on the fault impedance but, for a given network, on the following parameters:

- compensation degree (for networks compensated network);
- resistive current component value in the Petersen coil (I_R in Figure 7-33);
- faulty line contribution to the total network capacitance.

The protections settings and the definition of the phase angle (δ) between voltage and current depend on the conventions adopted to define the reference and the measurement positive direction.

Below the fault currents calculation is presented, in case of single phase fault to ground, for compensated and isolated networks, and then definition of the thresholds and of the angular sectors of intervention for the maximum zero sequence current directional protections are defined.

Single phase fault current calculation for compensated networks
The currents sum at the neutral node (Figure 7-33) requires that:

$$\vec{I}_f + \vec{I}_\alpha + \vec{I}_\beta + \vec{I}_L + \vec{I}_R = 0 \tag{7.5}$$

where:

- I_f: fault current;
- I_α: faulty line capacitive current;
- I_β: healthy line capacitive current;
- I_L: Petersen coil current;
- I_R: parallel resistance current.

[62] In the model, this angle is assessed by measuring the time that elapses between the zero-crossing of the voltage in a given direction, and the zero-crossing, in the same direction, of the current.

The healthy line capacitive current is:

$$\vec{I}_{\beta} = \sqrt{3} j\omega C \vec{V}_{ph-ph} = -3 j\omega C \vec{E} \tag{7.6}$$

The Petersen impedance is crossed by the currents:

$$\vec{I}_R = \frac{\vec{V}_0}{R} = -\frac{\vec{E}}{R} \tag{7.7}$$

$$\vec{I}_L = \frac{\vec{V}_0}{X_L} = -\frac{\vec{E}}{j\omega L} = \frac{j\vec{E}}{\omega L} \tag{7.8}$$

The total current measured by zero sequence toroidal CT installed at the start of the faulty line is therefore the sum of the (7.6), (7.7) and (7.8):

$$\vec{I}_{TOT} = \vec{I}_f + \vec{I}_{\alpha} = -(\vec{I}_R + \vec{I}_L + \vec{I}_{\beta}) = -\left(\vec{I}_{CM} + \vec{I}_{\beta}\right) = -\vec{E}\left[\frac{j}{\omega L} + \frac{1}{R} - 3 j\omega C\right] = -\vec{E}\left[\frac{1}{R} + j\left(\frac{-3\omega^2 LC + 1}{\omega L}\right)\right] \tag{7.9}$$

where $(\vec{I}_R + \vec{I}_L) = \vec{I}_{CM}$.

By the expression of the total current (7.9), it's possible to obtain the angle delta:

$$\delta = \angle(\vec{I}_{TOT}) = a\tan\left(-\frac{-3\omega^2 LCR + R}{\omega L}\right) = a\tan\left(-\frac{\vec{I}_L - \Sigma \vec{I}_{0,healthy}}{\vec{I}_R}\right) \tag{7.10}$$

With the 100 % compensation degree, from the expression (7.5) it is possible to define the coil current with the following expression whose value must be equal to that of the fault current that would be obtained without coil:

$$\vec{I}_L = \vec{I}_{\beta} + \vec{I}_{\alpha} \quad \rightarrow X_L = X_C \quad \rightarrow \omega L = \frac{1}{\omega C} \tag{7.11}$$

In case of over-compensated network, the (7.11) becomes:

$$\vec{I}_L > \vec{I}_{\beta} + \vec{I}_{\alpha} \quad \rightarrow \qquad X_L < X_C \tag{7.12}$$

while, if the network is under-compensated this formula can be applied:

$$\vec{I}_L < \vec{I}_{\beta} + \vec{I}_{\alpha} \quad \rightarrow \qquad X_L > X_C \tag{7.13}$$

The vector diagrams that describe the currents behavior in case of over-compensated and under-compensated networks are shown in Figure 7-34.

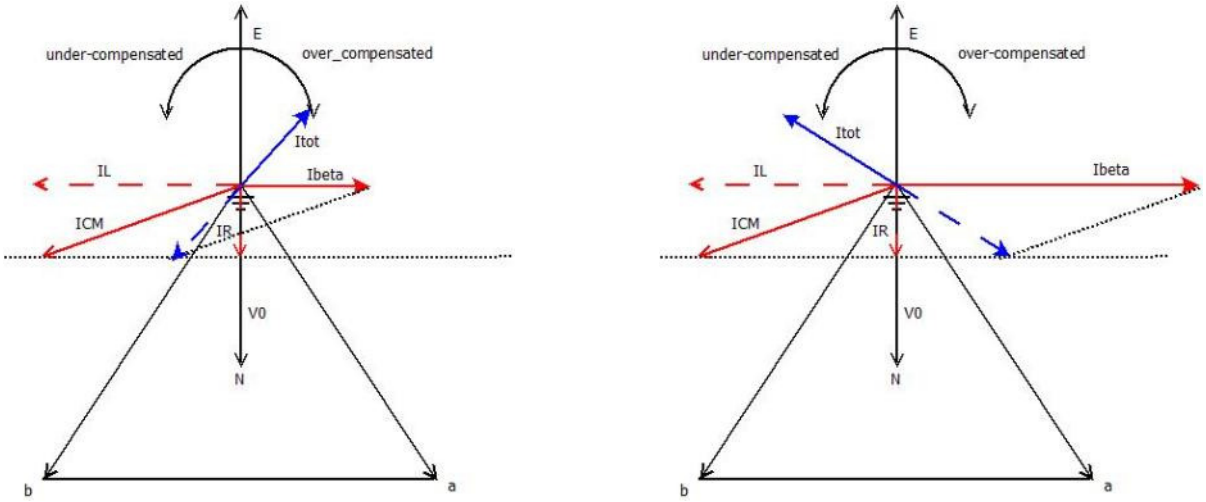

Figure 7-34: Fault currents dependence on the neutral compensation degree

Single phase fault current calculation for isolated networks

In this case there aren't the components I_L and I_R of the fault current, as shown in Figure 7-35, so the total fault current (I_{tot}) has a value greater than in case of compensated network, considering the same network capacitive parameters, and is always "orthogonal" with respect to the mains voltage.

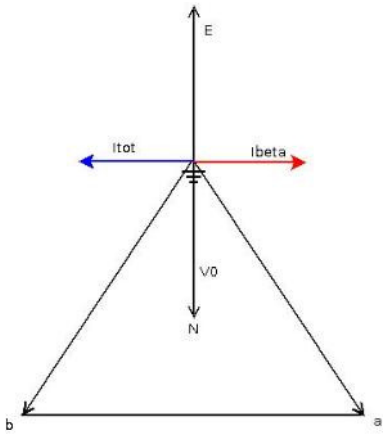

Figure 7-35: Voltages and currents phasor representation in case of single phase fault to ground with isolated network

Zero sequence sector of intervention definition

Once calculated the single phase to ground fault currents, the intervention area must be defined; for this definition it's important to know the vector conventions used. In particular, in the protections simulated, the angle δ between voltage and current is measured by placing as a reference point the I_{beta} axis in the positive direction. The angles measurement is assumed positive "counterclockwise", as shown in Figure 7-36.

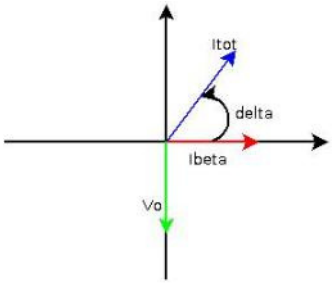

Figure 7-36: Implemented directional protection angles measurement convention

The directional relay sectors of intervention definition in the model must consider this convention. Therefore, using these conventions and considering the behavior of the current I_{tot} it's defined that:

- for Network Isolated (NI), the theoretical sector of intervention should be 180° (which represents the phase shift of 90° in delay of the zero sequence current with respect to the zero sequence voltage), however, in order to take account of the transducers measurement errors in the angles calculation, the angular sector of intervention has been defined with safety margins (Figure 7-37a):
  NI: $150° \leq \delta \leq 210°$

- for Network Compensated (NC), the theoretical sector of intervention should be between 90° and 270°, otherwise to avoid nuisance trip of the healthy line protections, due to the instrument transformer measure errors (the shift angle between I_{beta} and V_0 can be measured bigger than the 90° theoretical one), it's necessary to introduce a safety margin of 15°[63]. At the end for simulations need the sector of intervention is symmetric around 90° (Figure 7-37b):
  NC: $15° \leq \delta \leq 165°$

a) b)

Figure 7-37: Intervention sectors definition in blue, a) for isolated network (NI) and (b) for compensated network (NC)

In practice, it is often preferred to use a multifunction protection[64], i.e. able to operate properly in compensated and isolated networks. Such protection is programmable with two areas, totally independent, that allow to recognize ground faults in both the network configurations. Figure 7-38 shows the modeled intervention areas. If the angle falls in the overlapping area, the protection trips with the less delay (always the isolated network one).

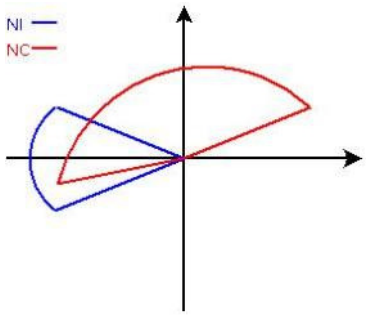

Figure 7-38: Multifunction directional protection intervention sectors definition

[63] This value has been chosen by the main Italian Distributor System Operator (DSO) as the results of the calculation of the instrument transducer measure errors, considering also the saturation effect.
[64] The need of this type for the earth protection derives from the DSO needing to be able to manage, in a compensated network, the network neutral status in accordance with operating or maintenance requirements (the protection default setting is for compensated network).

The simulated directional protection relay setting values are reported in Table 7-5. As for the other protection relays implemented, it's possible, if necessary, to set an intentional delay between the protection start and the tripping.
In some simulations, the intentional delay has been modified to obtain a huge reduction of the simulation times and the results file size. This operation has been carried out only in cases where the intentional delay duration has no influence on the simulation results.

Table 7-5: Maximum zero sequence current directional protection settings (values reported to the VT and CT secondary)

	Isolated network	**Compensated network**
Voltage Threshold	18 V	6V
Current Threshold	33 mA	33 mA
Angular Sector	150 ÷210°	15 ÷165°
Intentional Delay	0.4 s	1 s

7.6.2.3 Over/under frequency and voltage protection relays

The setting parameters for these protection relays are defined by Standard CEI 0-16 and are adopted in the implemented models (§ 1.2.1).
As input both of these protections have the line to line voltages measured through inductive voltage transducer with phase-to-phase primary winding connection (§ 7.6.1). The model circuit diagrams are shown in Figure 7-48.

The over/under voltage relays starting is verified after a comparison between the measured transducers voltage and the threshold values. For the frequency relays the frequency calculation is implemented in a model through a Phased Locked Loop (PLL). In particular, the voltage phase calculation, from which the frequency derives, is carried out according to the PLL operation logic. This device is based on the fact that network voltages Park space vector q-axis component is correlated with the voltages phases.
In fact, considering a three phase system, the Park transformation over rotation axes is expressed as follows:

$$\begin{bmatrix} v_\alpha \\ v_\beta \end{bmatrix} = \sqrt{\frac{2}{3}} \cdot \begin{bmatrix} 1 & -1/2 & -1/2 \\ 0 & \sqrt{3}/2 & -\sqrt{3}/2 \end{bmatrix} \cdot \begin{bmatrix} v_a \\ v_b \\ v_c \end{bmatrix} \tag{7.14}$$

where α and β are the Park space vector projections on fixed axis, that coincide with the real and imaginary axes of the complex plane where the input voltages phasors are defined (Figure 7-39).

By applying a rotation matrix to the previous conversion it's possible to define the Park transformation over dq-axes:

$$\begin{bmatrix} v_d \\ v_q \end{bmatrix} = \sqrt{\frac{2}{3}} \cdot \begin{bmatrix} \cos\vartheta & \sin\vartheta \\ -\sin\vartheta & \cos\vartheta \end{bmatrix} \cdot \begin{bmatrix} v_\alpha \\ v_\beta \end{bmatrix} \tag{7.15}$$

where the d and q components are the rotating Park vector projections on the axis d and q, which constitute the reference orthogonal frame rotating with respect to the fixed axis $\alpha\beta$ and offset with an angle ϑ, variable in time according to the rotation law.

The Figure 7-39 illustrates intuitively the PLL logic: the vector V is the Park space vector, rotating with respect to the fixed reference $\alpha\beta$ with angular speed ω; Φ is its phase with respect to this reference. The reference d-q is also rotating with respect to the reference $\alpha\beta$ and its position is defined by the angle ϑ, that appears in the transformation matrix. If the v_q component isn't zero, the reference frame d-q is not rotating in accordance with the vector itself and so it does not provide any information

on the phase (Figure 7-39a). On the contrary, if the angle ϑ has a value able to cancel the v_q the angles Φ and ϑ are equal and so the angle ϑ, known as imposed, provides information about the vector space phase (Figure 7-39b).

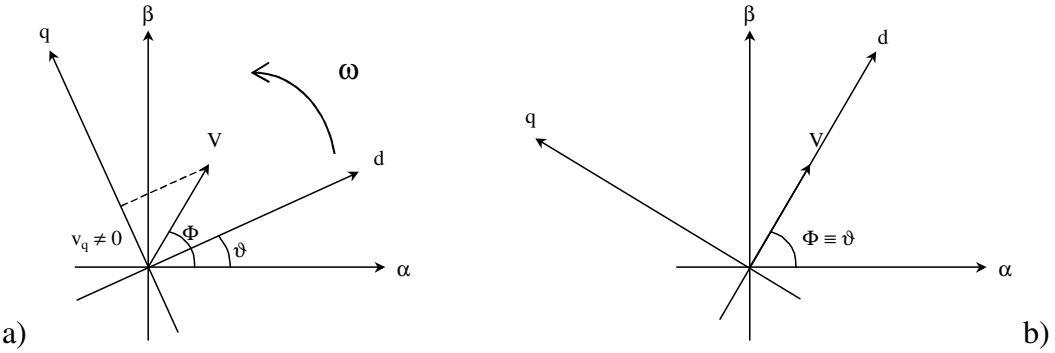

Figure 7-39: PLL principle operation diagram

Analytically, this can be demonstrated as follows. For small angles, the difference between the vector space phase and the d-q frame angle can be approximated by the following expression:

$$\Phi - \vartheta \approx \sin(\Phi - \vartheta) \tag{7.16}$$

developing:

$$\sin(\Phi - \vartheta) = \sin\Phi \cdot \cos\vartheta - \sin\vartheta \cdot \cos\Phi = \cos\Phi \cdot \left(\frac{\sin\Phi \cdot \cos\vartheta}{\cos\Phi} - \sin\vartheta \right) \tag{7.17}$$

recalling that, as v_α and v_β are defined in (7.14), it's possible to calculate:

$$\Phi = \arctan\left(\frac{v_\beta}{v_\alpha}\right) \quad \rightarrow \quad \frac{\sin\Phi}{\cos\Phi} = \frac{v_\beta}{v_\alpha} \tag{7.18}$$

By replacing the (7.18) in (7.17) it's obtained:

$$\sin(\Phi - \vartheta) = \cos\Phi \cdot \left(\frac{v_\beta}{v_\alpha} \cdot \cos\vartheta - \sin\vartheta \right) = \frac{\cos\Phi}{v_\alpha} \cdot \left(v_\beta \cdot \cos\vartheta - v_\alpha \cdot \sin\vartheta \right) = \frac{\cos\Phi}{v_\alpha} \cdot v_q \tag{7.19}$$

and, remembering that:

$$V \cdot \cos\Phi = v_\alpha \tag{7.20}$$

the expression (7.16) becomes the following:

$$\Phi - \vartheta \approx \frac{v_q}{V} \tag{7.21}$$

If the Park vector q-component is cancelled the phase is equal to the rotation angle ϑ imposed to the reference d-q and so it's possible to know the voltage vector phase. This procedure is included in the simulation model according to the block scheme shown in Figure 7-40.

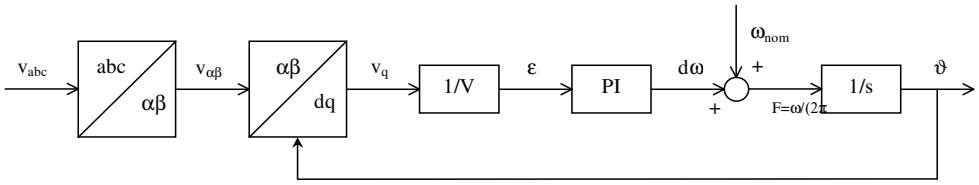

Figure 7-40: Network voltages phase calculation scheme

The v_q component is divided by the amplitude of the Park vector space to provide the error signal. This is sent to a Proportional-Integral controller which provides at its output the angular frequency variation from the nominal one; the d-q reference frame must rotate in accordance to this to cancel the voltage q-component. The rated angular frequency is added with this angular variation to calculate the frequency and this signal is integrated to obtain the angle ϑ, used by the Park transformation block.
The angle ϑ, thus obtained, represents the instantaneous value of the angle between the d-q rotating reference frame and the αβ fixed reference frame, and is continuously increasing in time (with reference to the example of Figure 7-41, i.e. $ϑ_1$ at the instant t_1 and $ϑ_2$ at the time t_2) and is scarcely significant to identify the voltage phase. To provide more clear information it has been used a different angle, called $ϑ_c$, defined as the difference between ϑ and the nominal angular frequency time integral (corresponding to a 50 Hz frequency). From the "physical" point of view, this corresponds to use a reference vector (V_{ref} in Figure 7-41) with zero phase and 50 Hz frequency to measure the three phase input voltages (represented by the Park vector V in Figure 7-41). If the voltage has a phase different from zero and a constant frequency of 50 Hz, $ϑ_c$ takes a constant value equal to the voltage phase; even if the voltage frequency differs from the nominal value, $ϑ_c$ hasn't constant behaviour, increasing or decreasing depending on frequency higher or lower than the nominal, correspondingly to the sliding between the reference vector and the three voltages.

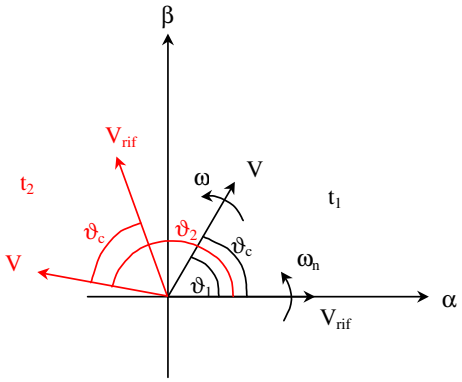

Figure 7-41: Identification of the variable $ϑ_c$

As an example some results concerning the voltage phase shift calculation during a three phase voltage dip are presented. Figure 7-42 shows the line to line voltages measured by the secondary winding of the phase to phase VT. These waveforms represent the input of the phase measurement system and are transformed to obtain the αβ and d-q components (Figure 7-43). The v_q divided by the Park vector magnitude represents the error signal that allows to calculate the angle ϑ and, consequently, the angle $ϑ_c$, shown in Figure 7-44. The other variable in green is an auxiliary one used to "freeze" the measure. Figure 7-44 shows that, at the moment in which the disturbance is detected, the phase measurement is inhibited and the angle $ϑ_c$ is forced to assume, and to maintain through the fault duration, the pre-dip value represented by this auxiliary variable. This value is obtained filtering the signal $ϑ_c$ with a second order filter obtaining a delay of about 12 ms[65]. After the fault and after a safety interval time of disturbance absence (in this case is equal to 10 ms), the phase measurement is

[65] The filter transfer function is $\frac{1}{(1+sT_{F1})(1+sT_{F2})}$ with T_{F1} = 1 ms and T_{F2} = 10 ms.

reactivated and the regulator resynchronizes the d-q rotating reference frame with the network voltages Park vector (v_q=0). Finally in Figure 7-45 the measured frequency is represented.

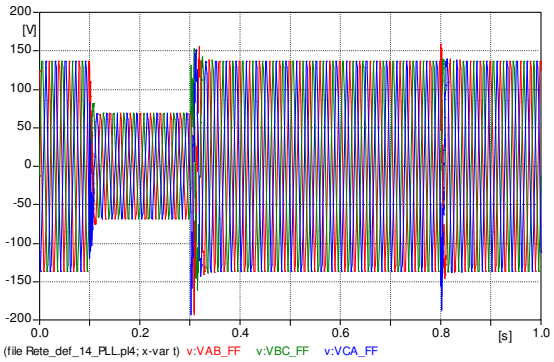

Figure 7-42: Line to line voltages of secondary VT connected phase to phase

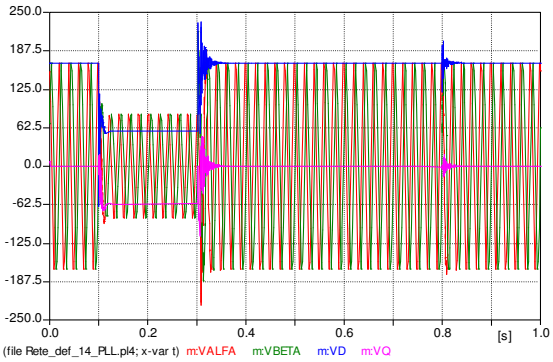

Figure 7-43: Components αβ and d-q line to line voltages of secondary VT connected phase to phase

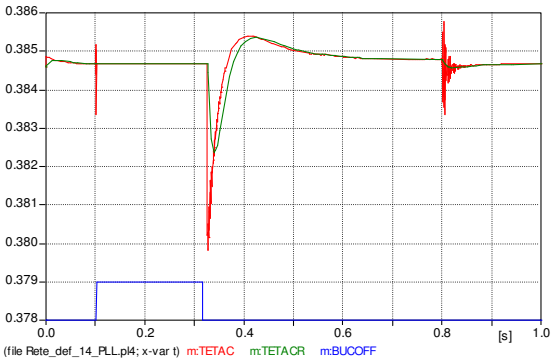

Figure 7-44: Phase ϑ_c measurement system output angle (red); internal variable for "freezing" the measure (green); fault detection output signal

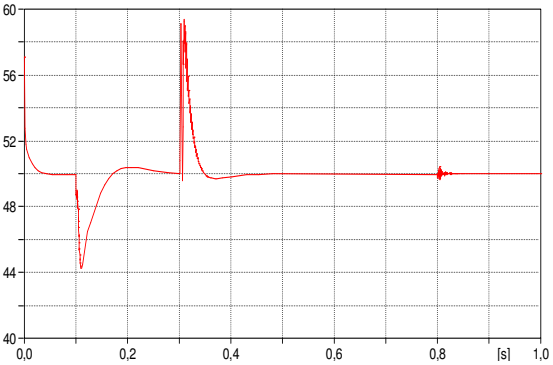

Figure 7-45: PLL frequency measured

In order to verify the regulator dynamic characteristics, the following figures show the transient step-response to perform the synchronization of the d-q rotating reference frame with the networks Park vector (coupling to the network transition). In particular, Figure 7-46 shows the angle ϑ_c, output of the phase measurement system, while Figure 7-47 shows the v_q network voltages component. The transient and the time of "coupling" are equal to 300 ms and are in line with the proportional integral regulator characteristics: phase bandwidth 70° and angular frequency 5 rad/s[66].

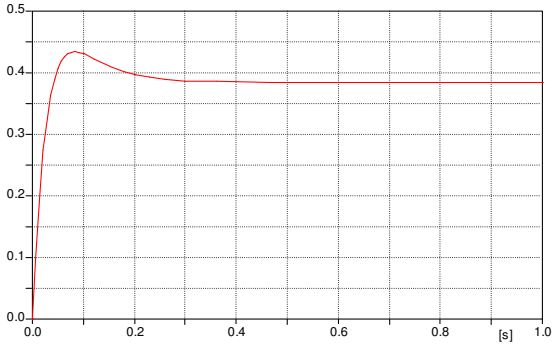

Figure 7-46: PLL Output Angle (ϑ_c)

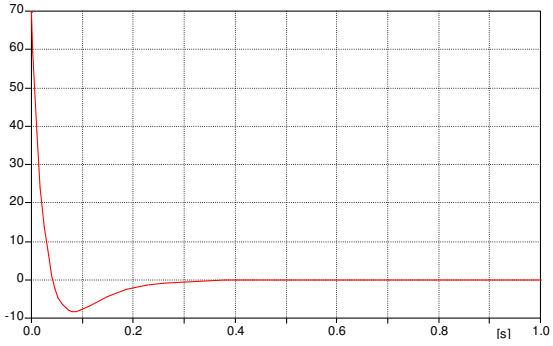

Figure 7-47: v_q network voltage

[66] K_p = 0.67 rad/s, K_i = 986.73 rad/s^2.

The method above described allows to measure the network voltages using the Park transformation. This procedure is defined for any type of steady state, not only sinusoidal, and can also be applied during the network disturbances (for example voltage dips or interruptions). However, if the system is sinusoidal the Park magnitudes take a constant values and the information about the phase is significant, while in a transient or unbalanced system these quantities assume variable values depending on the corresponding instantaneous values and so information about the phase may not be significant.

7.7 Operation protections simulations

The models of the different protection relay implemented have been verified by digital simulations to evaluate, preliminarily, the correct protection tripping in case of different types of fault without any kind of coordination between the devices, the only one is the chronometric selectivity obtained setting the relays with intentional delays.
In the modeled isolated network a 2MVA wind DG interfaced with electronic devices (as presented in Chapter 2) has been considered.

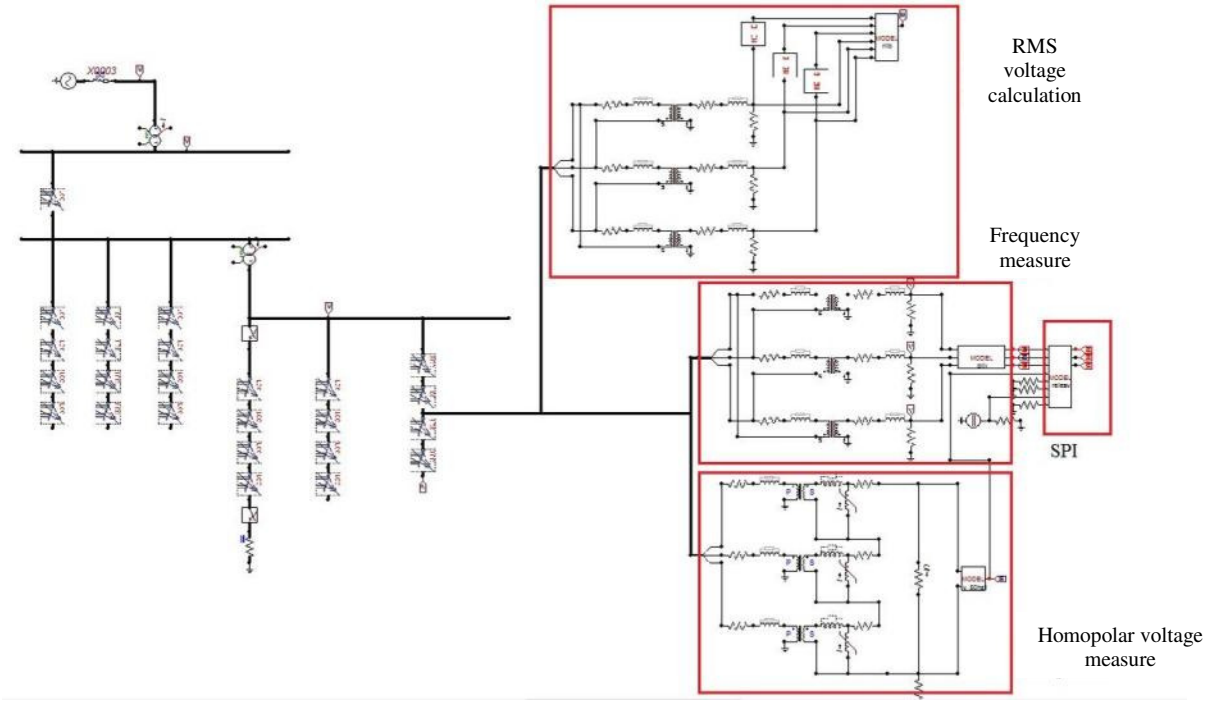

Figure 7-48: Network model simulated in environment ATPDraw

7.7.1 Three phase direct ground fault

A three phase fault on the DG connection line is simulated. The fault occurs at 0.4 s and is interrupted by the faulty line over-current protection relay (tripping without intentional delay I>>>, Figure 7-31). The MV bus-bar line to line voltages are shown in Figure 7-49, while the currents measured by the line protection are reported in Figure 7-50.

In this case, the fault characteristics does not determine the CT saturation. The time between sending the opening signal from the relay to the Circuit Breaker (CB) and the actual fault currents extinction depends on the mechanical opening time of the CB and on the time necessary for the currents to reach the null value.

The interface protection commands the DG disconnection from the network for the minimum frequency threshold tripping, as shown in Figure 7-51. During this simulation, the inverter characteristic measures, such as the frequency measured by relays after the interface protection tripping, are conditioned by the fact that the inverter isn't stopped by the relay itself but it's only disconnected from the network.

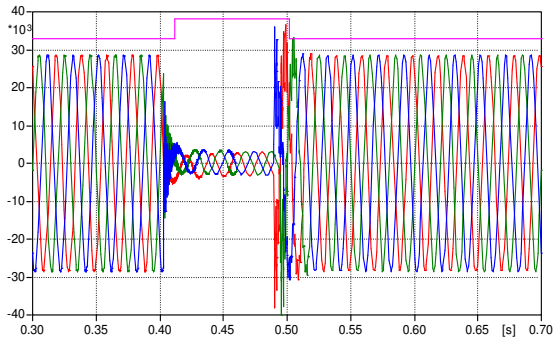

Figure 7-49: MV bus-bar line to line voltages and voltage dip detection signal

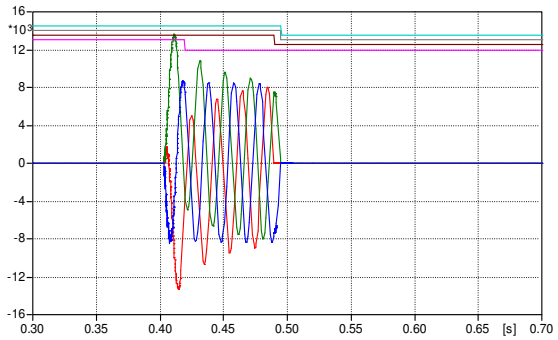

Figure 7-50: Fault current, CB control signal (pink), the real extinction currents time logic signals (brown, gray and cyan)

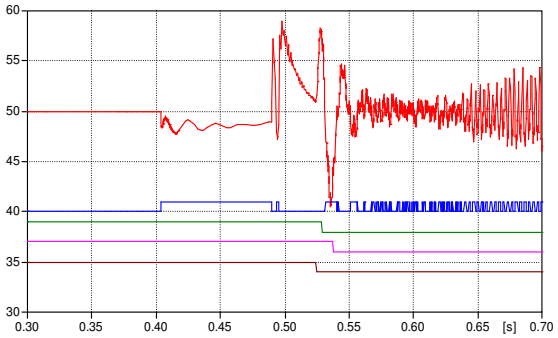

Figure 7-51: Frequency (red) with minimum frequency relay start signals (blue) and real currents extinction signals (a signal for each phase, curves green, pink and brown)

7.7.2 Three phase resistive fault

The simulated event is a three phase fault with fault resistance of 0,5 Ω, which occurs at t = 0.4 s and generates a voltage dip with residual voltage equal to 30% V_N. The protection tripping takes place after the over-current relay start (without intentional delay I>>>). The DG is disconnected from the network by the minimum frequency relay of the interface protection. The simulation has been carried out for a time sufficient to display the fast circuit breaker reclosing, which has been set up after a time of 400 ms by the protection tripping. The fault is not extinct, and after the reclosing, the protection relay trips for a second time as provided in the model.

Figure 7-52 represents the MV bus-bar line to line voltages during the transient voltage dip. In Figure 7-53 the faulty line currents are shown together with the over-current relay output signals, that drives the circuit breaker opening, and with the opening/closing effective states of each phase of the CB. Also in this case, the fault does not determine the CT saturation.

The interface protection causes the circuit breaker opening (and the DG disconnection) for the minimum frequency threshold tripping, as shown in Figure 7-54.

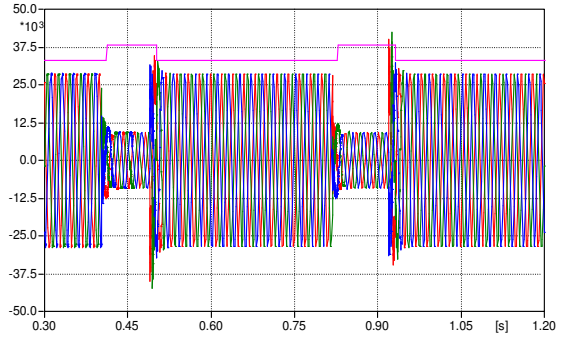

Figure 7-52: MV bus-bar line to line voltages and voltage dip detection signal

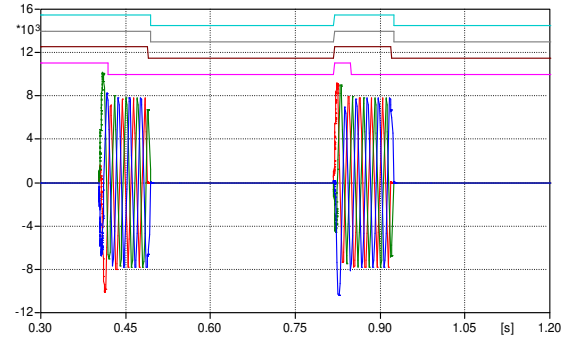

Figure 7-53: Fault current, over-current trip signal (pink) and the real extinction currents time logic signals (brown, gray and cyan)

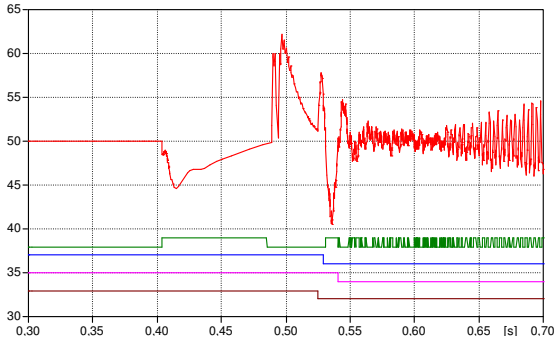

Figure 7-54: Frequency (red) with minimum frequency relay start signals (blue) and real currents extinction signals (a signal for each phase, curves green, pink and brown)

7.7.3 Three phase resistive fault with high impedance

A three phase fault with resistive fault impedance equal to 28 Ω occurs at 0.4 s without generating any voltage dip, as shown in Figure 7-55. The fault occurs in a line different from the DG installed one. The fault resistance is so big that the currents measured from the over- current relay are not sufficient to make it tripping without intentional delay. The relay trips instead for second threshold (I>>) with an intentional delay of 250 ms. The simulation results are shown in Figure 7-55 and Figure 7-56, where respectively the line to line network voltages and currents are shown. The simulation is sufficient to see the fast reclosing effect, but not a second protection trip.
The mains voltage increases due to the faulty line circuit breaker opening for the loads disconnection in this portion of the network.

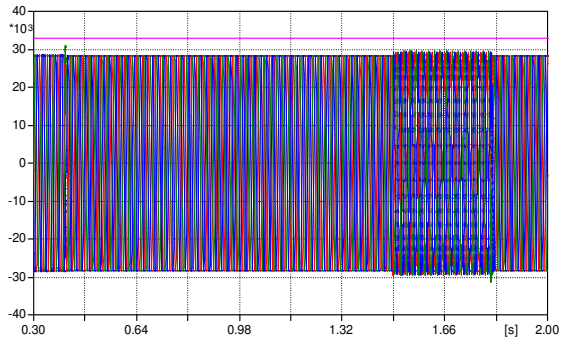

Figure 7-55: MV bus-bar line to line voltage with fault detection signal

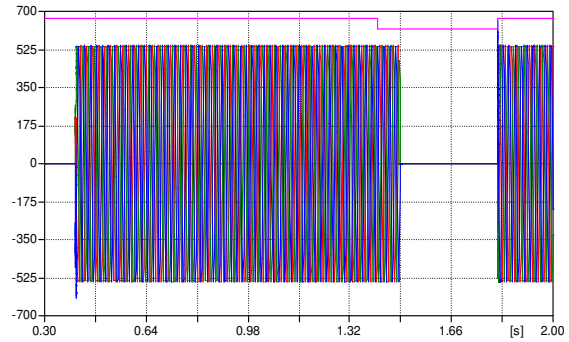

Figure 7-56: Fault current and over-current relay second threshold tripping signal (pink)

In contrast to the previous cases, the DG is not disconnected from the network since it's not installed on the faulty line, there is no risk of unwanted island. Correctly, the interface protection does not trip and the generator continues its normal operation. Since a voltage dip doesn't occurs, inverters FRT control logic aren't activated. Figure 7-57 shows the active and reactive power generated by the

inverter that remains connected to the network during the network disturbance, in particular the reactive power has a variable behaviour as a function of the voltage variations.

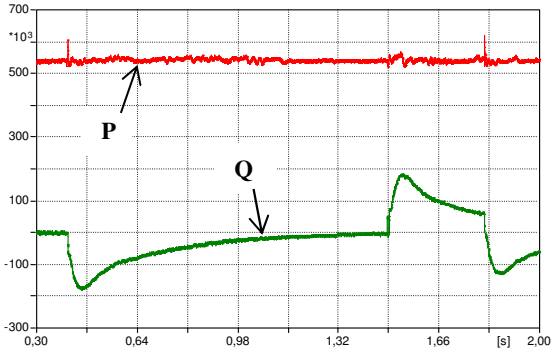

Figure 7-57: Active (red) and reactive (green) power delivered into the network

7.7.4 Single phase to ground fault

A single phase direct ground fault has been simulated on a line without DG installed, in this case a compensated network has been considered. The fault occurs at t = 0.4 s. In this case, the distributed generation doesn't see the voltage dip as shown in Figure 7-58.

The maximum current zero sequence directional protection is set according to the data reported in § 7.6.2 and correctly it detects the fault; Figure 7-58b shows the RMS zero sequence values of voltage and current detected by the relay and the angle between these two magnitudes (on the "secondary" ordinates axis on the right there is the scale for the reading of the zero sequence current RMS value, green curve).
As said, the inverter does not detect any voltage disturbance and continues to supply current without special control logic and limitation, as shown in Figure 7-58c.
For the isolated network, with a similar simulation, the directional protection selectivity has been tested in case of single phase ground fault. Also in this case, the network protection and the DG interface protection present the expected behavior.

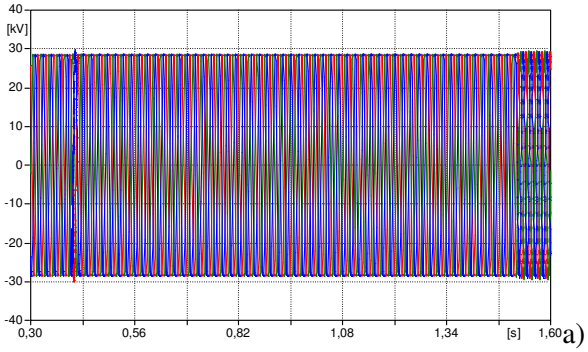

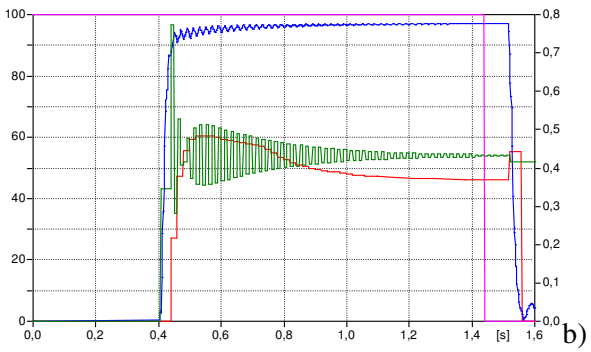

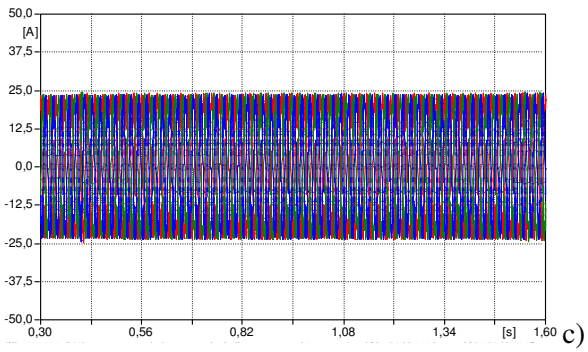

Figure 7-58:
a) MV bus-bar line to line voltages during a single phase fault;
b) directional protection maximum zero sequence current: zero sequence voltage (blue), zero sequence current (green), angle measured between the two (red) and the circuit breaker opening signal (pink);
c) MV side inverter current.

7.7.5 Unwanted island

Using the simulation models developed the problem of unwanted network island has been analyzed. In general the DG inverter islanding operation may occur as a result of the following conditions:

- a fault is detected and a feeder disconnecting device is opened but the disturbance is not detected by the DG protection devices;
- accidental opening of the line circuit breaker;
- intentional disconnection;
- human error or an act of nature.

There are many reasons for which islanding should be prevented with distributed generation. Safety, liability and maintaining the quality of power delivered to customers ranks high on the list of reasons:

- the utility cannot control voltage and frequency in the island, creating the possibility of damage to customer equipment that results from voltage or frequency excursions outside of the acceptable ranges;
- islanding may create a hazard for utility line-workers or the public by causing a line to remain energized that may be assumed to be disconnected from all energy sources;
- reclosing into an island may result in re-tripping the line or damaging the distributed resource equipment, or other connected equipment, because of out of phase closure;
- islanding may interfere with the manual or automatic restoration of normal service by the utility.

In order to avoid unwanted islands, it's mandatory equipping each grid-connected generating unit with an Interface Protection (IP) whose purpose is to detect the occurrence of a network disturbance and, in this case, to disconnect the generator from the public grid. Several methods for islanding detection have been proposed and developed [67] ÷ [75]. They can be classified into three main categories:

- *passive methods*, which are based only on the monitor of the local measurements at the DG's Point of Common Coupling PCC (such as voltage, frequency, phase and/or their rate of variation); in this case the island condition is detected when parameters run out of the required thresholds;
- *active methods*, which introduce deliberate changes or disturbances to the connected circuit and then monitor the response to determine if the grid with its stable frequency, voltage and impedance is still connected;
- *communication-based methods*: recent Standards have introduced the possibility of a forced trip of the IP, that is driven by an external signal under the control of distribution system operators.

Even though passive methods are easier and less expensive to implement with respect to the active ones, they show some difficulties about the proper setting of the admissible parameter ranges. Narrow ranges may lead to IP unwanted trips and unnecessary DG disconnections, while wide ranges may fail the island detection. The main drawback of this methods is the so called Non-Detection Zone (NDZ). In other words, passive methods are unable to detect islanding if the mismatch between the DG generated power and loads consumption in the island is small.
Such limitation is partially overcome by active island detection methods, which introduce perturbations in the current injected purposely by the inverter to unbalance the power generation and absorption. Even though more effective than passive methods, also active detection methods can have some limitations and drawbacks depending on the implementation method, for example:

- NDZ can still exists for some specific load impedances;
- unwanted trips can be caused by other disturbance signals coming from the grid;
- the perturbing signals injected into the grid may be disturbing for other grid connected systems.

In general, the reason why voltage and frequency of the island network portion present a displacement from the nominal values can be explained by taking into consideration the system simplified model shown in Figure 7-59.

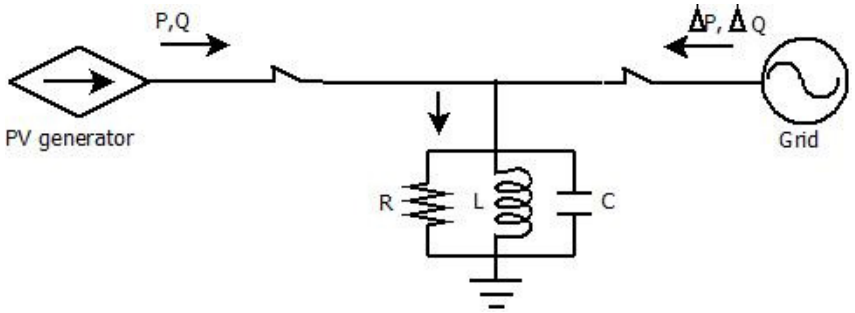

Figure 7-59: Generic circuit for the study of the unwanted island protections

In this model the network is represented as a an ideal voltage generator connected to the portion that can be operated in island by a three phase circuit breaker. The distributed generator, for example a photovoltaic generator, is represented as a current driven generator that injects constant power. This generator can be used as an equivalent model of all the generators connected to the part of the network that could operate in island. The loads are represented by RLC parallel equivalent circuits. This model represents a simplification compared to real situations, where rotating loads and non-linear ones are frequently connected, but it is still an explanatory of the phenomena under analysis[67].

7.7.5.1 Interface Protection Non-Detection Zone (NDZ)

Considering the passive methods, one problem is the interface protection Non-Detection Zone (NDZ), below the analytical calculation of this area is presented.
For the load in Figure 7-59 it's possible to define the quantities:

$$f_0 = \frac{1}{2\pi\sqrt{L_0 C_0}} \tag{7.22}$$

$$Q_f = R_0\sqrt{\frac{C_0}{L_0}} = \frac{Q_L Q_C}{P_R} \tag{7.23}$$

where:

- f_0= nominal resonance frequency;
- Q_f= quality factor;
- Q_C= capacitive reactive power;
- Q_L= inductive reactive power;
- P_R= active power;
- R_0= resistance value (in presence of the prevalent network with $V=V_n$ gives $\Delta P= 0$);
- C_0, L_0= capacitance and inductance loads values that in presence of the prevalent network ensure $\Delta Q=0$.

The parameters R_0, L_0 and C_0 will differ from those physical shown in Figure 7-59 (R, L, and C) of about ΔR, ΔL and ΔC. Considering the possibility to open the network circuit breaker by disconnecting the system generator + load from the network it's necessary to check the balance between generated power and absorbed one.

[67] This loads and network modeling can also be found in IEC62116 "Test procedure of islanding prevention measure for utility – interconnected photovoltaic inverters" Ed.1.0, 09 2008, that provides the requirement concerning the test procedures for the photovoltaic inverter anti-islanding protection.

Indicating ΔP and ΔQ the active and reactive powers supplied by the network to the load, while with P_{inv} and Q_{inv} the active and reactive powers injected by the inverter[68], therefore, the load powers are:

$$Q_{load} = Q_{inv} + \Delta Q \tag{7.24}$$

$$P_{load} = P_R = P_{inv} + \Delta P \tag{7.25}$$

It's possible to verify different conditions varying the power factor of the inverter, in particular cos(φ)=1 and cos(φ)≠1. Below it is assumed that the generation system connected to the network works with unity power factor, i.e. Q_{inv}=0.

Inverter operation with unity power factor
The island voltage is given by:

$$V_i = \sqrt{P_{inv}(R_0 + \Delta R)} \tag{7.26}$$

The resonance frequency of the load (with experimental values) can be expressed as:

$$f_i = \frac{1}{2\pi\sqrt{(L_0 + \Delta L)(C_0 + \Delta C)}} \tag{7.27}$$

The load reactive power unbalance when is connected to the network can be written as:

$$\begin{aligned} \Delta Q = Q_L - Q_C = V_0^2\left(\frac{1}{2\pi f_0(L_0 + \Delta L)} - 2\pi f_0(C_0 + \Delta C)\right) = \\ = V_0^2 \frac{1 - 4\pi^2 f_0^2 (L_0 + \Delta L)(C_0 + \Delta C)}{2\pi f_0 (L_0 + \Delta L)} \end{aligned} \tag{7.28}$$

From
(7.28) it's possible to obtain the following expression:

$$(L_0 + \Delta L)(C_0 + \Delta C) = -\frac{\Delta Q}{V_0^2}\frac{2\pi f_0(L_0 + \Delta L)}{4\pi^2 f_0^2} + \frac{1}{4\pi^2 f_0^2} \tag{7.29}$$

replacing the (7.29) in the resonance frequency expression (7.27) and considering the following relationships:

$$Q_L = \frac{V_0^2}{2\pi f_0 (L_0 + \Delta L)} \tag{7.30}$$

$$Q_C = Q_L - \Delta Q \tag{7.31}$$

the (7.29) can be rewritten in the following formula:

$$(L_0 + \Delta L)(C_0 + \Delta C) = \frac{1}{4\pi^2 f_0^2}\frac{Q_C}{Q_L} \tag{7.32}$$

[68] Very often the photovoltaic inverter operates at unity power factor (cos(ϕ) = 1) (ΔQ=0 var).

Substituting the expression (7.32) in the island resonance frequency, it's possible to obtain:

$$f_i = \frac{1}{2\pi\sqrt{\frac{1}{4\pi^2 f_0^2}\frac{Q_C}{Q_L}}} = f_0\sqrt{\frac{Q_L}{Q_C}} \tag{7.33}$$

It should be noted that the island frequency doesn't depend on the voltage and so it is independent on the inverter active power.

Not unitary power factor inverter operation

The island voltage calculation it's the same than in the previous case (7.26):

$$V_i = \sqrt{P_{inv}(R_0 + \Delta R)} \tag{7.34}$$

The inverter supplies a reactive power Q_{inv}, and during the island operating condition must be valid the following power balance:

$$Q_L - Q_C - Q_{inv} = 0 \tag{7.35}$$

$$Q_{inv} = \frac{V_i^2}{2\pi f_i L} - V_i^2 2\pi f_i C = V_i^2 \frac{1-(2\pi f_i)^2 LC}{2\pi f_i L} \tag{7.36}$$

where:

- $L=L_0+\Delta L$
- $C=C_0+\Delta C$

From (7.36) the island resonance frequency expression can be calculated in case of inverter working with $\cos(\varphi)\neq 1$:

$$f_i = \frac{1}{2\pi}\left[-\frac{Q_{inv}}{2CV_i^2} \pm \sqrt{\frac{Q_{inv}^2}{4C^2V_i^4} + \frac{1}{LC}}\right] \tag{7.37}$$

The frequency expressed as a function of the reactive components of the load is quite complex. However, in this case, it can be seen that the island frequency depends on the island voltage, on the inverter power supplied and the load resistance. Substituting the island voltage expression (7.34) in (7.37) it's possible to obtain:

$$f_i = \frac{1}{2\pi}\left[-\frac{Q_{inv}}{2CP_{inv}R} \pm \sqrt{\frac{Q_{inv}^2}{4C^2P_{inv}^2R^2} + \frac{1}{LC}}\right] = \frac{1}{2\pi}\left[-\frac{\tan(\phi)}{2CR} \pm \sqrt{\frac{\tan^2(\phi)}{4C^2R^2} + \frac{1}{LC}}\right] \tag{7.38}$$

Assuming the generator operation with power factor between 0.9 leading and 0.9 lagging, i.e. with an angle -0,451 rad ≤ φ ≤ 0.451 rad, Figure 7-60 presents the island frequency as a function of the power factor, where $f_{\cos(\phi)=1} = \frac{1}{2\pi\sqrt{LC}}$ represents the frequency at which the system could be if the generator works with unity power factor.

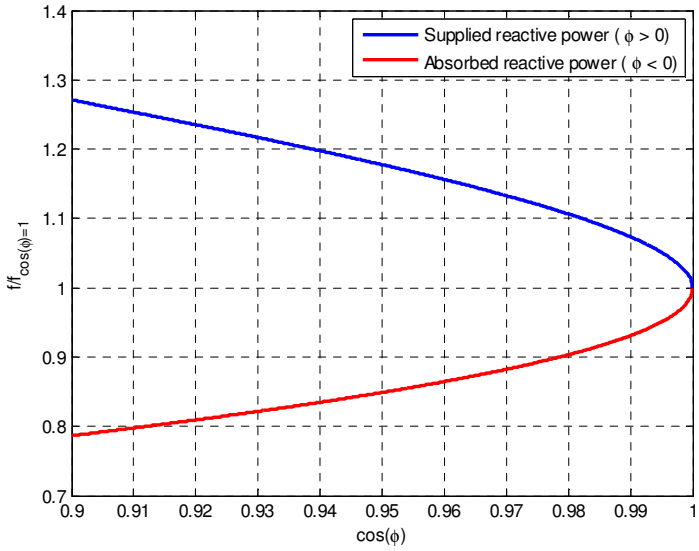

Figure 7-60: Representation of the islanding non-intervention area depending on the inverter power factor

Representation of the islanding non-intervention area

After the disconnection, the load is resonant with the frequency correlated to its components L and C values, thus causing a frequency variation. If due to this variation, the frequency reaches a value over a defined bandwidth around the nominal value, the anti-islanding protection relay trips. Otherwise the island operation is not detected and the system operates isolated from the rest of the network. This frequency range is the over/under-frequency protection Non-Detection Zone.

Considering the minimum and maximum frequency thresholds, the *over/under frequency protection relay intervention area*, considering the inverter operating condition at cosφ=1, is defined by1.

$$\frac{f_i - f_0}{f_0} = \frac{\dfrac{1}{2\pi\sqrt{(L_0+\Delta L)(C_0+\Delta C)}} - \dfrac{1}{2\pi\sqrt{L_0C_0}}}{\dfrac{1}{2\pi\sqrt{L_0C_0}}} = \frac{\sqrt{L_0C_0}}{\sqrt{(L_0+\Delta L)(C_0+\Delta C)}} - 1 \tag{7.39}$$

where f_i indicates the island frequency.

In accordance with the anti-islanding protection procedure adopted to disconnect the generator if the mains frequency deviates with a positive or negative variation from the nominal one over the two thresholds, the following condition has to be verified to avoid the protection tripping:

$$\frac{f_{\min} - f_0}{f_0} \le \frac{\sqrt{L_0C_0}}{\sqrt{(L_0+\Delta L)(C_0+\Delta C)}} - 1 \le \frac{f_{\max} - f_0}{f_0} \tag{7.40}$$

where f_{min} and f_{max} are the protection relay thresholds.

Rewriting suitably the (7.40) it's obtained:

$$\left(\frac{f_{\min}}{f_0}\right)^2 \le \frac{L_0C_0}{L_0C_0 + L_0\Delta C + \Delta L C_0 + \Delta L \Delta C} \le \left(\frac{f_{\max}}{f_0}\right)^2 \tag{7.41}$$

Considering only small variations of the parameters (ΔLΔC~ 0), the relation (7.41) can be written as:

$$\left(\frac{f_{\min}}{f_0}\right)^2 \le \frac{L_0C_0}{L_0C_0 + L_0\Delta C + \Delta L C_0} \le \left(\frac{f_{\max}}{f_0}\right)^2 \tag{7.42}$$

that is equivalent to:

$$\left(\frac{f_0}{f_{\max}}\right)^2 - 1 \le \frac{\Delta C}{C_0} + \frac{\Delta L}{L_0} \le \left(\frac{f_0}{f_{\min}}\right)^2 - 1 \tag{7.43}$$

The relation (7.43) represents the analytical relationship between the limits of the non-intervention area and the load variations with respect to the value that it should have to be equal to DG injection.

To find the relationship between this non-intervention area and the reactive power variations (since it's not linked to the active power because the load resistance is not involved in the non-intervention area definition), it must be taken into account that, in presence of prevalent network and in case of operation with unity power factor, the following expression for the reactive power exchanged with the network can be written:

$$\Delta Q = V^2\left(\frac{1}{2\pi f_0(L_0+\Delta L)} - 2\pi f_0(C_0+\Delta C)\right) = \frac{Q_L}{1+\frac{\Delta L}{L_0}} - Q_C\left(1+\frac{\Delta C}{C_0}\right) \tag{7.44}$$

Dividing the (7.44) by the load active power (P_R), it's obtained:

$$\frac{\Delta Q}{P_R} = \frac{(Q_L/P_R)}{1+\frac{\Delta L}{L_0}} - (Q_C/P_R)\left(1+\frac{\Delta C}{C_0}\right) = \frac{Q_f}{1+\frac{\Delta L}{L_0}} - Q_f\left(1+\frac{\Delta C}{C_0}\right) = Q_f\,\frac{-\left(\frac{\Delta C}{C_0}+\frac{\Delta L}{L_0}+\frac{\Delta C}{C_0}\frac{\Delta L}{L_0}\right)}{1+\frac{\Delta L}{L_0}} \tag{7.45}$$

Neglecting the variable terms with an order higher than the first, assuming that $1+\frac{\Delta L}{L_0} \approx 1$, the relation (7.45) can be rewritten as:

$$\frac{\Delta Q}{P_R} = -Q_f\left(\frac{\Delta C}{C_0}+\frac{\Delta L}{L_0}\right) \tag{7.46}$$

Replacing the (7.46) in the formula which expresses the non-intervention area relationship with the load parameters (7.43), the analytical relationship between the over/under frequency protection relay non-intervention area limits and powers is obtained[69]:

$$Q_f\left[1-\left(\frac{f_0}{f_{\max}}\right)^2\right] \le \frac{\Delta Q}{P_R} \le Q_f\left[1-\left(\frac{f_0}{f_{\min}}\right)^2\right] \tag{7.47}$$

Similarly the *over/under voltage protection relay non-intervention area* can be defined. In fact, the load voltage before (V_0) and after (V_i) the island operation can be expressed as:

[69] If $\Delta P=0$ then $P_R=P_{inv.}$

$$\frac{V_0^2}{R_0} = \frac{V_i^2}{R_0 + \Delta R} \tag{7.48}$$

from which it's derived:

$$\Delta R = 2\frac{\Delta V}{V_0} + \left(\frac{\Delta V}{V_0}\right)^2 \tag{7.49}$$

where $\Delta V = V_i - V_0$.

It has:

$$\frac{\Delta P}{P_R} = \frac{V_0^2}{R_0 + \Delta R} - \frac{V_0^2}{R_0} = -\frac{\Delta R / R_0}{\Delta R / R_0 + 1} \tag{7.50}$$

where expressing ΔR according to the (7.49) it's obtained:

$$\frac{\Delta P}{P_R} = \frac{1}{\left(\frac{\Delta V}{V_0} + 1\right)^2} - 1 \tag{7.51}$$

Considering the minimum and maximum voltage thresholds, the over/under voltage protection relay intervention area is defined by:

$$\left(\frac{V_0}{V_{\max}}\right)^2 - 1 \le \frac{\Delta P}{P_R} \le \left(\frac{V_0}{V_{\min}}\right)^2 - 1 \tag{7.52}$$

The non-intervention area of these two protections (7.47) and (7.52) can be represented on the ΔP, ΔQ plane, as shown in Figure 7-61. If the inverter supplies a not null reactive power, the NDZ is translated over the ΔQ axis as a function of the generator behavior (for example if it supplies capacitive Q the NDZ moves upwards).

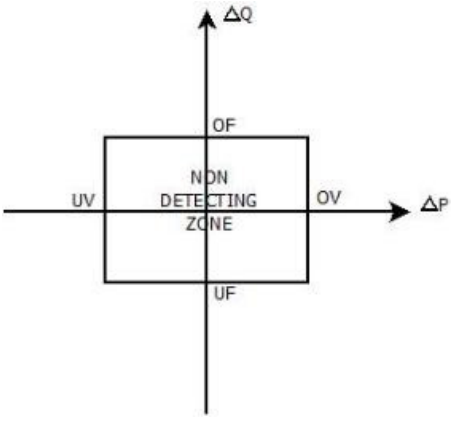

Figure 7-61: NDZ representation for frequency and voltage protection relays in the plane of active and reactive power variations

The unwanted island operation supported by DG in a real network situation, even if it may appear as a low probability event, it is actually verified in the Spanish network in 2009. In this case, a portion of MV network was disconnected from the main network for maintenance. In the isolated network, two 2.5 MW photovoltaic installations had supplied the island without the interface protections tripping to disconnect the DG, for a substantial balance between generation and loads. During the network circuit breaker closing for maintenance procedures, a pre-closing arc had been verified damaging the circuit breaker itself. The DSO involved, as a result of this incident, had carried out studies and simulations on island operation condition and the conclusions have been that this phenomenon may occur for power unbalance between load and generation up to 10% and can persist for several minutes [74][75].

As seen, the island voltage and frequency depend on the balance between the active and reactive powers delivered by the generators (P_g, Q_g) and those absorbed by the load (P_l, Q_l). Clearly, if the power balances are such that voltage and/or frequency deviate too much from the nominal values, i.e. beyond the interface protections tripping thresholds, the DG is disconnected from the network and the island is no longer supplied. It should be noted that, if the IP is inhibited, the inverters could supplying the island also for considerable voltage and frequency deviations from the nominal values, as a function of the design device, as shown by the simulation results shown in Figure 7-62 and Figure 7-63.
Using the network and DG models presented in Chapter 2, two different situation have been considered: in the first the power balance causes an increase in voltage and frequency (Figure 7-62) and in the second the network parameters decrease (Figure 7-63), always with DG interface protection disabled. In both cases, the inverters supplies the island, created at t = 0.6 s due to the healthy line circuit breaker opening.

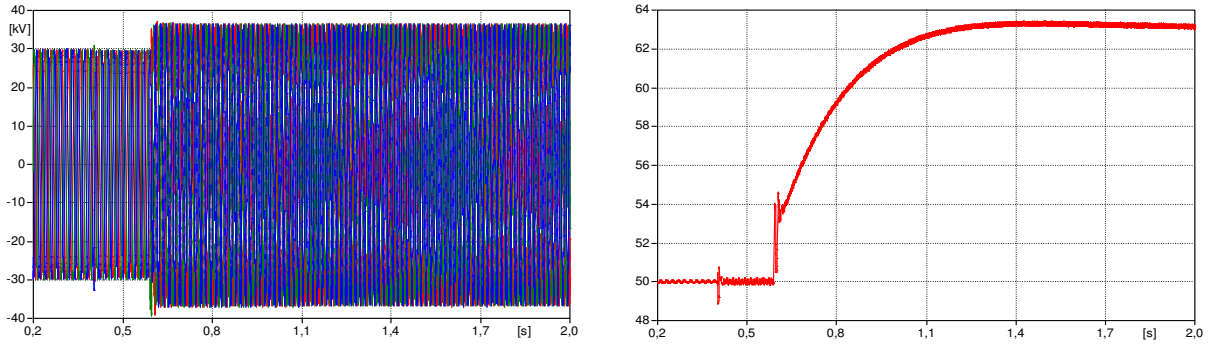

a) b)

Figure 7-62: Network island voltage (a) and frequency (b) in case of over-voltage and over-frequency condition

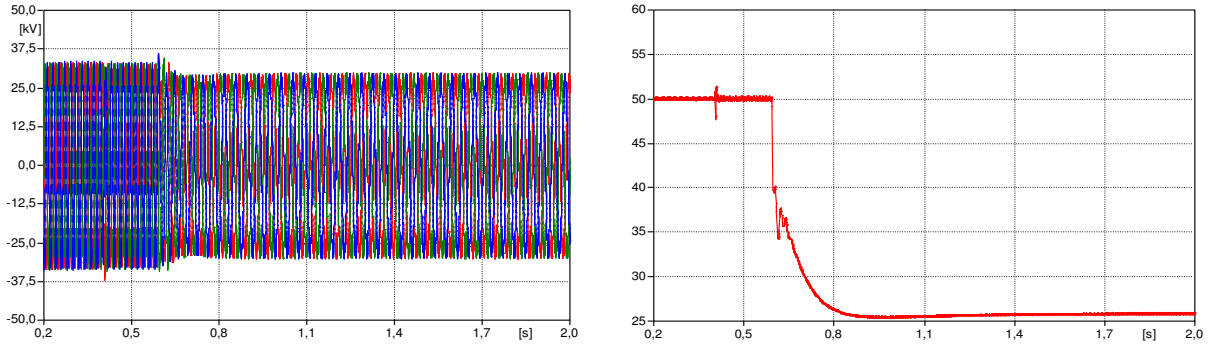

a) b)

Figure 7-63: Network island voltage (a) and frequency (b) in case of under-voltage and under-frequency condition

It's also been simulated the case of unwanted island due to a single phase fault to ground, which occurs at time t= 0.4s on the distribution network feeder with a wind PMSG connected. This is 2 MW

DG and works with power factor equal to 0.93. In the network there is a RL load, working with a power factor equal to 0.7, able to balance the active power supplied by the DG. Thanks to the factor correction capacitors, the load works with power factor of about 0.9, but considering the feeder capacitance to earth a balance between the DG reactive power delivered and the load absorbed one is reached. Theoretically in this case, neither island voltage or frequency present variations from the nominal values after the line circuit breaker opening; simulations confirm this behavior (Figure 7-64). The transient due to the line circuit breaker opening is too short to make the interface protection tripping and isn't sufficient to prevent the unwanted island so the DG remains connected. The zero sequence voltage, on the other hand, remains over the interface protection triggering threshold for the entire fault duration. The IP intentional delay, however, is greater than the line directional protection relay one, which trips as first.

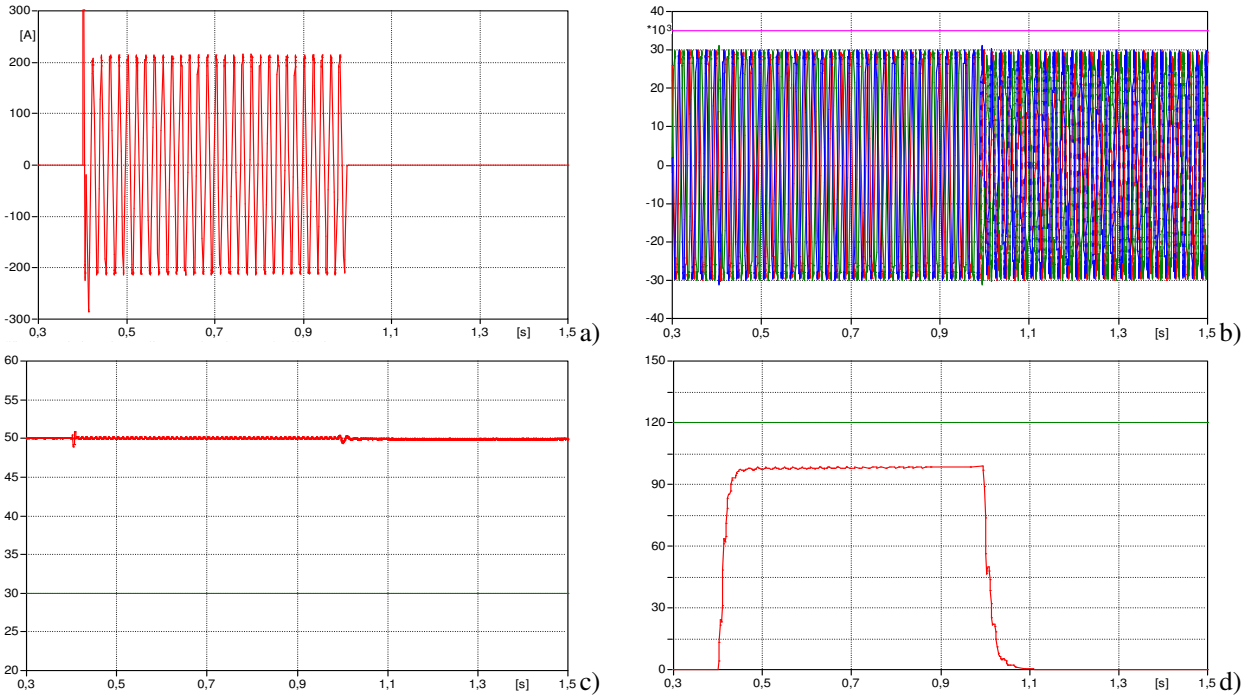

Figure 7-64: Unwanted island a) fault current, (b) network island line to line voltages and maximum/minimum voltage relay IP output signal (pink) with a scale factor of 35000, c) island frequency (red) and maximum/minimum frequency relay signal (green) with a scale factor of 30, d) zero sequence voltage (red) and output of the corresponding relay (green) with scale factor 120

7.7.6 Reclosing on island network

The unwanted island operation represents a risk factor for users and for those who work on the network and a problem for the network automation procedures, in particular for the reclosing. Since, in general, the island voltage and the frequency are not related to those of the rest of the network, despite of having similar values, it may happen that the automatic circuit breaker reclosing takes place with the voltages out of phase from the main network. This phenomenon can cause a damage of:

- line circuit breakers, as a result of the possible arc phenomena during the reclosing, especially if out of phase (the voltages across the circuit breaker terminals can be double than in case of reclosing in phase);
- loads since the voltage presents rapid variation;
- inverter, a step voltage variation causes the injection of high currents.

In the following, the last issue is analyzed, starting from the wind generators inverters models (Chapter 2), to simulate the inverter behavior during the circuit breaker closing.

Out of phase reclosing

It has been simulated a single phase resistive fault to ground, self-extinguished after a sufficient time to make the zero sequence line directional protection tripping, with the relative circuit breaker opening[70]. The inverter and the DG are connected to the faulty line. Since the inverter does not detect any voltage dip, continues to supply power allowing, under the generated and absorbed powers balance condition, the island operation. At time t=1 s the line circuit breaker automatic reclosing occurs, with the mains voltage out of phase than the island voltage. The simulation results are shown in Figure 7-65. In this case. it should be noted that the interface protection system has been bypassed[71] in order to run the inverter also for voltage and frequency levels over the protection tripping thresholds.

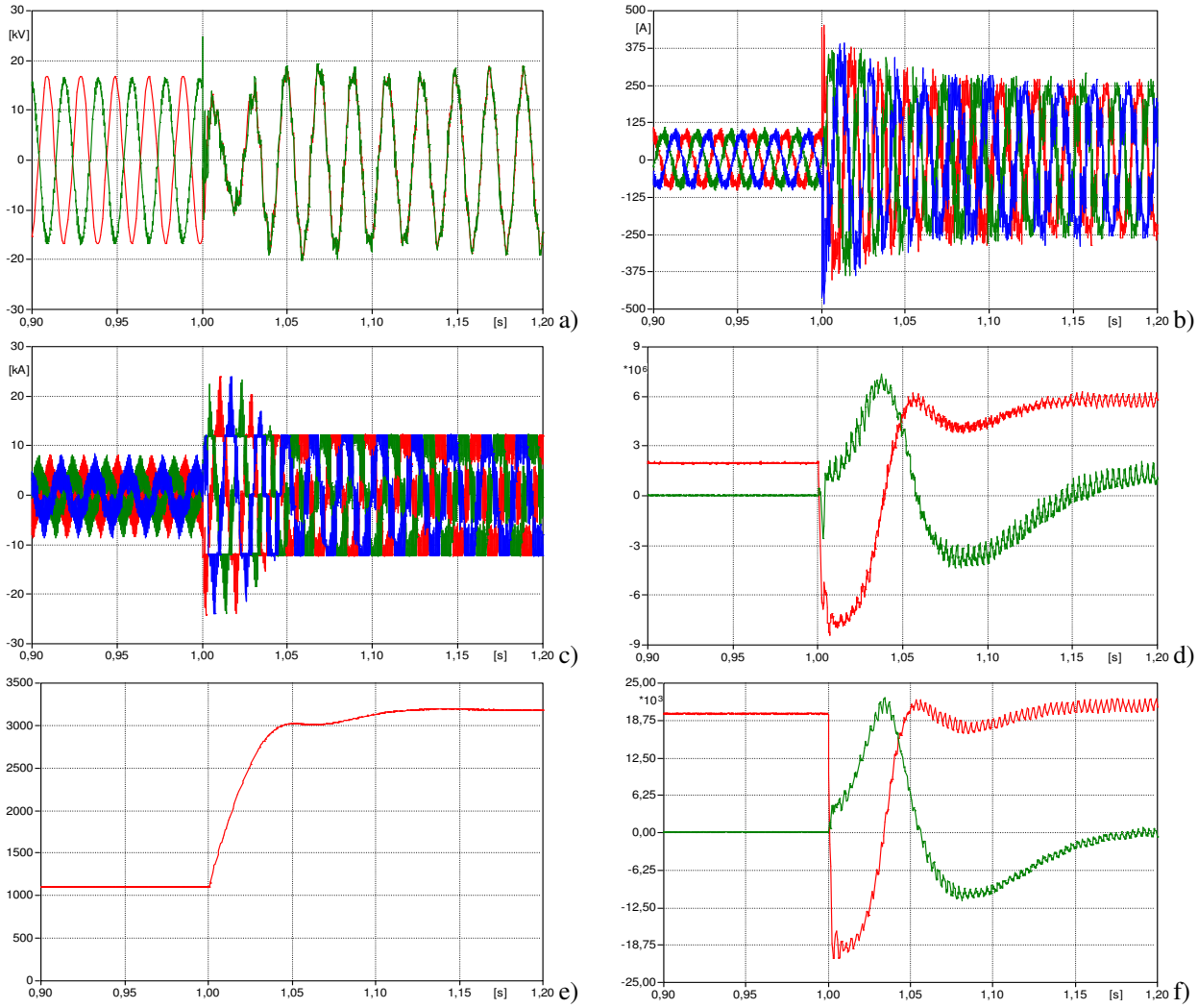

Figure 7-65: Inverter behavior in case of CB reclosing out of phase than the main network (a) island voltage phase "a" (red) and same mains voltage phase (green), (b) MV side inverter current, (c) LV side current inverter, (d) active (red) and reactive power (green), d) DC voltage, f) voltage on d-axis (red) and q-axis (green)

[70] In simulation, since this does not affect the results obtained and to shorten the simulation time, the intentional directional protections delays are decreased to 100 ms.

[71] The bypass of the IP has been simulated leaving the protection active without opening DG circuit breaker.

This figure shows that the reclosing in phase opposition cause a rapid transient of the network voltages and, consequently, their d-q components, sent to the inverter control through the PLL, show a step decrease over direct-axis. Due to this step (interpreted a short circuit in the network) the inverter:

- increases the injected currents (Figure 7-65b, c).;
- absorbs active power from the network (Figure 7-65d).

As a result of the active power absorption there is a DC voltage increase that cannot be limited by the braking chopper, designed to dissipate the only power from the primary source of the DG. The voltage increase is dangerous for the inverter components and has, as a further consequence, the instantaneous current limitation failure and the currents can reach values much higher than those switchable from the valves. The inverter can be damaged in case of circuit breaker reclosing in opposite phase, if there aren't specially safety systems.

In these considerations it has not been taken into account the possible "pitch" angle control effect to reduce the active power generated (which must be dissipated from the chopper, together with that one absorbed by the network). The time for power reduction implementation for devices similar as the one simulated are higher than the transients considered, supporting the assumptions made[72].

Reclosing in phase

The simulated system is the same as before but in this case the prevalent network voltage is in phase with the island one during the reclosing, as shown in Figure 7-66a. The inverter, in this case, is not subject to any type of significant transient during the reclosing, as demonstrated by the DC voltage and the currents, reported respectively in Figure 7-66b and in Figure 7-66c.

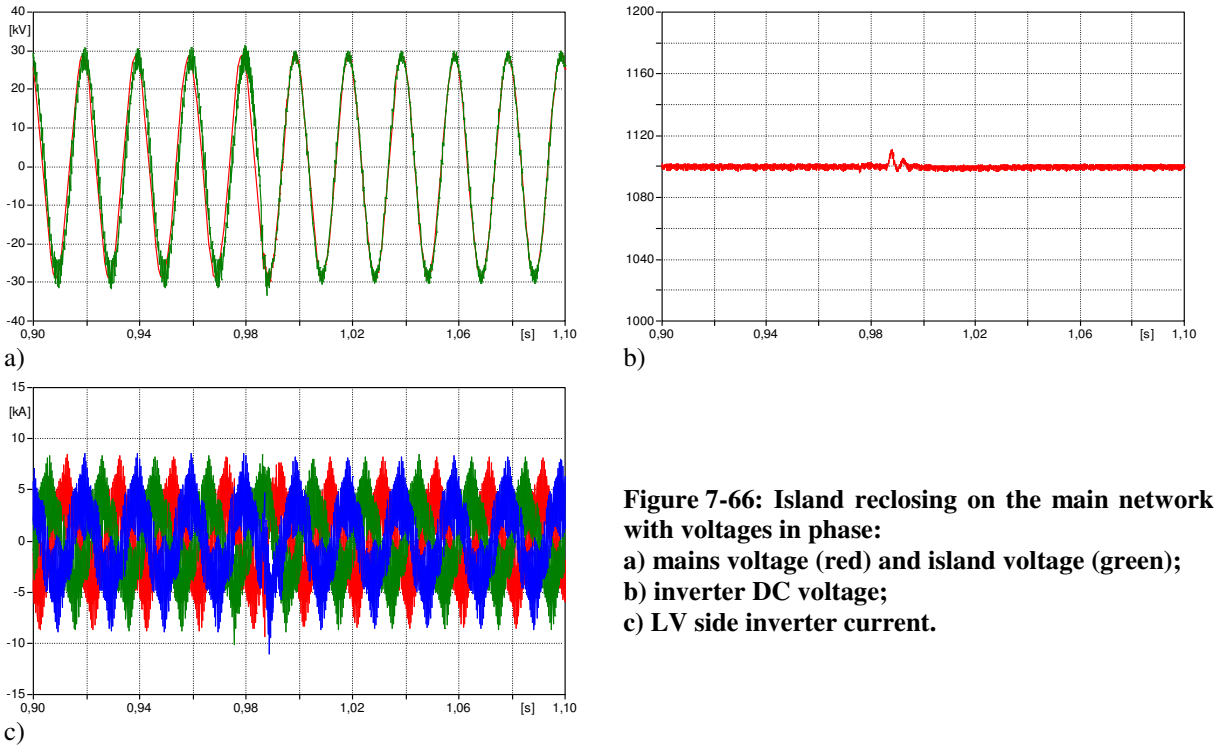

Figure 7-66: Island reclosing on the main network with voltages in phase:
a) mains voltage (red) and island voltage (green);
b) inverter DC voltage;
c) LV side inverter current.

[72] In case of machines with power equal to some kW, the pitch angle control response time is about 500ms.

Reclosing with a phase shift of 90°

In this case, the island voltage is shifted of 90° from the prevalent network when the circuit breaker recloses. The simulation results are shown in Figure 7-67. As seen in the reclosing out of phase simulation, the sudden phase shift of the voltage applied to the DG causes active power reversal flow and thus an increase in the DC voltage. The simultaneous braking chopper action and the current limitations bound the voltage rise within acceptable limits and the inverter resumes its normal operation after less than 60 ms. Under these conditions, the inverter components and valves, even if operating transiently in abnormal conditions, can overcome favorably the disturbance without damages.

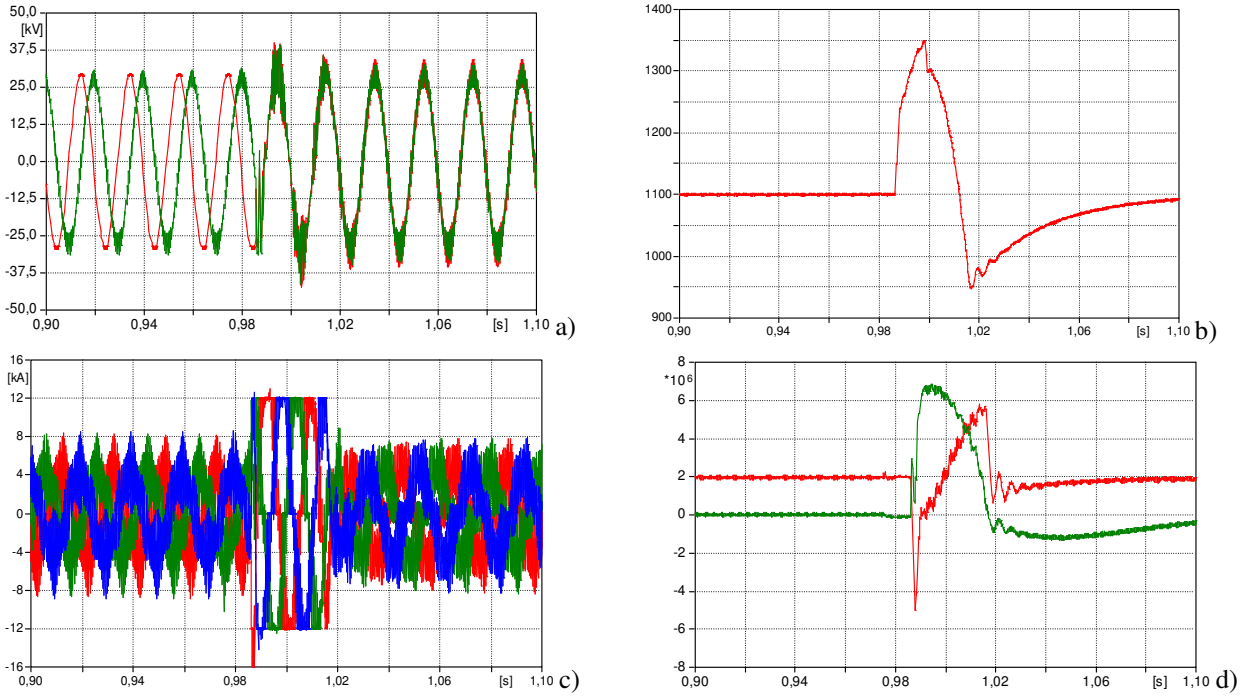

Figure 7-67: Island reclosing on the main network with phase shift of 90°: a) mains voltage (red) and island voltage (green), (b) inverter DC voltage, (c) LV side inverter current, d) active (red) and reactive (green) power

7.8 A protection coordination scheme

As anticipated, the typical network protection scheme requires, in case of fault, the faulty line circuit breaker opening. The Distributed Generation (DG) along the line is disconnected by the interface protection system and the following reclosing maneuvers involve all the feeder. Finally, in case of permanent fault, the faulty line segment selection procedures are carried out. From the perspective of an increase of DG connected to the network and of a Power Quality improvement, with a smaller number of users affected by interruptions, such protection scheme has some limitations:

- the whole feeder is affected by the circuit breaker opening, the DG cannot remaining connected to the network as for the Fault Ride Through requirements (Chapter 3);
- the whole DG connected along the feeder must be disconnected before the reclosing;
- the faulty line segment selection occurs with the circuit breakers opening and closing, affecting the whole feeder.

To overcome these limitations, it's necessary to introduce new protection schemes [76] ÷ [78]: in the following a network protection coordination proposal, based on logic selectivity, is presented. This proposal is characterized by:

- installation along the line of directional over-current and directional earth relays;
- communication channel to coordinate the protections;
- faulty line segment selection logic;
- coordinated interface protections management in order to reduce the unwanted island risk and to maintain as much as possible DG connected to the network.

7.8.1 Network protections coordination: the logic selectivity

The proposed protection scheme, as reported in the previous section, makes use of directional over-current relays which can exchange messages and commands between themselves and which can be coordinated with DG protection relays. The distribution feeder is subdivided in line segments, f.i. on the base of the number of connected users and generators, or with geographical or economic criteria. Protections are installed at the beginning and at the end of each line segment. These protections can exchange messages, and, in particular, two different logic commands can be sent/received:

- BLOCK: the receiving protection is disabled, so that it cannot trip;
- TRIP: the receiving protection is forced to trip, independently on its settings.

Also DG interface protections should be modified to be adapted. In particular, they should accept TRIP command and they should provide two different dead bands around the frequency nominal value.
In this scheme, the communication takes place only between adjacent network protection relays. The block signal is sent from a relay to the "previous" one along the direction of the protection intervention, while the tripping signal is sent to the one following[73]. The implemented protection model introduces a time lag in communications. In the model, all Circuit Breakers (CB) can interrupt fault currents and a delay of 70 ms between the receipt of the opening signal and the actual opening of the breaker has been inserted to simulate mechanical delays. Finally, currents are extinguished at the first zero crossing after the CB opening.
It's also necessary to provide a protection tripping back-up logic active in case of a communication failure or if the maximum times provided for the messages exchange is bigger than the allowed one. One possible solution could be to manage the fault detection according with the procedure already implemented in the passive networks, which requires the opening of the circuit breaker at the beginning of the faulty line.

In particular, when a fault occurs in a given line segment, the following actions take place:

1. each relay placed upstream the fault detects the fault current, following the direction from the MV bus-bar to the faulty point;
2. relays placed downstream the fault can detect a possible fault current coming from DG connected along the feeder beyond the faulty point. If the installed DG power is large enough, the fault current, which flows in the opposite direction in respect to current from the MV bus-bar, can start the protection relays;
3. each protection sensing a fault current, being from main grid or from DG, sends a BLOCK signal to the upstream relay, in the opposite direction of the measured current. In such a way, only the protection relays directly upstream and downstream of the fault are not blocked by any signal and the faulty line segment is identified;

[73] In this approach, the coordination between the protections is realized according to a distributed control logic, but the same can also be implemented by a central controller that supervises the operations.

4. the first non-blocked protection relay which trips sends a TRIP signal to the other one, in order to avoid non-synchronous trips of the two devices to different current levels;
5. a TRIP signal is sent to interface protections of the DG connected to the faulty line segment and downstream of it, while DG connected upstream should activate FRT strategy for handling the possible voltage dip resulting from the fault without disconnecting.

In such a way, the faulty line segment is disconnected from the grid, and all the DG located downstream of the fault is disconnected, avoiding island operations.
If the communication system is nonfunctional, or information exchange shows large time lags, protection functionalities are assured by the traditional protection scheme, which serves as back-up of the new scheme. In this case, faulty segment detection cannot be guaranteed, and all the feeder must be disconnected. Moreover, in this case, unwanted island operations are possible for some load conditions.

The block scheme of Figure 7-68 shows an example of protections coordination, according to the proposed logic, for a fault located in the second line segment.

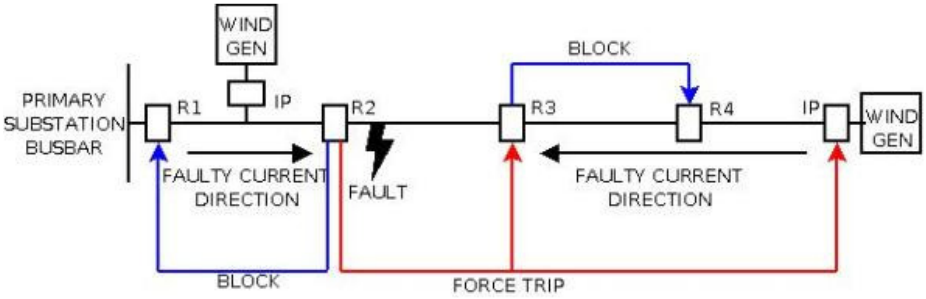

Figure 7-68: Example of fault detection with logic selectivity in an active network

It should be noted that the communication channel between the protection relays introduces inevitably intentional delays in the tripping time, according to the times required for communication. These delays would become negligible if the time for the information exchanges between the protection relays were extremely low (on the order of a few milliseconds). In fact, the messages between the protection devices, with the purpose of inhibiting the tripping of some of them, need a physical time ΔT_{com} to be received by the recipient[74]. During this time interval, the network protection relays, even if they have measured a sufficient current to trip without intentional delays, should bring in a state of waiting for a possible block signal that it would inhibit the action. Accordingly, there is a need to introduce an intentional delay ΔT_{I_ist} also for the over-current "instant" threshold relay. This delay may not be less than the time needed for the block signal exchange between two relays, i.e. $\Delta T_{I\_ist} > \Delta T_{com}$.
It is noted that the intentional delay introduction in the instantaneous over-current protection relay tripping involves an extension of the fault currents permanence in the network and, consequently, a longer duration of voltage dips (§ 7.9).

Then, the faulty line segment disconnection requires circuit breakers to be installed along the feeder, while, in common protection schemes, switch-disconnectors are employed along the distribution lines. The possibility to have two circuit breakers for each line segment, one upstream and one downstream, allows to select the faulty line segment without turning off the loads connected on the feeder itself, as reported in Figure 7-69.

[74] This time includes a time of sending and signal propagation, which depends on the communication type which is established between the relay and the physical component used for the transmission, and a time to receive and translate the signal.

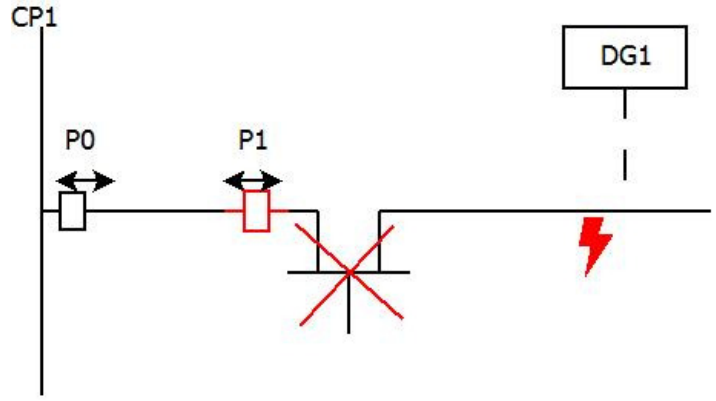

Figure 7-69: Installation of a single circuit breaker and faulty line disconnected

The coordination logic adopted in the example above can also be applied in case of feeder supplied by two distinct primary substations (Figure 7-70), with the exception that each network protection relay can communicate only with the DG interface protections connected in the two adjacent sections, always according to the logic of sending the forced tripping signal in the same direction as the fault current detected. In fact, in this case, only the generation included in the faulty line segment must be disconnected, while the remaining DG remains powered and connected.

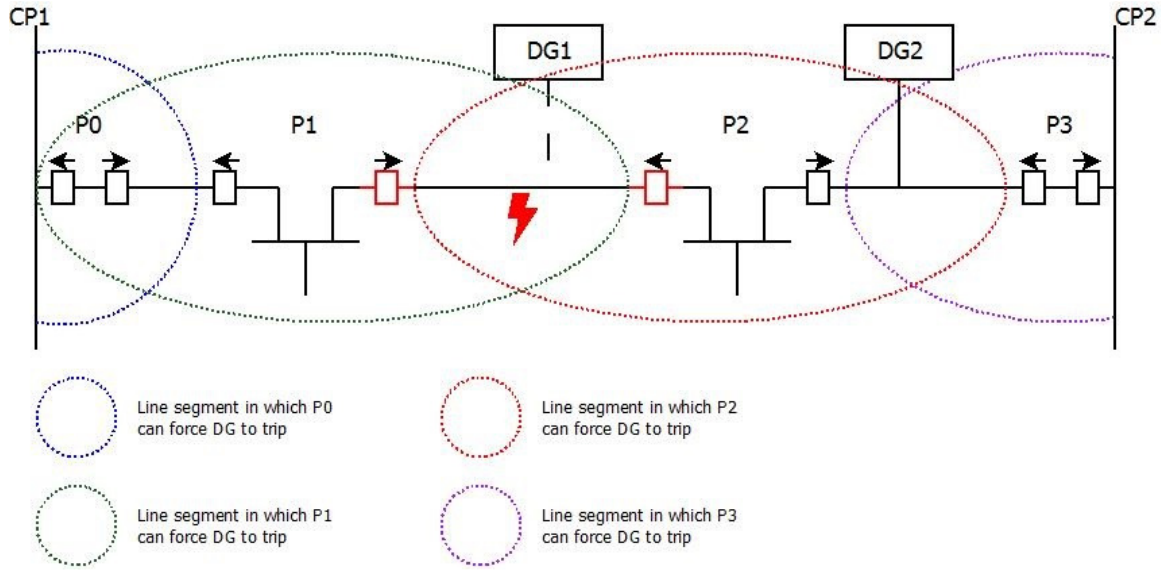

Figure 7-70: Example MV line fed by two different primary substations

7.8.2 Coordination logic verification

The proposed protection scheme has been tested for different fault cases with digital simulations performed in the ATPDraw environment. In the reported examples, the protection relays are named respectively R1, R2, R3 and R4 following the feeder direction; the communication time lag is supposed to be 20 ms. In addition, the DG model, already presented in the Chapter 2 has been modified to receive the signals from the line protection devices. These DG are controlled according to the FRT strategy to supply null active power during the voltage dip. It has been taken as reference the network showed in Figure 7-68.

Three phase fault with low impedance

In this example a three-phase fault occurring at t = 0.4 s in the second line segment is assumed. A total amount of power of 20 MVA[75] from DG is connected along the feeder, downstream the fault, so that the fault current from DG overcomes the I>>> current threshold of line over-current protection relays. Other wind generators are connected upstream of the faulty point, as well. Protection devices actions and the signals exchanged, for this example, are reported in Figure 7-71, while some simulation results are shown in Figure 7-72. This last shows that only relays R2 and R3 actually trips and only DGs connected downstream of the fault are forcedly disconnected, while generators located upstream perform FRT without disconnecting.

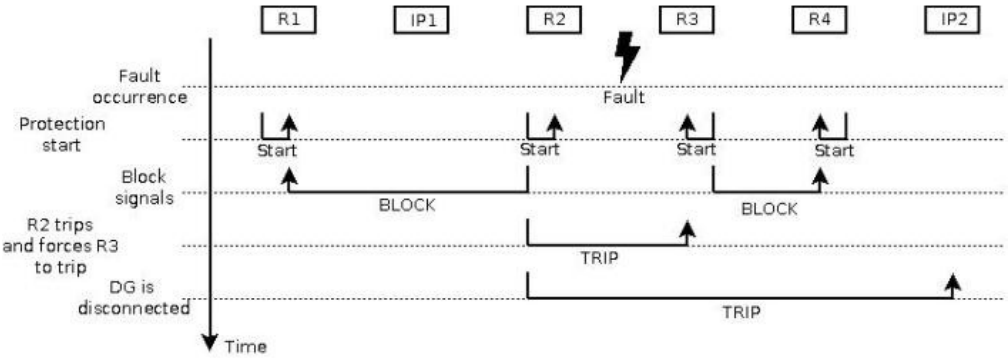

Figure 7-71: Events succession during a poly-phase fault along line

The simulation shows that the fault is detected properly by the protection relays and the faulty line segment is selected. The DG installed downstream the fault point is properly disconnected by a tripping signal sent from the protection "2" to the DG interface protection (Figure 7-72d). The DG connected upstream the fault, on the other hand, correctly implements the FRT strategy, leading to zero the power fed into the grid and then restarts after the mains voltage restoring (Figure 7-72e).

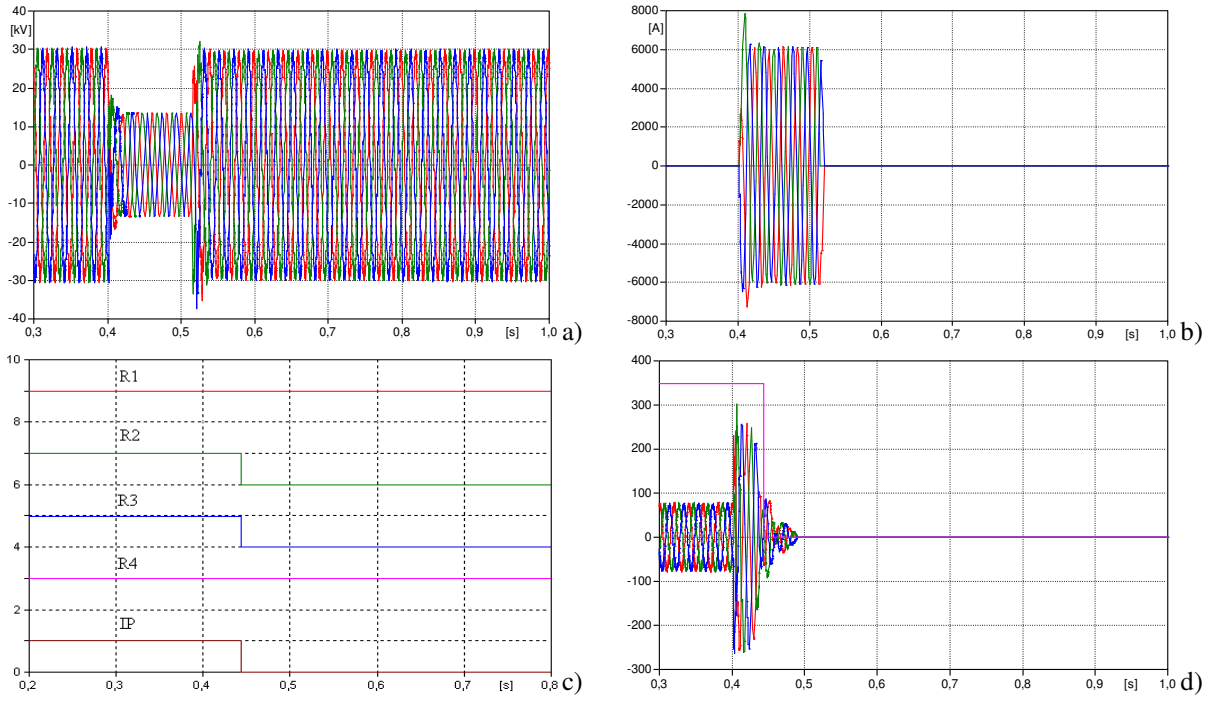

[75] This power amount is not related to the limit of power that can be installed on the MV feeder. This value has been used to simulate a big DG current that fed the fault.

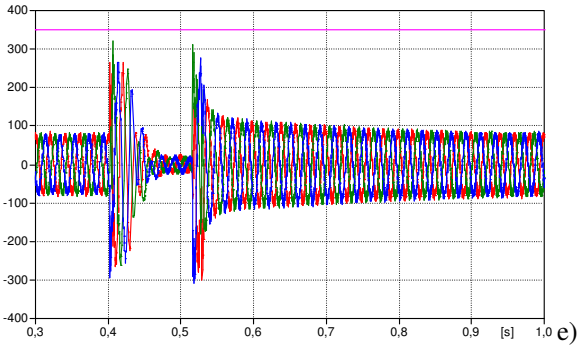

Figure 7-72: Example of logic selectivity in active networks with directional over-current relays.
a) voltage at the primary substation bus-bar,
b) fault currents,
c) output of relays (upper = close breaker, lower = open breaker),
d) AC output currents of the DG connected upstream of the fault,
e) AC output currents of the DG connected downstream of the fault.

Three phase fault with high impedance

The simulated case is similar to the previous one, but in this case the impedance fault isn't negligible (10 Ω). The fault current is not sufficient, in this case, to make the over-current protection relays tripping with threshold I>>>, while the second step threshold (I>>) is involved, with intentional delay equal to 100 ms. Also in this case, the logic selectivity scheme implemented recognizes and isolates the faulty line segment, minimizing the number of users disconnected from the network. It is also noted that a similar fault does not cause a voltage drop below 90% V_N and so any voltage dip condition is not detected by the DG. For this reason, it is not carried out any FRT strategies, but the generator, if it's not blocked by the signal sent to the interface protection, overcomes the disturbance continuing to supply the active power as before the fault. In addition, since the voltage and frequency parameters during fault differ only slightly from the nominal values, the interface protection is not started. The simulation results are reported in Figure 7-73.

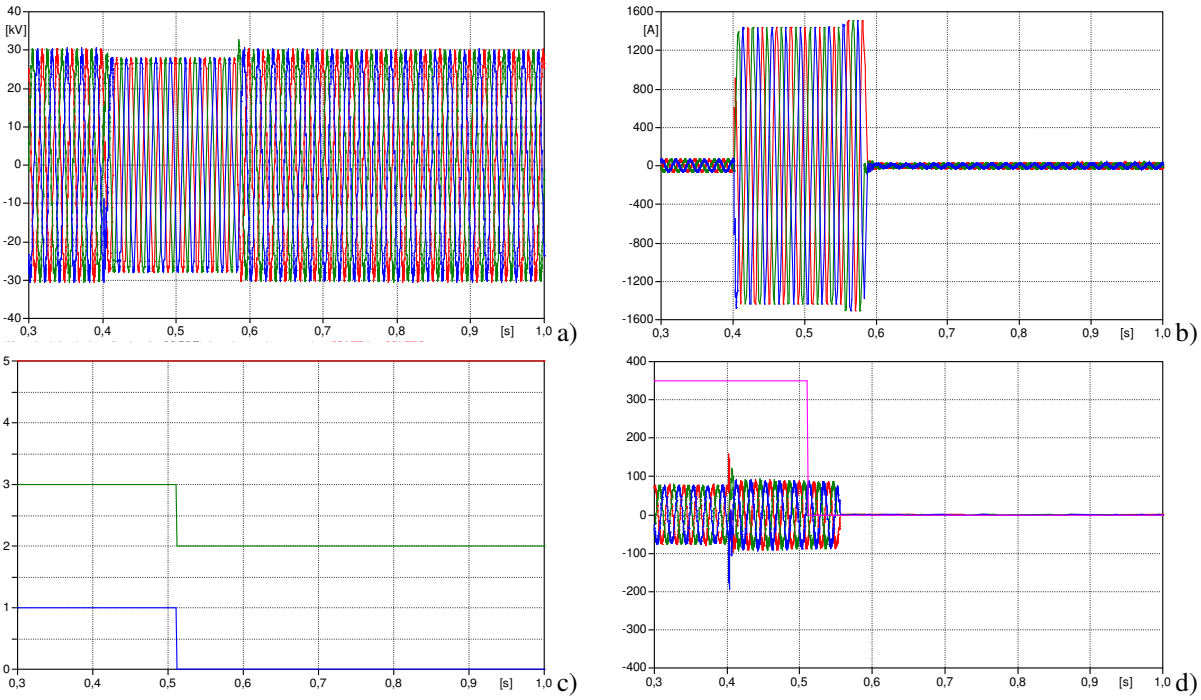

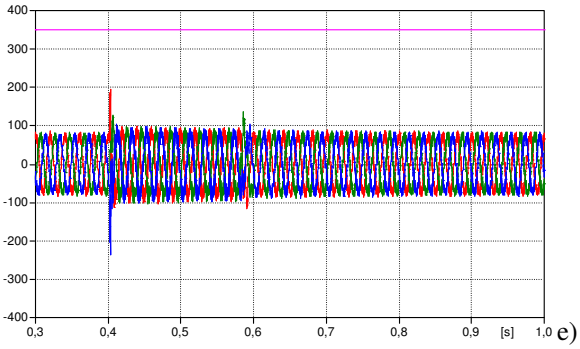

Figure 7-73: Simulation results obtained in the case of three phase fault with high impedance:
a) MV bus-bar line to line;
b) fault currents;
c) opening signals of the three CB along line (R1 red, R2 green and the R3 blue);
d) currents injected by the DG downstream the fault with the IP tripping signal;
e) currents supplied by the DG upstream the fault with the IP tripping signal.

Single phase to ground fault

The proposed protection scheme is suitable also in case of single phase faults. In the example reported, a single-phase fault to ground occurs at t = 0.2 s in the second line segment on the phase "a". The earth over-current directional relay plays the same role of the line over-current relays in the previous example. The grid is operated with the neutral connected to ground in the primary substation through an impedance, with a compensation degree of 90%. In this case, DG does not feel any voltage dip, so, the FRT strategies are not strictly necessary. In any case, the DGs connected downstream of the fault must be disconnected from the grid, in order to avoid island operations. Simulation results are shown in Figure 7-74.

Again, only the line protection relays close to the faulty point actually trip, while the others are blocked by the appropriate signals. The faulty line segment is detected and disconnected correctly and all the DGs located downstream of the fault are disconnected by the interface protections tripping.

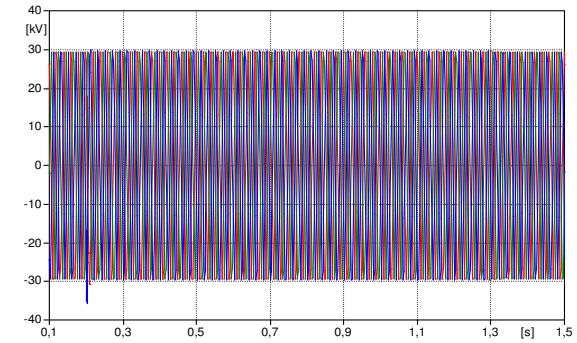

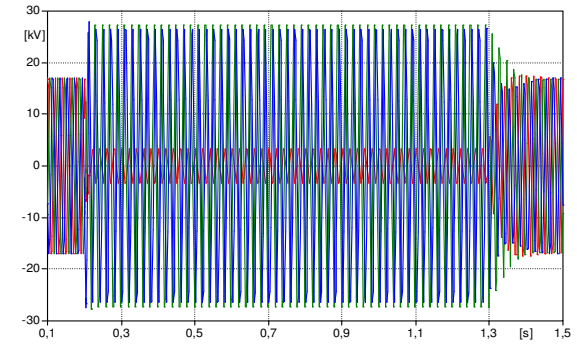

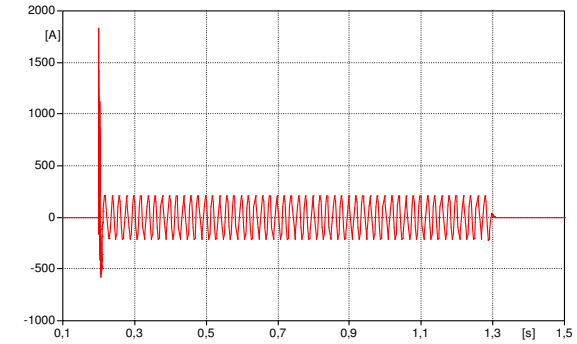

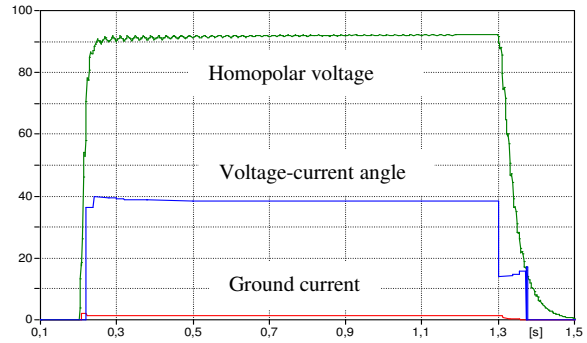

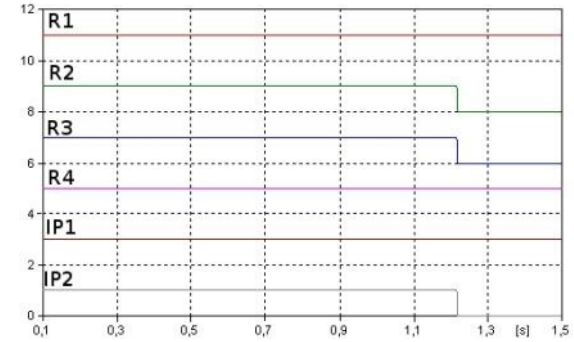

e)

Figure 7-74: Simulation results obtained in the case of a single-phase fault to ground:
a) MV bus-bar line to line;
b) MV bus-bar phase voltages;
c) fault current;
d) zero sequence voltage, ground current and angle between voltage and current measured by the protection R2;
e) tripping signals of line protections and interface protections.

Cross country fault

The response of the proposed protection scheme to a cross country fault (i.e. a single phase to ground fault on a feeder followed by a second single phase to ground fault on another feeder) has been simulated. In this case, protection relays models have been added to the second feeder of the simulated grid (protections are named R'x where x=1..3). The first fault occurs at t = 0,2 s on the phase "a" of the first feeder (in the second line segment), while the second fault appears at t = 0,23 s on the phase "b" of the other distribution line (in the first line segment). Both earth over-current directional relay and the line over-current directional relay of feeder 1 start, but, due to chronometric selectivity, only this last trips, for both feeders. Simulated responses are shown in Figure 7-75. In both feeders, the faulty line segment is correctly selected and disconnected from the grid.

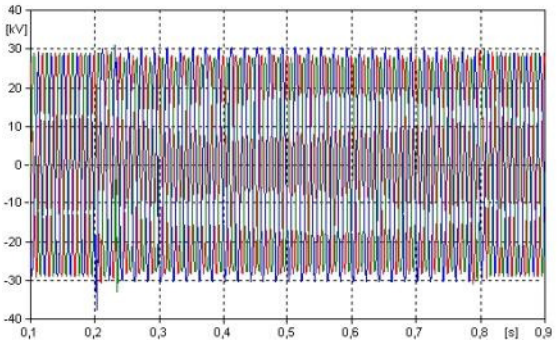

a)

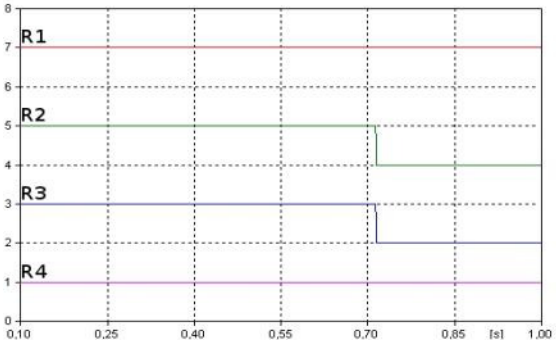

b)

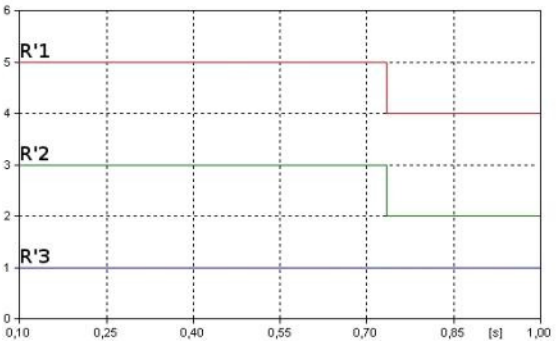

c)

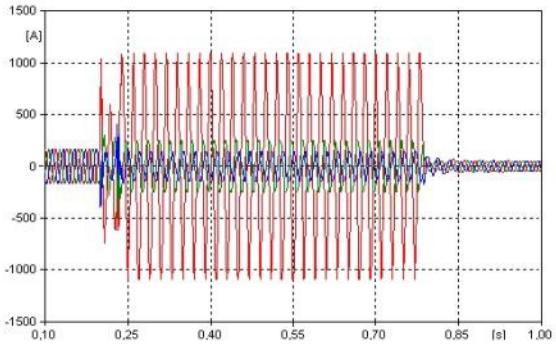

d)

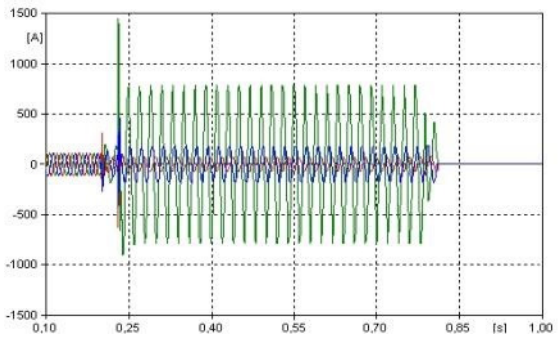

e)

Figure 7-75: Simulated waveforms in case of cross country fault:
a) line to line voltages at the MV bus-bar;
b) tripping signals of protections of feeder 1;
c) tripping signals of protections of feeder 2;
d) currents at the beginning of feeder 1;
e) currents at the beginning of feeder 2.

Automatic reclosing in presence of logic selectivity

The simulation has been carried out using the network configuration adopted in the previous example, and the automatic reclosing of the circuit breakers along the line is added. In this case, the three phase fault in the second line segment is self-extinguishing, and so the reclosing has good result and the line is re-fed. The distributed generators, installed upstream to the fault point, operate with the FRT logic to overcome the voltage dip, while those installed downstream receive a block signal from line protection relays to be disconnected from the network. In this simulation, any automatic generators restart have not implemented, and, therefore, the DGs located downstream the fault remain disconnected even after the mains voltage has been restored. Figure 7-76 shows the simulation results.

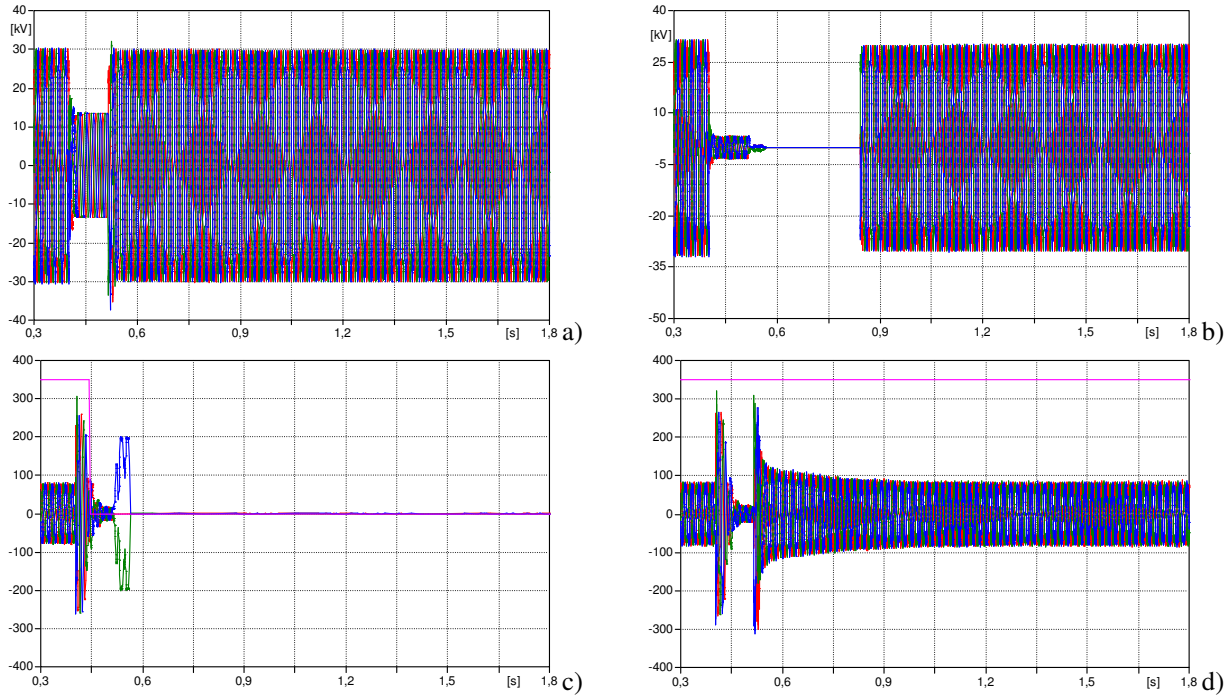

Figure 7-76: Simulation results in case of automatic reclosing (a) MV bus-bar line to line voltages, b) voltages at the bottom of the healthy line, (c) currents of the DG connected downstream the fault with the IP tripping signal, (d) currents of the DG connected upstream the fault with the IP tripping signal

Communication system failure

The same type of poly-phase fault considered before has been simulated supposing a failure in the communication system. Each protection is programmed to use standard settings if it does not receive BLOCK or TRIP signals after a given time it has detected fault currents.

The first protection installed along the line remains active, while the others are disabled, and it trips disconnecting all the feeder, independently on the fault location. All the DGs installed in the feeder are disconnected by their interface protections, not driven by external signals. Simulation results are shown in Figure 7-77; in particular, Figure 7-77a should be compared with Figure 7-72a, while Figure 7-77b with Figure 7-72b.

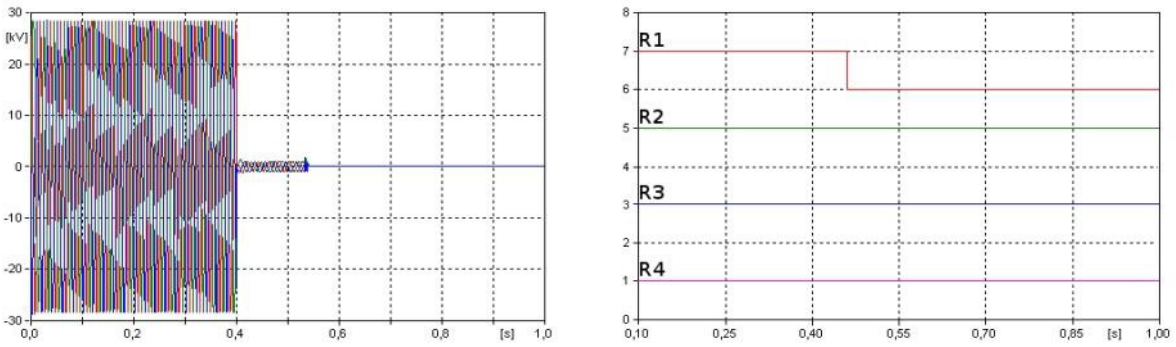

a) b)

Figure 7-77: Intervention of grid protection in case of communications failure: a) line to line voltages in the first line segment, b) line protection relays output.

7.8.3 Faulty line segment selection and reverse feeding

The proposed protections coordination scheme allows, with few modifications, to properly manage the network, maintaining the logic selectivity, even if line portions are reverse fed, due to the circuit breakers opening.

The network topology under exam is shown in Figure 7-78, where all the controlled circuit breakers and protection relays in the network are highlighted; the communication channels are not reported. For simplicity only the RELAY object is represented, even if in reality it's composed by two different functional blocks: the first is the over-current directional protection relay and the second one the directional earth relay.

The study takes into account four different conditions:

1. steady state initial condition (Figure 7-78);
2. first fault (Figure 7-79);
3. reverse feeding from an alternative primary substation (Figure 7-80);
4. second fault (Figure 7-81).

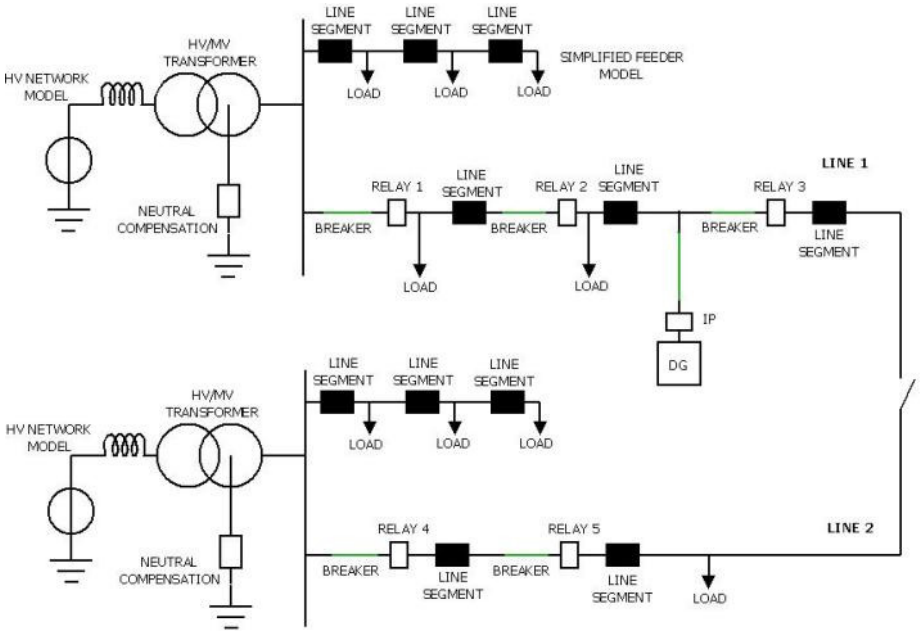

Figure 7-78: Network Diagram: initial condition

During the initial condition, line 1 and line 2 are fed by two different primary substations, and the distributed generator injects into the network an active power of about 2 MW.
The three phase resistive fault occurrence, as shown in Figure 7-79, starts the procedure described in the previous paragraph for the faulty line segment selection and the near circuit breaker opens, due to the logic selectivity implemented between the protection relays. A forced tripping signal is sent to the DG interface protection which, therefore, is disconnected from the network.
In this case, once isolated the faulty line segment, the circuit breaker recloses to allow the reverse feeding of line 1, as shown in Figure 7-79[76].

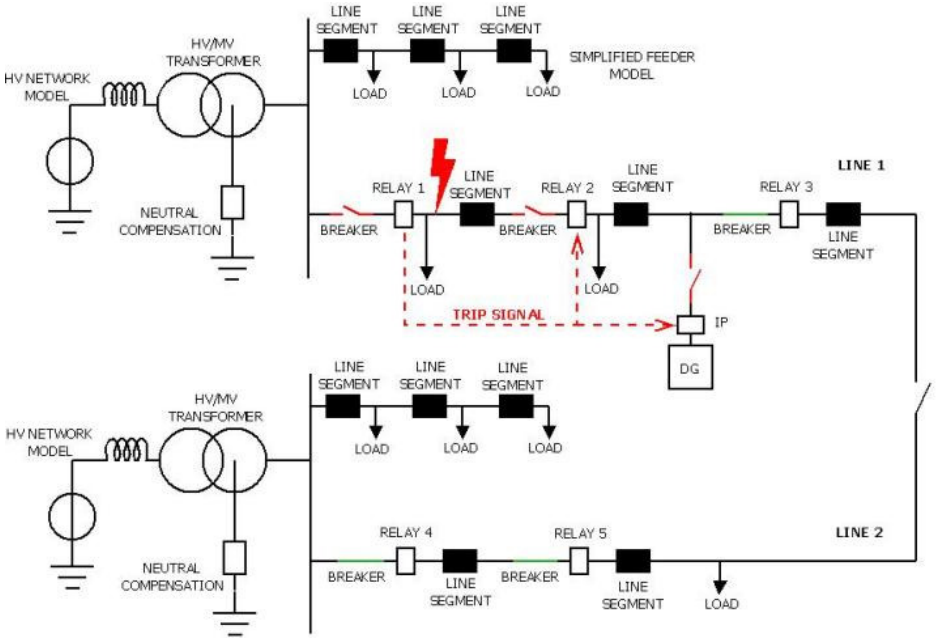

Figure 7-79: Network Diagram: first fault

[76] It should be noted that this procedure normally takes place after a cycle of automatic reclosing without positive results, while to make possible the second digital simulation it has been necessary to close the circuit breakers for reverse feeding, not implementing the reclosing.

During the first fault, it is necessary that the RELAY 3, the last of the line 1, is put in communication with the RELAY 5, placed at the bottom of the line 2, allowing to preserve the implemented logic selectivity functionality. In condition of reverse current feeding, however, the current in the line 1 has opposite direction than the normal supply condition: so it's necessary to reverse the intervention sectors angle of the over-current directional protection of the RELAY 3[77] (Figure 7-80). Substantially the RELAY 3 should be considered placed downstream the RELAY 5: the control signals exchange must be done according to the logic usually implemented.

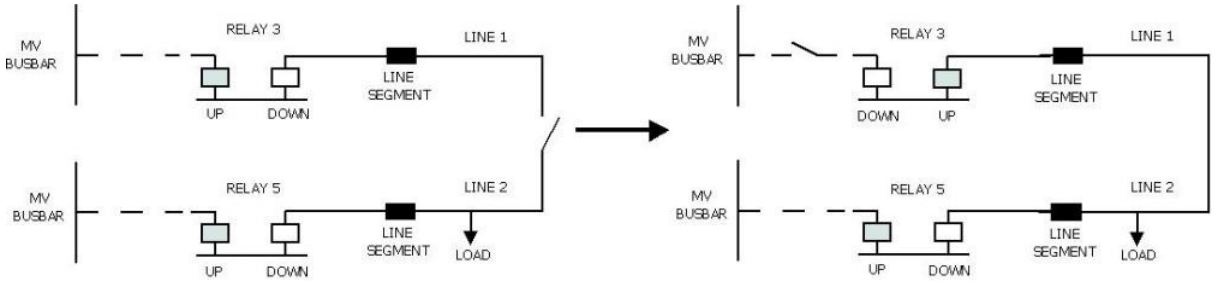

Figure 7-80: Over-current protection sectors of intervention

The Figure 7-81 shows the network scheme after the reverse feeding that allows to supply the last segment of the line 1, in favor of loads and DG connected; the distributed generators could restart to inject into the network the power produced from the primary energy source.

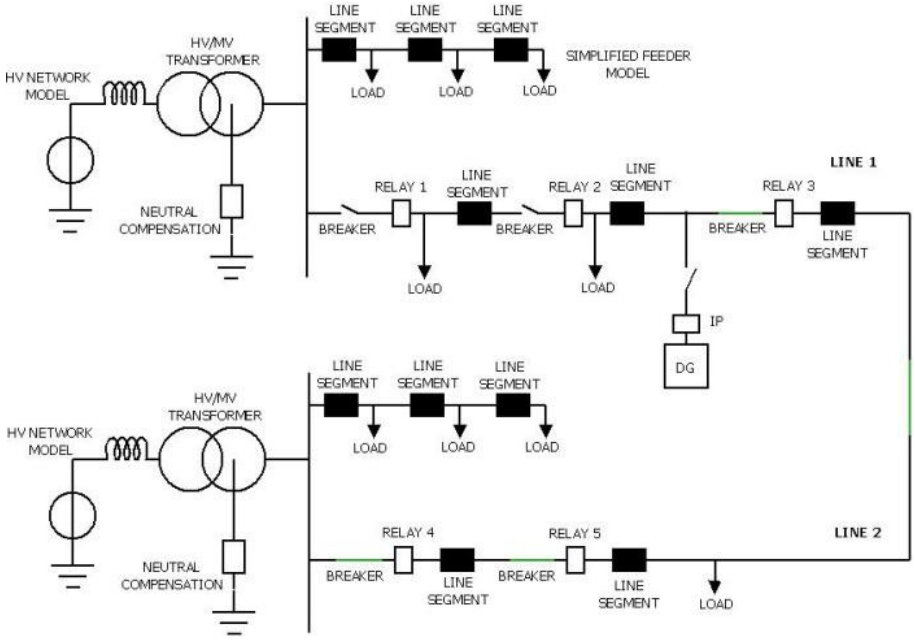

Figure 7-81: Network Diagram, condition of reverse feeding

[77] The reconfiguration of the directionality of the two protections is required to maintain the power supply to the load from Secondary Substation with the RELAY 3 during reverse feeding, in case of a fault downstream.

When the second fault occurs, as shown in Figure 7-82 (assumed resistive phase to phase fault) the over-current directional protections of the RELAY 4 and RELAY 5 will start: this last sends the block signal to the first, inhibiting its tripping. The fault current is also measured by over-current directional protection of the RELAY 3 which sends a stop signal to RELAY 5: in this way the only protection that trips is the one closer to the fault, allowing an effective faulty line segment selection.
The load at the bottom of the line 2 remains in fact fed upon the second fault; on the contrary, in the event of a lack of communication between the RELAY 3 and the RELAY 5, the second one would be tripped disconnecting the loads downstream.

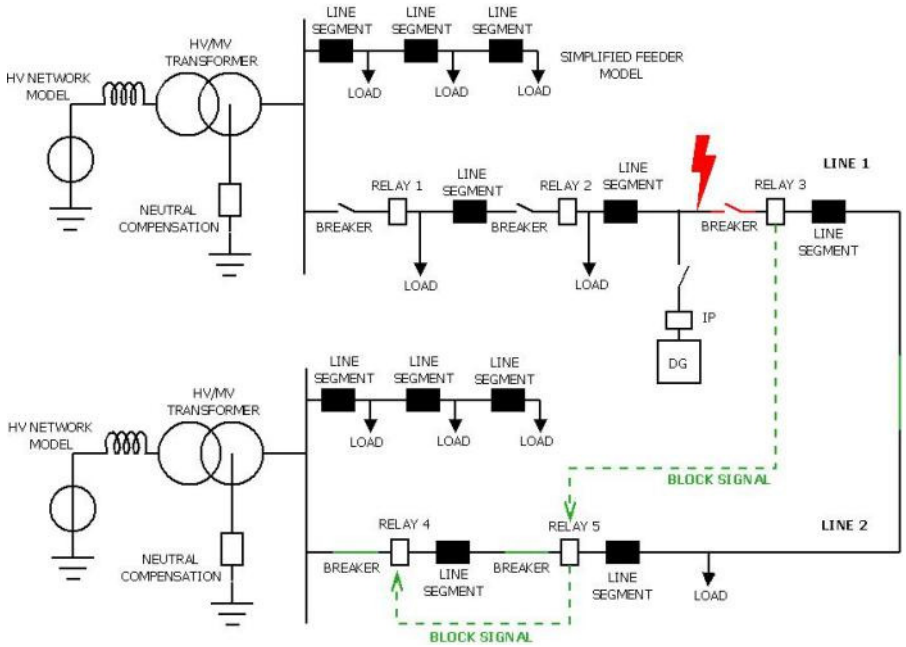

Figure 7-82: Network Diagram: second fault

The situation described above has been simulated in ATPDraw, introducing in the protection relay models the capability to reconfigure their own intervention areas as a function of the network configuration. Figure 7-83 represents the state of the different protection relays along the feeder during the simulation. Each Circuit Breaker (CB) refers to a RELAY, with the same number: the CB1 opening is due to the current measured during the first fault by the RELAY 1, while the CB2 opening has been forced by the tripping signal sent from the RELAY 1 to the RELAY 2. Upon the occurrence of the second fault, the only circuit breaker that is opened is the CB3 for the RELAY 3 tripping, which inhibits the RELAY 5 that sends block signal to the RELAY 4.

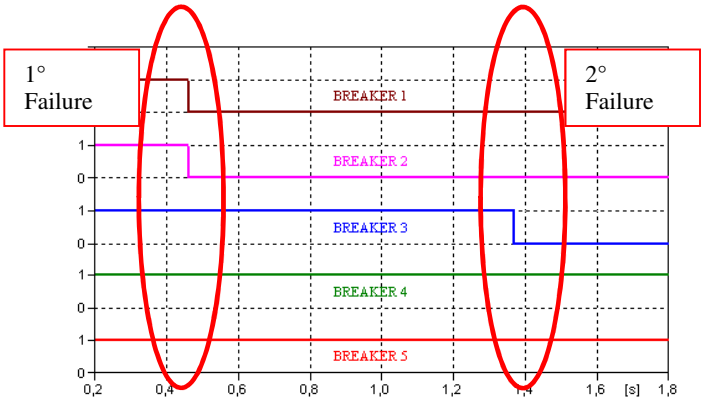

Figure 7-83: Circuit breakers states of the long line RELAY: 1 =closed, 0 =open

Figure 7-84a shows the MV line to line voltages at the DG connection point: both fault events are clearly visible, the first three phase resistive and the second two-phase resistive one; the reverse feeding starts at the time t = 1 s. In Figure 7-84b the DG currents supplied before and during the first fault are reported: after the RELAY 1 starting, a tripping signal is sent to the DG interface protection, causing the disconnection from the network. In this simulation a sequence to reconnect the DG to the network is not provided.

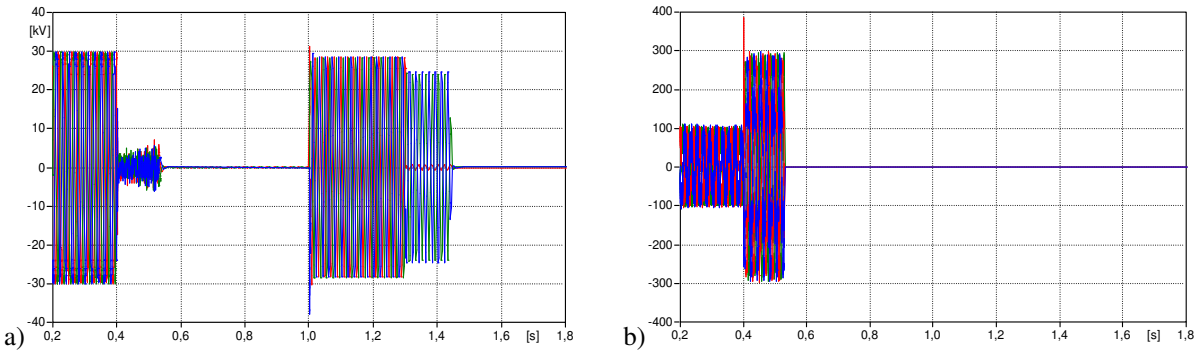

Figure 7-84: a) MV line to line voltages at the DG connecting point, b) MV inverter currents

The line lo line voltages in Figure 7-85a are measured at the load connection point at the bottom of the line 2. It's possible to see a slight perturbation of the voltage at the time t = 1 s due to the reverse feeding circuit breaker closing, while at the time t=1.3 s a phase to phase fault occurs with duration of 130 ms. Similar considerations can be made with respect to the measured currents, shown in Figure 7-85b: at the time of reverse feeding currents grow due to the load increase.

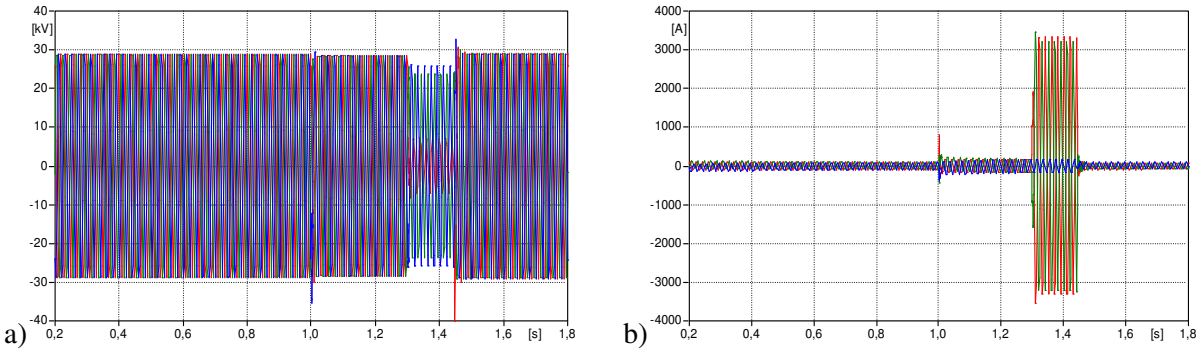

Figure 7-85: a) Bottom line 2 MV line to line voltages in, b) bottom line 2 RELAY 5 currents

7.9 Communication delays effects

The introduction of communication between the network protection relays makes it necessary to delay the tripping threshold of the over-current directional protection relays that usually don't present any intentional delay. This delay introduces:

- a longer permanence of the fault currents along the feeder;
- a longer duration of the voltage dips caused by faults that start the "instantaneous" tripping threshold of the over-current protection relay.

The fault currents permanence in the feeder for longer times produces an higher thermal stress for the line itself, identified by the index I^2t. This index, proportional to the line energy dissipated for the

Joule effect[78], grows linearly with the fault current permanence time. It is also possible to underline that the faults for which the protection relay trips instantaneously are those with the greatest magnitudes and, therefore, the most critical for the lines from a thermal point of view. Therefore it may be necessary to verify the design of lines where the protection devices with logic selectivity will be installed.

The elongation in the voltage dips duration is instead a phenomenon to be investigated in relation to the possible deterioration of the voltage quality. The voltage dips, as indicated in the Standard CEI EN 50160 [1], are classified according to duration and residual voltage, as shown in Figure 7-86, where the immunity curves of the class 2 and 3 equipment are highlighted, according to the CEI EN 61000-4-11 [79] and CEI EN 61000-4-34 [80]. The device of a given immunity class must be immune to voltage dips characterized by durations and residual voltages above the curve.

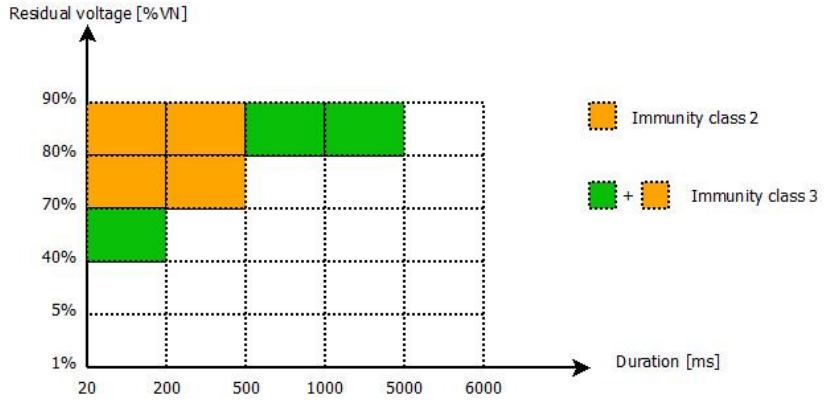

Figure 7-86: Voltage dips characterization in terms of residual voltage and duration and immunity curves of class 2 and 3

A first classification of the performance of a given network, or of a group of networks in a certain area and in a certain time period can be carried out by the voltage dips count in relation to the immunity curves, identifying indices for the networks performance characterization in terms of voltage dips, such as:

- N2a: the average number of voltage dips per measuring point that lie below the immunity curves class 2 (white + green cells in Figure 7-86);
- N3b: the average number of voltage dips per measuring point that lie below the immunity curves class 3 (white cells in Figure 7-86);
- R-DFI (Regulated Dip Frequency Index): index obtained by counting with weight 1 the voltage dips that fall below the immunity curve class 3, with weight 0 those that fall above the immunity curve class 2 and with a weight 0.5 events located between the two immunity curves.

An increase in the voltage dips duration would affect the events distribution in the classification table and, consequently, the network performance indices values.
The impact of the protection logic based on communication signals has been analysed considering the voltage dips statistics during the year 2011, recorded at national level by the QuEEN monitoring system of voltage quality[79], within its 400 primary substations, statistically representative of the Italian MV distribution network. In the following the detailed results are shown.

[78] It should be remembered that to avoid the cable damaging the I^2t must be less than the parameter k^2S^2, where k is a characteristic constant of the line type and of its insulation and S is the cable section in mm^2.
[79] http://queen.rse-web.it.

It's possible to see that not every voltage dip is influenced by the protection system proposed, so for the communication delay impact evaluation the following events will not be considered:

- voltage dips caused by faults in the HV transmission network that don't cause MV protection relays tripping, then the statistics reported below refer only to voltage dips with origin in the MV network;
- voltage dips with duration longer than 200 ms, times achieved nowadays with the network protection relays, which are not due to the "instantaneous" over-current protection tripping and are not affected by communication delays.

Therefore, in this analysis the duration of the only voltage dips classified in the first column of Figure 7-86 has been modified. In the next the voltage dips classifications obtained assuming different communication delays ($\Delta T_{communication}$) between 20 ms and 100 ms[80] are presented.

National Network, year 2011

Queen System Data					
	20-200 ms	**200-500 ms**	**500-1000 ms**	**1000-5000 ms**	**5000-60000 ms**
80 ≤ U <90	4668	2419	494	434	31
70 ≤ U <80	2480	1202	105	49	0
40 ≤ U <70	4625	1667	75	29	0
5≤ U <40	1786	501	45	10	0
1≤ U <5	18	4	0	0	0

$\Delta T_{communication}$=20 ms					
	20-200 ms	**200-500 ms**	**500-1000 ms**	**1000-5000 ms**	**5000-60000 ms**
80 ≤ U <90	4458	2629	494	434	31
70 ≤ U <80	2321	1361	105	49	0
40 ≤ U <70	4417	1875	75	29	0
5≤ U <40	1728	559	45	10	0
1≤ U <5	18	4	0	0	0

$\Delta T_{communication}$ =40 ms					
	20-200 ms	**200-500 ms**	**500-1000 ms**	**1000-5000 ms**	**5000-60000 ms**
80 ≤ U <90	4162	2925	494	434	31
70 ≤ U <80	2141	1541	105	49	0
40 ≤ U <70	4154	2138	75	29	0
5≤ U <40	1622	665	45	10	0
1≤ U <5	17	5	0	0	0

$\Delta T_{communication}$ =60 ms					
	20-200 ms	**200-500 ms**	**500-1000 ms**	**1000-5000 ms**	**5000-60000 ms**
80 ≤ U <90	3789	3298	494	434	31
70 ≤ U <80	1817	1865	105	49	0
40 ≤ U <70	3455	2837	75	29	0
5≤ U <40	1301	986	45	10	0
1≤ U <5	14	8	0	0	0

[80] In practice, it is proceeded to the events reclassification after having added the communication delay to the duration recorded by the monitoring system, maintaining the same residual voltage.

$\Delta T_{communication}$ =80 ms					
	20-200 ms	**200-500 ms**	**500-1000 ms**	**1000-5000 ms**	**5000-60000 ms**
80 ≤ U <90	3287	3800	494	434	31
70 ≤ U <80	965	2717	105	49	0
40 ≤ U <70	1685	4607	75	29	0
5≤ U <40	479	1808	45	10	0
1≤ U <5	13	9	0	0	0

$\Delta T_{communication}$ =100 ms					
	20-200 ms	**200-500 ms**	**500-1000 ms**	**1000-5000 ms**	**5000-60000 ms**
80 ≤ U <90	2652	4435	494	434	31
70 ≤ U <80	417	3265	105	49	0
40 ≤ U <70	522	5770	75	29	0
5≤ U <40	78	2209	45	10	0
1≤ U <5	6	16	0	0	0

Figure 7-87 shows the percentage increases of the Power Quality indices N3b considering an increase in the voltage dips duration. The analysis results are certainly bad than a real situation, because the study considers that all the voltage dips that originally have a duration of between 20 ms and 200 ms are prolonged. Since probably not every traditional network protection relay will be replaced with an "innovative" one, only the events occurred in lines with logic selectivity will be affected by an increase in the duration and it's therefore reasonable to expect that the Power Quality indices worsening is less pronounced.

In any case, the indices deterioration is a factor to be taken into account in the new network protection system evaluation. Finally, it should be pointed out that the voltage dips duration increasing is connected to the communication delays between the protection relays and therefore, in the final analysis, it depends on the technology used to implement this communication.

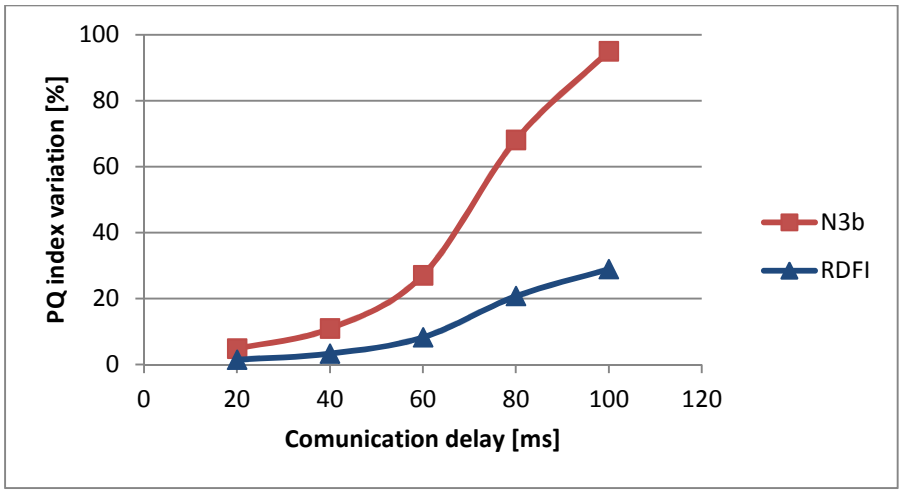

Figure 7-87: Power Quality indices of the network performance N3b and R-DFI considering different communication delays - national data 2011

7.10 Final Considerations

In this Chapter, after a brief description of the Italian protection system and of the reference Standards, a possible protection coordination scheme suited for mixed passive and active distribution networks has been presented. The protection coordination is made possible by introducing a communication channel to exchange the commands between the relays themselves and toward the Distributed Generators connected to the network. Central point of this approach is the use of directional over-current protection relays (to ensure the system selectivity in case of both poly-phase and single phase faults to ground) installed along the feeder in a radial distribution network. The main advantages of this protection scheme, than the traditional one, are:

- the faulty line segment selection, reducing the number of users disconnected;
- the possibility to accept reverse feeding;
- the reduction of the unwanted island operation probability.

The aim of the study is to assess the validity of this coordination scheme for different types of fault and different network configurations. The simulation results underline that the proposed protections coordination scheme allows to manage correctly passive networks and networks with distributed generators and to guarantee the logic selectivity also in presence of reverse feeding. The system is able to operate also in case of malfunction of the communications, even though with reduced performances similar to those obtained with the typical protection scheme for passive networks.

On the other hand, the proposed solution has some drawbacks due to the need of redundancy and communication time lags. This last issue introduces a thermal stress for the lines during the fault, quantifiable by the index I^2t, and a general voltage dips duration increasing, with negative effects on the network voltage quality performance. In particular, considering voltage dips recorded at national level by the QuEEN monitoring system during the year 2011, it is possible to verify that if the protection relays tripping delays are about tens of milliseconds (20 ms to 60 ms) the Power Quality indices vary in order of few percentage points. More significant worsening (up to 120 %) can be obtained in case of longer delay.

CONCLUSIONS

The network evolution toward an active network, with the increasing in the Distributed Generation (DG) installations, leads to analyse what impact the DG has both on the voltage quality in terms of Power Quality and on the distribution network operation and automation, even considering the Standards evolution about the requirements for the connection to the network.
In particular, the impact of the generation interfaced to the distribution network through power electronic devices (inverter) has been analysed in terms of:

- harmonics, flicker and operation with mains voltage unbalance;
- ability to overcome the voltage dips (Fault Ride Through - FRT) and mains voltage support;
- active and reactive power exchanges management;
- DG integration management in the most general network automation system proposing a protection coordination scheme based on the logic selectivity.

The analysis has been conducted through digital simulation in ATPDraw and DIgSILENT environments after the modeling of distribution network and distributed generation, with particular attention to the typologies and controls of the inverters (Chapter 2).
In detail the activity has been focused on photovoltaic and wind generation but the survey method used and the results can be extended to every type of distributed generators connected to the network through power electronic converters.

A laboratory experimental activity has also been carried out, supported by theoretical analysis/modeling, oriented to the functional tests for photovoltaic interface inverters, considering new requirements imposed by the recent national Standard (CEI 0-21). The tests have been performed both on an "old conception" inverter, i.e. designed according to the previous Standard, and on an "advanced" inverter, that is designed to provide the required functionalities even if not in full accordance with the Standard.

In general, all the activities have highlighted that the impact in terms of Power Quality (Chapter 1) and the capability to provide ancillary services to the network (Chapters 3 and 4) depend on the electronic network interface characteristics:

- design/capability, power configuration and modulation strategies (multi-level structures, interleaved solutions);
- management control strategy:
    - FRT (a condition of stand-by during the voltage dip is preferable to avoid the inverter current limitation operation and so the device is ready to exchange the pre-dip power with the network after the normal network conditions restoring);
    - the operation in presence of unbalanced steady state networks (control techniques optimized for these conditions are in fact not very effective to overcome the voltage dips for example those originated from two-phase faults, Chapter 5).

The main laboratory tests purpose is the deepening of issues to implement these new inverters capabilities, in particular it's resulted that "old conception" devices can satisfy the new Standard requirements with a firmware update and a capability curves revision (Chapter 6).

Finally, the connection to the network of distributed generators implies a critical revision of the network protection scheme even considering a greater level of network automation itself (Chapter 7). It has been proposed and analyzed a possible protections coordination scheme based on logic selectivity that can be applied with success both in passive and active distribution networks using directional over-current protections installed along the line and introducing a communication channel

to exchange the commands between the relays and toward the distributed generation connected to the network.

From the simulations, which took into account different types of network faults, it is clear that:

- the proposed protections coordination scheme allows to manage correctly passive and active networks:
    - thereby reducing the possibility of unwanted island operation;
    - allowing the line fault segment selection keeping the DG upstream the fault connected to the network, thanks to FRT logics, and reducing the number of users affected by the interruption;
    - confirming the possibility of reverse feeding the line keeping the logic selectivity even in this condition;
- the presence of the communication channels introduces delays that increase protection relay tripping time and this implies:
    - a greater thermal stress for the lines during failure, quantifiable by the index I^2t;
    - a general voltage dips duration increasing, with negative effects on the network performance in terms of voltage quality.

In conclusion the activity offers a general methodology for classification and analysis of the issues related to the DG connection through power electronic converters, regardless of the type of primary source, pointing out possible actions to be taken for their resolution. The results, especially in relation to the evolution of the protection systems in distribution networks, may represent a starting point for their laboratory and/or field activities to test the technological limits of the current products and evaluate their possible development to be effectively used in the future networks.

BIBLIOGRAPHY

[1] CEI EN 50160, "Voltage characteristics of electricity supplied by public electricity networks", Ed. 2010-12.

[2] CEI 0-21, "Regola tecnica di riferimento per la connessione di Utenti attivi e passivi alle reti BT delle imprese distributrici di energia elettrica", V2, December 2013, Italian Standard.

[3] CEI 0-16, "Regola tecnica di riferimento per la connessione di Utenti attivi e passivi alle reti HV ed MT delle imprese distributrici di energia elettrica", V1, December 2013, Italian Standard.

[4] IEC 61000-4-15 "Electromagnetic compatibility (EMC) - Part 4-15: Testing and measurement techniques - Flickermeter - Functional and design specifications", Ed. 2.0, 2010.

[5] D. G. Holmes, T. A. Lipo, "Pulse Width Modulation for Power Converters – Principle and Practice", IEEE, 2003.

[6] G. Chicco, J. Schlabbach, F. Spertino, "Operation of Multiple Inverters in Grid-Connected Large-Size Photovoltaic Installations", CIRED, Prague, 8-11 June 2009.

[7] D. G. Holmes, B. P. McGrath, "Opportunity for Harmonics Cancellation with Carrier-Based PWM for Two-Level and Multilevel Cascaded Inverters", IEEE Transactions on industry applications, Vol. 37, No. 2, March/April 2001.

[8] S. Kim, Y. Kim,K. Seo, S.Bang, K. Kim, "Harmonic analysis and output filter design of NPC multi-level Inverter", IEEE.

[9] J. Wang, D. Ahmadi, "A Precise and Practical Harmonic Elimination Method for Multilevel Inverter", IEEE Transaction on Industry applications, Vol. 46, No.2, March/April 2010.

[10] Waware, Madhukar; Agarwal, Pramod; "Use of multilevel inverter for elimination of harmonics in high voltage systems", Computer and Automation Engineering (ICCAE), 2010.

[11] K. A. Corzine, M. W. Wielebski, F. Z. Peng, J. Wang, "Control of Cascaded Multilevel Inverters", IEEE Transaction on Power Electronics, Vol. 19, No.3, May 2004.

[12] S. M. Samaun Imran, "Designing Transformerless Imbricated Cells Multilevel Inverter with Supercapacitor Storage", University of Dhaka, 2006.

[13] L. Chun-xi, M. Wei-ming, S. Chi, H. Wen-hua, "Research on Harmonics Suppression in High Power Middle Frequency 400Hz Inverter", IEEE, 2009.

[14] N. Golovanov, G. C. Lazaroiu, M. Roscia, D. Zaninelli, "Harmonic summation in power systems with power electronic interfaced loads", ICHQP 2010, Bergamo, Italy.

[15] F. medeiros, D. C. Brasil, P. F. Ribeiro, C. A. G. Marque, C. A. Duque, "A new approach for harmonic summation using the methodology of IEC 61400-21", ICHQP 2010, Bergamo, Italy.

[16] M. Brenna, F. Foiadelli, M. Roscia, D. Zaninelli, "Current Distortion Evaluation in Traction 4Q Constant Switching Frequency Converters", J. Electromagnetic Analysis & Applications, 2009.

[17] M. Brenna, R. Faranda, S. Leva, "Dynamic analysis of a new network topology for high power grid connecte PV System", IEEE, 2010.

[18] G. Carcangiu, C. Dainese, R. Faranda, S. Leva, M. Sardo, "New network topologies for large scale Photovoltaic System", IEEE Bucharest Power Tech Conference 2009, 28 June – 2 July, Bucharest, Romania.

[19] J. Schlabbech, A. Grob, G. Chicco, "Influence of Harmonic System Voltages on the Harmonic Current Emission of Photovoltaic Inverters", Powereng 2007, 12-14 April 2007, Setubal, Portogallo.

[20] A. Larsson, "The Power Quality of wind turbine", Chalmers university of technology, Sweden, 2000.

[21] A. Lazkano, K. Redondo, P. Saiz, J.J. Gutierrez, I. Azkarate, L:A. Leturiondo, "Case study: flicker emission and 3P power oscillations on fixed-speed wind turbines", 15th IEEE International Conference on Harmonics and Quality of Power, ICHPQ2012, Hong Kong, 17 – 20 June 2012, pp 1-6.

[22] R. Grünbaum, "Voltage and Power Quality control in wind power applications by means of dynamic compensation", Power-Gen Europe, 29-31 May 2001, Brussels, Belgium.

[23] H. Polinder, S.W.H. de Haan, M.R. Dubois, J.G. Slootweb, "Basic operation principles and electrical conversion systems of wind turbines", Converter technology and electric traction, June 2006, pp.1-6.

[24] L. Meegahapola, A. Perera, "Impact of wind generator control strategies on flicker emission in distributed networks", 15th IEEE International Conference on Harmonics and Quality of Power, ICHPQ2012, Hong Kong, 17 – 20 June 2012, pp 1-6.

[25] Rapporto Ricerca di Sistema RSE 11000902, "Sistemi elettronici di potenza connessi alla rete elettrica: studi, simulazioni e sperimentazioni", web site: http://www.rse-web.it, Italian language.

[26] J. Mur-Amada, A.A: Bayod-Rùjula, "Flicker emission of wind farms during continuous operation", IEEE Transaction on Energy Conversion, vol.17, Issue 1, March 2002, pp. 114-118.

[27] A.I. Estanqueiro, J.O. Tande, J.A. Pecas Lopes, "Assessment of Power Quality characteristics of wind farms", Power Engineering Society General Meeting, 2007, 24-28 June 2007, Tampa, USA, pp.1-4.

[28] IEC 61800-3: Adjustable speed electrical power drive systems - Part 3: EMC requirements and specific test methods Ed. 2.0, 2004.

[29] IEC 61400-21: Wind turbine generator systems – Part 21: Measurement and assessment of Power Quality characteristics of grid connected wind turbines, Ed. 1.0, 2001.

[30] A. Larsson, "Flicker and slow voltage variations from wind turbines", 7th International Conference on Harmonics and Quality of Power, ICHQP, Las Vegas, 1996.

[31] A. Lazkano, I. Azkarate, J.J. Gutierrez, J. Ruiz, L.A. Laturiondo, P. Saiz, "Measurement of the flicker characteristics of grid connected wind turbines: instantaneous frequency versus instantaneous phase estimation methods", 14th ICHQP, 26-29 September 2010, Bergamo, Italy.

[32] IEC 61000-4-15, "Electromagnetic compatibility (EMC) part 4: testing and measurement techniques – section 15: flickermeter functional and design specification", Ed. 2.0, 2010.

[33] T. Keppler, N.R. Watson, S. Chen, J. Avrillaga, "Digital flickermeter realizations in the time and frequency domains", Australasian Universities Power Engeneering Conference, AUPEC 2001, 23-26 September 2001, Perth, Australia, pp1-6.

[34] D.S.G. Barriel, G. Bonessi Menoni, T. di Lavello Mussi, D.N. Martin, "Flicker emission analysis of a wind farm", International Conference on Renewable Energies and Power Quality, ICREPQ2012, 28-30 March 2012, Santiago de Compostela, Spain, pp.1-6.

[35] A.A.V.V., "Wind in power, 2010 European statistics", available at web link http://ewea.org/fileadmin/ewea_documents/documents/statistics/EWEA_Annual_Statistics_2010.pdf.

[36] O.B.K. Hasnaoui, J. Belhadj, M. Elleuch, "Direct drive permanent magnet synchronous generator wind turbine investigation", in Journal of electrical systems, Vol. 4, Issue 3, September 2008, pp. 1-13.

[37] A. Dolara, R. Faranda, S. Leva, "Energy comparison of seven MPPT techniques for PV Systems", Journal of Electromagnetic Analysis and Applications, Vol.1 No.3, September 2009.

[38] IEC 60076-5, "Power transformer, capability to withstand short circuits", International Standard, Ed. 3.0, 2003.

[39] CEI EN 60904-3: Photovoltaic devices - Part 3: Measurement principles for terrestrial photovoltaic (PV) solar devices with reference spectral irradiance data, Ed. 2.0, 2008.

[40] J. Kearney, M.F. Conlon, E. Coyle, "Analysis of converter connected synchronous wind turbines to grid disturbances", 46th International Universities' Power Engineering Conference, UPEC 2011, 5-8 September 2011, Soest, Germany, pp.: 1-6.

[41] J. Conroy, R Watson, "Aggregate modelling of wind farms containing full-converter wind turbine generators with permanent magnet synchrounous machines: transient stability studies", Institution of Engineering and Technology, Journal on Renewable Power Generation, vol. 3, n, 1, 2009, pp. 39-52.

[42] J.A. Baroudi, V. Dinavahi, A.M. Knight, "A review of power converter topologies for wind generators", Journal on Renewable Energy, Vol 32, Issue 14, 2007, pp 1-17.

[43] Bin Wu, Yongqiang Lang, Navid Zargari, Samir, Kouro, "Power conversion and control of wind energy systems", Wiley and sons, 2011, Ed. 10.

[44] J. S. Thongam, R. Beguenane, A. F, Okou, M. Tarbouchi, A. Merabet, P. Bouchard, "A method for tracking maximum power points in variable speed wind energy conversion system", International Symposium on Power Electronics, Electrical Drives, Automation and Motion 2012.

[45] M. Örs, "Maximum power point tracking for small scale wind turbines with self excited induction generator", in Journal of Control Engineering and Applied Informatics, Vol. 11, Issue 2, Year 2009, pp. 30-34.

[46] R. Bharanikumar, A.C. Yazhini, A.N. Kumar, "Modeling and simulation of wind turbine driven permanent magnet generator with new MPPT algorithm", Asian Power Electronics Journal, Vol. 4, No. 2, August 2010, pp. 52-59.

[47] K. Belmokhtar, M. Lamine Doumbia, K. Agbossou, "Modelling and Power Control of Wind Turbine Driving DFIG connected to the Utility Grid", in Proc. of the International Conference on Renewable energies and Power Quality, ICREPQ 2011, Las Palmas de Gran Canaria (Spain), 13-15 April, 2011, pp. 1-6.

[48] J. Mur-Amada, A. A. Bayod-Rujula, "Flicker emission of wind farm during continuous operation", IEEE Transaction on Energy conversion, vol. 17, Issue 1, March 2012, pp. 114-118.

[49] Report Ricerca di Sistema, RSE 11000902A, "Sistemi elettronici di potenza connessi alla rete elettrica: studi, simulazioni e sperimentazioni", web site: www.rse-web.it, Italian language.

[50] J. Liang, B. Whitby, "Field oriented control of a permanent magnet synchronous generator for use in a variable speed tidal stream turbine", 46th International Universities' Power Engineering Conference, UPEC 2011, 5-8 September 2011, Soest, Germania, pp.: 1-6.

[51] A.A.V.V., "Codice di trasmissione, dispacciamento, sviluppo e sicurezza della rete", web site: http://www.terna.it/, Italian language.

[52] A.A.V.V., "Transmission Code 2007", web site: http://www.vde.com/.

[53] Florin Iov, Anca Daniela Hansen, Poul Sørensen, Nicolaos Antonio Cutululis, "Mapping of grid faults and grid codes", Risø-R-1617(EN), July 2007.

[54] A.A.V.V. "The Grid Code", disponibile sul sito web: http://www.nationalgrid.com/.

[55] E. Troester, "New german grid codes for connecting PV systems to the medium voltage power grid", 2nd International Workshop on Concentrating Photovoltaic Power Plants: Optical Design, Production, Grid Connection, DFarmstadt, 2009, pp. 1-4.

[56] R. Chiumeo, A. Florio, A. Mariscotti, M. Mazzucchelli "A voltage sag detection algorithm based on rectified voltage processing" - EPE-PEMC 2002 Dubrovnik & Cavtat.

[57] R. Chiumeo, R. Visintini, S. Quaia "Voltage sags effects on the operation of a synchrotron light source: experimental analysis and solution project" - EPE-PEMC 2002 Dubrovnik & Cavtat.

[58] Rapporto Ricerca di Sistema, 2001 - Project QUAFOR, "Studio e sviluppo di modelli di dispositivi Custom Power per la compensazione dei buchi di tensione", R. Chiumeo et alii, December 2001, Italian language.

[59] O.B.K. Hasnaoui, J. Belhadj, M. Elleuch, "Direct drive permanent magnet synchronous generator wind turbine investigation", in Journal of electrical systems, Vol. 4, Issue 3, September 2008, pp. 1-13.

[60] J. Kearney, M.F. Conlon, E. Coyle, "Analysis of converter connected synchronous wind turbines to grid disturbances", in Proc. of 46th International Universities' Power Engineering Conference, UPEC 2011, 5-8 September 2011, Soest, Germania, Vol. 1, pp. 1-6.

[61] C. Hochgraf, R.H. Lasseter, "StatCom controls for operation with unbalanced voltages", IEEE Transaction on Power Delivery, Vol. 13, Issue 2, 1998, pp.538-544.

[62] P. Mattavelli, S. Fasolo, "A closed-loop selective harmonic compensation for active filters", in Proc. of the Fifteenth Annual IEEE Applied Power Electronics Conference and Exposition, APEC 2000, Vol. 1 , pp. 399-405.

[63] A. Ortiz, M. Aredes, L.G.B. Rolim, E. Bueno, P. Rodriguez, "A new current control for the STATCOM based on secondary order generalized integrators", in Proc. of the IEEE Power Electronics Specialists Conference, PESC 2008, 15-19 June 2008, Rhodes, pp. 1-6.

[64] E. Di Marino, F. La Rocca, G. Valtorta, B. Ceresoli, "Variation of neutral earthing of MV networks from isolated to connected to ground through impedance: operation results and transition management", 17th CIRED, Barcelona, 12-15 May 2003.

[65] A. Cerretti, G. Di Lembo, G. Di Primio, A. Gallerani, G. Valtorta, "Automatic fault clearing on MV networks with neutral point connected to ground through impedance", 17th CIRED, Barcelona, 12-15 May 2003.

[66] B. Ceresoli A. Cerretti E. De Berardinis, A. Gallerani, P. Perna, G. Valtorta, "Neutral connection to earth in Medium Voltage networks: operation experience", 16th CIRED, Amsterdam, 18-21 June 2001.

[67] S. P. Chowdhurya, S. Chowdhurya, P.A. Crossleyb, "Islanding protection of active distribution networks with renewable distributed generators: A comprehensive survey", Electric Power System Research Journal, Volume 79, Isuue 6, 2009, Page(s): 984 – 992.

[68] D. Menniti, A. Pinnarelli, N. Sorrentino, G. Brusco, "Islanding detection active methods: implementation of simulation models using ATP-EMTP", 14th International Conference on Harmonics and Quality of Power (ICHQP), Bergamo, Italy, 26-29 Sept. 2010, pp. 1-8.

[69] Zhihong Ye; Kolwalkar, A.; Yu Zhang; Pengwei Du; Reigh Walling; "Evaluation of anti-islanding schemes based on nondetection zone concept", IEEE Transactions on Power Electronics, Volume: 19, Issue: 5, 2004, Page(s): 1171 – 1176.

[70] T. Thacker, F. Wang, R. Burgos, D. Boroyevich, "Islanding detection using a coordinate transformation based phase-locked loop", Power Electronics Specialists Conference 2007. PESC 2007, 17-21 June 2007, Orlando (USA), Page(s): 1-6.

[71] M.G.M. Abdolrasol, S. Mekhilef, "Robust hybrid anti-islanding method for inverter based distributed generation", IEEE Region 10 Conference, TENCON 2010, 21-24 Nov. 2010, Fukuoka (Japan), Page(s): 13-18.

[72] X. Zhu, C. Du, G. Shen, M. Chen, D. Xu, "Analysis of the Non-detection Zone with Passive Islanding Detection Methods for Current Control DG System", Twenty-Fourth Annual IEEE Applied Power Electronics Conference and Exposition 2009. APEC 2009, 15-19 Feb. 2009, Washington DC (USA), Page(s): 358 - 363.

[73] Zengqiang Mi, Fei Wang, "Power Equations and Non-Detection Zone of Passive Islanding Detection and Protection Method for Grid Connected Photovoltaic Generation System", Pacific-Asia Conference on Circuits, Communications and Systems, 2009. PACCS '09, 2009, Page(s): 360 – 363.

[74] F.J. Pazos, "Operational experience and field tests on islanding events caused by large photovoltaic plants", 21st International Conference on Electricity Distribution, CIRED2011, 6-9 June 2011, Frankfort, pp. 1-4.

[75] F:J. Pazos, "Power frequency over-voltages generated by solar plants", 20th International Conference on Electricity Distribution, CIRED2009, 8-11 June 2009, Prague, pp. 1-4.

[76] A. Cerretti, G. Scrosati, L. Consiglio, "Upgrade of ENEL MV network automation to improve performances in presence of faults and to deal DG", 21st International Conference on Electricity Distribution, CIRED2011, 6-9 June 2011, Frankfort (Germany), pp. 1-4.

[77] Belloni, Chiumeo, Gandolfi, Villa, "A protection coordination scheme for active distribution networks", 47th International Universities' Power Engineering Conference, UPEC, 4-7 September 2012, London, UK, pp.1-6.

[78] Report Ricerca di Sistema RSE 12000851, "Sistemi elettronici di potenza per la connessione della generazione distribuita alla rete elettrica: analisi del comportamento a fronte dei disturbi di rete", web site: http://www.rse-web.it, Italian language.

[79] CEI EN 61000-4-11 Electromagnetic compatibility (EMC) - Part 4-11: "Testing and measurement techniques, Voltage dips, short interruptions and voltage variations immunity tests", Ed. 2 – 2004.

[80] CEI EN 61000-4-34 Electromagnetic compatibility (EMC) - Part 4-34: "Testing and measurement techniques - Voltage dips, short interruptions and voltage variations immunity tests for equipment with input current more than 16 A per phase", Ed. 2, 2010.